SYNTHESIS AND CHARACTERIZATION OF LiFePO₄/C-POLYMER CATHODE MATERIAL FOR Li-ION BATTERY

A THESIS

Submitted in partial fulfilment of the
requirements for the award of the degree
of

DOCTOR OF PHILOSOPHY

in

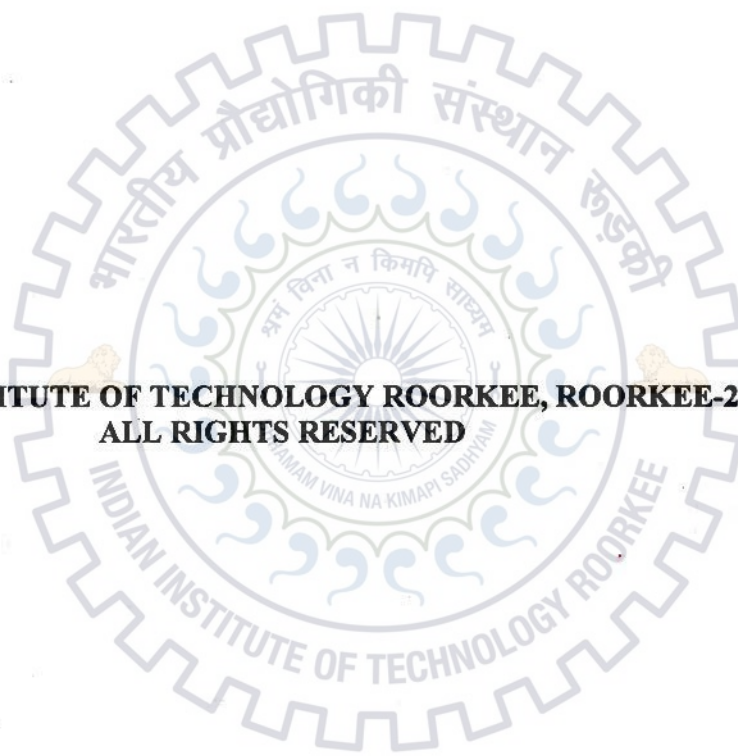METALLURGICAL AND MATERIALS ENGINEERING

by

RAJEEV SEHRAWAT

DEPARTMENT OF METALLURGICAL AND MATERIALS ENGINEERING
INDIAN INSTITUTE OF TECHNOLOGY ROORKEE
ROORKEE-247667 (INDIA)
JULY, 2015

INDIAN INSTITUTE OF TECHNOLOGY ROORKEE
ROORKEE

CANDIDATE'S DECLARATION

I hereby certify that the work which is being presented in the thesis entitled "**Synthesis and characterization of LiFePO$_4$/C-Polymer cathode material for Li-ion battery**" in partial fulfilment of the requirement for the award of the Degree of Doctor of Philosophy and submitted in the Department of Metallurgical and Materials Engineering of the Indian Institute of Technology Roorkee, Roorkee is an authentic record of my own work carried out during a period from July, 2010 to July, 2015 under the supervision of Dr. Anjan Sil, Professor, Department of Metallurgical and Materials Engineering, Indian Institute of Technology Roorkee, Roorkee.

The matter presented in this thesis has not been submitted by me for the award of any other degree of this or any other Institute.
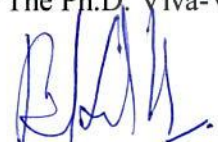
(Rajeev Sehrawat)

This is to certify that the above statement made by the candidate is correct to the best of my knowledge.

(Anjan Sil)
Supervisor

The Ph.D. Viva-Voce examination of **Mr. Rajeev Sehrawat** has been held on ___07/5/2016___

Chairman, SRC

Signature of External Examiner

This is to certify that the student has made all the corrections in the thesis.

Signature of Supervisor
Dated: ...7/5/2016...

Head of the Department
प्रोफेसर एवं विभागाध्यक्ष/Prof. & Head
धातुकर्म एवं पदार्थ अभियांत्रिकी विभाग
Metallurgical & Materials Engg. Deptt.
भा. प्रौ. सं. रुड़की/I.I.T. Roorkee

Abstract

Due to the economic liability of fossil fuels and increasing global warming concerns, it is required to develop alternative renewable and clean energy sources (such as solar, wind, and hydroelectric power) intensively at wide scale. These developments have raised a strong demand of high capacity energy storage systems with lower production costs and safety requirements. Li-ion batteries (LIBs) have been considered as one of the most promising energy storage system to meet these requirements. The first commercial Li-ion battery was developed by Sony Company in 1991. The ever increasing demand of producing a high energy storage system at lower cost drives the continuous research on various components of LIB. There are three key components in a LIB system: cathode, anode and electrolyte. The modern cathode materials have been prepared in their lithiated (discharged) state so that they can be paired with delithiated anode with a minimum possibility of accidental short-circuiting during the assembling of a battery. Hence, cathode materials always have a keen interest in research to enhance the storage capacity and fast charging of a LIB. The commonly used cathode materials are based on transition metals oxides or phosphates active material like $LiCoO_2$, $LiMn_2O_4$, and $LiFePO_4$ etc.

$LiFePO_4$ is a potential material for the cathode of Li-ion battery because it possesses superior performance as it has high discharge capacity of 170 mAh/g, flat discharge voltage (3.4 V) profile, excellent thermal stability both at the charged and discharged states, high cyclability, low cost and is environmental friendly. However, a few limitations such as nominal discharge voltage of 3.4 V vs Li/Li-ion, low electronic conductivity (10^{-9} S/cm), lower Li-ion diffusion coefficient and poor performance at low temperature restrict $LiFePO_4$ material from being used as cathode in commercial applications. The limitation of low redox voltage of 3.4 V for Fe^{2+}/Fe^{3+} couple can be solved by substituting Fe with the transition metals such as Ni, Co and Mn in the structure of $LiFePO_4$. The issues related to conductivity and diffusivity can be solved by 1) powder particles size reduction, 2) doping and 3) conductive surface coating such as with carbon and/or conducting polymers.

The reduced particle size of powder offers several advantages such as short diffusion length, improved electron propagation, large electrolyte/electrode interface area and modified chemical

i

potential. In view of the above advantages the particles size reduction can improve the high-rate capability and cycling stability of $LiFePO_4$ material.

The coating with conducting materials of carbon and polymers improves the electrical conductivity and Li-ion diffusivity of $LiFePO_4$ resulting in its improved capacity and rate capabiliy. The carbon coating is a potential approach to meet the theoretical capacity of $LiFePO_4$ at a nominal current rate. The effect of carbon coating is to impart high electronic conductivity, enhance the Li-ion diffusion in $LiFePO_4/C$ composite. Despite of many advantages carbon coating decreases tap density and volumetric density of cathode, and form inactive Fe_2P layer on $LiFePO_4$ active particles.

Substituting the inactive carbon and binder with electrochemically active polymer can enhance the electrochemical performance of $LiFePO_4$. The conducting polymers viz. polypyrrole, polythiophene and polyaniline are electrochemically active in the range of 2.2 - 3.8 V which overlaps with the redox range (3.4 V for Fe^{2+}/Fe^{3+}) for $LiFePO_4$. Therefore, these conducting polymers can act not only as conducting agent but also as host material for Li-ion insertion/extraction.

This PhD thesis aims at exploring and investigating different polymers coated $LiFePO_4/C$ cathode materials for lithium ion battery. Systematic studies on the synthesis, characterization, cell fabrication and electrochemical testing have been performed.

The thesis has been presented in six chapters.

Chapter 1 presents a brief overview on non-conventional and conventional energy sources, history of batteries development, and working principle of the lithium ion battery. This chapter also introduces several advantages of lithium ion battery over the other type of secondary batteries.

Chapter 2 presents a brief description of the various components of Lithium ion battery. The present status of various anode materials has been summarized. The detailed survey on cathode materials with main emphasis on $LiFePO_4$ has been conducted. The factors affecting the carbon coating on $LiFePO_4$ have been described. The promising methods of synthesis of electrochemically active polymers have been discussed. Finally the recent development on

ii

electrochemically active polymer coatings on the potential cathode materials has been summarized.

Chapter 3 deals with the synthesis and characterization of $LiFePO_4/C$ and polymers coated $LiFePO_4/C$. The $LiFePO_4/C$ nano-particles were synthesized by chemical precipitation method and the in-situ polymer coatings on $LiFePO_4/C$ were developed by oxidation polymerization method. Three types of electrochemically active polymer viz. polyaniline, polypyrrole and polythiophene have been used to coat $LiFePO_4/C$ material.

Chapter 4 presents the process of $LiFePO_4$ synthesis. The effects of 0.5 ml and 1.0 ml aniline monomers on structure and thickness of carbon coating as well as on the particle size of $LiFePO_4$ have been investigated. The decomposition of the polymer coatings has resulted in good graphitized carbon coating on the $LiFePO_4$ particles. The electrochemical study shows that discharge capacity of $LiFePO_4/C$ powder synthesized using 1.0ml aniline is higher than the powder synthesized using 0.5ml aniline. The higher rate capability and cyclability of $LiFePO_4$ synthesized using 1.0ml aniline were attributed to the smaller particle size, higher Li-ion diffusion coefficient and higher electronic conductivity.

Chapter 5 is broadly divided into three sections and presents the detailed investigation on mechanism of formation of polymer coatings viz. of polypyrrole, polythiophene and polyaniline on $LiFePO_4/C$ particles.

In section-I, the Polypyrrole coating on $LiFePO_4/C$ ($LiFePO_4/C$-PPy) particles has been discussed. The XRD pattern of the polypyrrole coated $LiFePO_4/C$ composite confirms the formation of two electrochemically active phases of $LiFePO_4$ and $Li_{0.05}FePO_4$. The less porosity in the polypyrrole coating grown in ACN solvent produces good connectivity of the core particles resulting in higher electrical conductivity and Li-ion diffusivity. The composite $LiFePO_4/C$-PPy polymerized in ACN shows appreciable rate capability of 82 mAh g^{-1} compared to 40 mAh g^{-1} for sample $LiFePO_4/C$ at higher current rate of 20C. The better rate capability of $LiFePO_4/C$-PPy polymerized in ACN was due to the higher electrical conductivity and higher Li-ion diffusivity as confirmed by electrochemical impedance spectroscopy (EIS) measurements.

The section-II presents the investigation on polythiophene coated $LiFePO_4$/C material. To suppress the growth of Li_3PO_4 impurity phases, polythiophene coating was developed on Li-deficient and Li-excess samples of $LiFePO_4$. It has been observed that only the polythiophene coated Li-deficient $Li_{0.95}FePO_4$ material was capable of suppressing the Li_3PO_4 impurity phase. Polythiophene with different quantities of 4, 6, 8 and 12 wt% were deposited on $Li_{0.95}FePO_4$ material and the resultant materials are designated as $Li_{0.95}FePO_4$/C-PTh(4), $Li_{0.95}FePO_4$/C-PTh(6), $Li_{0.95}FePO_4$/C-PTh(8) and $Li_{0.95}FePO_4$/C-PTh(12) respectively. The EIS measurements show that all the polythiophene coated $Li_{0.95}FePO_4$/C materials exhibit higher Li-ion diffusivity and low charge transfer resistance (R_{ct}). As the quantity of polythiophene increases in composites the conductivity also increase. The improved rate capability of $Li_{0.95}FePO_4$/C-PTh(8) composite was due to optimum quantity of polythiophene covering and interconnecting the $LiFePO_4$/C particles.

In section-III detailed investigations on the polyaniline coated $LiFePO_4$/C composite has been presented. The *in-situ* polyaniline coating on $LiFePO_4$ particles was done using three different oxidizing agents viz. $(NH_4)_2S_2O_8$, $KMnO_4$ and $K_2Cr_2O_7$. Polyaniline (PANI) samples have been grown separately by self oxidation process using the above oxidizing agents. XRD analysis reveals the formation of single phase pure active material $LiFePO_4$/C and mixed phase containing $LiFePO_4$ and $FePO_4$ for polymer coated $LiFePO_4$/C composite. The amounts of polymer in the polyaniline coated $LiFePO_4$/C composites synthesized using $(NH_4)_2S_2O_8$, $KMnO_4$ and $K_2Cr_2O_7$ are 14, 15 and 17 wt% respectively. Electrical conductivities of the composite materials were determined by Impedance spectroscopy method. The composite material synthesized with $(NH_4)_2S_2O_8$ has higher conductivity compared to those synthesized with $KMnO_4$ and $K_2Cr_2O_7$.

Chapter 6 presents the major conclusions of the present study and scope of the future work.

Acknowledgements

was not only a senior of mine; he was more than a friend, philosopher and guide for me in my research as well as in my personal life. My friends Rashmi Mittal, Pradeep Soni, Naveen Ohlyan and Nitin Phogat were like my family member in Roorkee. We shared lot of happy experience like travelling outing, party, dining... I will always remember those happy days when we were together.

During my stay at IIT Roorkee I was associated with several friends and colleague. I appreciate each one of them for their moral support and cooperation which helped to keep things in perspective. Thanks to Dr. Dharmendra Singh, Dr. Abhishek Singh, Dr. Deepa Mudgal, Dr. Paritosh dubey, Rashmi Rani, Himanshu panjiar, Kaushal Chauhan, Arun Narwal, Preeti Makkar, Ravi Kant, Sandan Kumar Sharma, Gajendra (Gajju), Sanjay Singh Rathore, Tilak Joshi and Ashish Selokar.

I express my deepest esteem to my parents and brothers (Sunil and Sandeep) for keeping their blessing over me. You're waited for many years to see this moment. Thank you for all sacrifices that you made. I know it was not easy. You all are always being with me in my memories. Without you I would never be standing where I am now. Thank for giving me strength and the spark of hope when everything looked hopeless. I am highly appreciative to my sister-in-law Mrs. Banita for her encouragement throughout.

The Author also like to thank everyone who supported him for completing this work successfully and express his apology that he could not mention everyone individually.

(Rajeev Sehrawat)

Contents

List of Figures

partially graphitized carbon

and LiFePO$_4$/C-PANI composites at 2C rate for 50 cycles

List of Tables

List of Publications

International Journals:

1. **Rajeev Sehrawat**, Anjan Sil "Synthesis and characterization of $LiFePO_4$-C/ PANI composite for cathode material of lithium ion battery", Advanced Materials Research, 585 (2012) 240 - 244.

2. **Rajeev Sehrawat**, Anjan Sil "Polymer gel combustion synthesis of $LiFePO_4$/C composite as cathode material for Li-ion battery", Ionics, 21, (2015) 673 - 685.

3. **Rajeev Sehrawat**, Anjan Sil "Effect of solvents on electrochemical performance of polypyrrole coated $LiFePO_4$/C cathode materials", Journal of Materials Science: Materials in Electronics, 26 (2015) 5175 - 5185.

Conferences:

1. International Conference (2012), International Conference on Advances in Materials and Processing Challenges and Opportunities (AMPCO 2012) organized by IIT Roorkee, Roorkee-247667 (U.K.)

2. International Conference (2014), International Conference, 'International Conference on Functional Materials' (ICFM-2014) organized by IIT Kharagpur, Kharagpur-721302 (W.B.)

3. International Conference (2014), International Conference 'International Conference on Innovations in Engineering and Technology' (ICCET'2014) at Penang (Malaysia), organized by International Institute of Engineers.

List of Abbreviations

DTA	Differential Thermogravity
EV	Electrical Vehicle
HEV	Hybrid Electrical Vehicle
HR-TEM	High Resolution Transmission Electron Microscope
SEM	Scanning Electron Microscope
CNT	Carbon Nanotubes
Ni-Cd	Nickel-Cadmium
SEI	Surface Electrolyte Interphase
FCC	Face Centered Cubic
XRD	X-ray Diffraction
PITT	Potentiostatic Intermittent Titration Technique
DMSO	Dimethyl Sulfoxide
CV	Cyclic Voltammetry
I_D	Intensity of Disordered
I_G	Intensity of Graphitic
I_p	Persistence Length
DBSA	Dodecylbenzenesulfonic Acid
TsOH	p-toluenesulfonic Acid
Na-PTSA	Sodium p-toluene Sulfonate
EC	Carbonate
DMC	Dimethyl Carbonate
ACN	Acetonitrile
TG	Thermogravimetry
SE	Secondary Electrons
BSE	Back Scattered Electron
EDS	Energy Dispersive Spectroscopy
TEM	Transmission Electron Microscopy
IR	Infrared
CCD	Charge Coupled Device
PVDF	Polyvinylidene Fluoride

NMP	N-methyl-2-pyrrolidinone
EIS	Electrochemical Impedance Spectroscopy
R_b	Bulk Resistance
R_{ct}	Charge Transfer Resistance
Z_w	Warburg Impedance
DC	Differential Capacity
CPE	Constant Phase Element
D_{Li+}	Li-ion Diffusivity
D	Diffusion Coefficient
L	Diffusion Length
XPS	X-ray Photoelectron Spectroscopy

INTRODUCTION

INTRODUCTION

Fossil fuel such as coal and petroleum are the major sources of energy to fulfill present demand of the society. The coal and petroleum are becoming more expensive due to their limited availability and non-renewable nature. The limited availability, pollution challenges and global warming are serious concerns of fossil fuel. So, it becomes an urgent need to decrease the amount of green house gases generation and pollution by using renewable energy sources. Renewable sources of energy such as solar, wind and hydro significantly rely on natural conditions hence these are not continuous sources. Due to this reason developments of renewable sources have raised a strong demand for high performance energy storage systems with higher safety and lower costs. The different storage technologies include batteries, ultra-capacitors, flywheels, and superconducting energy storage systems. From the above mentioned technologies battery is one of the most cost-effective energy storage technologies available, wherein energy is stored electrochemically.

Among the various energy storage systems, electrochemical energy storage devices have advantages of high versatility, efficiency, and flexibility. An electrochemical energy storage device is usually composed of a cathode and an anode; both are separated with a separator, soaked with electrolyte. Batteries and capacitors are the two typical electrochemical energy storage devices in which energy is stored in the form of chemical energy. Batteries have high energy density as compared to supercapacitors whereas supercapacitors have high power density but low energy density. The comparison of power density and energy density of batteries and supercapacitors is shown in Fig.1.1.

A traditional capacitor stores electrical energy by accumulating positive and negative charges on conducting electrodes separated by an insulating dielectric. A supercapacitor has conducting electrodes having large surface area separated by advanced electrolyte materials and provides a much higher storage capacity. The materials such as aqueous salts based, organic based and carbon based can be used as electrolyte for the supercapacitor. Although supercapacitor based on organic electrolyte can store higher energy density than aqueous electrolytes. But the power density of organic electrolyte based supercapacitors is usually lower than that of aqueous

electrolyte based supercapacitors. The electrode materials for supercapacitors mainly include carbon, transition metal oxides, and conducting polymers [Arbizzani et al, 1996]. A high performance supercapacitor can be developed by understanding the combined effect of various types of surface functionalities of carbon and pore structure [Jurcakova et al, 2009]. The storage capacity of supercapacitors can be improved using the nano-porous electrode material which provides higher surface area for the charge storage. One of the best materials is activated charcoal which is made up of rough and extremely small particles [Seredych et al, 2008]. The overall surface area of such a porous material is many times higher than the traditional metallic electrodes such as of copper and aluminium. The storage capacity of supercapacitor can be further improved by using mechanically aligned carbon nanotubes (CNTs) which provides higher surface area than activated charcoal.
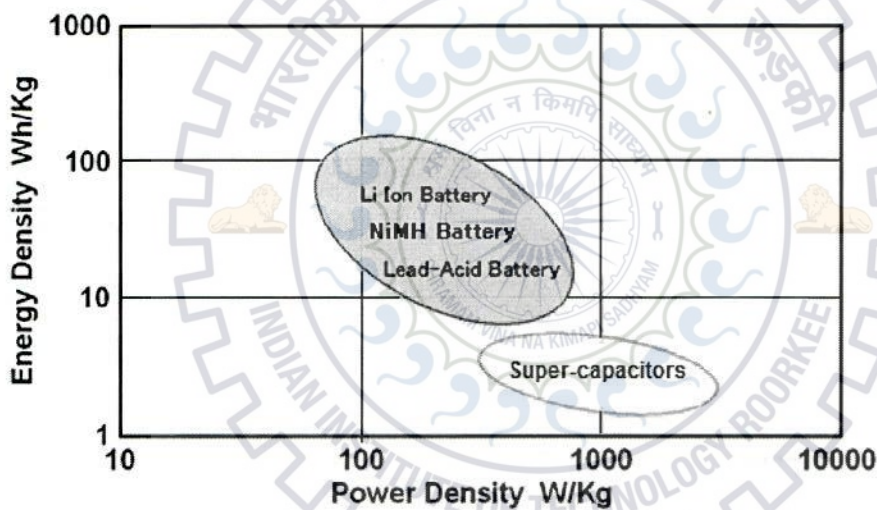
Fig. 1.1: A comparison between energy density and power density of batteries and super-capacitor.

There are a number of battery technologies under consideration for large-scale energy storage. Depending upon the materials of electrodes rechargeable batteries can be broadly classified as lead-acid, nickel-cadmium, nickel-metal hydride, zinc-air, and Li-ion battery. A lead-acid battery is the most matured and oldest battery technology which consists of a positive electrode of lead dioxide and a negative electrode of sponge lead, separated by a micro-porous material and immersed in an aqueous sulfuric acid electrolyte. Lead-acid batteries still represent a low-cost option for most applications requiring large storage capabilities. The low energy density and limited cycle life are common disadvantages of lead-acid battery. Although the Ni-Cd

batteries have superior cycle life, energy and power densities than that of Lead-acid batteries but they contain toxic heavy metals and suffer from severe self-discharging. Improvement in energy density and charging characteristics are still an active research area, with different additives under consideration for this class of battery. A comparison of volumetric energy density and gravimetric energy density of different battery technologies is shown in Fig. 1.2.

The light weight, high electropositive potential (– 3.04 V in reference with standard hydrogen electrode) and high chemical reactivity of lithium makes it most suitable metal for the batteries. Lithium-metal battery consists of an anode of lithium metal and cathode of metal oxides both dipped in the electrolyte. Lithium-metal batteries have extremely high specific capacities and are of light weight, which can boost the electric vehicles (EVs) and hybrid electric vehicles (HEVs). But these batteries suffer from two main problems. One is the growth of lithium dendrites and another is low columbic efficiency during the charging / discharging process. Both these problems act as barrier to develop these batteries. Although low columbic efficiency can be compensated by using higher amount of lithium but the formation of lithium dendrites is still a common problem with these batteries resulting in the dramatic failure leading to the fire and explosion to the battery [Xu et al, 2014]. Among all the commercially available batteries, lithium-ion (Li-ion) battery represents the current state-of-the-art technology in high energy storage device with higher safety, due to which they have occupied a prime position in the market for portable electronic devices, such as laptops, cell phones, and cameras. The concept of Li-ion battery was first demonstrated at the end of 1980s [Murphy et al, 1978]. The presence of lithium ion instead of lithium metal solve the problem of growth of dendrites to make the Li-ion battery safer than Li-metal. The other advantages of Li-ion batteries are long cycle life, very low self discharge (about 5% per month) and they do not suffer from memory effect. However, it is still challenging to achieve high power density and high energy density for EVs and HEVs from Li-ion batteries. In general, the power capability of Li-ion battery is hindered by the kinetic problems of the electrode materials used. To deliver high power densities, the electrode materials of Li-ion batteries must possess rapid ionic and electronic diffusion.

The three key components of a Li-ion battery are cathode, anode and electrolyte. The performance of a battery depends on the characteristics of these components. The schematic diagram of Li ion battery is shown in Fig. 1.3. At charged state all the Li-ions are at the anode side and at discharged state all the Li-ions are towards the cathode side. To avoid accidental

short-circuiting the assembling must be performed at the discharged state of the battery. So anode should be empty and cathode should be fully lithiated during the assembling of a battery. Therefore a Li-ion battery initially must be charged before it is used. During charging Li-ion hosted by cathode moves towards anode through the electrolyte. The oxide materials on positive side act as host for the Li-ion and hence this side is very critical in deciding the battery capacity.
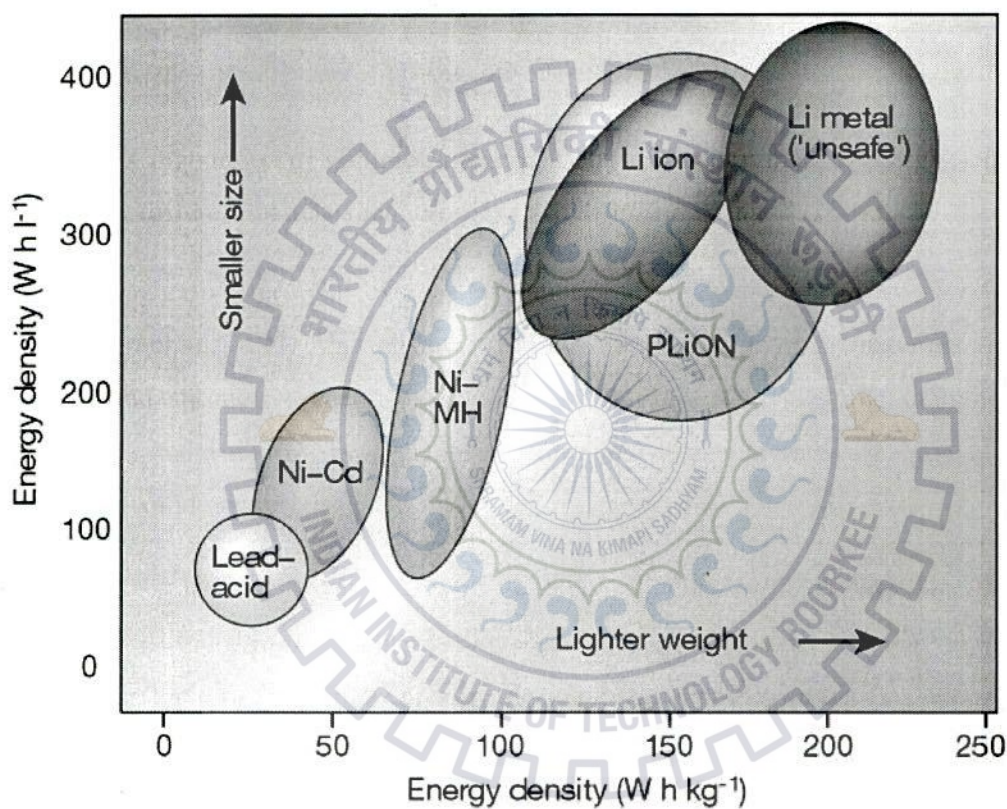
Fig. 1.2: Comparison of volumetric energy density and gravimetric energy density for different battery technologies (Tarascon and Armand, 2001).

The anode is the negative terminal of a battery and generally are made up of carbon based material (like graphite, CNT, graphene), alloying and de-alloying materials (silicon, germanium, tin and antimony), metal oxides/phosphides/sulfides/nitrides and titanium based materials ($LiTi_4O_5$ and $Li_4Ti_5O_{12}$). Carbon and titanium based materials are innovative and highly dominating anode materials.
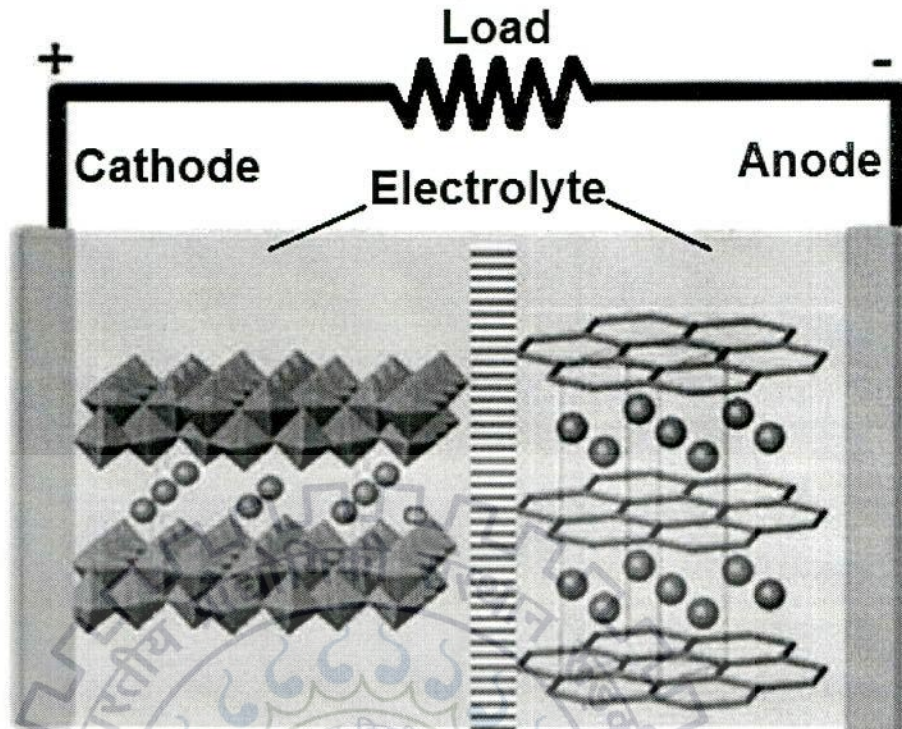
Fig. 1.3: Schematic diagram of Li ion battery.

A cathode is the positive terminal of a battery which holds the Li-ions at the discharged state. Since a Li-ion battery is always assembled in its discharged state, the storage capacity of a battery depends strongly on the capacity of the cathode material. The research on the cathode materials for Li-ion batteries has been focused on layered hexagonal-$LiCoO_2$, spinel-$LiMn_2O_4$, olivine-$LiFePO_4$, and their derivatives. $LiCoO_2$ is the cathode material that was used in the first commercial Li-ion battery introduced in market by Sony Inc. in year 1991. $LiCoO_2$ has been widely used in the small scale portable devices due to its high capacity. However, the use of $LiCoO_2$ has been limited in the bulk storage batteries due to Co. Due to limitation in availability and toxicity of Co, $LiCoO_2$ poses high cost and health hazard. The spinel $LiMn_2O_4$ is also a promising cathode material with moderate capacity, good thermal stability, low cost and non-toxicity. The $LiMn_2O_4$ was first proposed for use as cathode for Li-ion battery in the year 1984 [Thackeray et al, 1983]. The compound $LiMn_2O_4$ is less expensive as compared to $LiCoO_2$. Moreover Mn is non-toxic. But the two limitations are manganese dissolution and growth of inactive phase during the cycling, which make $LiMn_2O_4$ less suitable for the Li-ion battery.

LiFePO$_4$ was first proposed as a cathode material by Goodenough and coworker in the year 1997. The olivine structured LiFePO$_4$ is a potential cathode material for the Li-ion battery due to its excellent electrochemical properties viz. appreciable theoretical capacity (170 mAh/g) and flat discharge voltage (3.4 V). The properties such as excellent thermal stability, excellent structural stability, low cost, non-toxicity, and environment friendliness make the material more attractive cathode material for high energy density Li-ion battery. Several prototypes of electric and hybrid electric vehicles with batteries based on LiFePO$_4$ cathode have been demonstrated by a number of automobile companies.

The crystal structure of LiFePO$_4$ is distorted orthorhombic having space group of Pnma. The frame work of the oxygen atoms forms a distorted hexagonal close packed structure where Li and Fe atoms are located at the octahedral sites and P atoms are located at the 1/8 of the tetrahedral sites. During lithiation / delithiation material LiFePO$_4$ has slight (6.81%) volume change without undergoing any change in crystal structure. This small volume change during lithiation / delithiation accounts for the excellent structural stability and hence cyclic stability. The only limitation of the material is having low intrinsic electronic conductivity and low Li-ion diffusion. The low Li-ion diffusion was attributed to the structure of LiFePO$_4$ compound as the lithiation and delithiation are restricted only along the [010] direction. The material can only reach close to its theoretical capacity of (165 mAh/g) at very low current rate (0.1C). But due to low intrinsic electronic conductivity as well as low Li-ion diffusivity, a drastic fall in the theoretical capacity occurs even at moderate current rate, which restricts the use of this material as cathode for the high power application.

The limitation of low electronic conductivity can be solved by the different techniques like conductive surface coating, particle size reduction and super-valent ion doping. Doping is a direct approach to improve the electronic conductivity. The Li-site doping can improve the conductivity however this may reduce the Li-ion diffusivity, because the dopant at Li-sites blocks the one-dimensional path of Li-ion. While Fe site doping is an effective way to improve the intrinsic conductivity, but the tri-valent, tetra-valent and penta-valent doping at Fe site is not energetically favorable as these dopings show insufficient solubility. The low favorable energy was investigated only for divalent substitution on Fe sites however, these dopings do not introduce extra charge carrier and thus do not improve the intrinsic conductivity of LiFePO$_4$ [Islam et al, 2005]. Therefore we expect that doping is not an effective approach to improve the intrinsic conductivity of LiFePO$_4$.

The particles size reduction along with conductive surface coating is an efficient way to improve the power density of the material. The conducting materials such metals, carbon and conducting polymers can be used for coating to improve the conductivity of $LiFePO_4$. Carbon is a popular and most widely used coating material to improve the conductivity of $LiFePO_4$ compound. Besides improving the conductivity carbon coating restricts the growth of $LiFePO_4$ particles, and also acts as reducing agent to suppress the formation of Fe^{3+} impurity. However the presence of inactive carbon has the limitation to reduce the volumetric energy density of the cathode due to which, it affects adversely on the overall capacity of the battery. So, to gain high power density and high volumetric energy density a thin, uniform and continuous carbon coating on the surface of $LiFePO_4$ particles is desirable. The carbon coating thickness is related to the carbon content. High carbon content results in the higher coating thickness and improved conductivity of the material, but the higher thickness restricts the Li-ion penetration inside $LiFePO_4$ particle during charging / discharging process. The low carbon means thin carbon coating and less negative impact on the volumetric density, but the carbon below a certain quantity content results in partially coated $LiFePO_4$ particles. So, it is important to optimize the content of carbon to improve the utilization of the active material. However it is very difficult to optimize the carbon content without discussing the factors such as carbon structure, carbon distribution, and the effective surface area of the active material. In the total carbon content higher fraction of graphitic carbon gives better conductivity to the $LiFePO_4/C$. On the other hand small sized particles of active materials provide large surface area as compared to bulk particles. Hence smaller particles require higher carbon content to provide full coverage to active particles as compared to large particles.

To improve the rate capability of $LiFePO_4$ those electrochemically active conducting polymers should be use for coating which contain the charging / discharging range of $LiFePO_4$. Such polymer coated $LiFePO_4$ composites can deliver better rate capability without having an adverse effect on the volumetric energy. Polymers such as polyaniline, polypyrrole and polythiophene are electrochemically active in the range of 4 to 1 V and possess good electronic conductivity. So, these polymers are the superior coating materials for $LiFePO_4$.

In this PhD thesis the carbon coating on $LiFePO_4$ nano-particles has been optimized and the different electrochemically active conducting polymer coating on $LiFePO_4/C$ to deliver high capacity for rapid charging and discharging of the battery has been explored. The conducting

polymers such as polyaniline, polypyrrole and polythiophene are electrochemically active for Li-ion and are conductive in nature. Although the theoretical capacity of pure polyaniline, polypyrrole and polythiophene lies between 50 and 100 mAh/g but due to the gradually decreasing discharge potential it is difficult to use pure polymer as electrode for the Li-ion battery. Despite of intensive research efforts on polymer coated $LiFePO_4/C$ compounds, only few achievements have been attained so far. From the literature survey a few research gaps have been found. The investigation on different phases that develop on polymer coating of $LiFePO_4/C$ has not been performed so far, by the researchers, to the best of my knowledge. During in-situ polymerization oxidizing agent may react with $LiFePO_4$ and form electrochemically inactive phase(s) as product. So it is necessary to perform phase analysis to check the purity of electrochemically active phases after polymerization on $LiFePO_4$ particles. In addition to this Raman analysis to determine the structure of carbon and polymer coating has not performed for the polymer coated $LiFePO_4/C$ material. Further the effect of polymer chains formation on electrical conductivity and Li-ion storage capacity of $LiFePO_4$ has not been studied yet. Therefore an attempt has been made to study the effect of conducting polymers on the electrochemical properties of $LiFePO_4$.
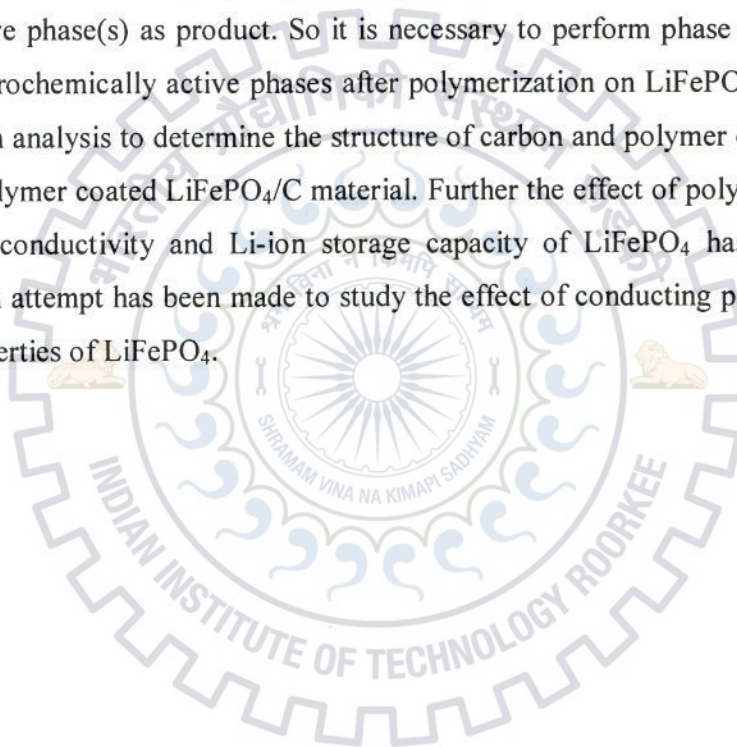
LITERATURE REVIEW

LITERATURE REVIEW

A lithium ion secondary battery is a device that delivers electrical energy stored in the form of chemical energy and vice-versa. The cathode, anode and electrolyte are three basic components of a Li-ion secondary rechargeable battery. During charging / discharging cycle of a Li-ion battery the electrodes cathode and anode are the component where Li-ion get absorbed or released. The electrolyte provides the path to Li-ion during the oxidation / reduction process and the charge neutrality was maintained by the flow of electron through the external circuit. So, that in an ideal battery system, the Li-ion transport number for the electrolyte is unity, where the Li-ion transport number is defined as the fraction of current carried by the Li-ion through the electrolyte [Klett et al, 2012]. The cathode and anode electrodes are separated by a microporus membrane which allows the Li-ion passage through electrolyte but prevent the short circuiting of the electrodes in the cell. The cell potential of the Li-ion battery is determined by the difference between chemical potentials of Li-ion at cathode and anode.

$$V = (\mu(c)_{Li-ion} - \mu(a)_{Li-ion})/e$$

2.1 Various components of Li-ion battery

Cathode, anode and electrolytic are the three basic components of a battery. During charging Li-ions migrate from cathode to anode through the electrolyte. So, during the charging process oxidation occurs at the cathode and reduction occurs at the anode of the battery assembly.

2.1.1 Electrolyte

An electrolyte is the component of a battery which allows the Li-ions migrate and acts as a barrier for the movement of electrons. The basic and desired properties of an electrolyte are listed below:

1. An electrolyte should have high ionic conductivity over a wide temperature range; this results high Li-ions diffusion and prevents polarization during operation of a battery.

2. Good thermal stability; ensures the battery operation under appropriate temperature.

3. Wide operating voltages; which prevents the degradation of electrolyte due to side reactions between electrodes and electrolyte.

4. Good mechanical property; which eases the manufacturing and enhanced safety.

5. Low cost.

6. Safety; high flashing point.

7. Non-toxic; environment friendly.

2.1.2 Anode

Anode is the negative electrode of Li-ion battery and holds the Li-ions during charging. So, the structural and electrochemical properties of anode materials are critical to the performance of the whole battery. Depending on the Li-ion battery performance and reaction mechanism the innovative anode materials have been classified into three main groups 1) intercalation / deintercalation materials, 2) alloying / de-alloying materials, and 3) conversion materials [Wang and Sun, 2012].

2.1.2.1 Intercalation / deintercalation materials

The intercalation / deintercalation materials are carbon based materials (such as porous carbon, carbon nanotubes, graphene), metal oxides (such as MoO_2, TiO_2), $Li_4Ti_5O_{12}$, etc; in which Li-ions intercalate / deintercalate during the redox reaction of the cell.

Carbon based materials with different morphologies and structure have been used as appropriate anode materials for Li-ion battery. These carbon based materials are very popular as anode in the Li-ion battery community due to advantageous features such as low cost high reversibility, ease of availability, good thermal and chemical stability [Marom et al, 2011, Scrosati et al, 2010, Goriparti et al, 2014]. The carbon based materials can be classified into two broad categories i) Soft carbon (graphitizable carbons) where crystallites are stacked almost in the same direction and ii) Hard carbon (non-graphitizable carbons) where crystallites have disordered orientation. The Soft carbon represents the present state of art for anode materials of Li-ion battery. Although Soft carbon shows very high reversible Li-storage capacity, their use has been hindered by the limitations such as high voltage hysteresis during discharging process and low storage capacity [Li, H. et al, 2009].

Hard carbon shows higher capacity lying in the range of $200 - 600$ mAh/g for a voltage range of $1.5 - 0$ V vs Li^+/Li. The voltage profile is mainly composed of two regimes, a sloping region in a voltage range of $1.0 - 0.1$ V with a capacity around $150 - 250$ mAh/g and a plateau region with a capacity around $100 - 400$ mAh/g. In hard carbon Li-ion diffusion is low due to which these materials show poor rate capability. Moreover hard carbon materials show low initial

columbic efficiency and low tap density. These limitations can be overcome by the use of metal coating or coating with thin layer of soft material [Wang, J., Liu, J.L. et al, 2012].

The carbon nanotubes (CNTs) were discovered in 1991. Depending upon thickness and number of coaxial layers the CNTs can be classified as single and multiwalled. CNTs were extensively investigated both as the composite materials and anode materials. From these two structures, maximum theoretical capacity was calculated to be 1115 mAh/g in LiC_2 symmetry for the SWCNT and is the highest capacity of the carbon based materials [Meunier et al, 2002]. However it is challenging to achieve the high columbic efficiency with the CNTs because of the presence of large structure defects and hysteresis in the voltage profile, during charge / discharge process. Eventhough CNTs have a number of advantages over the other carbon based materials. From the battery point of view CNT technology is not yet considered mature enough due to some open issues like mass production and cost.

Graphene is the honeycomb structure of sp^2-hybridized carbon atoms bonded in the two dimensional sheet of single atom thickness. Since their discovery in 1987, graphene has drawn much attention due to their attractive properties like, good electrical conductivity, high value of Li-ion mobility, good mechanical strength and high surface area [Meunier et al, 2002]. These properties make the graphene attractive to use as anode material in Li-ion battery. The theoretical lithium storage capacity of graphene is low as compared to graphite (372 mAh/g) [Brownson et al, 2002]. While the particles of a few number of graphene sheets together shows higher storage capacity than graphite. The highest storage capacity of 1116 mAh/g for graphene can be assumed when Li-ion trapped at the benzene ring in a covalent bond having LiC_2 stoichiometry. The additional storage capacity of the graphene is due to the presence of disorder (edge) / defects generating the additional active sites for the lithium storage [Pan et al, 2009].

Titanium based oxides have been gaining the attention as anode materials in the Li-ion battery community. The material is less expensive, has higher operating voltage ~ 1.55 V (vs Li^+/Li), safe and excellent cyclability as compared to carbon based materials due to small volume change (about 2 – 3 %) during charging / discharging process [Ma et al, 2012, Shen et al, 2010]. But the major issues with these materials are low theoretical capacity and low electronic conductivity (10^{-12} S/cm). Hence it is difficult to gain good rate capability for this electrode material. Different strategies have been adopted to improve the charge transport properties of

$Li_4Ti_5O_{12}$ including particle size reduction [Kavan et al 2003], doping with higher valence metal ions [Wolfenstine and Allen, 2008], and carbon coating [Park et al, 2008]. Template synthesis method was reported to have a very high rate capability for $Li_4Ti_5O_{12}$. The template of NH_4HCO_3 makes compaction of anode material, as required for establishing good electronic contacts with electrode, while its removal creates three dimensional interconnected network by creating small (~ 2 %) porosity. This method results in a high density material with excellent capacities retention at high current rates [Singh et al, 2013]. The operating voltage of $Li_4Ti_5O_{12}$ spinel is 1.55 V (vs Li^+/Li) which is slightly higher than the reduction voltage of electrolyte, due to which it would not form the SEI layer at the interface [Gu and Chen, 2012]. Molybdenum oxide based anode materials are also much attractive system due to its high electrochemical activity and high electrical conductivity. The two-dimensional nanobelt morphology of MoO_2 was found beneficial for Li-ion and electrolyte transportation which helps to achieve good cyclability and rate capabilities. The MoO_2 nanobelts synthesized by hydrothermal process shows excellent cyclability over 200 cycles at a current rate of 100 mA/g [Sen et al, 2014].

2.1.2.2 Alloy / de-alloy materials

This class of anode materials has property of alloying / de-alloying with the lithium metal during charging / discharging. Metals such as Si, Ge, Sn, Sb and Tin oxide are well known examples of this group. Alloying / de-alloying anode can fulfill the high power demand of electric vehicle and hybrid electric vehicle (HEV). This group belongs to the high capacity anode materials. The silicon and tin oxide deliver very high theoretical capacity upto 4211 mAh/g and 783 mAh/g respectively [Park et al, 2010]. Poor cycling performance due to large volume expansion in these materials during insertion / de-insertion of Li-ion is the major drawback of these materials.

2.1.2.3 Conversion materials

The oxides, phosphides, nitrides and sulphides of the transition metals (M_xN_y; M = Fe, Ni, Co, Cu and Mn and N = O, P, S and N) belong to this group of anode material. The reaction mechanism in this group of materials implies the reduction or oxidation of transition metal leading to the formation and decomposition of lithium compound [Li and Wang, 2013]. The general electrochemical reaction of conversion materials can be represented as.

$$M_xN_y + zLi\text{-}ion + ze^- \rightarrow Li_zN_y + xM$$
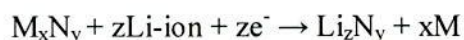
This group of anode materials delivers a good specific capacity in the range 500 to 1000 mAh/g with high reversible capacity [Poizot et al, 2012].

2.1.3 Cathode

A cathode is a positive electrode of an electrochemical system in which reduction takes place during the electrochemical discharging process of the battery. Cathode materials are typically oxides of the transition metals which undergo changes to higher oxidation states during delithiation. During oxidation of the transition metals large compositional variation leading to the phase changes takes place. So the structure that is stable over a wide range of composition must be preferred for the cathode material. The choice of a cathode material greatly affects the cost and performance of a Li-ion battery. The modern cathode materials were prepared in their lithiated (discharged) state so that they can be paired with delithiated anode with a minimum possibility of accidental short-circuiting during assembling. So a high capacity cathode material is required to store high number of Li-ion per unit mass or volume. The ideal cathode material should possess the following properties.

- The material can react with lithium reversibly and remains a stable structure during the process of intercalation / de-intercalation. This requirement is essential for extending the cyclability of lithium ion batteries.

- The reaction free energy change of the cathode material between charge and discharge states must be high enough to achieve high storage capacity.

- The material must have high electronic conductivity and fast lithium ion diffusion to facilitate fast charge transfer and deliver a high rate capacity.

- The material does not chemically react with the electrolyte during cycling. This is a basic safety requirement.

- The material should be of low-cost and environmental friendly.

2.2 History of cathode materials

2.2.1 Layered structure

The layered structure $LiMO_2$ (M = Co, Ni) can be demonstrated as consisting of alternate MO_2 slabs and lithium layers. Mizushima et al first demonstrated $LiCoO_2$ as cathode material for rechargeable lithium battery and is the most dominant material of this class [Mizushima et al, 1980]. Sony Corporation successfully introduced $LiCoO_2$ in 1991 to market and since then it

has been used in the small electronic devices [Nishi et al, 1990]. The structure of $LiCoO_2$ is hexagonal rhombohedral having space group $\bar{R}3m$ and lattice parameters a = b = 52.816 Å and c = 514.051 Å [Wang et al, 1999]. The material $LiCoO_2$ has good electrochemical stability which results in the long cyclability. But the limited availability of Co makes the $LiCoO_2$ material expensive, moreover Co is toxic which creates environmental problem. Therefore the research has focused from $LiCoO_2$ to its derivatives which replace the Co ion partially or fully to non toxic and high abundant metal ions in the structure. The delithiation of the material occurs through a series of phase transformations which involve monoclinic and then to hexagonal crystal symmetry [Bai et al, 2013]. The cell was fabricated in its discharged state and it was charged prior to use. The structure of $LiCoO_2$ remains stable if the 50% of Li-ions per formula unit take part in the charge / discharge process. The 50% ratio of Li-ions per formula unit gives a moderate cell capacity of 140 mAh/g, which is nearly half of the theoretical capacity (272 mAh/g) of $LiCoO_2$. The excess lithiation of $LiCoO_2$ results the structural change from hexagonal to monoclinic resulting to shrinkage along c-axis. The structural changes result cationic disorder in the crystal structure which results some Li-ions to enter on Co sites leading to the failure of electrochemical performance [Cho et al, 2001]. In order to improve the structural stability the material can be protected by surface coatings.

Cho et al reported the improvement in the material capacity by $AlPO_4$ coating on $LiCoO_2$ particles [Cho et al, 2003]. $AlPO_4$ coating of thickness of ~3 nm on the $LiCoO_2$ particles was deposited using the aqueous solution of Al and PO_4. $AlPO_4$ coated $LiCoO_2$ composite material shows good electrode capacity of 140 mAh/g at 1C rate with 99 % retention of capacity after 20 Cycles.

Cao et al have synthesized the carbon coated $LiCoO_2$ by ball milling followed by the calcinations at 600 °C [Cao et al, 2007]. Electrochemical observations of the carbon coated $LiCoO_2$ shows good improvement in the materials capacity as compared to that of bare material. The improvement in capacity was due to low charge transfer resistance and higher Li-ion diffusion delivered by the carbon coated $LiCoO_2$. ZnO coating can be deposited on the $LiCoO_2$ particles by solution mixing and calcinations. The ZnO coating protects the $LiCoO_2$ to cover from the resistive coating such as LiF, Li_2CO_3 and polycarbonate and other organic films generated when $LiPF_6$ based electrolytes were used. Although the ZnO lowers Li-ion diffusivity than in $LiCoO_2$ but the ZnO coating improves the electrochemical performance in two aspects. The coating 1) protects deposition of highly resistive LiF coating on $LiCoO_2$ and

2) prevents the dissolution of Co from the $LiCoO_2$ structure [Fang and Duh, 2006]. The Al_2O_3 coating of thickness $2 - 5$ nm on nano-$LiCoO_2$ was synthesized by atomic layer deposition and a good (250 %) improvement in the rate capability was achieved as compared to bare material. The composite material shows a discharge capacity of 133 mAh/g at 0.7C rate showing the good improvement in rate capability. Al_2O_3 coating acts as a barrier to deposit the thin undesirable products and improves the Li-ion transport. The interface of $LiCoO_2$ and electrolytic restricts the Co dissolution during charging and discharging of material resulting in improvement in the rate capability [Jung et al, 2010].

Although the metal oxides and carbon coatings have improved surface kinetics, suppress the deposition of inert coating on the particle surface (e.g. highly resistive LiF coating which develops on the $LiCoO_2$ active material during charging / discharging mechanism) and prevent the Co dissolution thereby improving the electrochemical performance of the $LiCoO_2$ electrode. But the presence of Co makes the material expensive and toxic. So, the research on $LiCoO_2$ cathode material has focused to substitute with the other transition metals either partially or fully, with environment friendly and more abundant like Ni and Mn. In this respect the materials $LiNi_{0.5}Mn_{0.5}O_2$ and $LiCo_{1/3}Ni_{1/3}Mn_{1/3}O_2$ were proposed to have good Li-ion storage capacity. Ohzuku et al initially reported the electrochemical performance of $LiNi_{0.5}Mn_{0.5}O_2$ [Ohzuku et al, 2001]. The capacity and rate capability of the material were further improved by selecting the suitable synthesis route. The $LiNi_{0.5}Mn_{0.5}O_2$ was synthesized by addition of $Li(OH)$ or Li_2CO_3 lithium salt to aqueous solution of $Ni(NO_3)_2$ and $Mn(NO_3)_2$. The precursor obtained from the Li_2CO_3 has more uniform distribution of Ni and Mn as compared to $Li(OH)$, resulting the final $LiNi_{0.5}Mn_{0.5}O_2$ material with a large Li layer spacing and small Li / Ni exchange. The perfect layered structure and uniform distribution of Ni and Mn in $LiNi_{0.5}Mn_{0.5}O_2$ synthesized using carbonate salt delivers higher specific capacity of 182 mAh/g [Lian et al, 2008]. The surface coating such as AlF_3 and $FePO_4$ on $LiNi_{0.5}Mn_{0.5}O_2$ particles have improved the conductivity and cycling performance [Lin et al, 2010, Liu et al, 2012]. The improvement in the cyclability of air quenched $LiNi_{0.5}Mn_{0.5}O_2$ was due to the formation of a stable electrode / electrolytic interface and low charge transfer resistance [Lin et al, 2010]. The lanthanum doped $LiCoO_2$ composite materials were synthesized by combustion synthesis method. The superior rate performance of $La_2Li_{0.5}Co_{0.5}O_2$ as compared to $LiCoO_2$ material was due to improved Li-ion movement. The fast Li-ion movement was due to lattice expansion of $La_2Li_{0.5}Co_{0.5}O_2$ as a result of lanthanum doping. The lanthanum doped $LiCoO_2$ cell also

contributes to the reduction of Co dissolution in electrolyte which results in the excellent cyclability of this cathode material [Ghosh et al, 2009].

The material system $LiCo_{1/3}Ni_{1/3}Mn_{1/3}O_2$ exhibits high discharge capacity, high thermal stability and good cyclability. The microemulsion synthesis of $LiCo_{1/3}Ni_{1/3}Mn_{1/3}O_2$ composite shows excellent electrochemical reversibility as cathode material. In this technique well crystallized nanoparticle (size ~ 45 nm) of $LiCo_{1/3}Ni_{1/3}Mn_{1/3}O_2$ was synthesized at low temperature. The $LiCo_{1/3}Ni_{1/3}Mn_{1/3}O_2$ cathode electrode exhibits a discharge capacity of 198 mAh/g when charging and discharging is done between 2.5 V and 4.6 V. The good electrochemical irreversibility of 4.4 % for $LiCo_{1/3}Ni_{1/3}Mn_{1/3}O_2$ cathode material makes the microemulsion route attractive as compared to other solid state synthesis routes [Lu et al, 2009].

The cyclability of the material was improved by surface coatings. Bai et al have performed the YPO_4 coating on the $LiCo_{1/3}Ni_{1/3}Mn_{1/3}O_2$ particles [Baia et al, 2013]. The 1.0 wt% of YPO_4 coated $LiCo_{1/3}Ni_{1/3}Mn_{1/3}O_2$ shows good cyclability and delivers a discharge capacity of 142.9 mAh/g after 50 cycles when discharged from 4.4 V. YPO_4 hinders the decomposition of electrolyte on electrolyte / electrode interphase during the repeating cycle and reduces the SEI formation in the cell. The suppression in the growth of SEI layer improves the Li-ion diffusion and cyclability of the material. Ni and Zr doped $LiCoO_2$ based system is another cathode material for rechargeable Li-ion battery. Sivaprakash et al synthesized $LiNi_{0.8}Co_{0.15}Zr_{0.05}O_2$ cathode composite by wet chemical synthesis route and observed the reduced discharge capacity as compared to $LiNi_{0.8}Co_{0.20}O_2$ [Sivaprakash et al, 2009]. The electrode $LiNi_{0.8}Co_{0.15}Zr_{0.05}O_2$ shows good cyclic stability of 98 % as compared to 63 % after 20 cycles for $LiNi_{0.8}Co_{0.20}O_2$ composite. The presence of Zr^{+4} prevents the local collapse of layered structure, resulting in enhanced structural stability.

In summary the $LiMO_2$ layered material have the ability to deliver good discharge capacity when charged to a higher voltage. The material is suffered from structural instability and lower efficiency at higher charging voltage.

2.2.2 Spinel $LiMn_2O_4$

The spinel $LiMn_2O_4$ is another promising cathode material for Li-ion battery and was first purposed by the Thackeray et al in 1983 [Thackeray et al, 1983]. The crystal structure consists of oxygen anions occupying the cubic close pack arrangement of FCC structure. The Li-ions

occupy the tetrahedral sites and Mn^{2+} ions occupy the octahedral sites. The material is not expensive and also environmental friendly. The discharging of $LiMn_2O_4$ occurs at two different voltages of 4 V and 3 V. The lithiation and delithiation processes occur through the three dimensional network of spinel structure rather than plane. The conductivity of the $LiMnO_2$ is lower as compared to $LiMO_2$ layered structure materials and capacity fading is another disadvantage of the spinel material. The capacity fading occurs due to the following factors: 1) The dissolution of Mn in the electrolyte solution results in the oxidation of electrolyte. The dissolution process is more prone at higher potentials > 4.4 V vs Li^+/Li. The dissolution degrades the quality of electrolyte and increase the charge transfer resistance. 2) The generation of a new electrochemically inactive phase masks on the surface of $LiMn_2O_4$ particles. Although the new phase does not reduce the kinetics of electrode (like electrical conductivity and Li-ion diffusion) but it is an electrochemically inactive, and therefore reduces the overall capacity of the electrode [Aurbach et al, 1999, Raja et al, 2009].

It is well known that in the structure of $LiMn_2O_4$, Mn-ions exists in two oxidation states, consisting of 50 % Mn^{4+} and 50 % Mn^{3+}. If the amount of Mn^{3+} exceeds the 50 %, the spinel $LiMn_2O_4$ exhibits Jahn-Teller lattice distortion. During the charging / discharging cycles of $LiMn_2O_4$ there exists a phase change from cubic to tetragonal due to the Jahn–Teller distortion. This phase change causes an anisotropic volume change which results in the severe damage to spinel $LiMn_2O_4$. The distortion due to mismatch between the tetragonal and cubic lattice affects the three dimensional Li-ion pathway, leading to the capacity fade of $LiMn_2O_4$ cathode material. For that reason, Jahn–Teller distortion is one of the most important causes of capacity fade for $LiMn_2O_4$ spinel [Li, X. et al, 2009]. Jahn–Teller distortion should be suppressed to have the excellent cycling performance of $LiMn_2O_4$ active materials. To reduce Jahn–Teller distortion, many research groups have tried to dope the Mn sites with other cation (such as Ni, Co, Cr, Mg, Fe, Al, etc.) and improve the cycle stability of $LiMn_2O_4$ spinel [Wolska et al, 2006, Takahashi et al, 2006, Li et al, 2009, Singh et al, 2009]. This approach can partially reduce Jahn–Teller distortion because it reduces the Mn content of spinel $LiMn_2O_4$. Apart from the Mn site doping, the excess of Li on Li sites is also reported as an effective approach to improve the rate capability of the material. $Li_xMn_2O_4$ (x = 1 to 1.4) was synthesized by solution growth technique as various synthesis condition. The thin film of $Li_xMn_2O_4$ was deposited on various substrates using spin coating method. On the basis of the electrochemical measurements the $Li_{1.4}Mn_2O_4$ film annealed at 700 °C for 2 hours deposited on Pt substrate was found to be the process - optimized [Das et al, 2006].

The cyclic performance of the spinal structure $LiMn_2O_4$ has been improved by doping it with the transition metals like Co or Ni. Zhao et al synthesized $LiCo_xMn_{2-x}O_4$ (for $0 < x < 0.16$) cathode material by sol-gel route to gain high purity, small particle size and narrow particle size distribution. The particle size in the range of $100 - 200$ nm was obtained using this technique. Higher structural stability of the $LiCo_xMn_{2-x}O_4$ spinel improves the cyclic performance of the cathode. The spinel structure for $x = 0.1$ shows good cyclic stability upto 20 cycles with specific capacity of 123 mAh/g for 0.1 mA/cm^2 [Zhao et al, 2009]. High voltage cathode material $LiCoMnO_4$ can be synthesized by 50 % substitution of Co at Mn site. A cell with $LiCoMnO_4$ as cathode material exhibits a discharge capacity of 95 mAh/g at a voltage plateau centered on 5.0 V. Since it is a high voltage cathode material so, $LiCoMnO_4$ has superior energy density [Kawai et al, 1999]. Partial substitution of Ni for Mn in $LiMn_2O_4$ structure also improves the performance of cathode. Shaju et al have synthesized spinel $LiMn_{1.5}Ni_{0.5}O_4$ for the cathode [Shaju et al, 2008]. $LiMn_{1.5}Ni_{0.5}O_4$ was synthesized using resorcinol-formaldehyde assisted solution method. The precursor formed was finally calcined at 700 and 750 °C to get nano-$LiMn_{1.5}Ni_{0.5}O_4$ (disordered) and $LiMn_{1.5}Ni_{0.5}O_4$ (ordered) structures respectively. The nano-$LiMn_{1.5}Ni_{0.5}O_4$ (disordered) structure has good rate capability and at 20C rate the material delivers 88 % of the capacity delivered at slow rate of 0.2C. The good rate capability of nano-$LiMn_{1.5}Ni_{0.5}O_4$ (disordered) is due to the low electrode impedance as compared to the electrode made of $LiMn_{1.5}Ni_{0.5}O_4$ (ordered) synthesized by conventional solid state method. Most of the nano-sized materials deliver higher rate capability compared with bulk materials as they possess low electrode impedance, higher contact area with current collector. Due to these factors nano-$LiMn_2O_4$ has been synthesized by many researchers and their electrochemical properties have been investigated [Shaju et al, 2008, Jiao et al, 2008].

The limitation associated with nano-sized material is that they cannot be packed as densely as micrometer sized material on the current collector. The nano-sized material pasted on the current collector has low tape density and the resulting material pasted on the current collector will be less as compared to micrometer sized material. Moreover the nano-sized material shows poor cycling performance because of difficult process ability to mix carbon black with the active material [Guo et al, 2008]. Raja et al has synthesized multi-faceted highly crystalline $LiMn_{1.5}Ni_{0.5}O_4$ cathode material by novel carbon exo-templating method [Raja et al, 2009]. The multi-faceted $LiMn_{1.5}Ni_{0.5}O_4$ cathode delivers a discharge capacity of 107 mAh/g at a high current density of 0.8 mA/cm^2 as compared to the discharge capacity of 59 mAh/g at the same current density for multi-faceted $LiMn_{1.5}Ni_{0.5}O_4$. The micrometer sized particles are cluster or

aggression of nanoparticles. The disadvantage of micrometer sized particles is that they give high electrode impedance. So, to reduce the electrode impedance conductive surface coatings of carbon or other conductive material is required.

2.2.3 Olivine LiMPO$_4$ (M = Fe, Ni, Co)

The olivine structure LiMPO$_4$ can be formed with transition metal ions such as Mn, Co, Ni and Fe. The redox potentials of LiMnPO$_4$, LiCoPO$_4$ and LiNiPO$_4$ are 4.1, 4.8 and 5.1V respectively which are higher than LiFePO$_4$ (3.4 V) [Xu et al, 2012].

2.2.3.1 LiMnPO$_4$

LiMnPO$_4$ shows the higher operating voltage of 4.1V (vs Li$^+$/Li) and a theoretical capacity of 170 mAh/g, so it can be used as high capacity cathode. But the material LiMnPO$_4$ suffers from Jahn–Teller lattice distortion due to presence of Mn^{3+} ions. The intrinsic electronic conductivity of the material is ~10^{-14} S/cm which is very low as compared to LiFePO$_4$ (~10^{-14} S/cm) [Delacourt et al, 2005]. This results in the material to possess very low capacity and rate capability [Delacourt et al, 2004]. The dissolution of Mn^{3+} is common for the LiMnPO$_4$ structure and such effect is enhanced with increase in temperature [Oh et al, 2010]. The volume change of 9.1 % was observed for the transformation of LiMnPO$_4$ to MnPO$_4$, due to Jahn–Teller effect which results a high strain on the boundary of two phases. The high strain on the boundary phase of LiMnPO$_4$ material results the poor electrochemical performance [Meethong et al, 2008]. The particle size reduction and making conductive surface coatings have improved the rate capability of the LiMnPO$_4$ material [Drezen et al, 2007]. Drezen et al have prepared LiMnPO$_4$ by sol-gel method and studied the effect of particle size on the capacity of material and found the discharge capacity of 150 mAh/g at C/20 rate for the particles of size 140 nm [Drezen et al, 2007]. Wang et al prepared the rod-like particles of carbon coated LiMnPO$_4$ by heating the precursor solution of binary solvent in autoclave at 240 °C [Wang et al, 2010]. They obtained the discharge capacity of 126 mAh/g at 0.01C rate for LiMnPO$_4$/C. Further the rate capability of the material was improved by isovalent ion doping. Ramar and Balaya have reported the effect of Fe and / or Mg doping on the rate capability [Ramar and Balaya, 2013]. High energy ball-mill was used to homogenize the material which was followed by the calcination at 650 °C under inert atmosphere. Composite LiMn$_{0.9}$Fe$_{0.05}$Mg$_{0.05}$PO$_4$/C has electrochemical performance by delivering specific capacity of 159 and 118 mAh/g at 0.1C and 1C scan rates respectively. The improved cyclic stability and rate capability were due to suppression in Mn dissolution and low electrode impedance of LiMn$_{0.9}$Fe$_{0.05}$Mg$_{0.05}$PO$_4$/C.

Although the performance of electrode has been improved, it is still challenging to develop the cathode electrode using $LiMnPO_4$ material.

2.2.3.2 $LiCoPO_4$

$LiCoPO_4$ is also a high energy density material having a redox potential profile at 4.8 V for $Co^{2+/3+}$. The high redox potential makes the material more attractive for the cathode electrode to deliver high energy density. Amine et al reported if extraction of Li-ion is limited to 0.42 per formula unit, the material delivers a discharge capacity of 70 mAh/g at 0.1C rate [Amine et al, 2000]. Crystallinity of the $LiCoPO_4$ electrode was not affected by the charge / discharge cycling as confirmed by X-ray diffraction analysis of the charged and discharged electrode. So, the initial irreversibility of the material was due to the low conductivity and electrolyte decomposition due to high redox potential of the material and was not due to the structural damage. Bramnik et al proposed that delithiation from the structure $LiCoPO_4$ occurs through three phases [Bramnik et al, 2007]. It was observed that, first phase $LiCoPO_4$ transforms to $Li_{0.7}CoPO_4$ after delithiation and the corresponding charge potential was observed at 4.9 V vs Li^+/Li. The phase $Li_{0.7}CoPO_4$ further transforms to $CoPO_4$ at a charge potential of 4.8 V vs Li^+/Li. The fully delithiated phase $CoPO_4$ is highly unstable in air and instantly change to amorphous state. The two phase delithiation mechanism is the characteristic of $LiCoPO_4$ and is independent on the synthesis method. The cell volume change for the transformation from $LiCoPO_4$ to $CoPO_4$ was observed to be ~7 % which is very close to the cell volume change for $LiFePO_4$.

2.2.3.3 $LiNiPO_4$

The material $LiNiPO_4$ has discharge potential of 5.1 V and is also a high energy density cathode material. The limitations of $LiNiPO_4$ material are, 1) high redox voltages of electrode decompose the most of common polymer electrolyte solutions, 2) extremely low electronic conductivity and 3) slow Li-ion diffusion [Wolfenstine and Allen, 2005]. So, for $LiNiPO_4$ electrode more stable electrolyte should to be used. $LiPF_6$ with sulfolane is highly resistant to oxidation upto 5.8 V [Amine et al, 2000]. Although it is difficult to get pure $LiNiPO_4$ phase [Okada et al, 2011]. Minakshi et al demonstrated the Sn / $LiNiPO_4$ anode / cathode system which shows Li-ion intercalation / deintercalation through aqueous LiOH electrolyte [Minakshi et al, 2011]. Single phase $LiNiPO_4$ was synthesized by annealing the precursor in air atmosphere and the electrochemical testing shows 45 % efficiency of the cell.

2.2.3.4 LiFePO$_4$

The olivine structured LiFePO$_4$ has gained the intense attention as a potential cathode material. The material LiFePO$_4$ is very near to an ideal cathode material having high theoretical discharge capacity of 170 mAh/g, moderate discharge potential 3.4 V (vs Li$^+$/Li), excellent thermal stability at charged and discharge state, low cost, environment friendly, high cyclability and flat discharge voltage. The excellent thermal stability enables the cathode to operate safely even at elevated temperature. At fully charged state the strong P–O covalent bonds stabilize the structure and restrict the O$_2$ release [Andersson et al, 2000]. The good structural stability of LiFePO$_4$ results slight change in unit cell volume (6.81 %) between lithiated and delithiated state which reveals excellent cyclability of the material [Wang et al, 2006].

The olivine LiFePO$_4$ has slightly distorted hexagonal close packed structure of oxygen anion atoms. The half of octahedral sites is occupied by Fe^{2+} and 1/8 sites is occupied by Li$^+$ So there are two types of octahedral units FeO$_6$ and LiO$_6$ with corner-sharing and edge-sharing respectively. The P^{5+} occupies the tetrahedral sites surrounded by the O^{2-}. The diffusion path for Li-ion is slightly curved along (010) direction. The structure of O^{2-} is slightly distorted from ideal hexagonal close packing (Fig. 2.1) due to cation-cation electrostatic repulsion [Padhi et al, 1997].
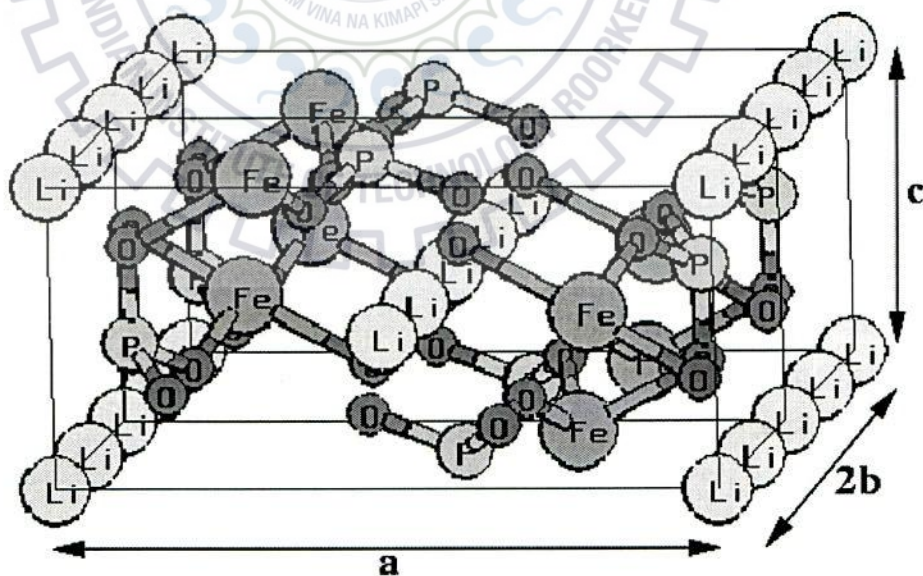
Fig. 2.1: Crystal structure of LiFePO$_4$.

Despite of many advantages in view of a cathode material, the LiFePO$_4$ has a few limitations viz.

1) Nominal discharge voltage of 3.4 V vs Li^+/Li which leads to low energy density of the electrode.

2) Low electronic conductivity (10^{-9} S/cm^2) leads to low rate capability.

3) Slow Li-ion diffusion which leads to the low rate capability.

4) Poor low temperature performance which restricts its use in low temperature energy storage applications.

These limitations restrict $LiFePO_4$ cathode material for its use in commercial application. The first principle calculation confirms that olivine structure offers lowest diffusion energy for Li-ion along the [010] direction in the crystal lattice. The theoretical value of intrinsic diffusion coefficient is of the order of ~10^{-8} (for $LiFePO_4$) to 10^{-7} cm^2/s (for $FePO_4$) [Wang and Hong, 2007]. But the observed values are found to be lower (~10^{-13} to 10^{-15} cm^2/s) than that of theoretical values. The low values are due to the blocking of a fraction of one dimensional Li-ion diffusion channels by the defects and impurities. The common defect observed in $LiFePO_4$ structure is Li-Fe anti-site defect in which Li and Fe exchange their position from their M(1) and M(2) respective positions. The anti-site defect blocks the diffusion path and effect the kinetic of Li-ion during charging and discharging mechanisms [Biendicho and West, 2011, Islam et al, 2005]. Different methods have been used to calculate the Li-ion diffusion coefficient. 1) Potentiostatic intermittent titration technique (PITT) was used by Lee et al and the diffusion coefficient were found in the range of 10^{-14} to 10^{-15} cm^2/s [Lee et al, 2013]. 2) Electrochemical impedance spectroscopy technique was used by Tang et al and they found the diffusion coefficient in the lower range of 10^{-18} to 10^{-14} cm^2/s [Tang et al, 2011]. 3) Chen et al have performed the CV test to measure the diffusion coefficient and found the diffusion coefficient of order of 10^{-9} cm^2/s which was near to the theoretical value of the diffusion coefficient for $LiFePO_4$ [Chen et al, 2014].

The operating temperature of the electric vehicle (EV) lies between − 40 °C and + 50°C. The poor performance of the Li-ion battery at low and high temperature is the major technical barrier in the field. The material $LiFePO_4$ loses its specific capacity rapidly at low temperature especially below 20 °C. The influence of temperature becomes more significant at higher rate of charging / discharging. The loss of capacity at low temperature is attributed to the limited electrode kinetics, low Li-ion diffusivity, low electrolyte conductivity, and high charge transfer resistance at the electrode / electrolyte interface.

Goodenough et al explained the mechanism of charging and discharging of the $LiFePO_4$ by proposing the shrinking core model [Goodenough et al, 1997].

Shrinking core model: According to this model, during intercalation process Li-ion is transported to $FePO_4$ structure by filling the sites starting from surface to interior of particle. The filled Li sites creates highly enrich Li phase. An interphase develops separating the highly enrich Li to nearly vacant Li sites. At the starting of intercalation the Li rich phase forms a shell on the Li deficient core. Further discharging of electrode fills the vacant sites in Li deficient phase which are next to filled sites, causing the movement of interphase toward the core of particle. The Li deficient core phase goes on shrinking at the cost of Li rich and finally discharging leads to the complete lithiation of particle creating a single Li enrich phase. Similarly during charging, delithiation starts from the outer surface of Li enrich phase creating a Li deficient phase. During the delithiation the Li deficient shell grows at the cost of Li-ion enrich core. At fully delithiated state only Li deficient phase exists.
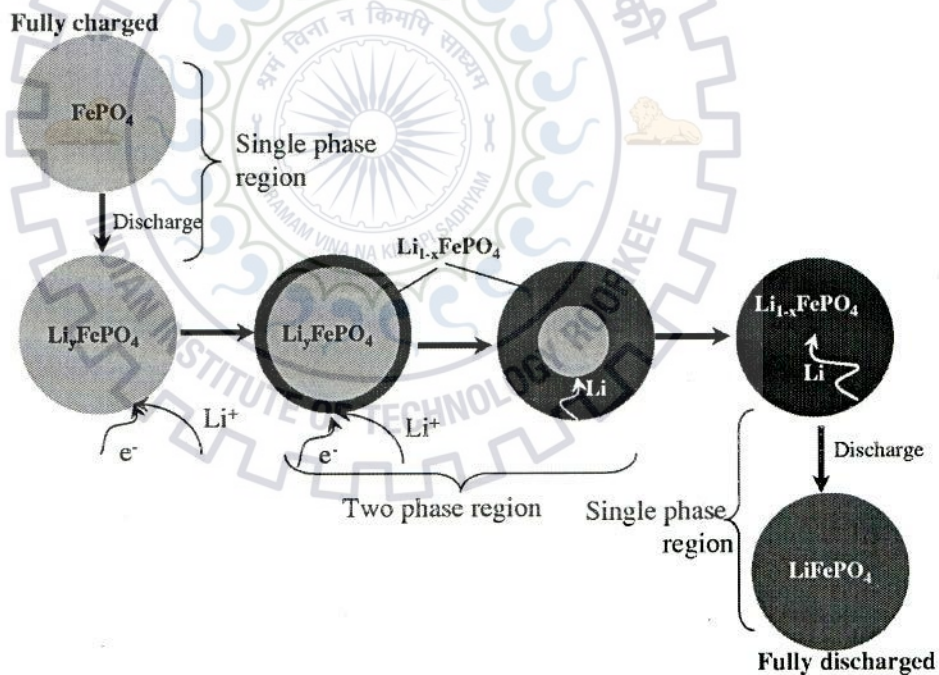
Fig. 2.2: Shrinking-core model showing the movement of phase boundary during charging / discharging [Srinivasan et al, 2004].

2.3 Synthesis method of LiFePO₄

To improve the electrochemical performance of $LiFePO_4$ or $LiFePO_4/C$ various synthesis processes have been used by the researchers. The synthesis methods must be optimized to get high purity and homogeneity in $LiFePO_4$ particles along with thin and uniform carbon coating. The different methods of synthesis have their different advantages and disadvantages.

2.3.1 Solid state synthesis

Solid state reaction is widely used method for synthesis of ceramic materials. In this method stoichiometric amount of starting materials were grinded to homogenize the mixture and the mixture was calcined to get the final ceramic material. The theoretical capacity of ~ 95 % for $LiFePO_4$ can be achieved at room temperature by good optimization of the solid state reaction conditions like calcination time, temperature and ratio of the raw materials used [Yamada et al, 2001]. The agglomeration and particle size range can be reduced by addition of carbon inhibitor [Huang, 2001]. The disadvantages of the solid state reaction method is long heating time, several intermediate grinding steps, irregular morphology, wide particle size range, agglomeration and inhomogeneous from composition point of view [Franger et al, 2003].

2.3.2 Hydrothermal synthesis

Hydrothermal synthesis method has the advantages of low cost and less energy utilization as it requires low temperature and less time as compared to solid state synthesis process [Song et al, 2010]. In this method of synthesis the stoichiometric amounts of the reactants were dissolved in the water or other solvent and heated above the boiling point at high pressure in the sealed autoclave. The sealed autoclave was heated preferably in the microwave oven to give uniform heating throughout the volume of material. Hydrothermal method has the advantage of growing the highly crystalline, fine particles with controlled morphology and low synthesis temperature [Ellis et al, 2007]. The hydrothermal method can tune the particle size and morphology by controlling the variables such as temperature, time and concentration of the reactants [Pei et al, 2012].

2.3.3 Sol-gel synthesis

The sol-gel method of synthesis is wet-chemical technique widely used for the synthesis of ceramic materials. The better mixing of the reactant insures the high purity, homogeneity and small particle size of the material synthesized using this technique. In this method the precursors were mixed in a solvent to form a solution. The solution was then heated to evolve the mother liquid to form a polymeric gel network containing the liquid and solid phase. The polymeric gel was then dried by heating. For the synthesis of $LiFePO_4$ the source of lithium (e.g. Lithium acetate, Lithium hydroxide or lithium carbonate), iron (e.g. Iron acetate or Iron chloride) and phosphate (Orthophosphoric acid or Ammonium dihydrogen phosphate etc.) were mixed in a fixed amount to form a precursor. An in-situ carbon coating can be produced by adding the source of carbon like acetates, citrates or oxalate to the precursor before heating

[Yang et al, 2004]. The sol-gel technique is regarded as one of the best methods to prepare the $LiFePO_4$ and carbon coated $LiFePO_4$ with controlled particle size and / or high quality (continuous, uniform and thin) carbon coating to improve their electrical conductivity with minimal Li-ion diffusion path length.

2.3.4 Chemical precipitation method

The chemical precipitation method is also a solution method which can be used to synthesize $LiFePO_4$ material. For the synthesis of $LiFePO_4$ the sources of lithium, iron and phosphate were used to mix in the aqueous solution. The parameters such as pH and temperature of the solution were adjusted to give high purity of the $LiFePO_4$ powder. The highly crystalline $LiFePO_4$ material was synthesized with the narrow particle size range of $100 - 200$ nm using this method [Delacourt et al, 2006]. The method has the advantage of simple synthesis procedure and required low energy consumption for the synthesis of highly pure, homogeneous and well crystalline powder. For the synthesis of doped materials post heat treatment is required in the range of 400 to 700 ºC under controlled environment [Sarkar et al, 2014, Yang et al, 2009]. The temperature and time for heat treatment is lower compared to other synthesis process as the crystalline $LiFePO_4$ phase is already formed during the precipitation.

2.3.5 Polymerization restriction method

Polymerization restriction method is a promising method used for the synthesis of carbon coated $LiFePO_4$ for the application of high rate capability cathode. It may be considered as a combination of sol-gel and chemical precipitation method. In this method the source of iron and phosphate were added along with the organic monomer units. The precipitates of $FePO_4$ form and start growing. When the size of $FePO_4$ particles reaches within the specific range the organic monomer units start polymerizing to restrict the size of $FePO_4$ growing particles and $FePO_4$ / polymer composite forms. The $FePO_4$ / polymer composite was further calcined with lithium source in the inert atmosphere to form the carbon coated $LiFePO_4$ material. During calcination carbonization of polymer coating takes place along with the particle size restriction of $LiFePO_4$. This method is used to deposit carbon coating on the single crystallites of $LiFePO_4$ having a size range of $20 - 40$ nm. The material synthesized using this method delivers a discharge capacity of 168 mAh/g at 0.6C and 90 mAh/g at 60C indicating a high power performance of $LiFePO_4$ electrode [Wang et al, 2008]. Different organic monomers can be used to restrict particle size and decompose to carbon coating [Jiang and Jiang, 2012, Chen et al, 2013].
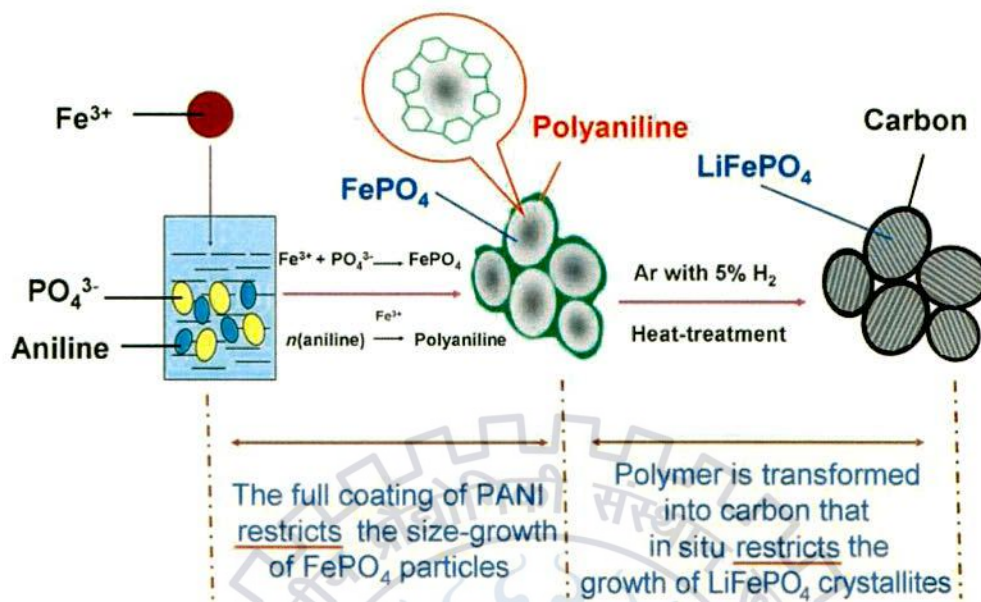
Fig. 2.3: In-situ growth of polyaniline and carbon coating showing the restriction of size of LiFePO$_4$ particles [Wang et al 2008].

2.4 Approaches to solve the limitations of LiFePO$_4$

Different experimental approaches such as substituting Fe with other transition metals, particle size reduction, doping and conductive coatings have been proposed to solve the limitations associated with LiFePO$_4$. The low redox voltage of 3.4 V for Fe^{2+} / Fe^{3+} couple can be solved by substituting Fe in the structure of LiFePO$_4$ with the transition metals such as Mn, Co and Ni. According to different active redox couples, the voltage is 4.1 V for LiMnPO$_4$, 4.8 V for LiCoPO$_4$ and 5.1 V for LiNiPO$_4$, therefore these materials may be used to improve the volumetric energy density (energy/volume or Wh/L) of the olivine structure. Conductivity and diffusivity related issues can be solved by 1) particle size reduction, 2) doping and 3) conductive surface coating. The issues related to temperature dependence of the materials can be solved by selecting the suitable electrolyte and coating materials.

2.4.1 Particle size reduction

Advantages of particle size reduction

i)   One of the most important aspects of nano-sized particle is fast charging / discharging of materials, implying that the material is suitable for high rate capability. Reducing the particle size to nano-sized range shortens the diffusion length resulting in reducing the diffusion time required for Li-ion during charging / discharging of the material,

according to the relation, $t = L^2/D$, where L is diffusion length, D is diffusion coefficient of the ion and t is the diffusion time [Guo et al, 2008, Kumar et al, 2009].

ii)   The electron propagation in the structure of particle can be improved by reducing the particle in the nano-size range.

iii)   Large surface area of nano-sized particles provide higher electrolytic / electrode interface area. This provides higher flux of conducting species [Bruce et al, 2008].

iv)   The particles of nano-size range can accommodate good strain as compared to micron-sized particles[Meethong et al, 2007]

v)   The thermodynamic aspect of nano-sized particles is modified chemical potential which results in higher potential and storage capacity of electrode prepared using these materials [Balay et al, 2006].

Disadvantages

1) Particles size below a certain limit in nano range show poor cycling performance and have difficult process ability to mix conducting carbon black and of cathode electrode fabrication [Wu et al, 2009].

2) It is difficult to control size and dimension during synthesis of nano-sized material [Bruce et al, 2008].

3) Large particle / electrolyte contact area leads to the undesirable reactions which involve the electrolyte decomposition resulting in the loss of cyclability and reversibility of the cell [Wagemaker and Mulder, 2013].

4) For the nano-sized particles it is difficult to maintain interparticle contact resulting in low packing density of the active particles which reduce the volumetric density of the electrode [Bruce et al, 2008].

So, it is highly promising and challenging to use the nanoparticles as the active material for the Li-ion battery. The nano-sized particle offers higher specific surface area delivering higher flux of Li-ion across the material / electrolyte interphase, but at the same time decreasing the specific charge due to undesirable side reactions between the electrode material and electrolyte. So, advantages are often linked with the disadvantages for the nano-size material. Applications such as EV / HEVs require both high energy and high power densities which can be supplied by nano-structured materials. In an invention excellent electrochemical properties of nano-crystalline $LiFePO_4$ of particle size 50 nm were reported [Delacourt, et al, 2006, United States Patent]. This nano-crystalline $LiFePO_4$ was synthesized by chemical precipitation method in

the solvent of water (50 % volume) and DMSO (50 % volume). The material delivers discharge capacity of 85 % of the theoretical value at a charge / discharge rate of 1C. The nano-crystalline $LiFePO_4$ material has a very low capacity degradation of ~ 0.04 % per cycle upto 200 charge / discharge cycles at 5C rate.

2.4.2 Supervalent doping

Doping of $LiFePO_4$ with the supervalent cation also improves the rate capability and cyclability of the material. Doping with the foreign atom makes the structure more flexible to the phase transformation by expanding the Li-ion diffusion channel [Meethong et al, 2009]. Many studies confirmed that supervalent ion doping to the $LiFePO_4$ raise the electronic conductivity upto 8 orders of magnitude. Doping in the bulk material was initially doubted on the basis of instability of the nonstoichiometric compound [Ravet et al, 2003]. X-ray photoelectron spectroscopy (XPS) studies of Fe site doped Mg confirmed the low binding energy of O (1s) and Li(1s). The low binding energy by doping has reduced the interaction between O and Li which favors the higher Li diffusivity [Wang, D. et al, 2005]. Later Wagemaker et al confirmed the Zr, Nb and Cr supervalent cation doping in the structure of $LiFePO_4$. The supervalent cation doping of upto 3 % atomic substitution can be hosted in the lattice $LiFePO_4$ material synthesized by solid state route at 600 °C [Wagemaker et al, 2008]. The presence of foreign atom in the crystal lattice of $LiFePO_4$ may be deleterious if it occupies on the Li-ion sites [Yonemura et al, 2004]. Ouyang et al have studied the Cr doping on Li sites of $LiFePO_4$ by first principle calculations and Monte-carlo simulations and investigated that Cr doping on Li sites do not improve the electrochemical performance of $LiFePO_4$ [Ouyang et al, 2004]. The Cr has higher energy barrier as compared to Li implying that Cr doping on Li sites blocks the one dimensional diffusion path for Li-ion during the charging / discharging process of $LiFePO_4$.

2.4.3 Conductive surface coating

The electrochemical performance of $LiFePO_4$ can be improved by the conductive surface coatings such as 1) metals, 2) metal oxide, 3) carbon and 4) conducting polymers. These conductive coatings improve the materials conductivity and Li-ion diffusivity which results better capacity and rate capability of $LiFePO_4$.

2.4.3.1 Metallic coating

Metallic coatings such as of Cu, Ag have improved the conductivity of material resulting in improved rate capability of the $LiFePO_4$. The Cu and Ag particles of size 100 nm were

dispersed with $LiFePO_4$ particles to impart enhanced conductivity and cyclability of the cathode electrode. About 1 wt% of Cu or Ag delivers good conductivity and restricts the particle size of $LiFePO_4$ [Croce et al, 2002]. The surface of $LiFePO_4$ particles were modified by Ag using continuous stirring of $LiFePO_4$ in aqueous $AgNO_3$ solution and the filtered material was further calcined at 500 °C to decompose the undesirable salts. The Ag coating improves rate capability by improving the conductivity of the $LiFePO_4$ electrode [Park et al, 2004]. It was also investigated that formation of metallic compound Fe_2P along with small amount of Li_3PO_4 takes place during the calcination for the synthesis of carbon coated $LiFePO_4$. The highly conducting phase Fe_2P forms due to the reduction of $LiFePO_4$ in the presence of carbon in the temperature range of 600 to 800 °C. The Fe_2P metallic is the initial layer that forms on the $LiFePO_4$ structure followed by the carbon coating. An optimum amount (5 – 10 %) of Fe_2P greatly enhanced the electrochemical performance of $LiFePO_4$ [Rho et al, 2007]. Although metal dispersion results in significant improvement in the electrochemical performance of the $LiFePO_4$ but it is difficult to achieve the uniform metal dispersion on the surface of $LiFePO_4$ without affecting the structure. Furthermore metals get oxidized to form insulating film on the negative electrode to affect the cyclability. High cost metal dispersion makes the composite expensive and should not be used for bulk production of $LiFePO_4$ cathode.

2.4.3.2 Oxide coating

Oxide coatings such as TiO_2, ZrO_2 and CeO_2 have performed to enhance the electrochemical performance of the $LiFePO_4$ material. Chang et al deposited TiO_2 coating by sol-gel process and investigate the effect of coating on cyclic performance at different temperature [Chang et al, 2008]. TiO_2 coating on the surface of $LiFePO_4$ particles has improved the cyclability by reducing the Fe dissolution in the electrolytic when measurements were performed at 55 °C temperature. The TiO_2 coating also improves the conductivity of electrode to have better capacity and rate capability. The nano-structured ZrO_2 oxide coating can be deposited by chemical precipitation method. The ZrO_2 coated $LiFePO_4$ shows better rate performance by improving the Li-ion kinetics at the electrolyte / electrode interface. Liu et al investigated the redox behavior of CeO_2 coated $LiFePO_4$ in 1M Li_2SO_4 electrolyte solution [Liu et al, 2009]. They observed that 2 wt% CeO_2 on $LiFePO_4$ particles perform good rate capability and cyclability at elevated temperature by improving the particle to particle contact and Li-ion diffusivity. The cyclic performance of the electrode is improved in the presence of metal oxide coating as it also protects the electrode material from HF attack. HF forms in the electrolyte during moisture attack on $LiPF_6$ and make the electrolyte acidic. The metal oxide coating reacts

with HF to form metal fluorides and maintains the neutrality of the electrolyte [Chen et al, 2010]. But the drawback of metal oxide coatings is same as of metal coating that, it is difficult to disperse uniform metal oxide on $LiFePO_4$ particles.

2.4.3.3 Carbon coating

The carbon coating is a potential approach to meet the theoretical capacity of $LiFePO_4$ material at nominal current rates. The effect of carbon coating is to impart high electronic conductivity and fast Li-ion diffusion in $LiFePO_4$/C composite. Electrons spread over the entire surface of $LiFePO_4$ particle through carbon coating and impart higher conductivity to the bulk material, resulting in improved kinetics of charging / discharging of $LiFePO_4$ material. The carbon coating helps to slow down the growth of $LiFePO_4$ particles resulting in fine $LiFePO_4$ particle. Ravet et al was the first to introduce the carbon using sucrose and cellulose as carbon sources on $LiFePO_4$ particles [Ravet et al, 2001]. The carbon coating reduces separation between oxidation / reduction peaks of cyclic voltammetry (CV), implying that introducing carbon as coating material has better reversibility of $LiFePO_4$/C electrode by reducing the polarization of electrode [Liu, et al 2006]. So, the overall effect of carbon coating is to provide high electronic conductivity, fast Li-ion diffusion, restrict the particles growth resulting in fine $LiFePO_4$ particles and reduce the electrode polarization. These effects improve the rate capability of the cathode. Table 2.1 shows an improved rate capability of $LiFePO_4$/C and it is compared with the rate capability of $LiFePO_4$.

Table 2.1 Comparison of rate capability of pristine $LiFePO_4$ and $LiFePO_4$/C.

S. No	Rate capacity of LiFePO₄ [Lee et al, 2013]	Rate capability of LiFePO₄/C (8 wt % of carbon) [Chen et al, 2014]
1	~ 130 mAh/g at 0.2C rate	135 mAh/g at 0.2C rate
2	~ 110 mAh/g at 0.5C rate	130 mAh/g at 0.5C rate
3	~ 50 mAh/g at 1C rate	120 mAh/g at 1C rate

But the various factors such as content, thickness, structure, distribution, morphology, surface area and porosity, impart different properties to $LiFePO_4$/C composite materials. The properties of carbon are discussed below.

2.5 Factors effecting carbon coating

2.5.1 Effect of carbon content

Since carbon is electrochemically inactive and has density 61 % of the density of $LiFePO_4$ so, the addition of carbon adversely affects the volumetric energy density of $LiFePO_4/C$ electrode. The addition of 15 wt% carbon decrease the 22 % of the volumetric energy density and also decrease the gravimetric energy density by 15 % for the $LiFePO_4/C$ electrode [Chen and Dahna, 2002]. In order to have good conductivity and higher energy densities values, amount of carbon must be optimized. But it is not easy to optimize the weight of carbon as the amount of carbon depends upon structure and structure of carbon varies according to the synthesis conditions. Zhang et al made $LiFePO_4/C$ composite by solid state reaction method, having different carbon amounts and investigated that $3 - 10$ wt% of carbon is optimum to impart higher specific capacity [Zhang et al, 2005]. Jin et al reported the specific capacities of $LiFePO_4/C$ composites having carbon from 0 to 10 wt% and investigate that 5 wt% of carbon delivers maximum capacity and better cyclability of all the samples synthesized using hydrothermal method [Jin et al, 2008]. The $LiFePO_4/C$ composite was synthesized by one-step microwave method and it was investigated that 4.6 wt% of carbon delivers excellent specific capacity of 152 mAh/g and 59 mAh/g at 0.2C and 20C rate respectively [Zhang et al, 2009]. In another study $LiFePO_4/C$ was synthesized by sintering the precursor at 750 °C in reduced atmosphere (N_2-5%H_2) and they optimized 7 wt% of carbon to give specific capacity of 98.3 mAh/g at 5C rate [Chang et al, 2009]. In all the research the optimized amount of carbon is different and depends upon the synthesis methods. But the amount of carbon should be kept as low as possible in the range of $2 - 3$ wt% in order to improve the tape density, volumetric and specific capacity of the $LiFePO_4/C$ composite electrode [Chena et al, 2002].

2.5.2 Carbon coating thickness

The carbon is usually derived from the organic materials mixed with the precursor before calcinations. The organic materials of the precursor decompose to residual carbon in the inert atmosphere. The thickness of coating increases with the amount of organic precursors added and size of $LiFePO_4$ particles. Small sized $LiFePO_4$ particles provide larger surface area. So, a higher amount of organic precursor is required to optimize the thickness for small particles. Usually carbon in the coating reduces the Li-ion diffusion, electronic conductivity and tape density of $LiFePO_4$. Thin and uniform carbon coating is preferred for easy diffusion and high tape density. But a low carbon content imparts less electronic conductivity due to the presence of partially coated $LiFePO_4$ particles. So, in order to balance the good electronic conductivity,

higher tape density and fast Li-ion diffusion, the carbon coating thickness must be optimized. Chao et al has optimized the carbon coating thickness to 4 – 8 nm (for 2.28 wt% of carbon) in order to impart good discharge capacity [Cho et al, 2009].

2.5.3 Structure of carbon

The structural formation of carbon on the surface of $LiFePO_4$ significantly affects the electrochemical performances of the cathode [Hu et al, 2004]. Raman spectroscopy has been used to characterize the structure of carbon coating by the ratio of intensity of defected carbon to graphitic carbon (I_D/I_G) peaks [Doeff et al, 2003, Bhargava et al, 1996]. The higher graphitization is achieved for low I_D/I_G value which favors the good conductivity of carbon. The formation of carbon structure depends upon the carbon sources and synthesis conditions.

The choice of different carbon source affects the structure of carbon formed during the synthesis of $LiFePO_4$/C. A higher fraction of graphitic carbon is formed during the synthesis of $LiFePO_4$/C using sucrose as carbon source [Kim, J.K., Cheruvally, G. et al, 2008]. The naphthalene-tetracarboxylicdian-hydride organic precursor as carbon source forms higher fraction of graphitic carbon and improves the rate capability of $LiFePO_4$/C composite [Wilcox et al, 2007]. Nakamura et al added the organic material Pyrene as carbon source and improved the fraction of conducting carbon [Nakamura et al, 2006]. The addition of pyromellitic acid $(C_6H_2(COOH)_4)$ with iron nitrate before the calcination process gives low I_D/I_G values. They also found that addition of ferrocene with pyromellitic increases the amount of carbon formed on the surface while the structural characteristic of carbon remains unaltered [Wilcox et al, 2007]. Recently, Nien et al deposited carbon on the surface of $LiFePO_4$ particles by pyrolysis of polymers like polystyrene, polyethylene oxide, polybutadiene and styrene-butadiene-styrene [Nien et al, 2009]. Polystyrene due to the presence of large number of aromatic ring structure produced highly graphitic carbon in the $LiFePO_4$/C composite resulting in superior electrochemical properties.

Recently the graphene coating has gained great potential for the high performance of $LiFePO_4$ due to unique structure, superior electronic conductivity and high surface area. Ding et al introduced the graphene coating on $LiFePO_4$ particles by co-precipitation method [Ding et al, 2010]. It was observed that a 1.5 wt% of graphene delivers a discharge capacity of 160 mAh/g at 0.2C rate and the capacity retained of 110 mAh/g at 10C rate. The high rate capability of the $LiFePO_4$/graphene material is due to the following two reasons: 1) particles size control by the graphene oxide added at the precursor level and 2) the graphene nano-sheets act as conducting

medium for the interconnection of the LiFePO$_4$ particles to reduce the particle to particle contact resistance.

2.5.4 Carbon distribution

The diffusion of Li-ion is restricted only along [010] direction of the structure. So, in order to have fast diffusion of Li-ion the distribution of carbon on the surface of LiFePO$_4$ particles should be uniform and continuous. Carbon can be distributed on the surface of LiFePO$_4$ by ex-situ and in-situ methods of deposition. The ex-situ method is direct introducing the carbon on the already prepared LiFePO$_4$ particles, where in-situ method is carbon addition during the synthesis of LiFePO$_4$. The ex-situ method has the advantage of choice of the direct addition of highly graphitic carbon or high surface area carbon by mechanical mixing. Limitation of this method is to deposit non-uniform carbon distribution on the LiFePO$_4$ surface. Fang et al have introduced the graphene nano-sheets on LiFePO$_4$ particles by mechanical mixing and a unique plane-to-point conductive network was formed between single or few graphene sheets [Su et al, 2010]. The graphene network provides highly conducting path to electrons and delivers high capacity at fast discharging current rate. Kim et al deposited the conducting carbon by both in-situ and ex-situ methods of carbon addition [Kim, J.K., Choi, J.W. et al, 2008]. They form the in-situ carbon coating by carbonization of sucrose during the synthesis of LiFePO$_4$/C composite and observed that 6 wt% carbon gives the best electrochemical property. The in-situ carbon coating shows higher discharge capacity as compared to the coating formed by mechanical mixing. The higher discharge capability of in-situ carbon coated LiFePO$_4$ is due to better distribution of carbon on the surface of LiFePO$_4$ as the carbon formed by decomposition of sucrose is thin and uniform comparative to ex-situ coated LiFePO$_4$. A high performance cathode of LiFePO$_4$/C composite should have nano-sized LiFePO$_4$ particles with continuous and thin coating of highly conducting carbon. Wang et al successfully deposited the uniform and thin carbon coating on the 20 – 40 nm sized LiFePO$_4$ particles by in-situ polymerization restriction technique [Wang et al, 2008]. They grow in-situ thin polyaniline coating on the surface of FePO$_4$ growing particles. The polyaniline coverage stops the growth of FePO$_4$ particles and the residue was further calcined by homogeneously mixing with Li(CH$_3$COO) at 700 °C under inert and reducing atmosphere (Ar-10%H$_2$). During calcinations polyaniline decompose to carbon as thin coating on LiFePO$_4$ crystallites.
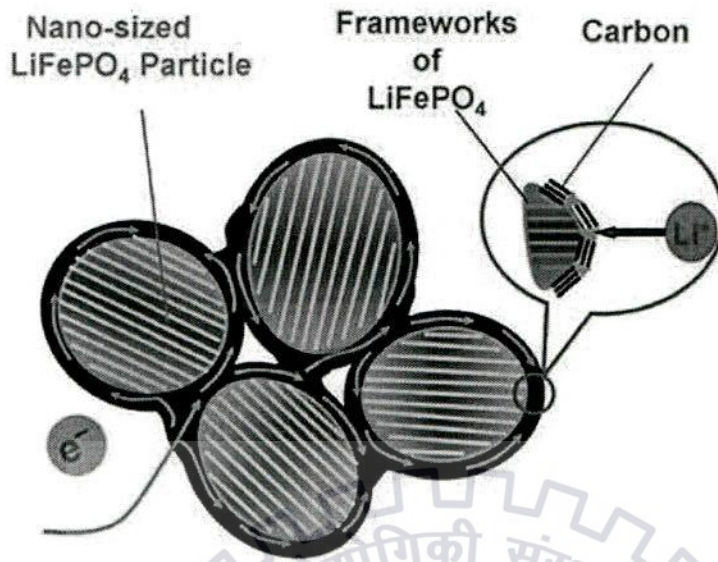
Fig. 2.4: Design of complete carbon coating on nano-sized LiFePO₄ [Wang et al 2008].

A lot of work has been done in order to deposit thin and uniform carbon coating on the LiFePO₄ surface. But it is still challenging to deposit thin and uniform carbon coating on the surface of irregular shape and agglomerated particles.

Despite of many advantages carbon coating provides some limitations as given below:

1 Decreases tap density of the cathode

2 Decreases volumetric density

2.6 Conducting polymer coating

Conducting polymers are the class of polymer having conductivity from semiconductor to well into the metallic range. The conducting polymers have the pie-conjugation system in the long polymer chain. The conductivity of these polymers can be tuned by the doping and de-doping of the pie-conjugation system. Two types of doping involve in the conjugated polymers viz. p-doping and n-doping. The p-doping involves the oxidation by removing an electron leaving the positive charge on polymer chain. Similarly n-doping involves the reduction by adding the electron or negative charge on the polymer chain [Mike et al, 2013]. The reduction and oxidation in polymer chains can be induced either by chemical species (Iodine, sodium-naphthaline) or by the electrochemical process. The positive or negative charge that develops during p-doping and n-doping becomes delocalized through the polymer chain and is neutralized by attaching a counter ion (dopant). For an example the n-doping results in the ionic complex of the negatively charged polymer chain attached with the Li-ion. The conductivity of

these conducting polymers can be controlled by level of doping [Freund and Deore, 2007, page 7]. The reactions shown below represent the p-doping and n-doping in the polyethylene.

p-doping $(CH)_n + 3/2ny(I_2)$ $\longrightarrow$ $[(CH)^{y+}(I_3^-)_y]_n$

n-doping $(CH)_n + yLi$ $\longrightarrow$ $[(CH)^{y+}(Li\text{-}ion)_y]_n$

The aromatic polymers with pie-conjugation such as polyaniline, polypyrrole and polythiophene have non-degenerate ground states. The ground state degeneracy of these polymers is weakly lifted corresponding to highly conjugated quinoid ring (Fig. 2.5) as compared to benzenoid ring. The mechanism of conduction in these polymers can be well understood by the formation of polaron and bipolaron.
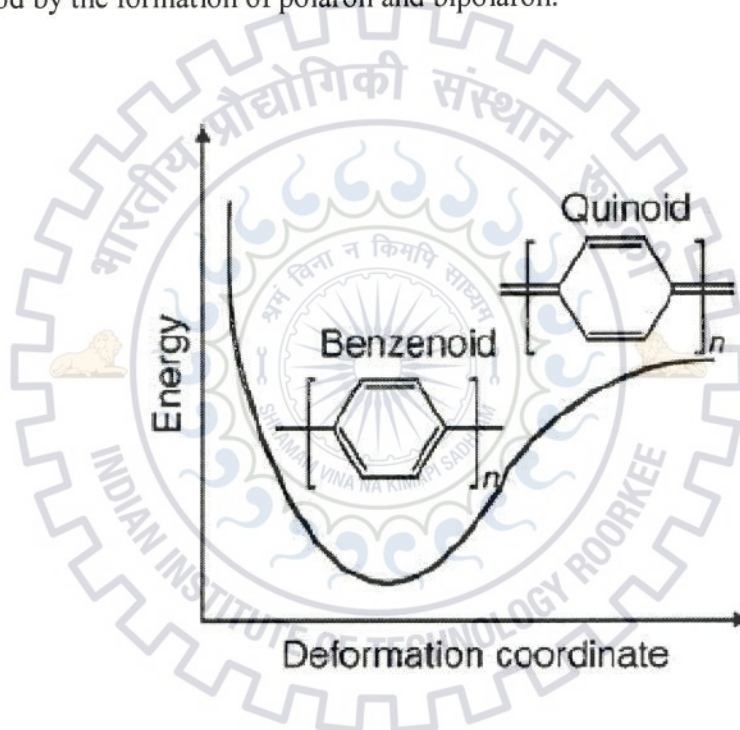
Fig. 2.5: Non-degenerate ground states of aromatic polymers.

The removal of an electron from the pie-conjugated polymer chain results the formation of radical cation. This radical cation which is partially delocalized over a segment of polymer chain is known as 'polaron'. Further removal of an electron from the polymer chain results two possibilities viz. 1) the electron may be removed from the different location of the polymer chain and creates there an independent polaron or 2) the removal of electron from the same location of the chain and creating there a dication separating the domain of quinoid bonds within the sequence of aromatic type bonds. This dication is referred as a bipolaron. Relatively lower energy is required for the formation of a bipolaron as compared to the formation of two distinct polarons. When doping level becomes sufficiently high it becomes possible the two

polarons may combine to create a single bipolaron [Han et al, 2003]. A bipolaron created have higher effective concentration of charge carrier as compared to polaron, due to which a bipolaron have higher conductivity [Hou et al, 2014].

Recently, work has focused to improve the electrochemical properties of $LiFePO_4$ by conducting polymers coating. Conducting polymers are highly attractive coating materials as they improve the electronic conductivity and Li-ion diffusivity of $LiFePO_4$/Polymer composite materials. Another attractive property of the conducting polymer is during discharging the polymers do not dissolve in the electrolytic keeping the shape of the electrode unchanged. The flat discharge voltage which brings the structural instability in the good capacity ceramic electrode is not the problem in case of polymer electrodes [Vernitskaya et al, 1997].
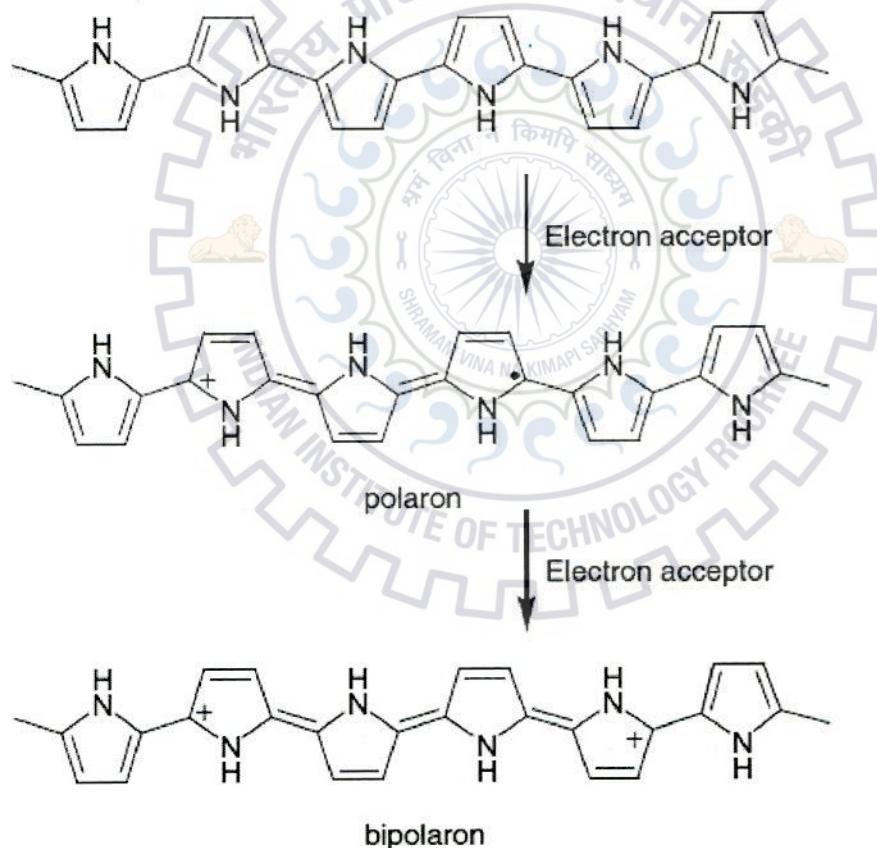
Fig. 2.6: Mechanism of formation of polaron and bipolaron [Freund and Deore, 2007, page 15]

So, polymer materials electrodes have good flexibility. The improving materials stability on the electrode, good electronic conductivity and ability to store Li-ion are advantages of conducting

polymers coating over carbon coating. However carbon is electrochemically inactive and its incorporation with LiFePO$_4$ decrease the tape density of the electrode. So, the advantages of the conducting polymer coating on the carbon coating are:

1) The conducting polymers are electrochemically active, but carbon is electrochemically inactive.

2) The conducting polymers show good binding ability as compared to carbon, so less quantity of binder is required for the fabrication of electrode.

3) The conducting polymer coating can be performed under mild processing conditions (they can be synthesized or processed at normal temperature and in air atmosphere) as compared to carbon coating (requires high temperature calcinations and inert environment) [Yin et al, 2012].

4) They also show good flexibility as compared to carbon coating [Yin et al, 2012]. The chain flexibility of polymers can be calculated by the factor known as persistence length (I$_p$). For the flexible polymers the value of I$_p$ is as low as of order of few angstroms [Li et al, 2006].

Properties 1) and 2) increase the tape density by improving the utilization of the electrochemically active material on the electrode.

The conducting polymers which are electrochemically active can be used as the coating material on the LiFePO$_4$ crystalline particles. The electrochemically active conducting polymers such as polyaniline, polypyrrole, polythiophene, polyacene and poly-3,4-ethylenedioxythiophene (PEDOT) have been used to cover the LiFePO$_4$ particles as they show good conductivity and are electrochemically active between 2 – 4 V [Huang and Goodenough, 2008, Bai et al, 2010, Xie et al, 2006].

2.6.1 Polyaniline coating

Among the conducting polymers, polyaniline is an important conducting polymer for the application in Li-ion battery. The properties like high conductivity, facile synthesis, thermal and chemical stability makes it suitable for the energy storage devices [McManus et al, 1987, Huang et al, 2003, Chandrakanthi and Careem, 2000]. The emerladine salt form of polyaniline is the highest conducting form of polyaniline. The emerladine base form of polymer is the non-conducting form and can be converted to the emarldine salt form by protonic acid doping.
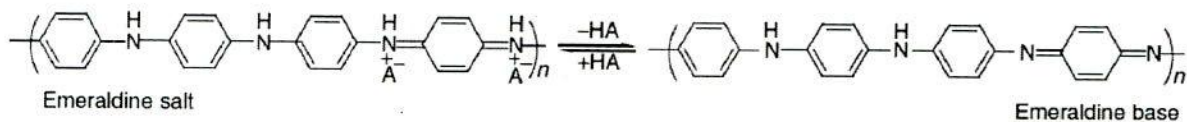
Fig. 2.7: Protonic acid doping of Polyaniline [Focke et al, 1987].

The advantages of polyaniline coating are

1. The polyaniline is an electrochemically active material, so it acts as the host material to store the Li-ion. The storage capacity of polyaniline is 95 mAh/g at 1C rate.

2. Polyaniline acts as binder to sustain more strains during charging / discharging of electrode to have higher cyclability.

3. Polyaniline reduces the polarization at electrolytic / electrode interface to impart easy exchange of conducting species and results in higher reversibility of the electrode.

Yang et al have used emerladine salt form of polyaniline as the cathode material in the Li/polyaniline battery [Yang et al, 1996]. The maximum theoretical capacity of 81 mAh/g was achieved and the material performed well upto 200 cycles with a columbic efficiency of 95 %. The reactions at cathode and anode during charging of the Li/polyaniline cell are shown below:

Charging: Emeraldine salt $- e^- + ClO_4^{2-} \rightarrow$ Emeraldine salt$^+$ ClO_4^{2-} Cathode

Charging: $Li^+ + e^- \rightarrow Li$ Anode
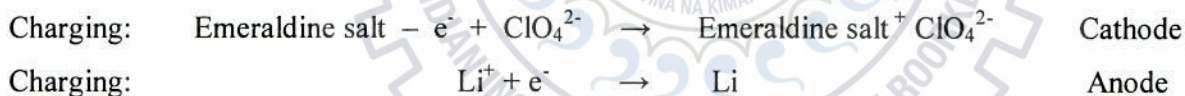
Polyaniline can be synthesized by chemical oxidation and electrochemical methods. The electrochemical synthesis is the simple and one step method of synthesis of polyaniline. This method of synthesis allows better control on conductivity and morphology of synthesized polyaniline. The control on conductivity was associated by the control on the charge supplied by the electrochemical device during the polymerization process, which controls the level of doping on the polymer chains [Heeger et al, 2001]. Although the chemical oxidation method has less control on the conductivity but the method of synthesis has advantages of mass production, better conductivity and solubility in the organic solvents [Chabukswar and Bhavsar, 2010]. The physical and chemical properties of polyaniline depend on the level of doping, oxidizing agent and solvent used for polymerization. On increasing the ratio of oxidizing agent to aniline monomers the conductivity and yield of the synthesized polyaniline increase. Pron et al have carried out the polymerization using different oxidizing agent ($K_2Cr_2O_7$, H_2O_2, $(NH_4)_2S_2O_8$ and KIO_3) with HCl doping [Pron et al, 1988]. It was observed

that polyaniline synthesized using KIO_3 oxidizing agent delivers higher conductivity and H_2O_2 shows the least conductivity. Moreover the rate of reaction in H_2O_2 is least resulting in very slow polymerization. Further the conductivity of polyaniline can be tuned by primary doping and secondary doping of inorganic acids. Zhang et al synthesized the polyaniline doped with the different inorganic acids such as, H_2SO_4, HBF_4, HCl, H_3PO_4 and investigated the morphology, size and electrical conductivity that depend upon the nature of inorganic acid [Zhang et al, 2002]. The HCl doped polyaniline has better electrical conductivity as compared to the other doping acids. The better electrical conductivity of HCl doped polyaniline was due to small sized doping ion as the conducting species. Further it was also investigated that on decreasing the ratio of dopant / aniline monomer the probability of formation of one dimensional structure reduces and the reaction product has a fraction of particulate structure. These structural effects are also temperature dependent. It was found that if the temperature of the polymerization becomes above 4 °C a particulate structure forms due to fast rate of reaction, so that polymerization in all the direction occurs and the resulting in polyaniline granular morphology.

The emeraldine salt form of polyaniline can be used as conducting additive which provides efficient conducting path for the charge species. MoS_2/polyaniline nanowires composite with an optimum of 33 wt% of polyaniline shows good rate capability of 1064 mAh/g retaining 92% of initial reversible capacity at the end of 50 cycles [Yang et al, 2013]. The $LiCoO_2$/polyaniline (15 wt%) composite material without conductive additives shows higher discharge capacity as compared to $LiCoO_2$ with acetylene black as conductive additive. The higher discharge capacity of $LiCoO_2$/polyaniline was due to better conductivity of polyaniline as compared to acetylene black. Moreover polyaniline is electrochemically active and contributes to the overall storage capacity [Zeng et al, 2013].

2.6.2 Polypyrrole coating

Polypyrrole is an attractive conducting polymer due to the pie-conjucation system in the polypyrrole backbone [Vernitskaya and Efimov, 1997]. The electrons from the pie-conjuction system move through the polymer chain resulting to impart the conductivity. Although the pristine polypyrrole imparts low conductivity $\sim 10^{-6}$ S/cm^{-2} and is insoluble in most of the solvents. This poor conductivity of polypyrrole restricts the applications in the field of engineering and technology. The conductivity of polypyrrole can be improved upto few tenth of S/cm^2 by doping and by selecting the suitable solvent for the synthesis [Kang and Geckeler,

2000, Ko et al, 1990]. Doping of polypyrrole improves the conductivity by the formation of polaron and bipolaron. These polaron and bipolaron are delocalized upto four benzene rings of the polypyrrole chains. Doping with dodecylbenzenesulfonic acid (DBSA), p-toluenesulfonic acid (TsOH) greatly improve the conductivity and solubility of the polypyrrole making it suitable for the many applications including the Li-ion battery. The doping of polypyrrole with Na-PTSA improves and stabilizes the conductivity of polypyrrole [Kaynak et al, 2009]. The stability and conductivity of the polypyrrole depend on the nature of solvent used for the polymerization of pyrrole monomers. If the polymerization of pyrrole monomers was carried out in the aqueous solvent (H_2O) the formation of hydroxyl and carbonyl group takes place. These groups localize the polaron and bipolaron at the location where they attached on the polymer chain. Moreover hydroxyl and carbonyl groups restrict the growth of long polymer chain during polymerization and due to this they are also known as terminal groups. The short polymer chains formed in the presence of these terminal groups shows low conductivity as compared to long polymer chains [Ko et al, 1990]. The stability of polypyrrole also reduces in the presence of these terminal groups due to evolution of CO_2 from the polymer chain [Wanekaya et al, 2006]. So, in order to get higher conductivity and stability the polymerization of the pyrrole should be processed in the non-aqueous solvent.

The great attractive property of polypyrrole is that it is electrochemically active and shows the Li-ion storage capacity of 72 mAh/g (vs Li^+/Li) especially in the range of 2.0 to 4.5 V. Since the range 2.0 to 4.5 V covers the electrochemical activity of most of cathode materials therefore polypyrrole is suitable coating material for the cathode materials. The Li/polypyrrole cell exhibits more than 90 % columbic efficiency and high cyclability, upto 1400 cycles at 0.1 mA/cm^2 current density [Osaka et al, 1994]. The reaction mechanism of the polypyrrole during charging of electrode can be understood by the following reaction:

At Cathode $\quad (Polypyrrole)^0 - e^- + PF_6^- \quad \rightarrow \quad (Polypyrrole)^+ PF_6^-$

At Anode $\qquad\qquad\qquad Li^+ + e^- \quad \rightarrow \quad Li$
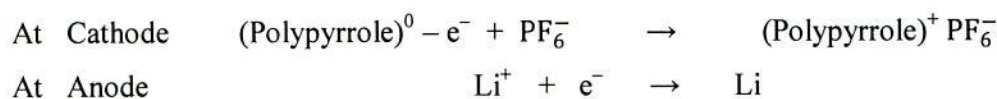
During charging polypyrrole releases an electron and becomes positively charged. The anion PF_6^- from the electrolytic intercalates with the positively charged polypyrrole and forms the $(Polypyrrole)^+ PF_6^-$ complex. The electron released by the polypyrrole chain moves through the external circuit and combines with the Li-ion present in the electrolytic solution and deposit at the anode in the form of lithium. If two PF_6^- anions are accommodated then the estimated theoretical capacity becomes 144 mAh/g. However in practice only one anion is accommodated

in one polypyrrole unit leading to the theoretical capacity of 72 mAh/g [Wang, G.X. et al, 2005].

The polypyrrole synthesized using $FeCl_3$ as oxidizing agent and doped with the Na-PTSA has electrical conductivity of 3 S/cm. The electrochemical cell was fabricated using the electrolyte of composition 1M $LiPF_6$ in a mixture of ethylene carbonate (EC) and dimethyl carbonate (DMC) (1:1 by volume). The polypyrrole electrode delivers an initial capacity of 69 mAh/g which is very close to theoretical capacity. The capacity reduces with cycling and becomes stable after 15 cycles.

A promising field for the polypyrrole is to form the protective coating on the surface of semiconductor ceramic materials to protect the structural instability generated by stress generated during extraction of the Li-ion. The conducting polypyrrole is suitable coating material for $LiMPO_4$ (where M = Fe, Mn, Ni, Co) and $LiMn_2O_4$ (spinel) and $LiCoO_2$ which have good Li-ion storage capacity but suffered from low conductivity. The optimized amount of polypyrrole in the $LiFePO_4$/polypyrrole coating was estimated to 10 wt% in order to exhibit good capacity and cyclability upto 50 cycles [Wang, G.X. et al, 2005]. The better cyclability and high capacity of the $LiFePO_4$/polypyrrole was due to the lower charge transfer resistance as compared to $LiFePO_4$. The electrochemically grown $LiFePO_4$/C-polypyrrole composite material was deposited on the stainless steel mesh used as cathode without addition of binder and acetylene black. The electrochemical measurements show the good cyclability and improved rate capability of $LiFePO_4$/C-polypyrrole as compared to $LiFePO_4$/C with binder [Huang et al, 2006].

2.6.3 Polythiophene coating

Among the entire conducting polymers, polythiophene is unique because of its distinct electrochemical, optical and magnetic properties [Groenendaal et al, 2000, Guimarda et al, 2007]. The conductivity of polythiophene comes in the range of a few S/cm and depends upon the synthesis parameter viz. time, temperature and solvent used for the synthesis [Guimarda et al, 2007]. Along with the conducting property, polythiophene also shows lithium storage capacity which leads the material to contribute in the Li-ion insertion / deinsertion mechanism. Carradini and Mastragostino initially reported, polythiophene as a cathode material in the rechargeable lithium battery [Corradini and Mastragostino, 1987]. The doped polythiophene shows the lithium storage capacity of nearly 100 mAh/g. The material shows an average

discharge voltage of 3.7 V (vs Li^+/Li) which is very close to the discharge voltage of olivine $LiFePO_4$ = 3.4 V (vs Li^+/Li) [Jeon et al, 2010]. Electrochemical and chemical oxidations are two broad methods which are used for polythiophene synthesis. Electrochemical method of synthesis has attracted great attraction as the polythiophene synthesized using this method shows desirable morphology and good conductivity. On the other hand chemical oxidation method has gained less attraction regarding morphology and electrical conductivity. Kwang et al have synthesized the polythiophene chemical oxidation method in the chloroform solvent and obtained the conductivity of 20 S/cm for the slow oxidation reaction using $FeCl_3$ oxidizing agent [Ryu et al, 2004]. The Li/Polythiophene cell was prepared using the electrolytic solution of 1M $LiPF_6$ dissolved in 1:1(v/v) mixture of EC and DMC. The specific capacity of the polythiophene electrode was 20 mAh/g and shows good cyclability upto 100 cycles of charging and discharging at 3.7 V (vs Li^+/Li). The discharge capacity of the electrode was further improved by optimizing the ratio of monomer to oxidation at 1:3. The polythiophene electrode delivers the discharge capacity of ~ 50 mAh/g for the Li/polythiophene cell discharged between 3.3 to 3.8 V [Bai et al, 2010]. The charging / discharging process can be explained using the equations as shown below.

Charging: Polythiophene - e^- + ClO_4^{2-} →   Polythiophene$^+$ ClO_4^{2-} Cathode

Charging: Li^+ + e^- →   Li   Anode

During charging the cathode of polythiophene releases an electron to become a cation which intercalate with ClO_4^{2-} anion. The electron released at cathode move to the lithium anode through external circuit [Bai et al, 2010].

Polythiophene have been studied as coating material for the cathode materials like $LiFePO_4$, LiV_3O_8 and sulphur in secondary lithium battery. The polythiophene shell protects the materials dissolution in electrolytic and provides better conductivity to improve cyclability of the electrode. For the LiV_3O_8/polythiophene the 15 wt% of polythiophene gives the best electrochemical performance. The cathode of LiV_3O_8 shows the discharge capacities of 248.5 and 87.8 mAh/g at 1C and 3C rate which further decrease rapidly after 50 cycles. The LiV_3O_8/polythiophene composite shows improved specific capacity of 200 mAh/g at 3C rate and retained a specific capacity of 198 mAh/g upto 50 cycles showing good cyclic stability. The improved electrochemical performance of LiV_3O_8/polythiophene was due to reduction in charge transfer resistance by polythiophene coating [Guo et al, 2014]. In the similar way the

discharge capacity of the composites $LiFePO_4$/polythiophene and S-polythiophene has improved the utilization of core material by improving the conductivity [Bai et al, 2010, Wu et al, 2011].

2.7 Objective and problem formulation

The overall objective of this thesis is to develop the high performance $LiFePO_4$ based cathode materials, where high performance refers to high rate capability with promising cyclability. A low cost process which restricts particle growth is chemical precipitation method by polymer coating is employed for the synthesis of $LiFePO_4$/C. The particles grown using this method have small size which reduces the diffusion length for Li-ion. To, overcome the limitation of slow Li-ion diffusion and low electrical conductivity of $LiFePO_4$ material, the coating of conducting polymers which are electrochemically active such as polypyrrole, polythiophene and polyaniline is performed.

In the present research work we have selected polypyrrole, polythiophene and polyaniline polymers as coating material to improve the electronic conduction and Li-ion diffusion. These polymers are being selected for the coating on $LiFePO_4$/C particles as, i) they are electrochemically active in the range of 2.2 - 3.8 V which overlaps with the redox range (3.4 V for Fe^{2+}/Fe^{3+}) for $LiFePO_4$ core particles, ii) they have good electronic conductivity and Li-ion diffusivity, iii) they have good binding ability towards the ceramic particles. Therefore, these conducting polymers not only act as conducting agent but also as host material for Li-ion insertion/extraction. From the health point of view polypyrrole has limited cytotoxic effect, while there is no data available for the other conducting polymers [Balint et al, 2014 and Ibarra et al, 2015].

Although polyacetylene is another material which has advantages of having higher electrical conductivity and charge storage capacity as compared to the polymer used in the present research work. However, polyacetylene is not an ideal battery material. It degrades in air, is chemically stable only in liquid solutions, and is brittle. Where the advantages of the polymers used in the present research work are having good flexibility, high columbic efficiency and binding ability for the oxide material [Sengodu et al, 2015].

After going through the literature critically the problem and objective of the present study have been formulated as:

- To synthesize carbon coated LiFePO$_4$ particles using chemical precipitation method and restriction of LiFePO$_4$ particle size by in-situ polymerization.

- To deposit in-situ polymer coatings (of polyaniline, polypyrrole and polythiophene) on LiFePO$_4$/C particles by chemical oxidation method.

- To study the different phases that exist after polymer coating on LiFePO$_4$

- To study the morphology of LiFePO$_4$/C and polymer coated LiFePO$_4$/C particles

- To study the weight fraction of carbon and polymers for LiFePO$_4$/C and polymer coated LiFePO$_4$/C composite material

- To study the structure of carbon and confirm the polymerization of monomer units in the coatings region using Raman spectra

- To study the electrochemistry (i.e. capacity, cyclability and rate capability) of LiFePO$_4$/C and polymer coated LiFePO$_4$/C materials as cathode for electrochemical cell

- Study the conductivity of LiFePO$_4$/C and polymer coated LiFePO$_4$/C as cathode of the electrochemical cell.

EXPERIMENTAL PROCEDURE

CHAPTER-3

EXPERIMENTAL PROCEDURE

This chapter describes the preparation and characterization of LiFePO$_4$/C and polymers coated LiFePO$_4$/C composite materials. The LiFePO$_4$/C particles were synthesized by the chemical precipitation method followed by *in-situ* polymer coating using the oxidation polymerization method. Three different electrochemically active polymers viz. polyaniline, polypyrrole and polythiophene have been used to coat LiFePO$_4$/C material. The synthesized LiFePO$_4$/C and polymer coated LiFePO$_4$/C materials were characterized using X-ray diffractometer, scanning electron microscope operated with field emission gun, Raman spectrometer, transmission electron microscope and thermal analyzer. The cell is assembled and tested inside Ar-filled glove box having oxygen and moisture levels below 0.1 ppm. Fig. 3.1 shows schematically flow diagram of experimental work.
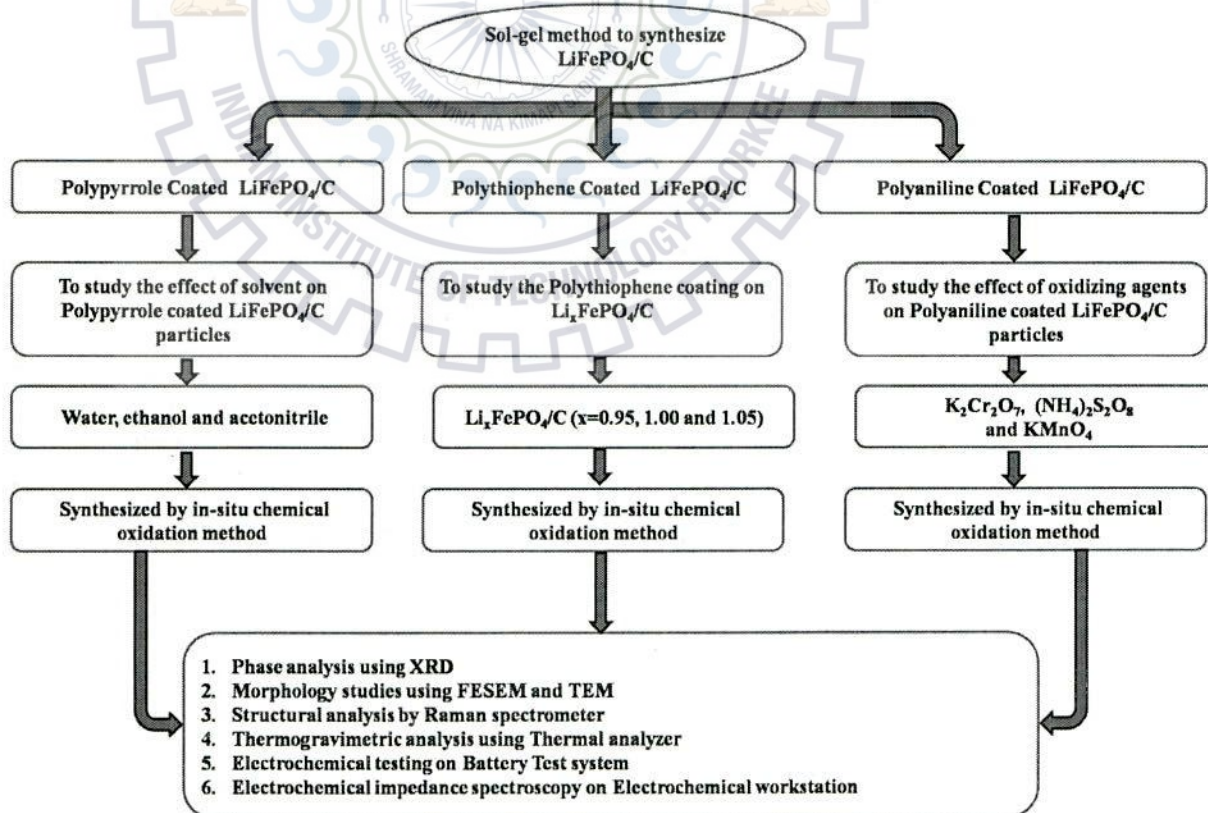
Fig. 3.1: Schematic flow diagram of experimental work.

3.1 Purification of monomers

In the presence of light or at room temperature aniline, pyrrole and thiophene monomers degrade or polymerize. Due to this monomers were purified before they were used for polymerization and remaining, of them are kept in brown bottle below 5 °C to avoid degradation. The photograph of purification process is shown in Fig. 3.2. The setup for purification consists of a round bottom flask (of capacity 500 ml) placed on a temperature controlled heater. The round bottom flask was connected to a straight condenser where cold water circulates using a pump placed in the cold water bath. The other end of condenser was inclined down and connected to a double neck round bottom flask. For the purification, monomers of aniline, pyrrole and thiophene were heated just above their boiling point. During the boiling, vapors of monomers pass through the condenser where they were condensed to pure liquid phase again and the purified liquid was collected on the double neck round bottom flask. After some time whole liquid was purified and impurities remain behind in the round bottom flask placed on the heater. All the monomers were purified three times before they were used for the polymerization.

Fig. 3.2: Arrangement for purification of monomers.

3.2 Materials synthesis

3.2.1 Synthesis of LiFePO₄/C

The synthesis of LiFePO$_4$/C was performed in two steps. In the first step, two solutions were prepared separately with 0.5 ml and 1.0 ml of aniline monomer (99.5 %, GR, Merck) containing 2.62 gm of (NH$_4$)H$_2$(PO$_4$) (99 %, GR, Merck) in 200 ml of millipore water. The mixing was carried out with the help of a magnetic stirrer for 30 minutes and during the process 3.7 gm of FeCl$_3$ (98 %, Merck) dissolved in 100 ml of millipore water was added dropwise into the solutions. NH$_4$Fe(HPO$_4$)$_2$ precipitates (white) start forming instantaneously in the solution.
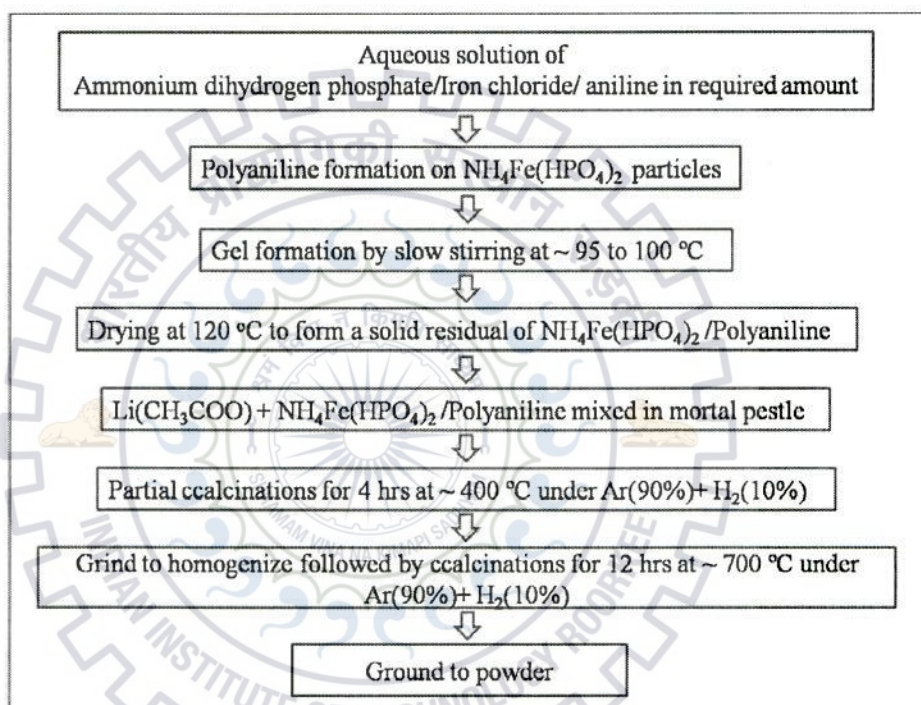
Fig. 3.3: Flow chart for the synthesis of LiFePO$_4$/C.

The white color of solution turns into light green due to the formation of polyaniline on the surface of NH$_4$Fe(HPO$_4$)$_2$ particles 4 hours after the addition of aqueous solution of FeCl$_3$. The solution was further heated for 2 hours at 65 °C to increase the growth of polyaniline and color of the solution changes from light green to dark green. The solution was heated between 95° and 100 °C under continuous stirring to evaporate the water content and after 6 – 8 hours of heating a dark green residue of solid polymer gel was formed on the surface of NH$_4$Fe(HPO$_4$)$_2$. In the second step, the synthesized material was ground in a pestle-mortar with Li(CH$_3$COO) (99 %, Loba chemie.) maintaining molar ratio of 1:1 between Li and Fe. The mixture was heated at 400 °C for 4 hours under the Ar(90%)+H$_2$(10%) gas flow and was further grinded in a pestle-mortar for 30 minutes to homogenize the mixture. The material was heated at 700 °C in a

tubular furnace for 15 hours under $Ar(90\%)+H_2(10\%)$ gas atmosphere. The calcined material was washed thoroughly with deionized water and acetone to remove chloride content to get pure $LiFePO_4/C$ powder.
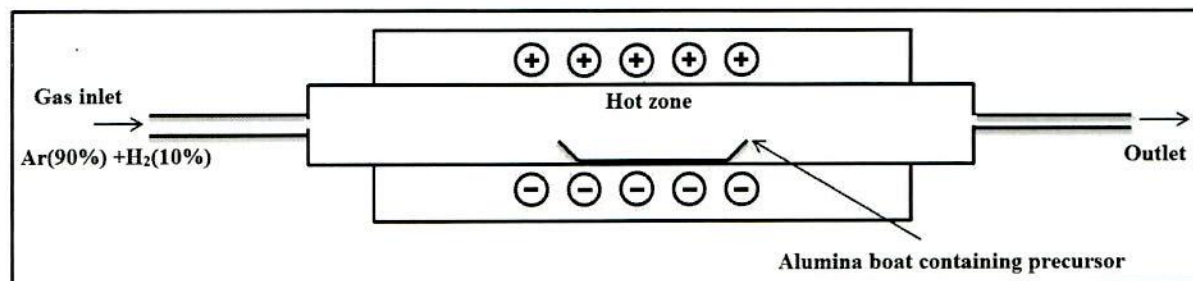
Fig. 3.4: Schematic of tubular furnace for calcination.

3.2.2 Synthesis of polypyrrole

For the synthesis of polypyrrole, three suspensions each one containing 1 ml of pyrrole (99.8 %, Sigma Aldrich) monomer in 40 ml of each solvent (water, ethanol and acetonitrile (ACN)) were prepared separately and stirred at 0-5 °C. In each suspension 0.95 gm of sodium p-toluene sulfonate (Na-PTSA) (99 %, Sigma Aldrich) was added. Further 7.25 gm of $FeCl_3$ dissolved in 20 ml of corresponding solvent was added dropwise in the suspensions prepared. The color of the solution changes from transparent to black on the addition of $FeCl_3$ solution showing the formation of polypyrrole precipitates inside the suspension. The molar ratio of the additive Na-PTSA to pyrrole was 1:3 and oxidizing agent to pyrrole was kept at 3:1. The reaction was carried out for 4 hours with continuous stirring. After 4 hours the solution was filtered and washed with their respective solvents. The filtered material was dried in vacuum oven for 12 hours at 60 °C.

3.2.3 Synthesis of polypyrrole coated $LiFePO_4/C$ composite

For the synthesis of polypyrrole coated $LiFePO_4/C$ ($LiFePO_4/C$-PPy) composites, 1 gm of $LiFePO_4/C$ powder was added into 40 ml solvent each of water, ethanol and ACN and was sonicated for 15 minutes to prepare the corresponding suspensions. 1 ml of pyrrole monomer was added in each suspension under continuous stirring at temperature between 0 – 5 °C. After homogenization for 30 minutes with continuous stirring, 0.95 gm of Na-PTSA was added in the above suspensions followed by the addition of $FeCl_3$ (7.25 gm) dissolved in corresponding solvents to each suspension. After 30 minutes of polymerization the solutions were filtered and washed with the corresponding solvents. The synthesized materials were dried in vacuum oven for 24 hours at 60 °C to get the $LiFePO_4/C$-PPy composite. The $LiFePO_4/C$-PPy composite

materials synthesized in each of ACN, ethanol and water solvents were designated as $LiFePO_4/C$-PPy(ACN), $LiFePO_4/C$-PPy(ethanol) and $LiFePO_4/C$-PPy(water). The detailed steps for the synthesis of $LiFePO_4/C$-PPy by chemical oxidation method are shown in Fig 3.5.
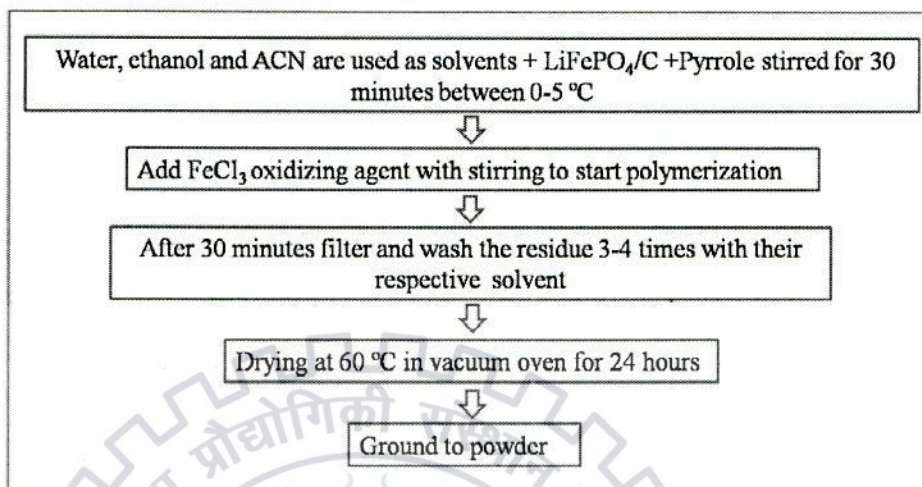
Fig. 3.5: Detailed steps for the synthesis of $LiFePO_4/C$-PPy.

3.2.4 Synthesis of Li_xFePO_4/C (for x = 0.95, 1.0 and 1.05)

For the synthesis of Li_xFePO_4/C (for x = 0.95 and 1.05) the molar ratio of Li and Fe was maintained at 0.95 : 1 and 1.05 : 1 respectively, while all other processing steps were remained same as described in the synthesis of $LiFePO_4$.

3.2.5 Synthesis of polythiophene coated Li_xFePO_4/C composites

The conducting polythiophene coated Li_xFePO_4/C was synthesized in CH_2Cl_2 and ACN binary organic solvents. 1 gm of Li_xFePO_4/C (x = 0.95, 1, 1.05, 1.10) powder was added in 50 ml CH_2Cl_2 solvent maintained at 0 °C. The suspensions were magnetically stirred for 30 minutes to homogenize and an addition of 0.5 ml thiophene to each of above suspension was made. A freshly prepared solution containing 4.01 gm anhydrous $FeCl_3$ (maintaining a molar ratio $FeCl_3$/thiophene = 4:1) in 25 ml ACN was added to the above suspensions of monomer units with continuous stirring. The polymerizations were carried out for 30 minutes at 0 – 5 °C without stirring. All the three suspensions were filtered and washed several times with acetone and then with ACN. The materials were dried after washing in vacuum oven at 60 °C for 24 hours to get the polythiophene coated Li_xFePO_4/C (x = 0.95, 1, 1.05, 1.10). The various steps for the preparation of $Li_{0.95}FePO_4/C$-PTh are mentioned in the flow diagram (Fig. 3.6).

Different amounts of thiophene monomer were added in the above process with a fixed amount of $Li_{0.95}FePO_4/C$ to deposit different amounts of polythiophene in $Li_{0.95}FePO_4/C$-PTh composite.
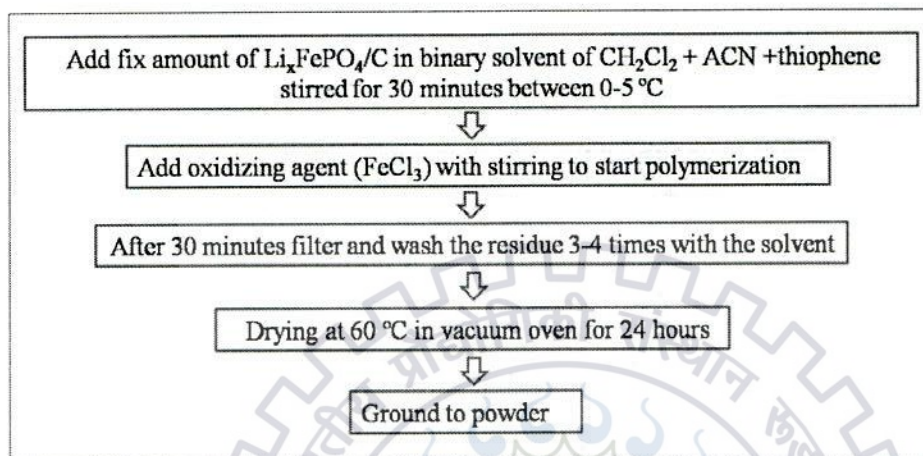
Fig. 3.6: Detailed steps for the synthesis of $Li_{0.95}FePO_4/C$-PTh.

3.2.6 Synthesis of polyaniline coated LiFePO₄/C

Polyaniline coated $LiFePO_4/C$ composite material was synthesized by polymerization of aniline monomers using different oxidizing agents viz. $(NH_4)_2S_2O_8$, $KMnO_4$ and $K_2Cr_2O_7$. A precursor solution was prepared by adding fixed amount of $LiFePO_4/C$ material in 100 ml water containing 2 ml aniline monomers under continuous stirring.
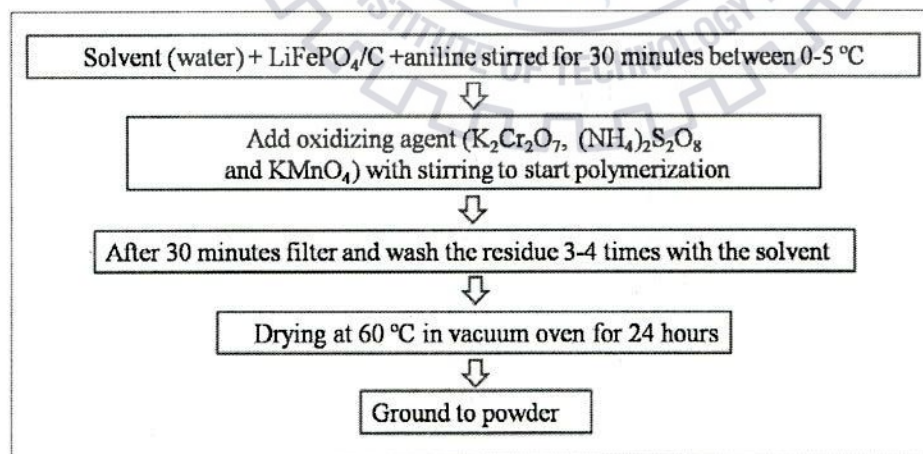
Fig. 3.7: Flow diagram of the synthesis of Polyaniline coated $LiFePO_4/C$.

Precooled aqueous solutions of oxidizing agents $(NH_4)_2S_2O_8$, $KMnO_4$ and $K_2Cr_2O_7$) weighing 10 wt% of aniline monomers were prepared. These oxidizing agents and HCl (2 mol) were added in the above precursors with continuous stirring in order to proceed the reaction for 30

minutes at 0–5 °C. The particles was filtered and washed with millipore water and acetone. Final material was obtained by drying the powder in vacuum oven at 60 °C for 24 hours.

3.3 Physical characterization

3.3.1 X-ray diffraction

The X-ray diffraction (XRD) is a characterization technique which can be used for determination of different properties of matter such as crystal structure, residual stress, grain size, grain orientation etc. When a X-ray beam is incident on a crystal it produce beams at specific angles depending on the wavelength of X-ray, crystal orientation and crystal structure (*d*) in accordance with the Bragg law. The Bragg's law is written as:

$$n\lambda = 2dSin\theta \qquad (3.1)$$

where *n* is an integer, λ wavelength of X-rays, *d* the inter-planer spacing in the crystal structure and θ the diffraction angle. The different atomic planes in the crystal structure act as the diffraction grating and the reflected beams interfere constructively while they satisfy the Bragg's relation (3.1).
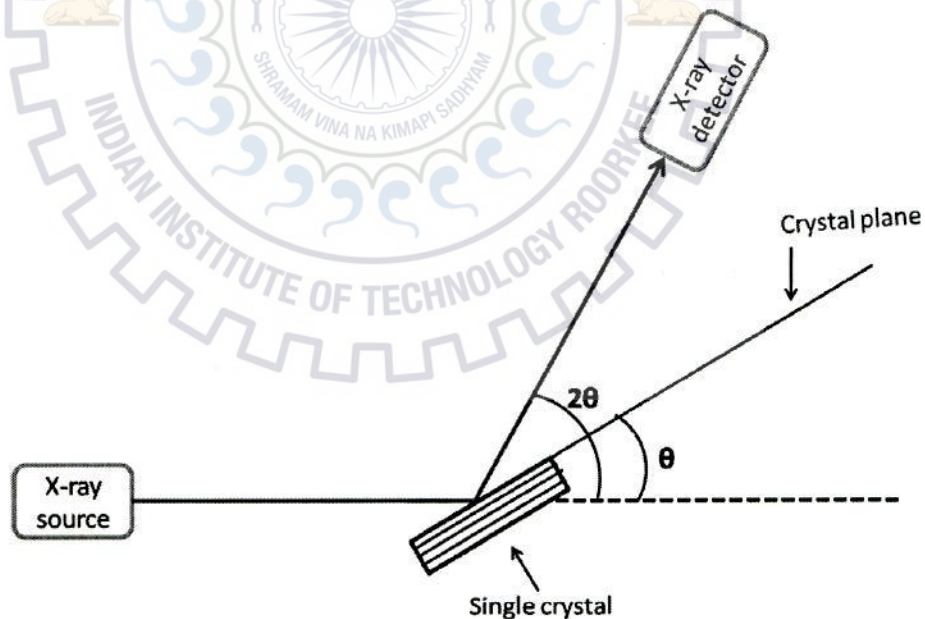
Fig. 3.8: Schematic of diffraction of X-rays by a crystal.

This relation (3.1) demonstrates that diffraction effects are observable only when wavelength of interacting radiation is approximately of same size as the size of the grating. Since the distances between atoms or ions are of the order of 10^{-10} m, the diffraction method requires X-rays with similar wavelengths region of the electromagnetic spectrum. Through X-ray spectra one can

identify the different phases and their lattice parameters. Since for a crystal d is fixed the Bragg's law can be devised by continuously varying either λ or θ during the experiment. There are three main diffraction methods depending upon the way in which λ and θ varied. Laue method was the first diffraction method ever used in which a beam of white X-ray (of varying λ) is allowed to fall on a fixed single crystal. For a fixed crystal θ is fixed so a particular set of planes diffract that particular wavelength which satisfies Bragg's law. Therefore in *Laue method* the diffracted beam has a different wavelength. In *Rotating crystal method* a single crystal is mounted with one of its axes perpendicular to the monochromatic X-ray beam.

A cylindrical film is placed around this crystal and the crystal is rotated about the chosen direction. During rotation of the crystal a particular set of lattice planes will make the correct Bragg angle for reflection. The reflection intensities are located on the imaginary cones with axis coincident with the axis of rotation of single crystal. The *Rotating crystal method* can be used to determine the unknown crystal structure. In *Powder diffraction method* the crystal to be examined is reduced to a very fine powder and placed in the path of a monochromatic X-ray. Each particle of the powder is a tiny crystal oriented at random with respect to the incident beam. Just by chance, some of the particles will be correctly oriented. This pack of fine powder is equivalent in fact to a single crystal rotated not about one axis but about all possible axes. Every particle of the powder is a tiny crystal oriented at arbitrary with respect to the incident beam. Just by chance, some of the particles will be suitably oriented so that their particular set of planes, can reflect the incident beam. Other particles will be correctly oriented for other set of planes and so on. The method is especially recommended for determining lattice parameters with high precision and for the identification of phases, whether they occur alone or in mixtures such as alloys and compounds. The relative intensity of diffraction beam of the powdered sample is affected by six factors viz. polarization factor, structure factor, multiplicity factor, Lorentz factor, absorption factor and temperature factor. On the basis of these six factors the intensity of diffracted beam in the powder method can be determined by using the relation:

$$I = |F|^2 p \frac{1 + \cos^2 2\theta}{\sin^2 \theta \cos 2\theta}$$

(3.2)

where I = relative integrated intensity, F = structure factor, p = multiplicity factor, and θ = Bragg angle.

XRD patterns of samples were obtained on X-ray diffractometer (Bruker AXS, D8 advance) using CuK_α radiations (λ = 1.5418 Å) with a scanning rate of 1.5 °/min and the phase analysis of the pattern was performed using XRD software (PANalytical, X'Pert HighScore Plus 2.2.0). The measured diffraction patterns were compared to powder diffraction files of ICDD database.

3.3.2 Thermogravimetry (TG) analysis

Thermogravimetry (TG) analysis is a thermal analysis technique by which mass of a sample is measured as a function of temperature while the sample is subjected to a controlled temperature program. During the record of a TG curve, mass is normally plotted on the y-axis and temperature or time is on x-axis. TG data can also be represented as the derivative of TG which is known as differential thermogravimetry (DTG) curve, which is a plot of rate of change of mass with respect to time or temperature against time or temperature respectively. TG is a quantitative technique and can be used to estimate the amount of a particular substance present in the mixture. In the present study TG analysis has been performed for the $LiFePO_4/C$ to estimate the carbon content and for polymer coated $LiFePO_4/C$ to estimate polymer content in their respective samples. TG of samples $LiFePO_4/C$ was performed in air atmosphere from room temperature to 750 °C by heating at 10 °/min. The polymer contents in the samples were estimated by TG analysis in the argon gas atmosphere from room temperature to 800 °C at the heating rate of 10 °/min and the samples were held at that temperature for 3 hours to decompose all the polymer content. All the TG measurements of the samples were performed using thermal analyzer (Seiko Instruments, EXSTAR TG/DTA 6300). The other processes such as oxidation, reduction, sublimation, decomposition etc can be investigated by the TG technique. The only limitation of this technique is that it does not give information about the reactions that do not have mass change with respect to temperature.

3.3.3 Scanning electron microscope

The scanning electron microscope (SEM) is an electron microscope in which a magnetically controlled beam of electron is directed towards the specimen. When a beam of electrons fall on to the specimen, different types of signals such as secondary electrons (SE), back scattered electrons (BSE), X-rays etc. are emitted by the specimen.
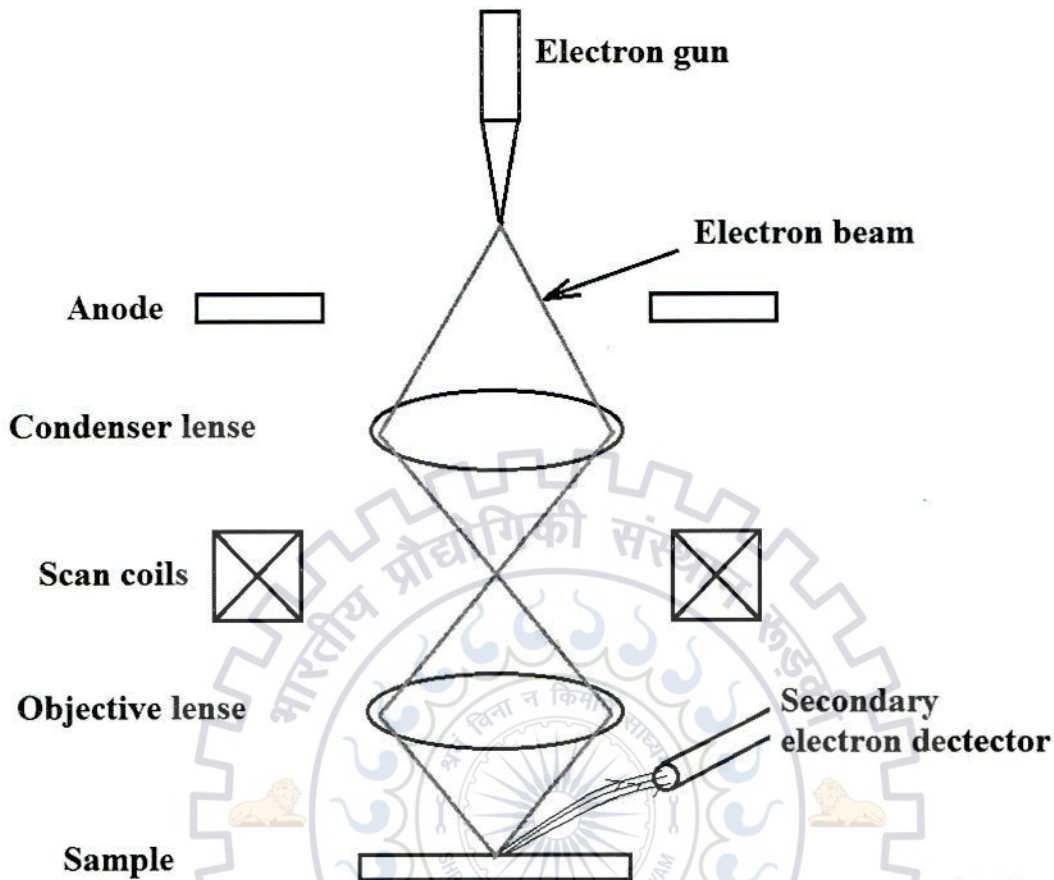
Fig. 3.9: Schematic diagram of SEM.

A SEM can be used for imaging purpose in SE mode, compositional analysis in the BSE mode and elemental analysis in the X-rays mode of detection. Since in a SE mode the specimen emits a large number of secondary electrons coming out from the outer surface, therefore this mode is used to study the topography of the specimen. In the BSE mode the intensity of back scattered electron depends on the atomic number of specimen, so this mode is employed to compositional analysis of the specimen. A specimen with different compositions gives rise to different *atomic number contrasts* by using BSE. Further energy dispersive spectroscopy (EDS) can be performed for elemental analysis of the specimen. The SEM is equipped with EDS detection system which detects the X-ray signals emitted by the specimen. When an electron jumps from higher energy shell to lower energy shell of an atom, an X-ray photon is emitted which is a characteristic property of an element. The EDS spectrum has intensity counts on y-axis and energy spectrum of X-rays signals on x-axis. The EDS detector is a Si-Li semiconductor fitted with a beryllium window. The beryllium window allows to enter the

signals coming from elements with atomic number greater than that of beryllium but for signals coming out from the elements having atomic number less than beryllium do not have sufficient energy to pass the beryllium window. Due to this reason the signals from hydrogen, helium and beryllium itself are not detectable.

The LiFePO$_4$/C and polymer coated LiFePO$_4$/C were studied using SEM built-in with field emission gun (FESEM). The FESEM microscopy was performed to examine the morphology of carbon coating and polymer coating on LiFePO$_4$ particles. The powdered samples were dispersed on the double sided carbon tape pasted on the aluminium stub. To avoid charging of the sample during microscopic observation, the dispersed material on metallic stub was gold coated by sputtering for 50 seconds with a deposition current of 30 mA using a BAL-TEC (SCD 005) sputter coater. A FEI Quanta 200F, was used at an accelerating voltage of 25 kV with a working distance of ~ 10 mm.

3.3.4 Transmission electron microscope (TEM)

Transmission Electron Microscope (TEM) is an electron microscope in which a high energy beam of electron passes through a thin specimen (< 100 nm). The electron beam interacts with the specimen during the transmission and a highly magnified image is projected on to the fluorescent screen or to be detected by a charged coupled device camera. The electron beam was controlled by the different magnetic lenses which are free from most of optical defects.

A TEM generally consists of one condenser lens as collimator to (control the spot size and intensity) electron beam before it comes to specimen, and a few objective and projector lenses to magnify the image. Depending on the position of first projector lens there are two different modes of operation of TEM which are *image mode* and *diffraction mode*. In the *image mode* first projector lens is focused on image plane of the objective lens where as in the *diffraction mode* it is focused in the back focal plane of the objective lens as shown in Fig. 3.10. The high resolution transmission electron microscopy (HR-TEM) is the imaging mode of TEM that allows the direct imaging of atomic planes of specimen. The high quality HR-TEM images can only be obtained for highly crystalline, extremely thin or well dispersed powdered specimens. If an electron beam of high energy is incident on a very thin and crystalline specimen it will be elastically scattered by some of the constituent atoms. The electron beam can be considered as a wave motion and can be diffracted in a similar way as of light or X-rays. So the diffraction pattern of electron beam must satisfy the Bragg's relation (3.1).
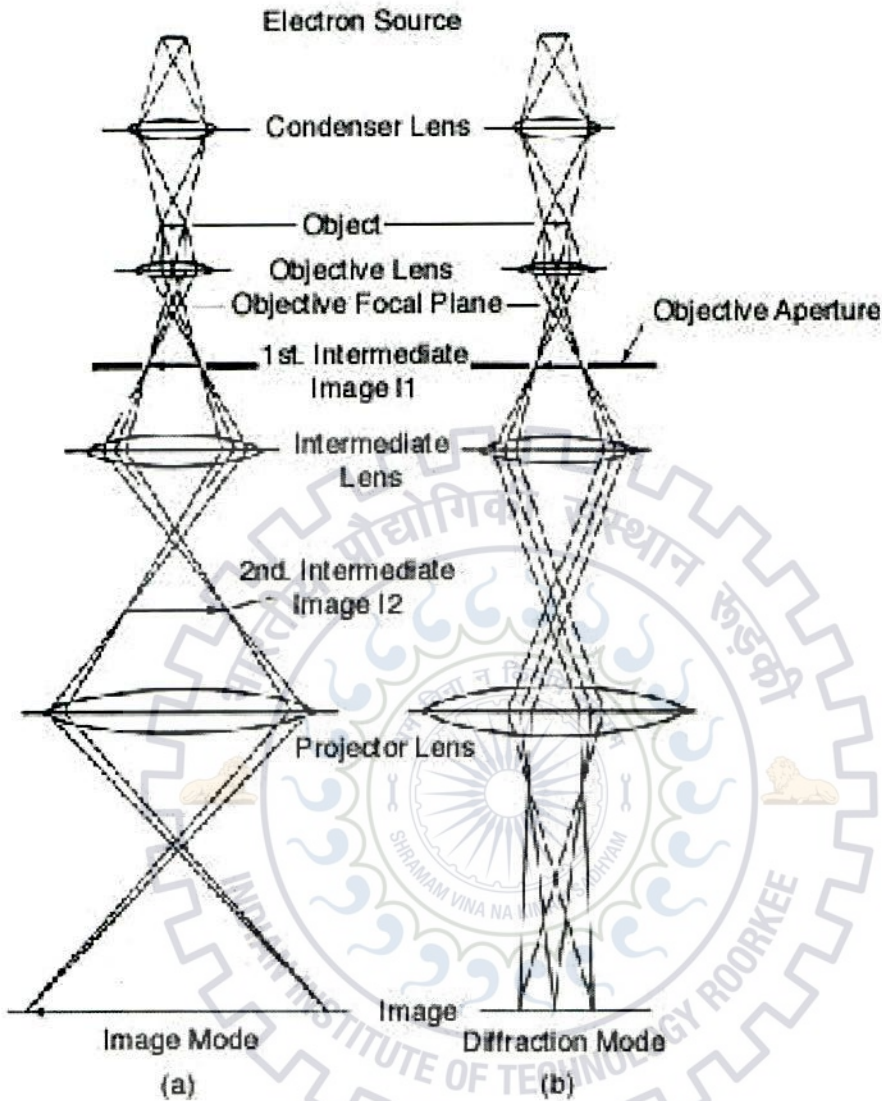
Fig. 3.10: Ray diagram of *Image* and *Diffraction mode* of TEM.

Since, a very short wavelength (λ=0.0037 nm for an operating voltage of 100 kV) of electrons used in the TEM and for most of the cases interplaner spacing (d) ~ 0.4 nm, then from Bragg's law, the diffraction angle (2θ) = 0.26 °. Hence, there will be strong diffraction pattern from the planes which are almost parallel to the electron beam. For small values of θ the Bragg's law can be written as:

$$n\lambda = 2d\theta \tag{3.2}$$

The diffraction pattern of a single crystal specimen consists of a periodical array of spots arising from the several sets of planes parallel to the electron beam. If the specimen is a

polycrystalline material then diffraction pattern is the sum of individual patterns and the spots are not randomly distributed but fall on the concentric rings. To understand the final image on the camera there are different contrast mechanisms, which contribute to the appearance of the TEM image. In the *diffraction contrast* intensity of scattering is greatly increased for particular orientations of the specimen. The objective aperture can then be used to form the image thus giving strong and weak contrast from the regions which are diffracting strongly and weakly respectively. *Mass-thickness contrast* arises because of areas of higher atomic number or greater thickness, which scatter electrons more strongly thereby appearing dark in bright-field images and bright in dark-field images. It is particularly useful for imaging non-crystalline materials (such as polymers) and biological samples. If the objective aperture is allowed to stop all the diffracted beam then background of the image will be bright, this is known as *bright field* imaging. If the objective aperture is allowed to select the diffracted beam then background of the image will be dark, this is known as *dark field* imaging. The morphology of LiFePO$_4$/C, carbon coating, and polymer coating on the LiFePO$_4$ particles were observed using TEM (FEI-TECHNAI-20) with an accelerating voltage of 200 kV. The samples of LiFePO$_4$/C and polymer coated LiFePO$_4$/C were prepared by dispersing a small amount of powder in ethanol followed by the ultrasonication. A few drops of suspension were placed on the carbon-coated copper grids and were allowed to dry under vacuum.

3.3.5 Vibrational spectroscopy

Raman and infrared (IR) spectroscopies are referred as vibrational spectroscopy. The techniques of Raman and IR have some similarities, yet they are governed by completely different selection rules. IR bands arise from an interaction between light and the oscillating dipole moment of a vibrating molecule, whereas Raman bands arise from an oscillating induced dipole caused by light interacting with the polarizability of a vibrating molecule. Because of wide variety of chemical structure and physical ordering present in the polymer systems, the vibrational spectroscopy is quiet interesting for these systems. The different applications of vibrational spectroscopy are that, it can be used, 1) as an identification tool for the complex polymer systems, 2) to determine the polymer structures in the wide range of length scale such as stereoregularity, chain conformation and crystallinity, 3) to determine other dynamic properties such diffusion and electronic conductivity [C.M. Snively and J.L. Koenig, 1999].

3.3.5.1 Raman spectroscopy

The Raman spectroscopy is based on inelastic or Rayleigh scattering of monochromatic light or laser from the molecular levels of a specimen. A very small amount of the scattered light (ca. 10^{-5} % of the incident light intensity) is shifted in energy from the laser frequency due to interaction between the incident electromagnetic waves and the vibrational energy levels of the molecules in the sample. In particular, the vibrational state of molecule changes as shown in Fig. 3.11. The scattering of light from a molecule results in the frequency shift which is known as Raman effect. Plotting the intensity versus shifted frequency results in Raman spectrum of a sample.

A Raman spectrometer typically consists of four major components viz, 1) excitation source (laser), 2) sample illumination system and light collection optics, 3) wavelength selector (filter or spectrophotometer), 4) detector (CCD). A sample is normally illuminated by a laser beam in the ultraviolet, visible or near infrared range of the electromagnetic spectrum. Scattered light is collected by a lens and is sent through interference filter to obtain Raman spectrum of a sample.
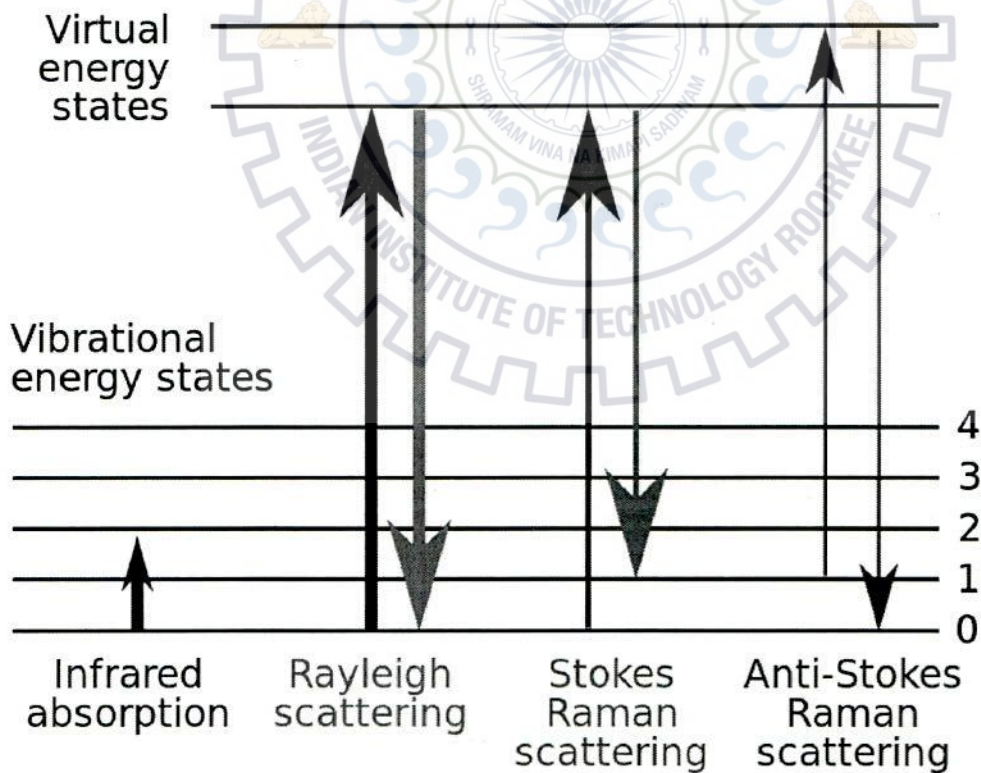
Fig. 3.11: Transition between two energy levels having different vibrational levels.

The major Raman active modes of vibration for carbon which generally appears at 1359 cm^{-1} and 1580 cm^{-1} are assigned to D-band and G-band respectively [Sood et al, 2001]. The peak associated to D-band is related to defect or disorder present in the graphitic carbon. The defects may be of diamond like (sp^3-hybridised) carbon or may be due to poor graphitization of carbon [Rengan et al, 1992]. The ratio of peak intensity of D-band to G-band is an indicator of the extent of defect structure in the graphite. The Raman spectroscopy is useful to determine conducting properties of polymers such as polypyrrole, polythiophene and polyaniline by the formation of polaron and bipolaron polymer structures. Raman confocal micro-spectrometer system (in Via, Renishaw) was used to characterize the carbon coating on the samples for its graphitization and polymers deposited in the LiFePO$_4$/C-PPy composites. The samples were illuminated using He-Ne laser of wavelength of 514 nm as the excitation source to obtain Raman spectra. The spectra data were further processed using Renishaw WIRE 2.0 software. The peak de-convolution and Gaussian curve fitting were performed using Origin 8.0 software.

3.3.5.2 IR spectroscopy

IR spectroscopy is very useful technique to determine the polymer structures. A unique problem which Raman spectroscopy faces is that most of the polymers fluoresce strongly when exposed to the laser radiation. Because of this difficulty associated with Raman spectroscopy the quality of Raman spectra of fluorescent polymers is typically less than IR spectra. This problem can be reduced by using IR spectroscopy.
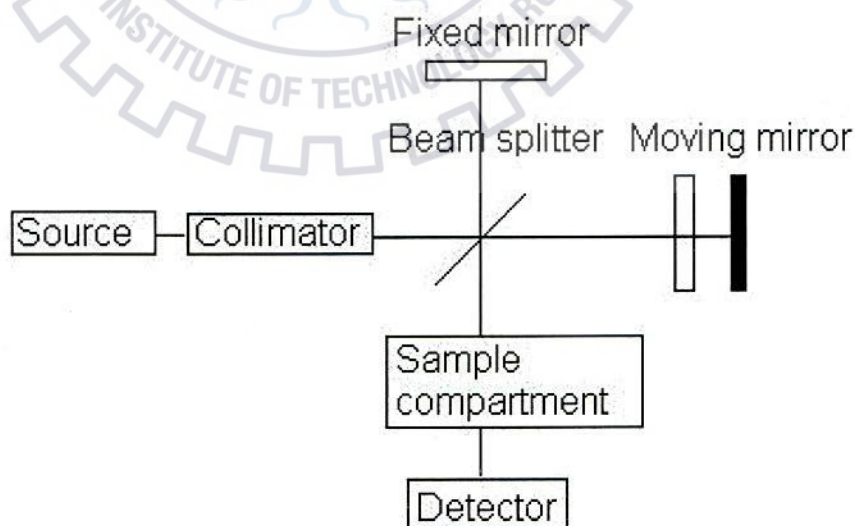
Fig. 3.12: Schematic diagram of IR spectrometer.

IR spectroscopy is sensitive to many chemical groups that possess the significant dipole moment such as C-H and C=O which are commonly found in polymers. An IR spectrometer

usually consists of an excitation source, sample compartment, a set of mirrors and detector. The schematic diagram of IR spectrometer is shown in Fig. 3.12. Solid sample is mixed with potassium bromide. This powder is then compacted into a thin pellet which is analyzed under spectrometer. The polymer gel of polyaniline was characterized using IR spectrometer (UV-1500, Shimadzu Japan).

3.4 Electrochemical measurements

3.4.1 Preparation of electrode

Cathodes were prepared for the testing of $LiFePO_4/C$, $LiFePO_4/C$-PPy, $LiFePO_4/C$-PTh and $LiFePO_4/C$-PANI materials. Slurry was prepared out of the active material (80 wt%), polyvinylidene fluoride (PVDF) binder (10 wt%) and carbon black (10 wt%). Initially the active material and carbon black were dry mixed and then slurry was made by adding binder mixed with N-methyl-2-pyrrolidinone (NMP).
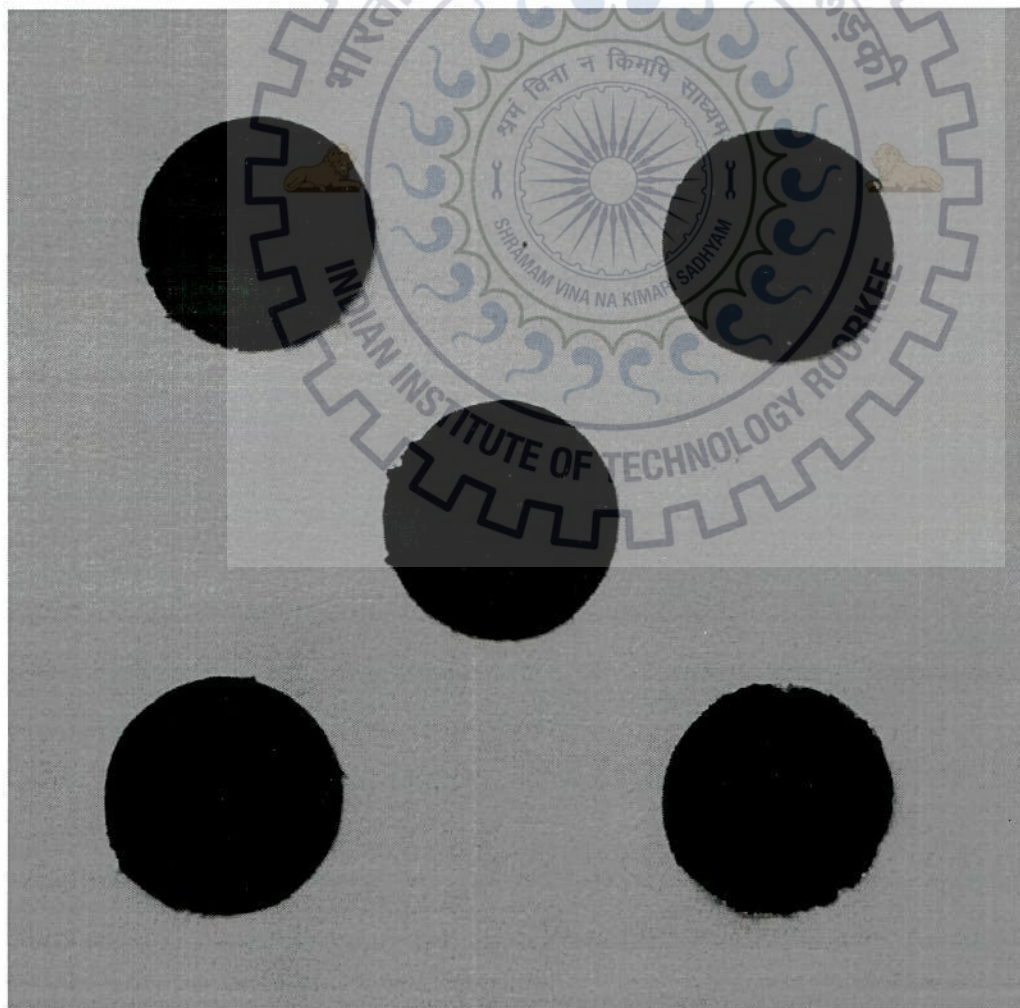
Fig. 3.13: Cathodes used in the cell testing.

The slurry was spread uniformly onto an aluminum foil using doctor blade technique. The material on the foil was dried at 80 °C for 24 hours under vacuum and was pressed using a hydraulic press for 30 seconds at a pressure of 500 kN/m^2 to develop good adherence of the cathode material with the foil. The foil coated with the material was punched into a circular disk having an area of 1 cm^2 containing the $1 - 3$ mg/cm^2 of the cathode material.

3.4.2 Cell fabrication

Teflon cell was assembled for the electrochemical testing of the cathodes prepared. A lithium foil used as a counter electrode was placed with a polypropylene microporous separator (Celgard 2400) membrane. The movement of Li-ion was through the electrolyte prepared by dissolving LiPF$_6$ (1M) in a solution of ethylene carbonate and dimethyl carbonate (EC/DMC=1:1 v/v) (Mitsubishi Chemical Corp.). The cell was assembled in an argon gas filled glove box (MBRUN, MB 200 G) with controlled atmosphere maintaining both oxygen and moisture contents less than 0.1 ppm. The complete schematic diagram of the cell is shown in Fig. 3.14.
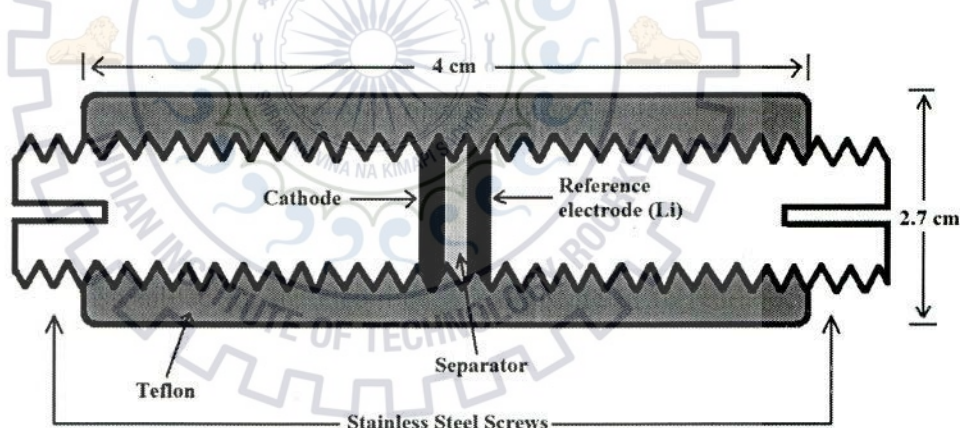
Fig. 3.14 Schematic diagram of Teflon cell used for the electrochemical testing.

3.4.3 Electrochemical testing

The electrochemical testing of LiFePO$_4$/C, LiFePO$_4$/C-PPy, LiFePO$_4$/C-PTh and LiFePO$_4$/C-PANI has been performed on the Teflon cell. After the Teflon cell assembling it was kept undisturbed in the glove box for 6 to 7 hours to get stabilized through soaking of electrolyte by cathode and anode electrodes. Soaking of electrolyte essentially improves the ionic contact between electrode and electrolyte. After stabilization the cell was connected to the battery test system (Arbin Instruments, BT-2000).

3.4.3.1 Measurements of capacity and cyclability

The discharge capacities of the cathode of $LiFePO_4/C$, $LiFePO_4/C$-PPy, $Li_{0.95}FePO_4/C$-PTh and $LiFePO_4/C$-PANI can be calculated by cell testing at different C-rates on the battery test system. 1C-rate is defined as the rate at which a cathode of capacity X mAh, while discharging under ideal condition should deliver a current of X mA for 1 hour. Since the theoretical capacity of $LiFePO_4$ is 170 mAh/g, therefore the electrode of $LiFePO_4$ is to deliver a current of 170 mA for 1 hour. The charging and discharging of the cell was tested in the potential window of 2.2 to 4.2 V (vs Li^+/Li) at different C-rates of 0.1C, 0.2C, 0.5C, 1C, 2C, 5C, 10C and 20C. The constant current is applied to the battery and the resulting change in the cell potential as a function of time is measured. For a single complete charge / discharge cycle the gravimetric capacity is derived from the total charge passed per unit mass of the active material and can be calculated as:

$$Capacity = \frac{I \times t}{m}$$

(3.3)

where I (mA) is the current at which the cell has been tested, t is time in hours and m is weight of active material in gram.

To measure the cyclability of the active material, the cells have been tested for 50 cycles at a particular C-rate and the percentage capacity failure after 50th cycle was calculated for each electrode. The cyclability measurements for all the samples were performed at 2C rate and the cells were also tested from 2.2 to 4.2 V.

3.4.3.2 Differential capacity

In order to investigate the rate capability of polymer coated $LiFePO_4/C$ composites, a factor 'differential capacity (DC)' as expressed below, has been devised

$$DC = \frac{Discharge\ capacity\ of\ LiFePO_4/C(PPy) - Discharge\ capacity\ of\ LiFePO_4/C}{Discharge\ capacity\ of\ LiFePO_4/C}$$

(3.4)

3.4.3.3 Cyclic voltammetry measurement

Cyclic voltammetry (CV) measurement of the samples of $LiFePO_4/C$ has been performed from 2.2 to 4.1 V at a constant voltage rate of 0.1 mV/s. The cyclic voltammogram is a plot of

voltage along x-axis and current on y-axis, and consists of a pair of oxidation / reduction peaks. The good overlapping of each cycle of a CV measurement reveals little capacity loss per cycle. The oxidation / reduction peaks are always symmetric to the theoretical discharge voltage of the active material of the electrode. The narrow potential difference between oxidation / reduction peaks reflects the small polarization of electrode resulting in higher reversibility.
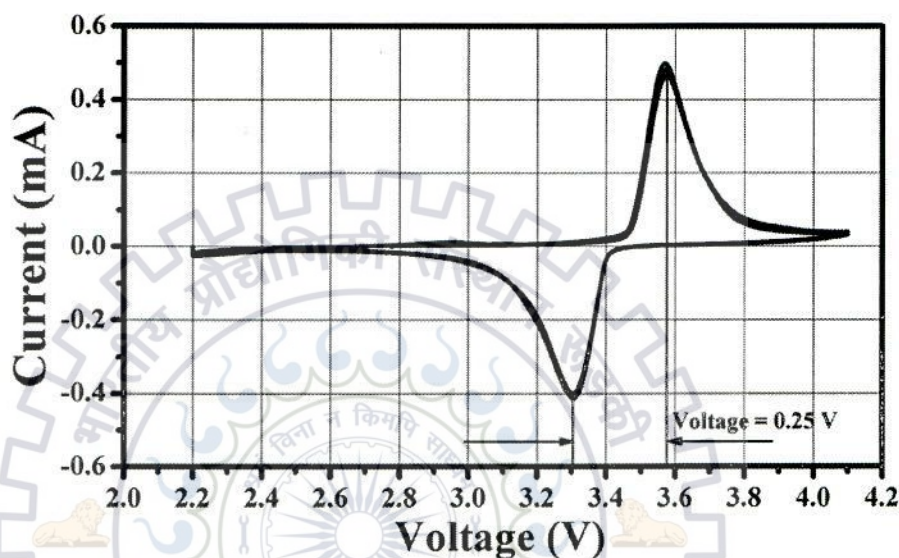
Fig. 3.15: Cyclic voltammogram of $LiFePO_4$.

3.4.3.4 Electrochemical impedance spectroscopy (EIS)

Electrochemical Impedance Spectroscopy (EIS) is a widely used technique to investigate electrochemical systems. EIS provides several informations such as grain boundary geometry, thickness of electrically-active grain boundaries, and conduction mechanism at grain and grain boundaries [Biendicho and West, 2012]. Generally, a sinusoidal alternate voltage excitation signal of amplitude 5 mV is applied to the system under study during an EIS experiment and the alternate voltage response is measured. The Nyquist plot of the EIS measurement is the plot of Imaginary vs real parts of the complex impedance of the cell at different frequencies of measurement. The plot consists of a semicircle or depressed semicircle starting from high frequency to intermediate frequency and a straight line in the low frequency region. The profiles of impedance spectra can be explained by equivalent circuit of the Nyquist plot shown in the inset of Fig. 3.16 [Mukherjee et al, 2013]. The high frequency intercept (Fig. 3.16) on real impedance axis corresponds to resistance (R_s) of the electrochemical cell, offered by the separator, electrolyte and at interface of electrode and current collector [Mahajan et al, 2011]. Medium frequency intercept on real impedance axis corresponding to R_{ct}. The R_{ct} is attributed

to charge transfer resistance offered during the electrochemical reaction of cell which is associated with the electrode / electrolyte interface and particle / particle contact resistance during the electrochemical reaction of the cell [Chen et al, 2014]. The straight line starting from the edge of medium frequency side of semicircle to low frequency region corresponds to Warburg impedance (Z_ω) which reflects the Li-ion diffusion in the cathode electrode. R_{ct} represents all Faradic reactions that occur on the electrode surface. These reactions can be reversible or irreversible. In contrast, *constant phase element (CPE)* describes non Faradic charge storage mechanisms and is angle made by the straight line with x-axis in the Warburg region of Nyquest plot [Katare et al, 2005]. The Nyquist plot can be simplified by using the model of electronic equivalent circuit. The electronic equivalent circuit has R_s in series with a parallel combination of *CPE* and R_{ct} in series with Z_ω [Katare et al, 2003].
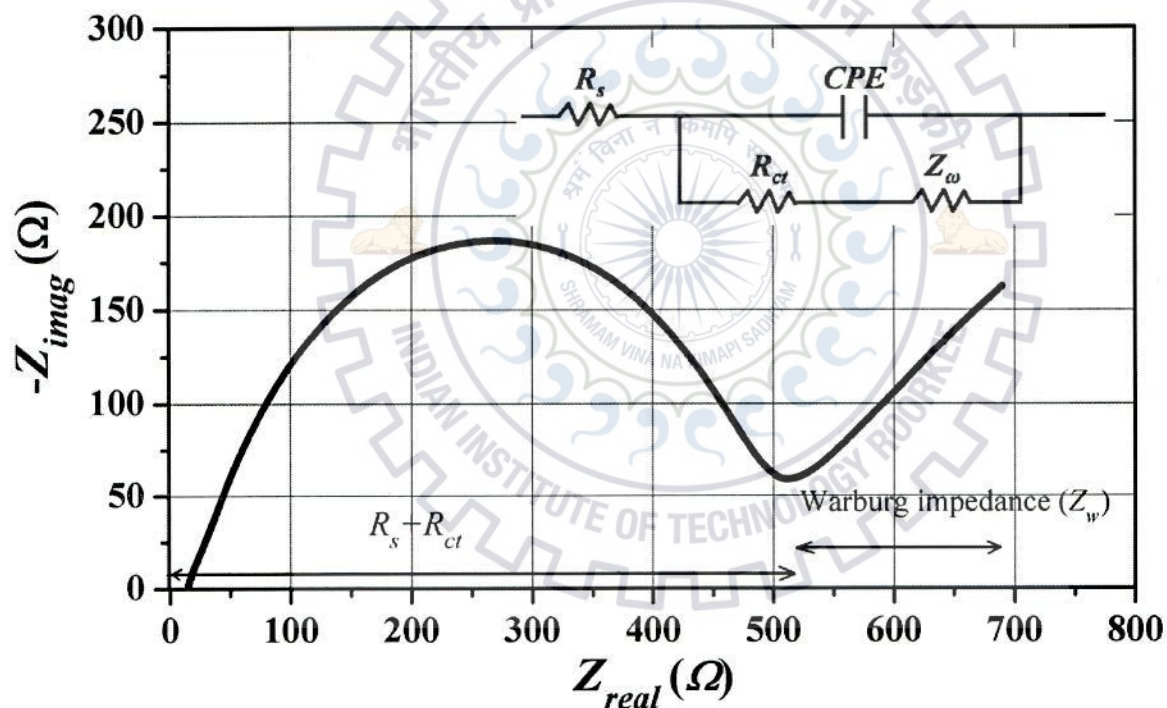
Fig. 3.16: Nyquest plot of EIS measurement of a sample of LiFePO$_4$.

All the EIS analyses of the cells were carried out on the electrochemical workstation (Gamry Instruments, INTERFACE 1000) in the frequency range from 0.1 Hz and 100 kHz and at a voltage of amplitude 0.5 mV. The diffusivity of Li-ion (D_{Li+}) has been calculated in the low frequency region of EIS using the expression.

$$D_{Li^+} = \frac{R^2 T^2}{2 A^2 n^4 F^4 c^2 \sigma_\omega^2} \tag{3.5}$$

where R is gas constant (8.314 J mol^{-1}K^{-1}), T is absolute temperature (300 K) of electrode during measurement, A is area of cathode–electrolyte interface, n is the number of electrons per molecule during oxidization (for LiFePO$_4$, $n=1$), F is the Faraday constant (96487 Coulomb mol^{-1}), c is the molar concentration of lithium ion (mol cm^{-3}), σ_ω is the Warburg factor. Warburg factor can be calculated from the following relation

$$Z_{real} = R_s + R_{ct} + \sigma_\omega \omega^{-1/2} \tag{3.6}$$

The slope of the plot Z_{real} vs. $\omega^{-1/2}$ in the low frequency region yields the σ_ω where ω is the angular frequency of the applied alternating current. The electrochemical reversibility can be estimated by exchange current density (i_0) factor of the electrode and can be calculated as [Sarkar et al, 2013]:

$$i_0 = \frac{RTA}{nFR_{ct}} \tag{3.6}$$
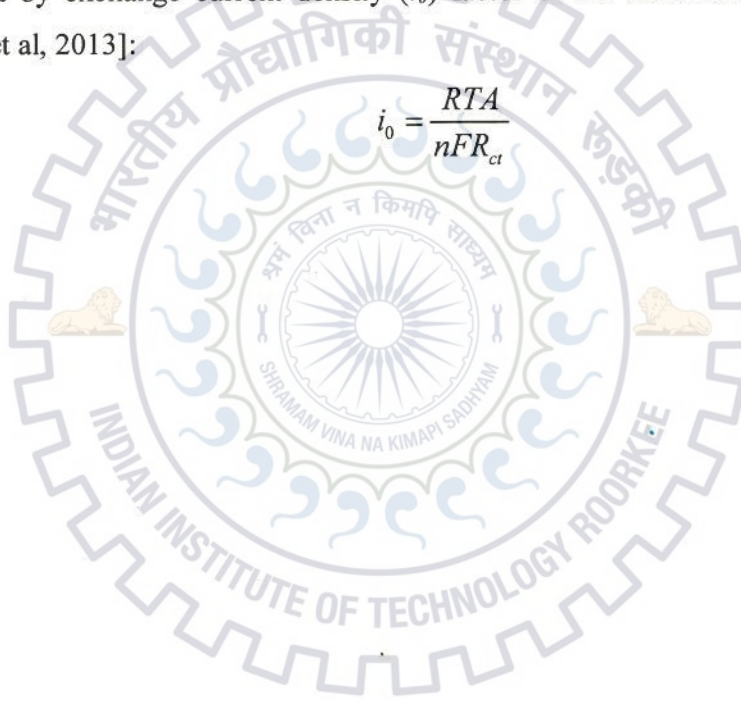
RESULTS AND DISCUSSION-
PRISTINE LiFePO$_4$/C

RESULTS AND DISCUSSION-PRISTINE LiFePO₄/C

This chapter presents the results and discussion on the synthesis and characterization of carbon coated $LiFePO_4$. The carbon coated $LiFePO_4$ was prepared by in-situ polymerization of polyaniline on sol-gel synthesized $(NH_4)Fe(HPO_4)_2$ followed by complete decomposition of polyaniline into carbon coating. The process of synthesis has been described in previous chapter (Chapter 3). The process adopted in the present work has yielded well graphitized and uniform carbon coating. The results and discussion on synthesis and characterization are described in the following sections.

4.1 Analysis of physical characterization

4.1.1 Structural analysis of polymer gel coated $(NH_4)Fe(HPO_4)_2$

The XRD patterns of as synthesized polymer gel coated $(NH_4)Fe(HPO_4)_2$ are shown in Fig. 4.1. The polymer gel formation was considered in two cases of 0.5 ml aniline and 1.0 ml of aniline additions during the formation of $(NH_4)Fe(HPO_4)_2$.
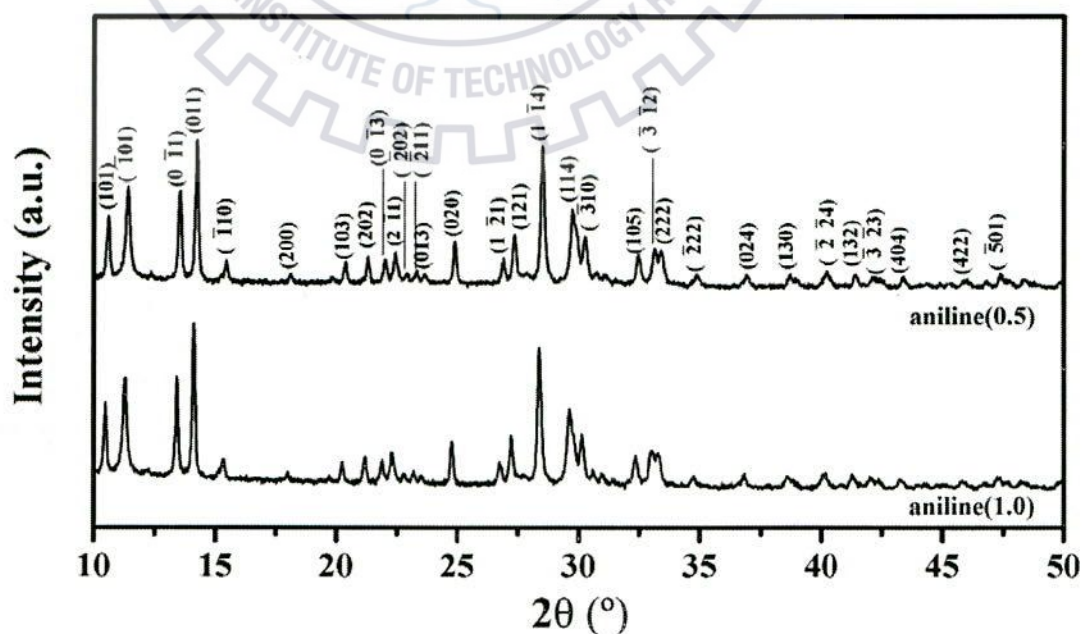

Fig. 4.1: XRD patterns of aniline (0.5) and aniline (1.0) samples.

The polymer gel coated $(NH_4)Fe(HPO_4)_2$ synthesized with 0.5 ml aniline and 1.0 ml aniline are designated as aniline(0.5) and aniline(1.0) respectively. The peaks of the XRD patterns correspond to the phase $(NH_4)Fe(HPO_4)_2$ and are matched with data base file JCPDS No. 01-085-1141 implying the formation of single phase material. The broad and low intensity polyaniline peak which appears at ~ 25 ° is not observed in the XRD patterns (Fig. 4.1) [Singla et al, 2011]. This is perhaps due to negligible contribution of the polyaniline content to give rise to perceptible intensity in the XRD pattern.

4.1.2 Morphology of polymer gel coated $(NH_4)Fe(HPO_4)_2$

The FESEM micrographs of the solid polymer gels are shown in Fig. 4.2 which reveal the layered morphology of the polyaniline formed on the surface of $(NH_4)Fe(HPO_4)_2$ particles. The FESEM micrograph confirms that the average particle size of the sample aniline(1.0) is < 100 nm and is smaller than that of sample aniline(0.5) which have particle size in the range of 300 to 400 nm. This is due to the fact that if the amount of initially added aniline monomer is higher, then the amount of the polyaniline also becomes higher which pose an early limitation on the $(NH_4)Fe(HPO_4)_2$ growing particle. Hence the $(NH_4)Fe(HPO_4)_2$ particles synthesized along with the 1 ml of aniline have relatively smaller size as compared to the particles synthesized with 0.5 ml aniline. Agglomeration of $(NH_4)Fe(HPO_4)_2$ particles through the polyaniline coating is also evident from the FESEM micrographs of both aniline(1.0) and aniline(0.5) samples

Beyond an optimum quantity (1 ml) of monomer the separate polyaniline rod formation takes place as confirmed by FESEM microstructure Fig. 4.2 (c). With the aniline monomer limited to 0.2 ml, the formation of polyaniline is insufficient and partial coating develops as observed under FESEM in Fig. 4.2(d). The polymer films subjected under FESEM often leads to the development of film cracking at the operating voltage suitable for inorganic oxide materials characterization. During FESEM imaging the high voltage electron beam has interacted with the polymer and has caused burning or cracking of the polyaniline which is deposited on $(NH_4)Fe(HPO_4)_2$ particles. The cracking in the polymer coat as indicated by the arrow mark in the micrograph (Fig. 4.2 (b)) is an indirect evidence of the polymer films that was formed on $(NH_4)Fe(HPO_4)_2$ particles.
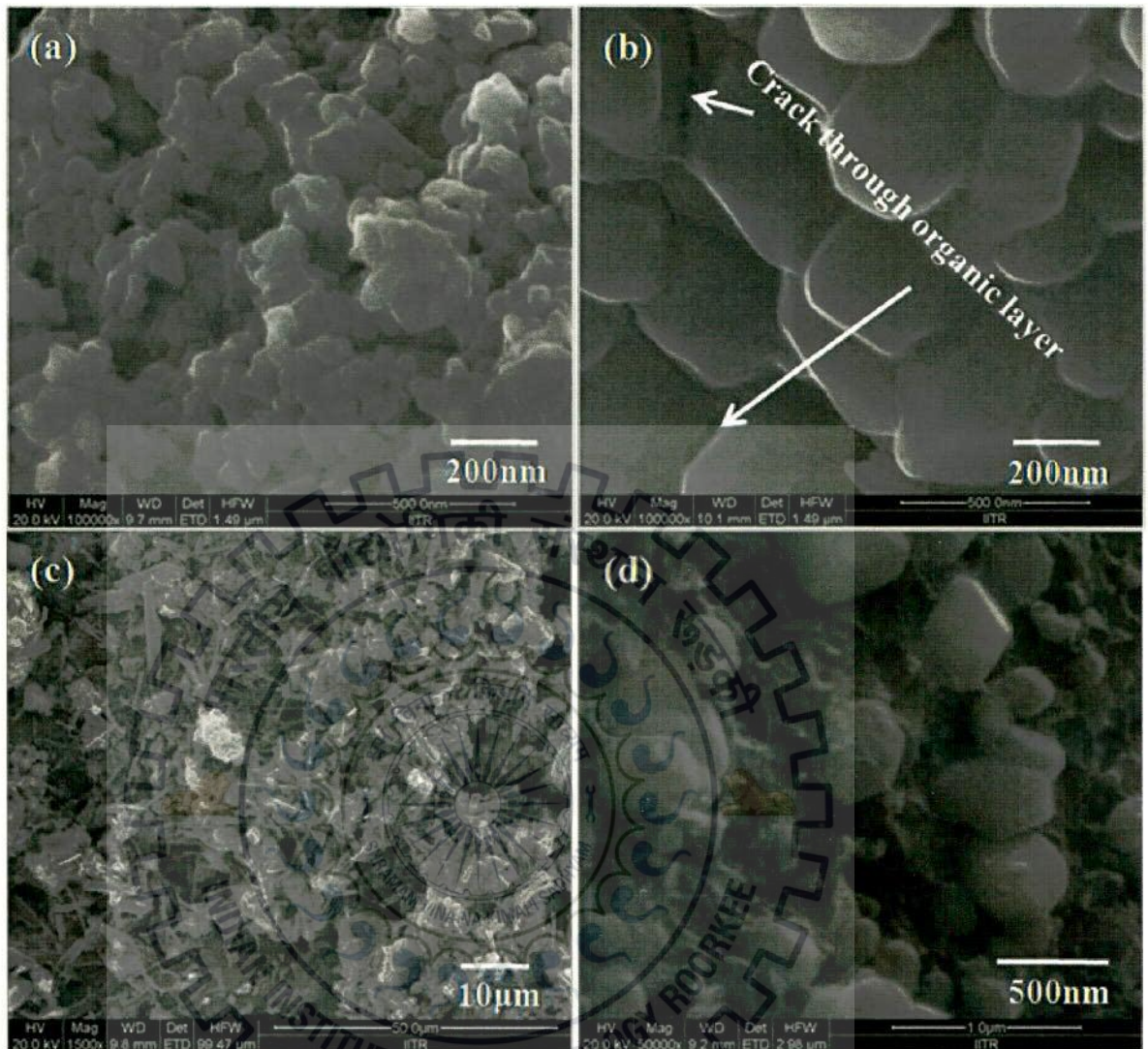
Fig. 4.2: The FESEM micrograph of (a) aniline(1.0), (b) aniline(0.5), (c) coating using 1.5 ml aniline and (d) coating using 0.2 ml aniline.

4.1.3 IR spectroscopy of polymer gel coated $(NH_4)Fe(HPO_4)_2$

IR spectra of aniline(0.5) and aniline(1.0) samples prepared with KBr are shown in Fig. 4.3. The spectrum of the sample aniline(0.5) shows the peaks at 507, 614, 898, 1055, 1134, 1240, 1426 and 1625 cm^{-1} whereas, 508, 614, 891, 1053, 1133, 1244, 1422 and 1625 cm^{-1} are the peak positions for the sample aniline(1.0). All these peaks confirm the formation of polyaniline in both the samples. The bands at 507 cm^{-1} and 508 cm^{-1} are due to bending deformation in polyaniline aromatic ring [Kang et al, 1998]. The 614 cm^{-1} peaks for aniline(0.5) and aniline(1.0) are assigned to C–H out of plane bending vibration in benzene ring of polyaniline [Kulkarni et al, 2011].
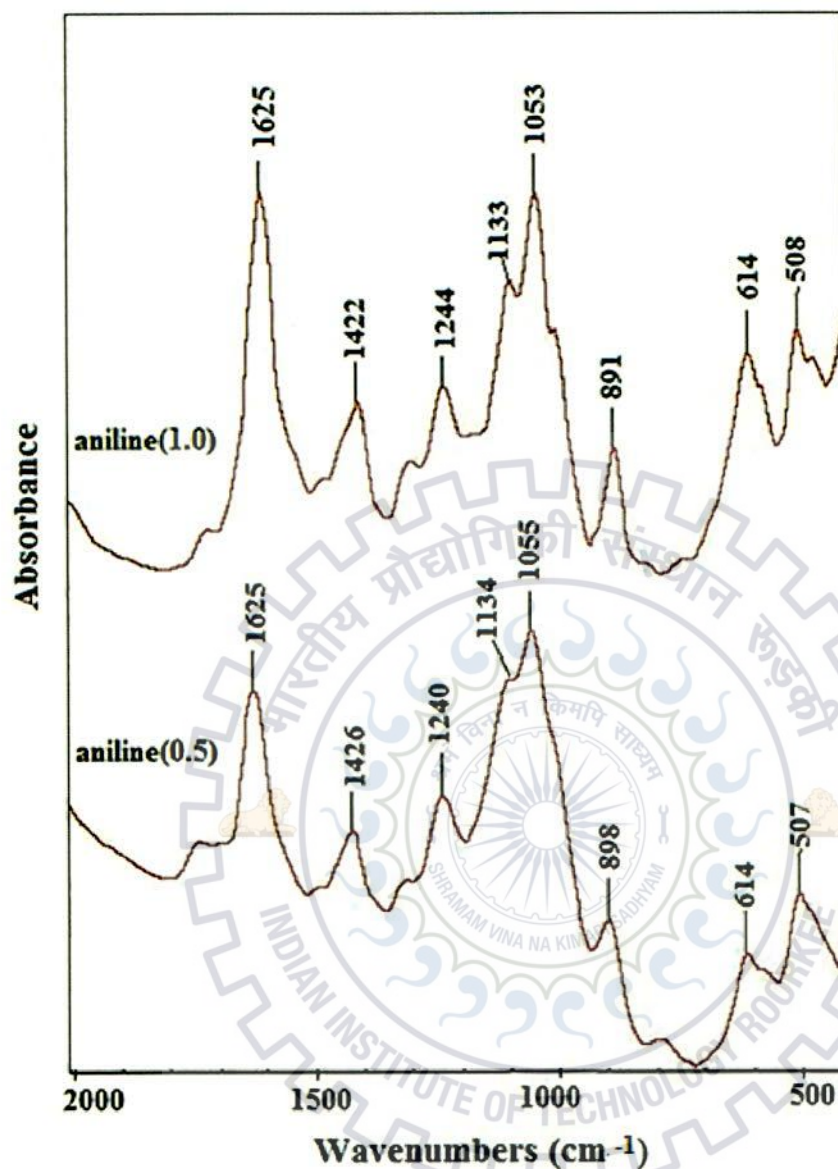
Fig. 4.3: IR spectra of aniline(1.0) and aniline(0.5)

Vibration corresponding to C–H out of plane bending in 1, 2, 4 tri-substituted ring gives rise to the peaks at 898 cm^{-1} and 891 cm^{-1}, and the peaks occur when synthesis is done in ammonium rich solvent [Kang et al, 1998]. The peaks at 1055 cm^{-1} and 1053 cm^{-1} are attributed to internal mode of vibration of PO_4^{-3} ions [Zaghib and Julien, 2005]. The characteristic shoulder peak of polyaniline at 1134 cm^{-1} and 1133 cm^{-1} due to Q=N=Q (Q is quinoid benzene ring of polyaniline) stretching were observed and appears to be very weak due to PO_4^{-3} group [Wang et al, 2006]. The peaks at 1240 cm^{-1} and 1244 cm^{-1} are due to C–N stretching between three benzene (BBB) rings in polyaniline [Kang et al, 1998]. The broad peaks at 1426 cm^{-1} and 1422

cm^{-1} are one of the three deformations due to ν_4 mode. The absorption band at 1625 cm^{-1} is attributed to the bending vibration of oxygen in water molecule [Scaccic et al, 2002].

4.1.4 Structural analysis of LiFePO$_4$/C

Fig. 4.4 shows the XRD patterns of LiFePO$_4$/C composites synthesized using aniline(0.5) and aniline(1.0). The LiFePO$_4$/C powders synthesized using aniline(0.5) and aniline(1.0) are designated as LFP(0.5) and LFP(1.0) respectively. The peaks in XRD pattern match well with the pattern of LiFePO$_4$ (JCPDS card 01-081-1173) having orthorhombic crystal structure with space group Pnma (62). The cell parameters as calculated by XRD data are a = 10.31 Å, b = 5.99 Å, c = 4.68 Å giving rise to unit cell volume V$_{cell}$ = 289.02 Å^3 for the sample LFP(0.5). Similarly for the sample LFP(1.0) the cell parameters are a = 10.32 Å, 6.00 Å, c = 4.68 Å yielding the unit cell volume V$_{cell}$ = 289.82 Å^3 for sample LFP(1.0).

The peaks corresponding to carbon are not present in the XRD patterns which may be due to negligible amount of the carbon present in the sample to give rise to perceptible intensity in the pattern. Moreover, a fraction of carbon is perhaps in the disordered form, this will further be confirmed by Raman spectroscopy.
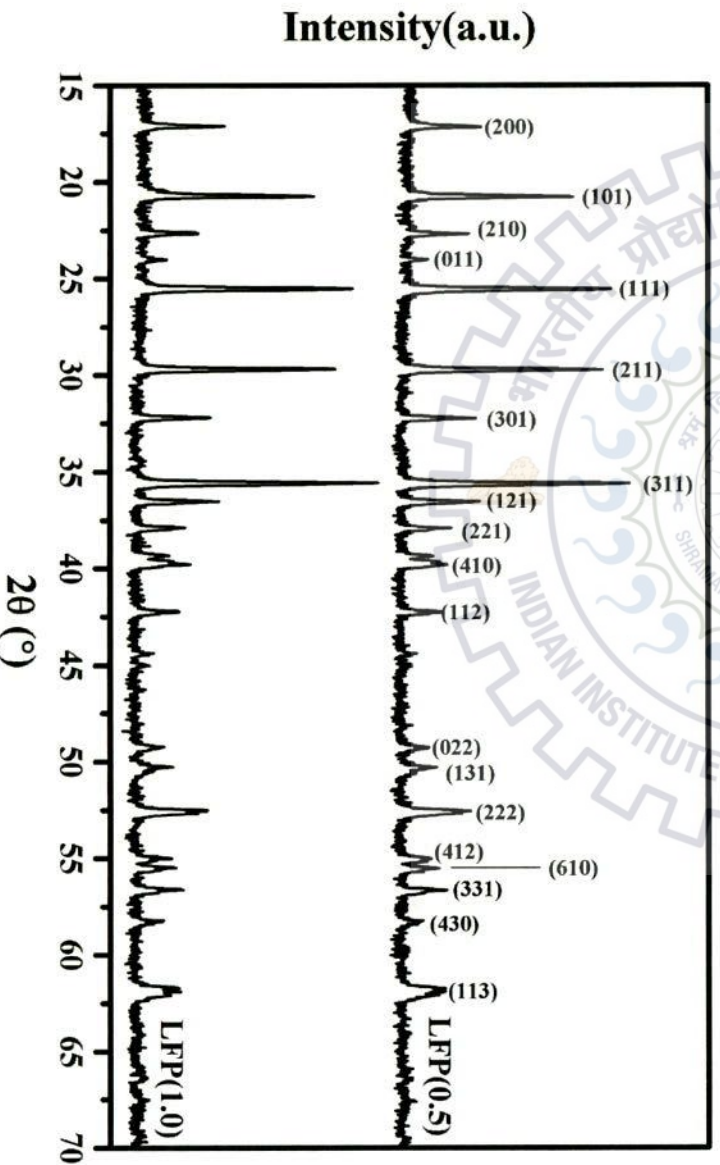
Fig. 4.4: XRD patterns of LFP(0.5) and LFP(1.0).

4.1.5 Morphology of LiFePO₄/C

Fig. 4.5 shows the FESEM micrograph of synthesized LiFePO$_4$/C. The micrographs confirm agglomeration of particles through the carbon present on the surface of LiFePO$_4$ particles. EDS confirms the presence of Fe, P, O and C elements. As estimated from the EDS analysis the molar ratio of Fe, P and O is nearly 1 : 1 : 4. The FESEM micrograph shows that the crystallites of LiFePO$_4$ synthesized using aniline(0.5) have larger particle size (~500 nm) than that synthesized using aniline(1.0) (~100 nm) and this was further confirmed by TEM images.
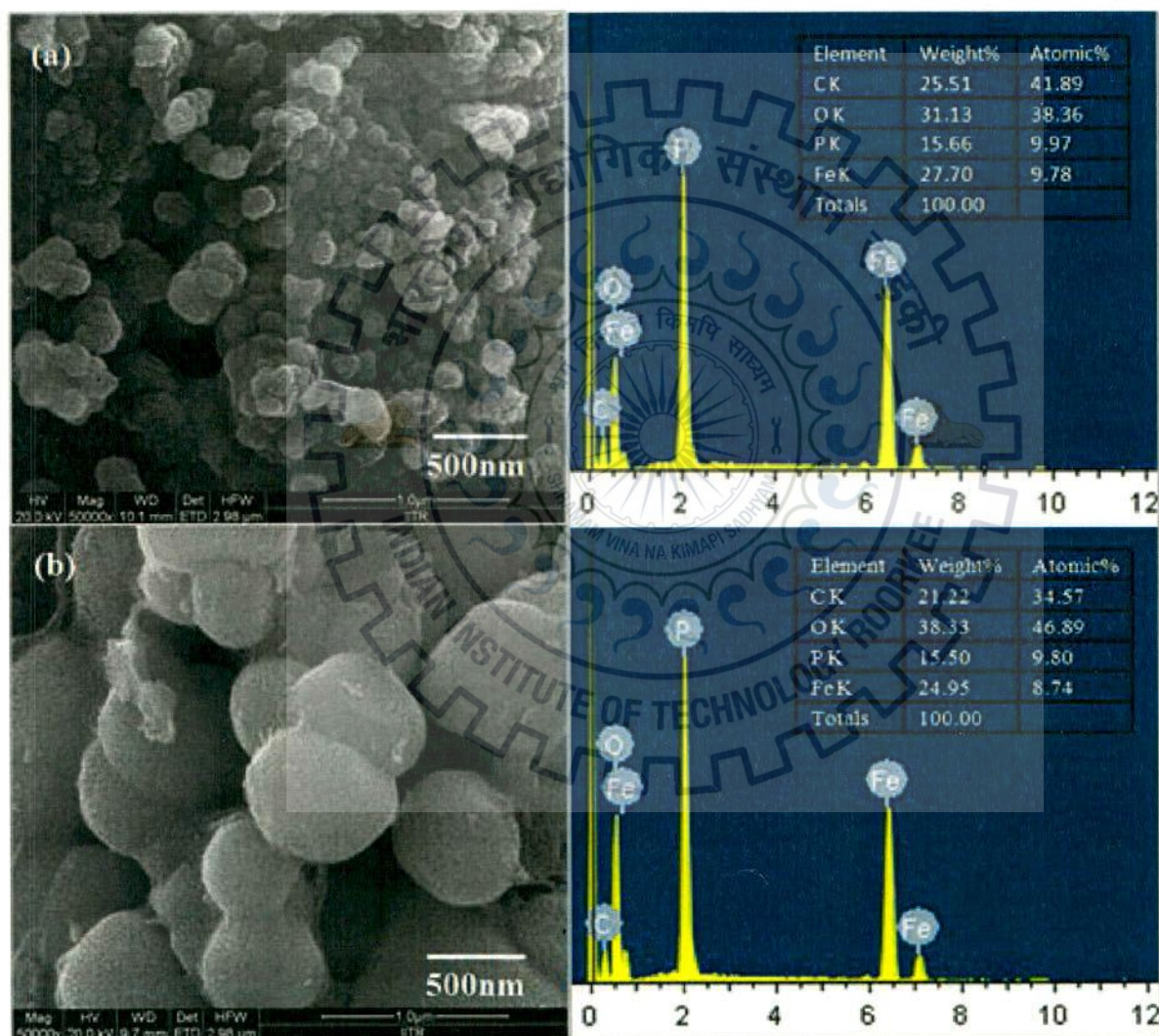
Fig. 4.5: FESEM micrograph of (a) LFP(1.0): particle size ~ 100 nm and, (b) LFP(0.5): particle size ~ 500 nm along with EDAX spectra.

4.1.6 Raman spectroscopy of LiFePO₄/C

The structure of carbon formed by the decomposition of polyaniline is of great importance as the electrochemical properties of LiFePO$_4$ are greatly affected by the structure of carbon. The

structural formation of carbon on the surface of $LiFePO_4$ was characterized by Raman spectroscopy. The Raman spectra of both the $LiFePO_4$/C materials are shown in Fig. 4.6.

The two broad bands at 1350 cm^{-1} and 1590 cm^{-1} represent D-band and G-band respectively of graphitic carbon. The G-band originates due to the formation of highly ordered graphitic carbon and is assigned to E_{2g} optical mode. The E_{2g} mode is doubly degenerate Raman active optical mode arising of carbon atoms movement in graphene plane towards and away from each other [Wilcox et al, 2007, Kostic et al, 2009]. The D-band occurs due to breaking of symmetry viz. finite size of graphite with edges treated as defects and stacking disorder [Reich and Thomsen, 2004]. The growth of different carbon structures can be assessed by the shape of D-band. I_D and I_G are defined as intensities of defect and graphitized bands respectively, the intensity ratios ($R = I_D/I_G$) have been calculated from the pattern given in Fig. 4.6. The R values are 0.97 and 0.98 for carbon coatings for the samples LFP(1.0) and LFP(0.5) respectively, showing the amount of graphitized carbon is marginally larger than the carbon in disordered form [Dresselhaus, et al, 2010]. The formation of graphitic carbon in the coating is essential as it favors the electronic conductivity through the carbon network during charging / discharging of the cell.
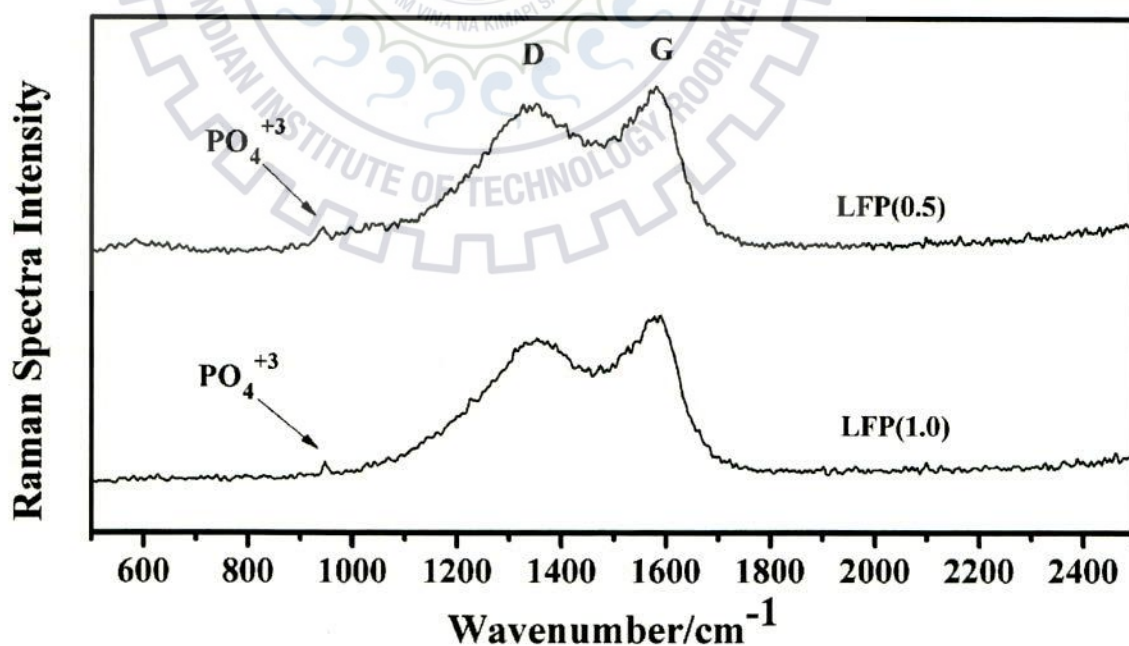
Fig. 4.6: Raman spectra of the samples LFP(0.5) and LFP(1.0).

4.1.7 TEM analysis of LiFePO$_4$/C

The transmission electron microscopy was performed to observe the carbon distribution on LiFePO$_4$/C particles. The interplaner spacing and carbon coating thickness were calculated by Image-J software. The interplaner spacing estimated from HR-TEM images of Fig 4.7(b) and Fig. 4.7(d) is 2.99 Å corresponding to the d$_{211}$ plane spacing.
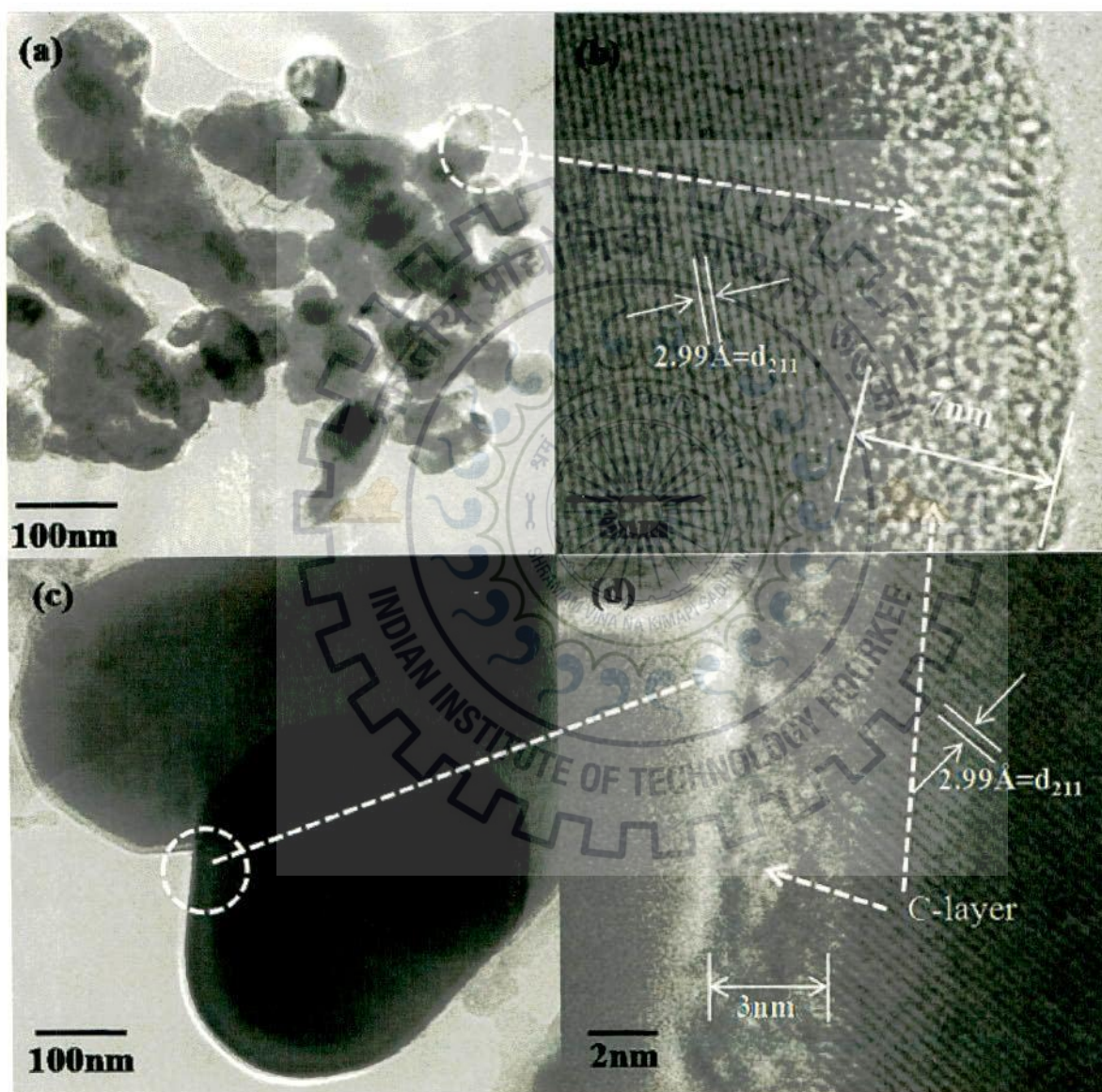
Fig. 4.7: LiFePO$_4$/C material synthesized using aniline(0.5): (a) Particles morphology, (b) lattice image of the LiFePO$_4$ overlapped with partially graphitized carbon; LiFePO$_4$/C materials synthesized using aniline(1.0): (c) Particles morphology, (d) lattice image of LiFePO$_4$ overlapped with partially graphitized carbon.

The beam was focused randomly on the particles of sample LFP(1.0) and of LFP(0.5). TEM images in Fig. 4.7(a) and Fig. 4.7(c) show the particles of LFP(1.0) are smaller as compared to LFP(0.5). The TEM images in Fig. 4.7(a) and 4.7(c) show that $LiFePO_4$ particles are joined each other under the cover of continuous and complete carbon coating. Interconnectivity of the particles via carbon coating helps to enhance the electrical conductivity of bulk materials. The graphitized carbon shell is the path of electrons movement through the surface of particles during charge / discharge cycles of the electrode prepared with the synthesized materials $LiFePO_4/C$.

The HR-TEM images clearly show the carbon shells form a continuous coating on $LiFePO_4$ particles having shell thicknesses of ~ 3 nm and ~ 7 nm for samples LFP(0.5) and LFP(1.0) respectively. Although a powder having small particle size always possesses higher surface area as compared to the powder of larger particle size. So for the same content of coating material the powder with small particle size should possesses thin coating. But in the present experiment the addition of content of coating material viz. aniline was doubled for the sample with small particle size (LFP(1.0)) as compared to the sample with larger particle size (LFP(0.5)). Hence in the sample LFP(1.0) with smaller particle size has large carbon coating thickness as compared to that of sample LFP(0.5).

4.1.8 TG Analysis of $LiFePO_4/C$

TG analysis of samples LFP(1.0) and LFP(0.5) was performed in air atmosphere over a range of room temperature to 750 °C. Oxidation of standard $LiFePO_4$ material starts at 300 °C and completes at 600 °C under air atmosphere. This oxidation produce two phases $Li_3Fe(PO_4)_3$ and Fe_2O_3 as the reaction products, which results a weight gain due to addition of oxygen from the air. Due to the oxidation, weight gain of the reaction products $Li_3Fe(PO_4)_3$ and Fe_2O_3 was estimated to be 5.07% [Vujkovic et al, 2003]. Further, in the temperature range between 350 ° and 500 °C, carbon combustion also takes place in the presence of air which results in the weight loss. Hence the total carbon content in $LiFePO_4/C$ material can be estimated by taking into account of the weight gain due to oxidation.

$$Carbon\ content\ (wt\%) = Total\ wt.\ loss(wt\%) + 5.07 \qquad (4.1)$$
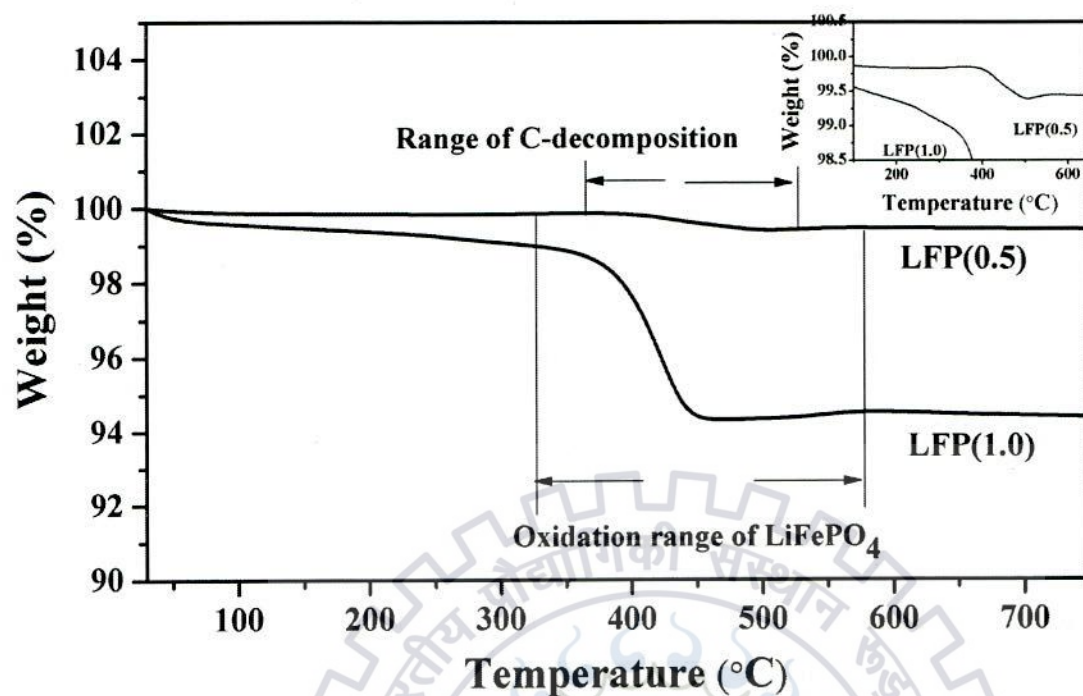
Fig. 4.8: TG traces of LFP(1.0) and LFP(0.5).

It can be seen from the TG traces (Fig. 4.8) of samples LFP(1.0) and LFP(0.5) that a minor weight losses of ~ 0.50 % and 0.16 % have taken place when the samples are heated upto 150 °C and the weight loss is due to moisture removal. The net weight loss between 300 ° and 600 °C were estimated as 4.60 wt% and 0.45 wt% for LFP(1.0) and LFP(0.5) samples and according to above equation, the estimated wt% of carbon was 9.67 and 5.52 for the samples LFP(1.0) and LFP(0.5) respectively. Carbon combustion occurs between 350 ° and 500 °C, which is evident from the TG trace of the samples. The weight loss between 360 ° and 450 °C is quite significant for the sample LFP(1.0), whereas, the loss is nominal in the case of LFP(0.5). The marginal weight gain by the samples beyond 450 °C shows the oxidation process continues even after the completion of the complete carbon removal.

In a control experiment 1.0 ml and 0.5 ml aniline monomers were made to undergo polymerization in presence of FeCl₃ to find out the polymer yields which were found to be 0.8671 gm and 0.4386 gm respectively. The yields were estimated to be ~ 85 % and ~ 86 % for 1.0 ml and 0.5 ml aniline respectively. The experimental results are summarized in the Table 4.1. So the decomposition of 0.8671 gm and 0.4386 gm of polyaniline yields ~ 0.3686 gm and 0.2076 gm of carbon as coating material on the surface of LiFePO₄.

Table 4.1: Weight of carbon in LiFePO$_4$/C by addition of aniline monomer.

Aniline (volume) (ml)	Aniline (weight) (gm)	Polyaniline (weight) (gm)	Polymerization (Yield) (%)	Weight of LFP (gm)	Wt% of carbon in LFP/C(gm)	Weight of carbon (gm)
1.0	1.02	0.8671	85	3.84	9.67	0.3686
0.5	0.51	0.4386	86	3.81	5.52	0.2076

4.2 Electrochemical measurements of LiFePO$_4$/C

4.2.1 EIS of LiFePO$_4$/C

The EIS of samples LFP(1.0) and LFP(0.5) were performed to know their conducting behavior. Fig. 4.9 shows the impedance spectra are semicircular profile in high to intermediate frequency region and slanted straight line on real impedance axis in low frequency region. The sample LFP(1.0) and LFP(0.5) show R_{ct} values of 500 Ω and 710 Ω respectively. Low R_{ct} value for the sample LFP(1.0) is due to good electronic conductivity of carbon rich LFP(1.0) sample. Although the carbon layer is present on the surface of LiFePO$_4$ particles for sample LFP(0.5), but the particle of sample LFP(1.0) have higher amount of carbon in the coating region to impart higher electrical conductivity.
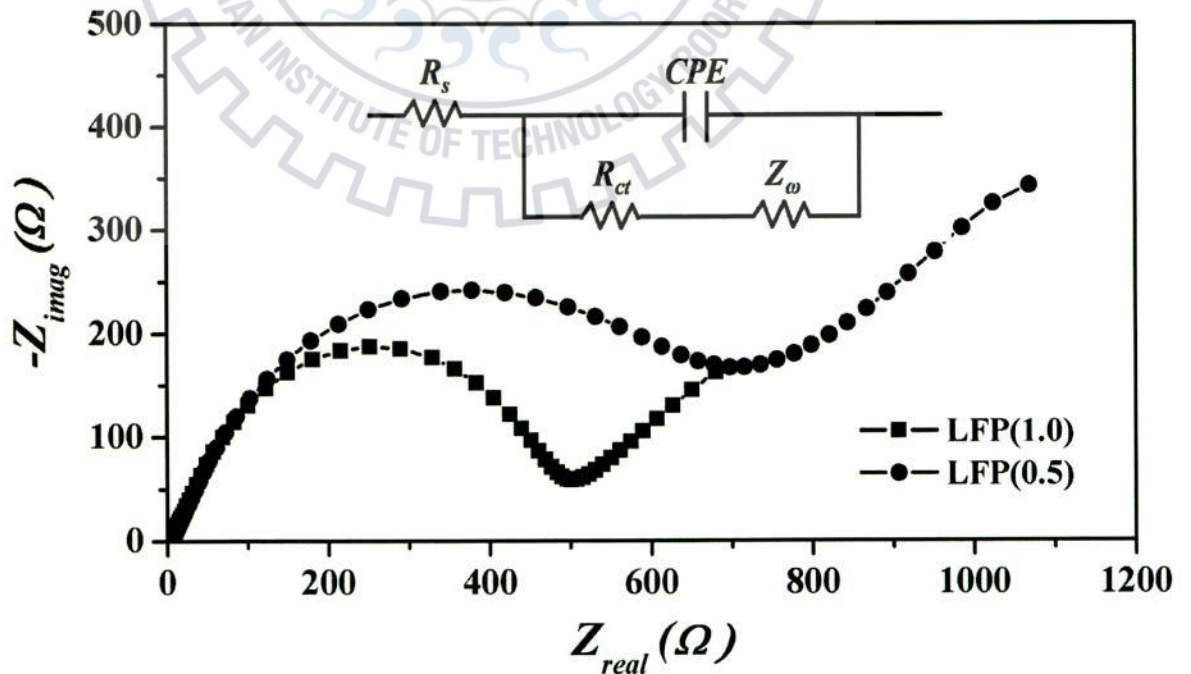

Fig. 4.9: Electrochemical impedance spectra of LFP(1.0) and LFP(0.5).
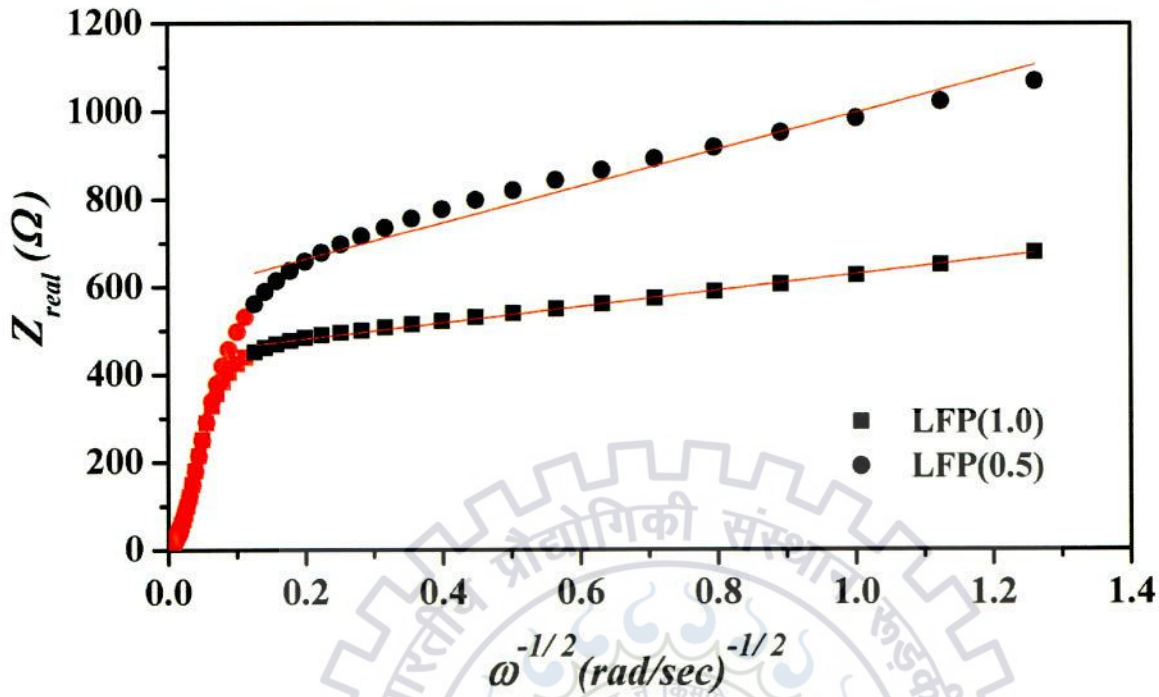
Fig. 4.10: Linear fitting of Warburg impedance of sample LFP(1.0) and LFP(0.5).

The electrochemical reversibility of the electrode material can be determined by i_0 which is calculated by using the relation (3.6). The sample LFP(1.0) reflects good electrochemical reversibility by showing better i_0 of 6.94×10^{-5} mA/cm^2 as compared to 5.17×10^{-5} mA/cm^2 for LFP(0.5). The D_{Li+} has been calculated using the equation (3.5). The σ_ω can be calculated from the slope of linearly fitted Z_{real} vs $\omega^{-1/2}$ line (Fig. 4.10) in the low angular frequency region. The D_{Li+} of samples LFP(1.0) and LFP(0.5) are 6.82×10^{-15} cm^2/s and 1.35×10^{-15} cm^2/s respectively. The EIS parameter such as R_{ct}, i_0, D_{Li+} and slope of linearly fitted Z_{real} vs $\omega^{-1/2}$ line of samples LFP(1.0) and LFP(0.5) are reported in Table 4.2. The higher D_{Li+} of the sample LFP(1.0) reflects the better kinetic performance of Li-ion during charging / discharging of electrode.

Table 4.2 EIS parameter of electrodes of LFP(1.0) and LFP(0.5)

Sample	$R_{ct}(\Omega)$	i_0 (mAcm^{-2})	D_{Li^+} (cm^{2}sec^{-1})	σ_ω (Ω rad$^{1/2}$ sec$^{-1/2}$)
LFP(1.0)	500	6.94×10^{-5}	6.82×10^{-15}	186
LFP(0.5)	710	5.17×10^{-5}	1.35×10^{-15}	418

The sample LFP(1.0) has higher carbon content in the coating region which provides the full coverage to LiFePO$_4$ particles resulting in faster Li-ion diffusion as compared to that of LFP(0.5).

4.2.2 Electrochemical cell performance of LiFePO$_4$/C

The galvanostatic charging / discharging of LFP(1.0) and LFP(0.5) samples were determined between 2.2 V and 4 V at various current rates of 0.1C, 0.2C, 0.5C, 1C, 2C, 5C and 10C. The discharge profiles of samples are shown in Fig. 4.11. The highest discharge capacities of 159 mAh/g and 152 mAh/g were obtained at 0.1C rate for the samples LFP(0.5) and LFP(1.0) respectively. At 0.1C and 0.2C rates, the sample LFP(0.5) shows a higher capacity as compared to that of LFP(1.0). As the rate of charging / discharging further increases to 1C, both the materials show nearly same discharge capacities. Sample LFP(1.0) shows higher discharge capacity of 94 mAh/g as compared to 82 mAh/g for LFP(0.5) at 2C rate. The sample LFP(1.0) shows higher rate capability of 60 mAh/g at 10C rate. Fig. 4.12 shows the rate capabilities of the samples for 5 cycles at every current rate of 0.1C, 0.2C, 0.5C, 1C, 2C, 5C and 10C.
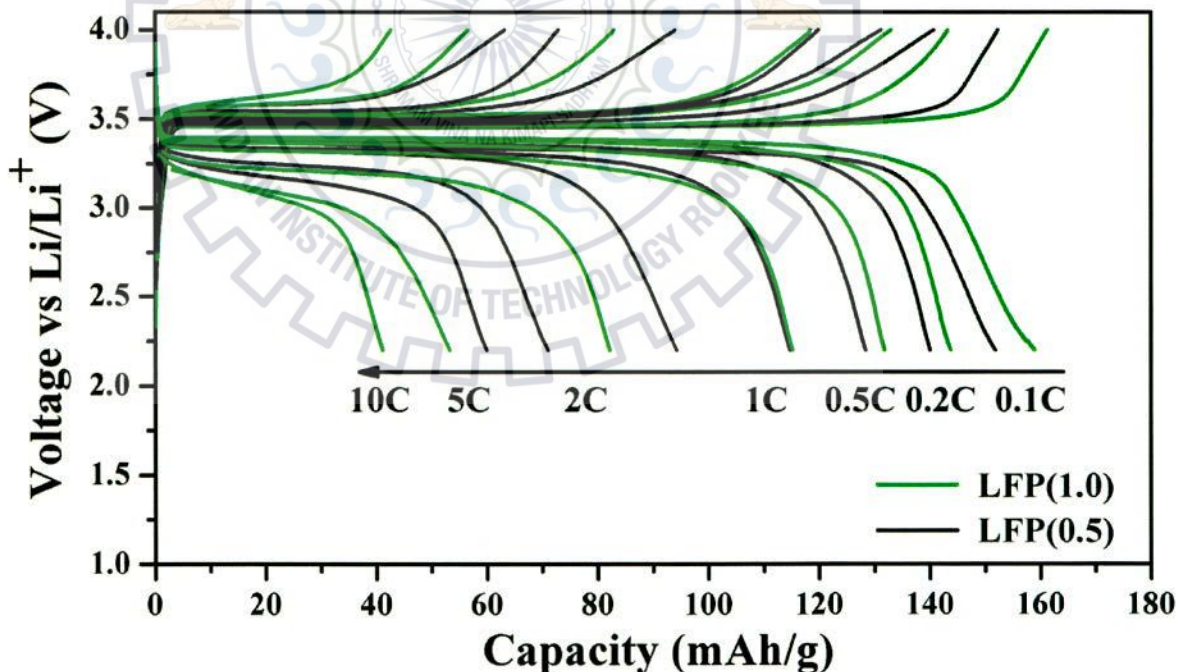

Fig. 4.11: Discharge profile of LFP(1.0) and LFP(0.5) at different current rates.

The poor rate capability of sample LFP(0.5) is attributed by the low electronic and low ionic conductivities as confirmed by EIS. The Fig 4.13 shows the cyclic stability of the samples at

1C (20 cycles) and 2C (50 cycles) rates. The sample LFP(1.0) shows good cyclic stability as compared to LFP(0.5).
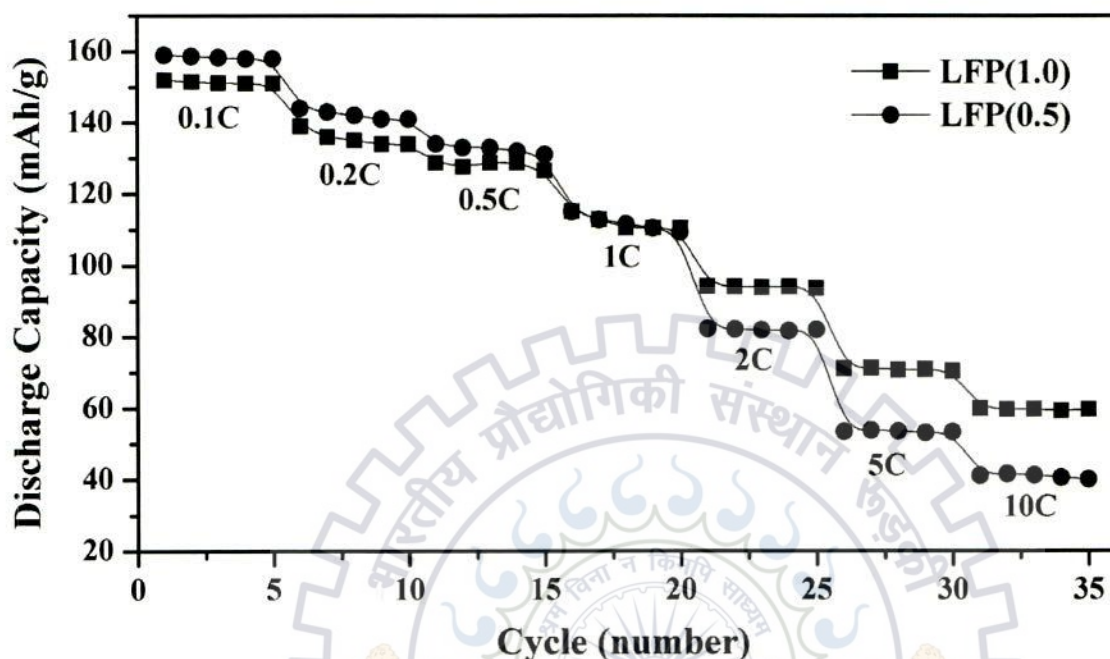
Fig. 4.12: Discharge capacities delivered by LFP(1.0) and LFP(0.5) for every cycle at different current rates upto 35 cycles.

At low current rate (0.1C) the Li-ion diffusion is slow enough that the particle size and carbon coating do not have significant effect on conduction so that the better discharge capacity of LFP(0.5) was due to lower fraction of inactive carbon present in the composite material. At 0.2C rate the discharge capacity of sample LFP(1.0) was slightly reduced as compared to LFP(1.0). This is due to the availability of lower fraction of LiFePO₄ active material for sample LFP(1.0) as confirmed by the TG analysis in section 4.1.8. The carbon network formed on the LiFePO₄ particle was electrochemically inactive to store Li-ions. This electrochemically inactive carbon reduces the tap density of LiFePO₄ active material on the aluminium foil. So, overall effect of higher carbon quantity at low current rate was to decrease the specific capacity of electrode for sample LFP(1.0). At faster rate of charging and discharging particle size, quality (graphitization) of carbon coating, coating thickness and coating uniformity play a major role [Dominko et al, 2005, Cho et al, 2009].

Fig. 4.13 Cyclic performance of LFP(1.0) and LFP(0.5) at 1C rate (20cycles) and 2C rate (50cycles).

The quality of carbon was measured by Raman spectroscopy and it was found that same level of graphitization was gained in the carbon coatings for both samples. But the thin carbon coati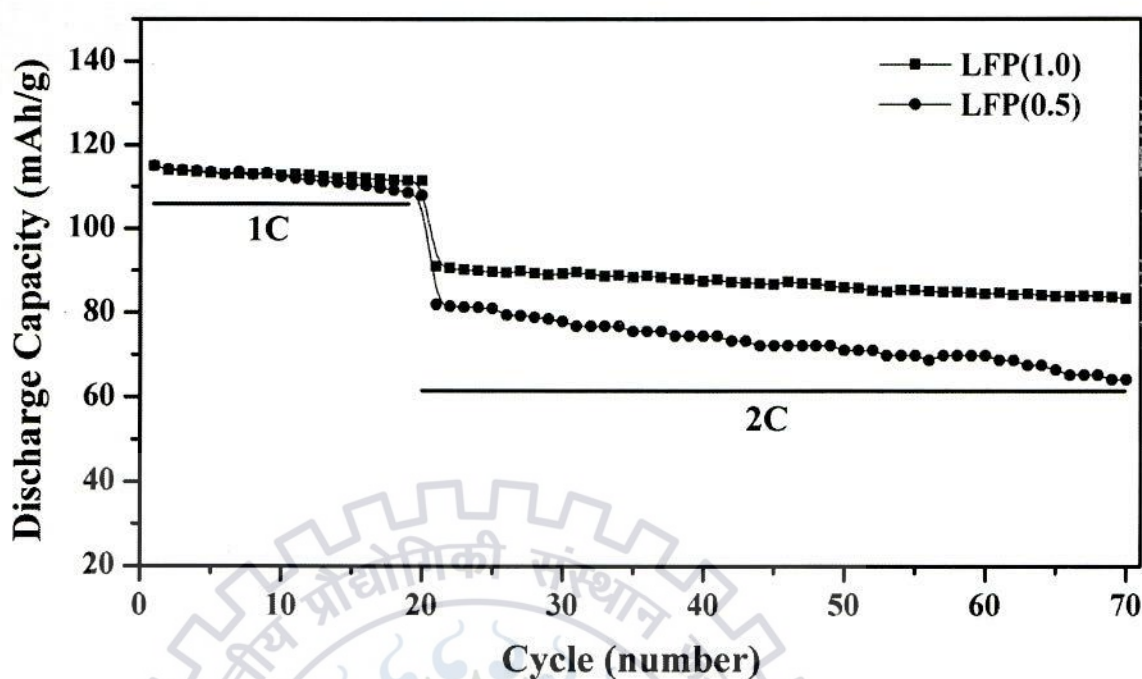ng and larger particle of sample LFP(0.5), affect adversely the material capacity when charging / discharging occurs at a faster rate. Thin carbon coating may not be sufficient to give better coverage to LiFePO₄ which results less conductivity. EIS analysis under section 4.2.1 reveals that the sample LFP(1.0) shows better Li-ion diffusion and better electronic conductivity. The larger particle size of LFP(0.5) enhances the diffusion length resulting to increase the diffusion time for Li-ion due to which the material is not able to charge / discharge to it full capacity. So, the net effect is the decrease in discharge capacity of material LFP(0.5) at higher 2, 5 and 10C rates. The better reversibility as reflected by exchange current density for sample LFP(1.0) electrode reflects the good cyclability of the material.

4.2.3 CV test of LiFePO₄/C

Fig. 4.14(a) and (b) show the cyclic voltammograms of samples LFP(1.0) and LFP(0.5) for 3 cycles at constant voltage rate of 0.1 mV/s respectively, showing a single reduction and oxidation peak between 2.2 to 4.1 V. The good overlapping of CV profile for every cycle indicates a very low or little capacity fade of material per cycle of the cathode materials. The

peaks in the cyclic voltammogram reveal fast conduction of Li-ion at 3.56 V and 3.31 V for sample LFP(0.5) and, 3.53 V and 3.33 V for sample LFP(1.0) respectively.
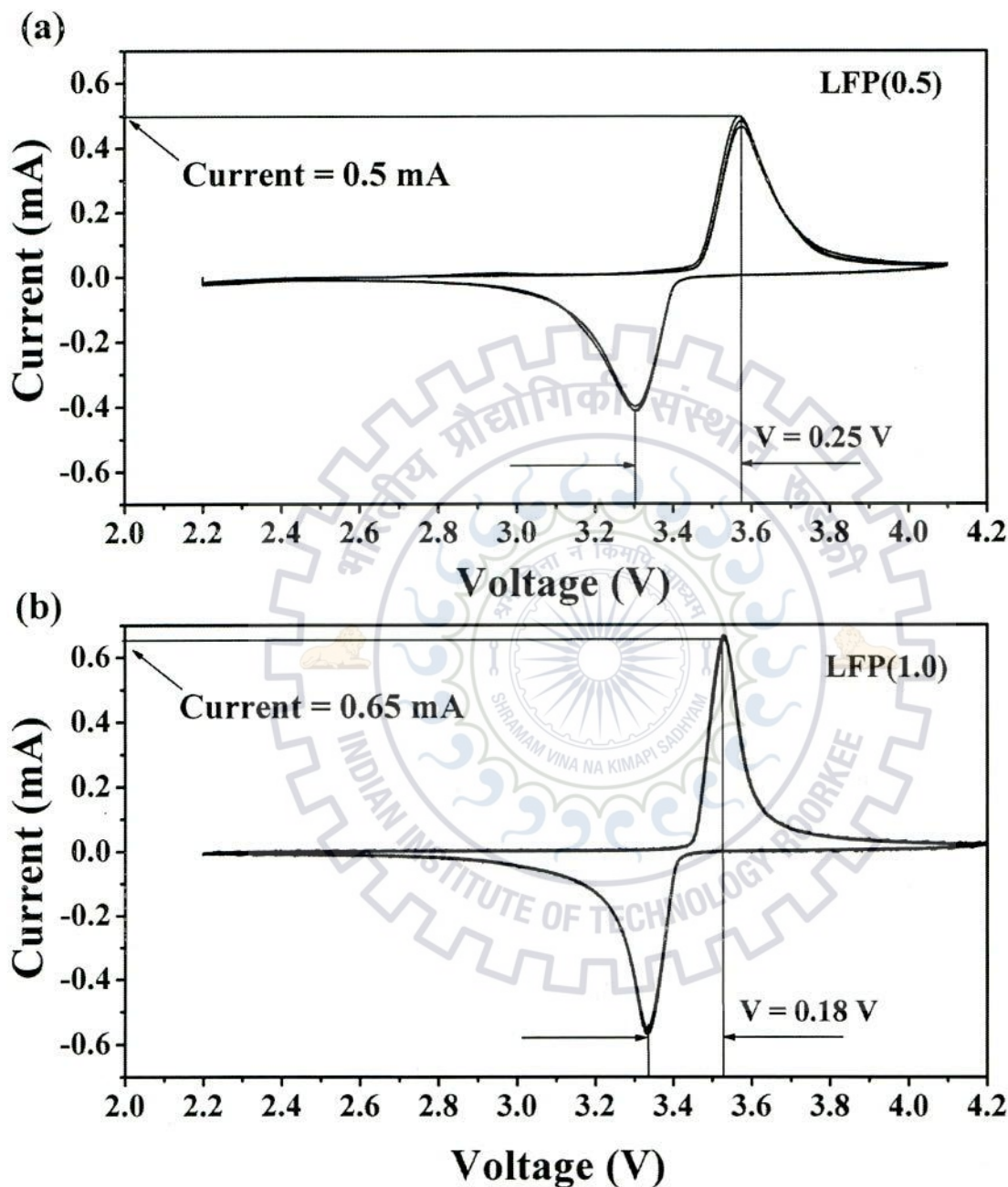
(a)

(b)

Fig. 4.14: (a) Cyclic voltammograms of LFP(0.5), and (b) LFP(1.0) at a scanning rate 0.1 mV/s.

From the cyclic voltammograms it was found that the potential differences between the oxidation / reduction peaks are 0.25 V and 0.18 V for samples LFP/C(0.5) and LFP/C(1.0) respectively. The narrow potential difference between oxidation / reduction peaks for sample

LFP/C(1.0) reflects the small polarization of electrode resulting in higher reversibility and lower impedance to the moving charge [Zhang et al, 2010]. The higher reversibility reflects good cyclability of the cathode material. So, the profiles of CV tests for both the samples are in accordance with the cyclability and EIS measurements.

Summary

In this chapter, LiFePO$_4$/C materials have been characterized and electrochemically tested as cathode material for the high rate capability of Li-ion battery. During polymerization the growth of (NH$_4$)Fe(HPO$_4$)$_2$ particles were restricted by polyaniline coating while the growth of LiFePO$_4$/C were restricted by carbon coating during calcination. The carbon on LiFePO$_4$ particles with coating thickness of ~ 3 nm and ~ 7 nm for 0.5 ml and 1.0 ml of aniline respectively were formed by the decomposition of polyaniline coating. The higher fraction of graphitic carbon in the coating was observed for sample synthesized using 1.0 ml aniline monomer which improves the conductivity of LiFePO$_4$/C particles. The sample LFP(0.5) shows higher discharge capacity as compared to LFP(1.0) at slow C-rate. While sample LFP(1.0) shows better rate capability and cyclic stability as compared to sample LFP(0.5). The improved rate capacity and cyclability of LFP(1.0) is attributed by small particle size and uniform carbon coating. Further the better reversibility of the sample LFP(1.0) was confirmed by narrow voltage difference between peak currents in a cycle.

RESULTS AND DISCUSSION- POLYMER COATED LiFePO$_4$/C

RESULTS AND DISCUSSION-POLYMER COATED LiFePO₄/C

The conducting polymers viz. polypyrrole, polythiophene and polyaniline are electrochemically active over the voltage range of 2.2 – 3.8 V. This redox range of polymers overlaps with the redox range (3.4 V for Fe^{2+}/Fe^{3+}) for $LiFePO_4$. Therefore, these conducting polymers can not only act as conducting agent but also act as host material for Li-ion insertion / extraction to improve the cyclability and rate capability of $LiFePO_4$ material. This chapter consists of results and discussion on the characterization and electrochemical testing of *in-situ* deposited conducting polymers on $LiFePO_4/C$. The chapter has been divided in to three major sections to present the results on the effects of polypyrrole, polythiophene and polyaniline coatings separately on $LiFePO_4/C$.
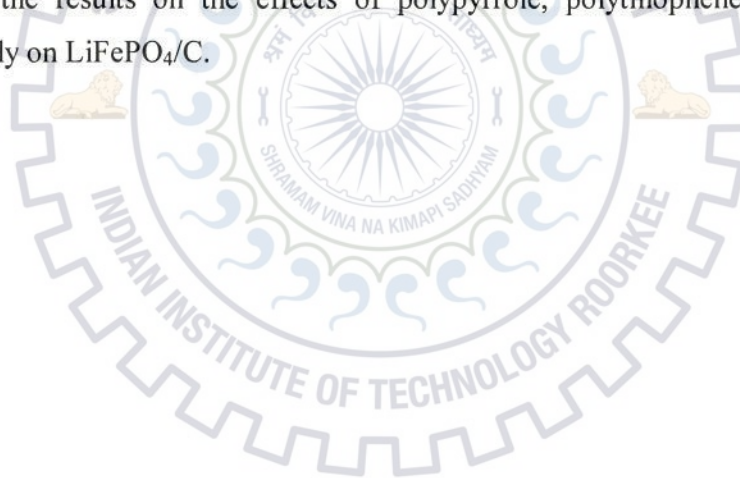
5.1 RESULTS AND DISCUSSION- POLYPYRROLE COATED LiFePO$_4$/C
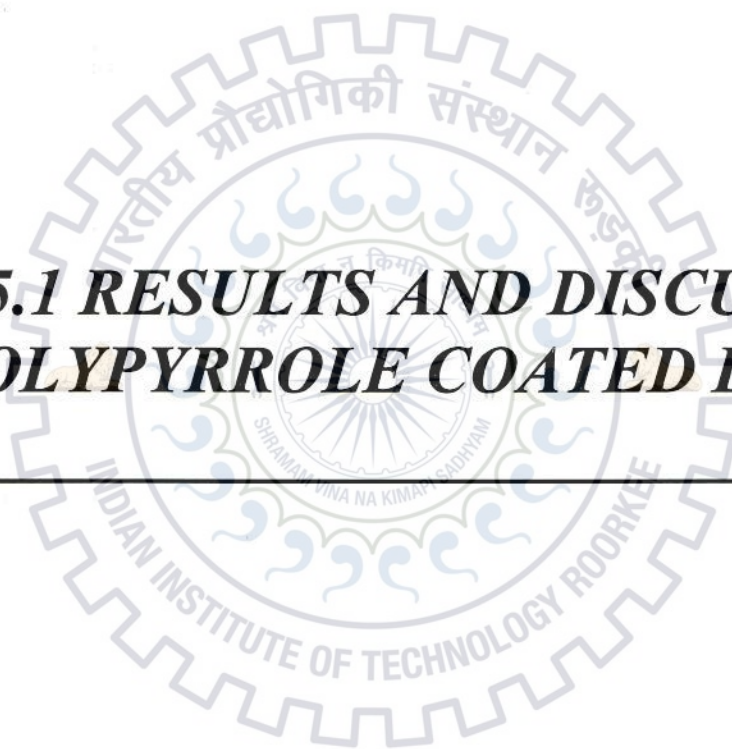
5.1 RESULTS AND DISCUSSION- POLYPYRROLE COATED LiFePO₄/C

In this section, the investigation on polypyrrole coated LiFePO$_4$/C particles designated as LiFePO$_4$/C-PPy has been discussed. Polypyrrole shows the electronic conductivity due to delocalization of pie-electrons in the conjugated pie-bond system [Wanekaya et al, 2006]. The conductivity of polypyrrole can further be improved by using suitable solvent and doping with Na-PTSA or inorganic dopants ClO$_4^-$, BF$_4^-$ and NO$_3^-$ [Wanekaya et al, 2006, Machida and Miyata, 1989]. The doping with Na-PTSA as compared to inorganic dopants results in good and stable electronic conductivity of polypyrrole [Kaynak et al, 2009]. In the present study, effect of nature of solvents viz. water, ethanol and acetonitrile (ACN) on the conducting and electrochemical properties of LiFePO$_4$/C-PPy samples have been investigated. The conductivity and morphology of deposited polypyrrole vary depending upon the nature of solvent such as polarity and different groups present in the solvent molecules. The study has indicated that ACN solvent derived LiFePO$_4$/C-PPy has highest rate capability among the composite materials prepared in three different oxidizing agents used.

5.1.1 Physical characterization

5.1.1.1 XRD analysis of LiFePO₄/C-PPy

Fig. 5.1 shows the XRD patterns of pristine polypyrrole synthesized using water solvent and LiFePO$_4$/C-PPy composite materials. The LiFePO$_4$/C-PPy composite materials synthesized in each of ACN, ethanol and water solvents are designated as LiFePO$_4$/C-PPy(ACN), LiFePO$_4$/C-PPy(ethanol) and LiFePO$_4$/C-PPy(water). The diffraction patterns show that material consists of two phases of LiFePO$_4$ (JCPDS file No. 01-083-2092) and Li$_{0.05}$FePO$_4$ (JCPDS file No. 98-10-8284). The formation of Li$_{0.05}$FePO$_4$ phase implies that lithium depletion has taken place due to the lithium abstraction by the polymer coating of polypyrrole because the polymer is electrochemically active. Both the phases of LiFePO$_4$ and Li$_{0.05}$FePO$_4$ are reported to have same capacity [Yamada et al, 2006]. Also mention from the reference that though the second compound is lithium deficient. The characteristic peaks of carbon and polypyrrole are not visible in the XRD patterns (Fig. 5.1) this may be due to amorphous nature of polypyrrole coating and carbon content in the materials is significantly low. Moreover, a fraction of the carbon is in disordered form that is confirmed by Raman spectroscopy of the sample.

Table 5.1 Shows the angular position and intensity of the major peaks in the XRD patterns of Li$_{0.05}$FePO$_4$ (JCPDS file No. 98-10-8284) and LiFePO$_4$ (JCPDS file No. 01-083-2092) materials. The resolved and unresolved peaks of Li$_{0.05}$FePO$_4$ in the XRD pattern are also indicated.

S. No.	2θ(degree) LiFePO$_4$	Peak Intensity LiFePO$_4$(I=I$_{2θ}$*10 0 /I$_{max}$)	2θ(degree) Li$_{0.05}$FePO$_4$	Peak Intensity Li$_{0.05}$FePO$_4$(I=I$_{2θ}$*100 /I$_{max}$)	Peak status of Li$_{0.05}$FePO$_4$ LiFePO$_4$/C-PPy XRD pattern
1	17.17	38.0	18.04	69.4	Resolved
2	20.81	76.2	20.644	94.0	Unresolved
3	25.6	83.3	25.777	88.9	Unresolved
4	29.73	78.2	30.819	79.2	Resolved
5	35.61	100	36.663	100.0	Unresolved
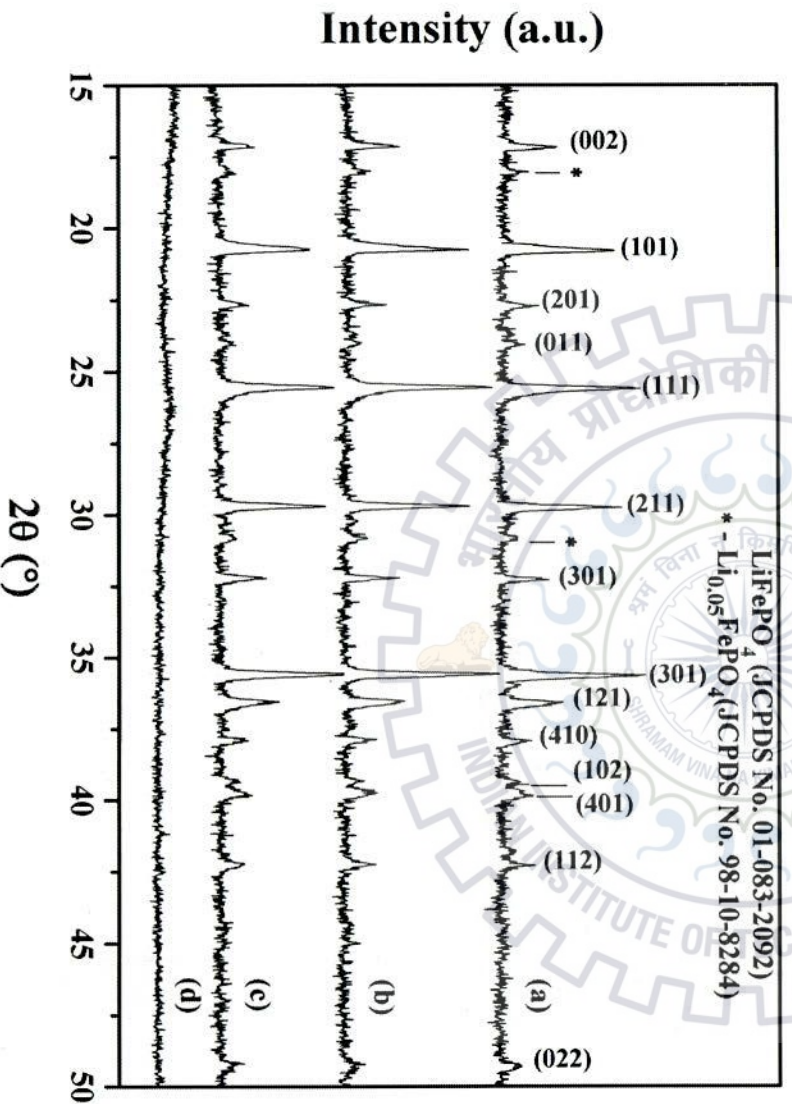
Fig. 5.1: XRD patterns of (a) LiFePO$_4$/C-PPy(ACN), (b) LiFePO$_4$/C-PPy(ethanol), (c) LiFePO$_4$/C-PPy(water) and PolyPyrrole(water).

5.1.1.2 TG analysis

Fig. 5.2 shows the TG profiles of the samples LiFePO$_4$/C-PPy(water), LiFePO$_4$/C-PPy(ethanol), LiFePO$_4$/C-PPy(ACN) and pristine polypyrrole heated at the rate of 10 °C/minute from room temperature to 800 °C. The materials were held at the temperature of 800 °C for 1 hour in order to remove the polypyrrole content completely by decomposition. A nominal weight loss was occurred over the temperature range from room temperature to 120 °C for all the samples due to the removal of water molecules. Above 120 °C, a gradual weight loss of the materials takes place upto 800 °C due to the decomposition of polypyrrole coating material. The polypyrrole content in LiFePO$_4$/C-PPy(water), LiFePO$_4$/C-PPy(ethanol), LiFePO$_4$/C-PPy(ACN) were estimated as 6.9, 5.5 and 6.6 wt% respectively.
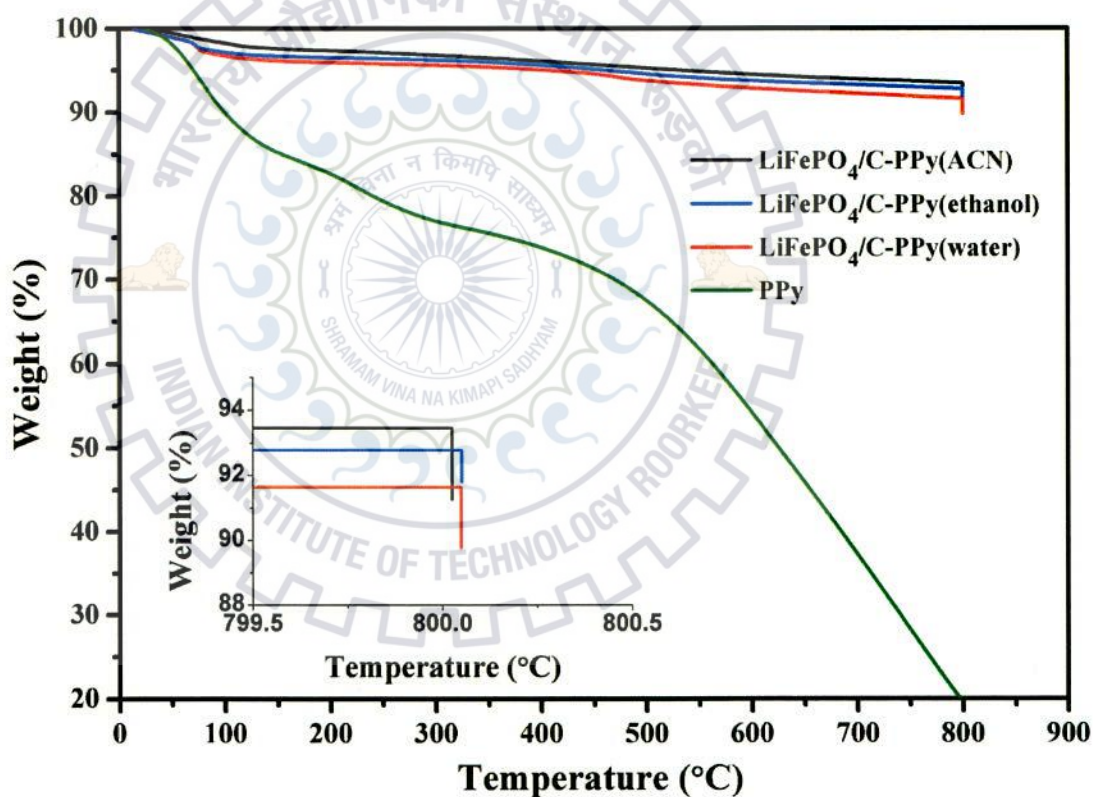
Fig. 5.2: TG plots of LiFePO$_4$/C-PPy(water), LiFePO$_4$/C-PPy(ethanol), LiFePO$_4$/C-PPy(ACN) and polypyrrole measured at a heating rate of 10 °C/min in Argon gas atmosphere.

5.1.1.3 Morphology of LiFePO$_4$/C-PPy

FESEM micrographs of the pristine polypyrrole and LiFePO$_4$/C-PPy composites are shown in Fig. 5.3. The Fig. 5.3(a-c) show the morphologies of pristine polypyrrole synthesized in ACN,

ethanol and water solvents respectively. The micrographs of polypyrrole synthesized in water and ethanol solvents show similar morphologies. Whereas, the polypyrrole powder prepared in ACN solvent has low porosity and smooth surface than that of powder synthesized in water and ethanol.

Fig. 5.3(d-f) show the FESEM micrographs of the composites LiFePO₄/C-PPy(ACN), LiFePO₄/C-PPy (water) and LiFePO₄/C-PPy (ethanol) respectively. The micrographs show that the morphologies are the same for the polypyrrole coating and of pristine polypyrrole synthesized in the same solvent. The polypyrrole in the composites LiFePO₄/C-PPy (water) and LiFePO₄/C-PPy (ethanol) provide partial coverage of the LiFePO₄/C. It is also observed that the polypyrrole chains grow separately in the coating region. The surface roughness and porosity of the polypyrrole coating is higher in the composites LiFePO₄/C-PPy(water) and LiFePO₄/C-PPy(ethanol) as compared to that of LiFePO₄/C-PPy(ACN). The micrograph in Fig. 5.3(d) suggests that LiFePO₄/C-PPy(ACN) composite is largely covered by the polypyrrole.

The polymerization process involves the formation of radical cation of pyrrole due to its oxidation by FeCl₃.

$$FeCl_3 \rightarrow Fe^{3+} + 3Cl^- \qquad (5.1)$$

$$Pyrrole + Fe^{3+} \rightarrow Pyrrole^+ (radical\ cation) + Fe^{2+} \qquad (5.2)$$

During polymerization the pyrrole radical cation combines with other similar radical cation for chain propagation of the polymer. But if the polypyrrole synthesis is processed in water or ethanol the active centers of the growing chain were attacked by the –OH and C=O nucleophilic groups instead of free pyrrole radical cation produced in the reaction 5.2 [Rodrıguez et al, 2000]. Due to the attack of –OH and C=O, polypyrrole chains become hydrophobic to the solvent resulting in the lowering of active centers. The lowering of active centers on a polymer chain reduces the chain growth and formation of aggregates of polypyrrole takes place. So, the polypyrrole synthesized in the water or ethanol solvents have more porosity and surface roughness as compared to the ACN derived polypyrrole [Ko et al, 1990].
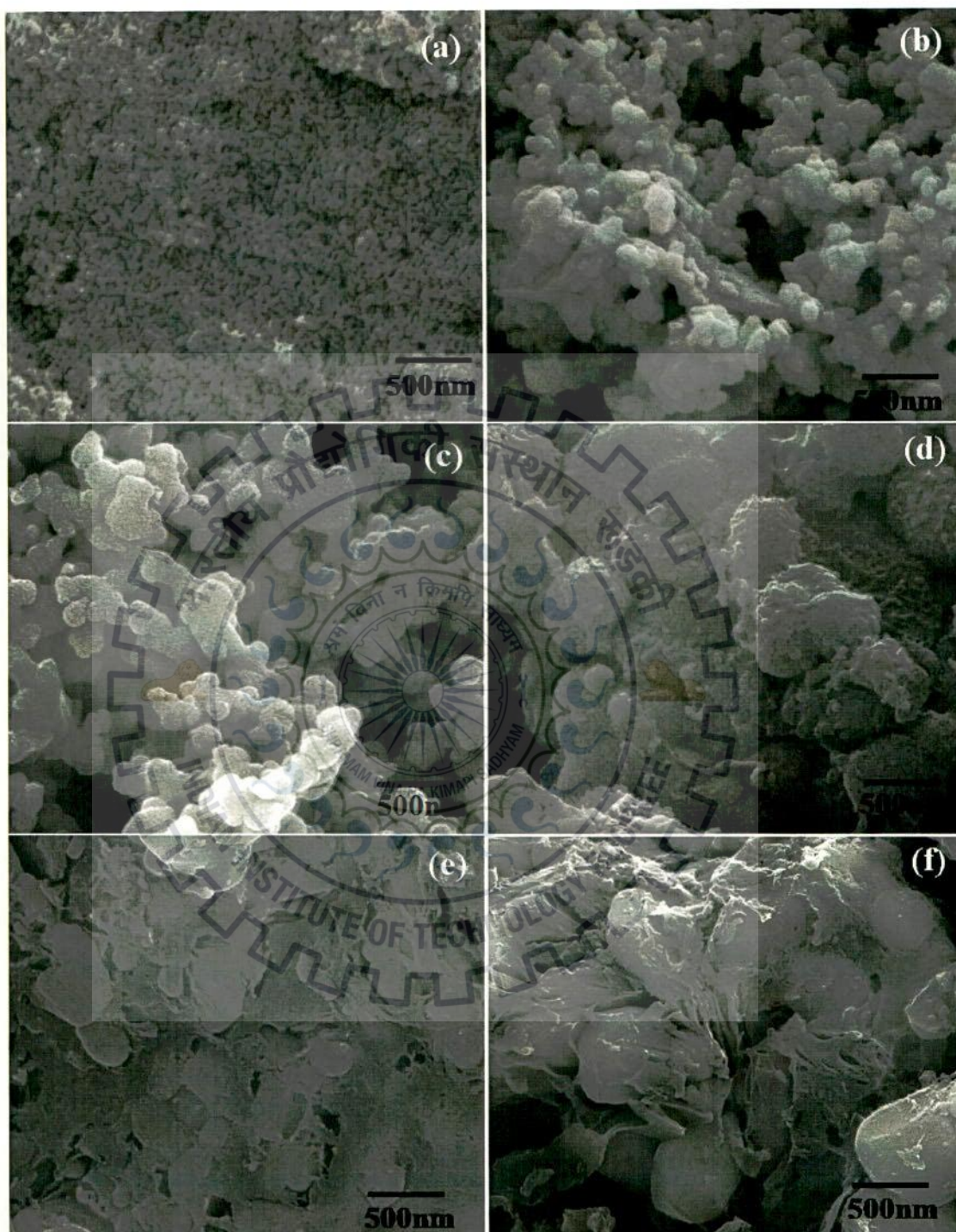
Fig. 5.3: FESEM micrographs showing morphology of polypyrrole synthesized in (a) ACN, (b) ethanol, (c) water, (d) LiFePO₄/C-PPy(ACN), (e) LiFePO₄/C-PPy(water) and (f) LiFePO₄/C-PPy(ethanol).

5.1.1.4 TEM analysis of polypyrrole and LiFePO$_4$/C-PPy

Fig. 5.4 (a, b and c) show the TEM images of polypyrrole samples synthesized in ACN, ethanol and water solvents respectively. Polypyrrole particles synthesized in ACN solvent are interconnected and surrounded by each other from all the direction to form a thin sheet. But the polypyrrole particles synthesized in water and ethanol solvents have similar morphology.
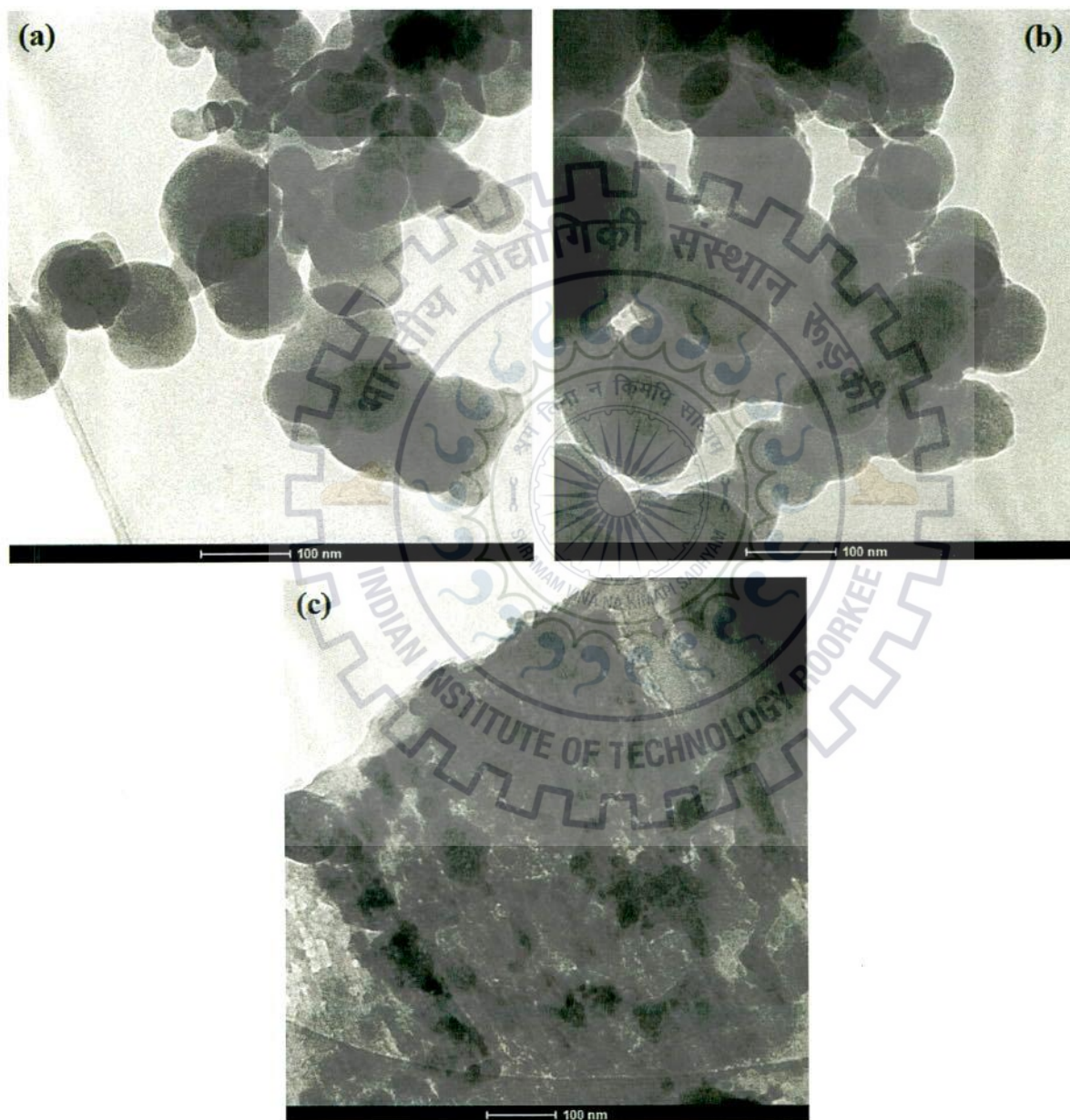
Fig. 5.4: TEM images of polypyrrole synthesized in (a) ethanol, (b) water and (c) ACN solvents.

These particles have irregular arrangement to give low powder density as compared to the polypyrrole synthesized in ACN solvent. Similar morphologies have already been obtained for these samples which can be seen through respective FESEM micrographs under section 5.1.1.3. Fig. 5.5(a-c) show the TEM micrographs of LiFePO₄/C-PPy(ACN), LiFePO₄/C-PPy(ethanol) and LiFePO₄/C-PPy(water) composite materials. The effective surface coverage of the LiFePO₄/C particles with the polypyrrole synthesized in ACN solvent can be observed in the micrograph of Fig. 5.5(a).
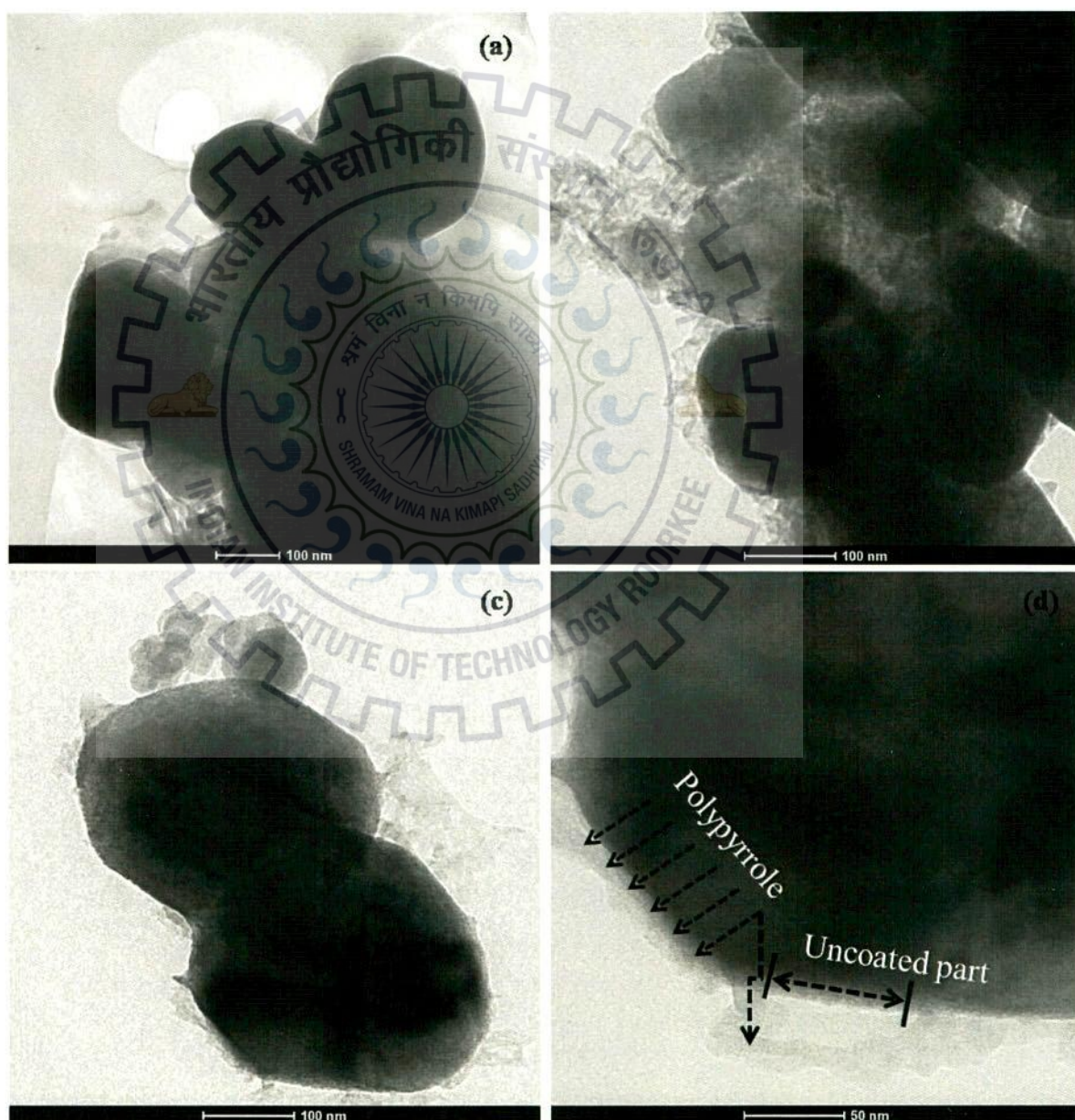
Fig. 5.5: TEM images of (a) LiFePO₄/C-PPy(ACN), (b) LiFePO₄/C-PPy(ethanol), (c) LiFePO₄/C-PPy(water) and (d) LiFePO₄/C-PPy(water) at higher magnification.

Though the $LiFePO_4$/C particles are present in the agglomerated state, however, the regular (nearly spherical) shape of the particles remains unchanged after surface coating with the polymer. The particle size of all the $LiFePO_4$/C-PPy composites are in the range of 100 – 200 nm. Fig 5.5(d) presents a high resolution micrograph of the particle shown in Fig. 5.5(c) from which the incomplete polypyrrole coating on the $LiFePO_4$/C particle prepared in water solvent can be seen.

5.1.1.5 Raman spectra analysis

The structure of carbon and polypyrrole coatings that developed on the $LiFePO_4$ particles is important for assessing the electronic conductivity and Li-ion diffusivity of the $LiFePO_4$/C material. Raman analysis was performed to know the structure of carbon and polypyrrole. The broad and high intensity bands at 1350 cm^{-1} and 1580 cm^{-1} in Raman spectra of $LiFePO_4$/C signify the D and G-bands of carbon (Fig. 5.6). The D-band originates because of defects associated with finite graphene size such as edges with special shapes and atomic defect within a graphene layer, leading to breaking of symmetry in the structure [Dresselhaus et al, 2010]. The A_{1g} mode of vibration, occurs at the k_1 (edge) point of first Brillion zone and gives rise to D-band. For the infinite graphitic size the polarizability gets cancelled, therefore A_{1g} mode of vibration is Raman inactive. But for finite graphitic polarizability exists due to which graphitic carbon becomes Raman active. So, the intensity at 1350 cm^{-1} is attributed to A_{1g} mode for finite size of graphitic carbon or at the edges of larger graphitic carbon [Tuinstra and Koenig, 1970].

The G-band represents highly ordered graphitic carbon. The Fig. 5.6 shows the Gaussian fitting of the Raman spectra with de-convolution of D-band and G-band for $LiFePO_4$/C and $LiFePO_4$/C-PPy composites to measure the R values. The Gaussian fitting and peak de-convolution were performed using the 'Magic Plot' software package. The values of R for $LiFePO_4$/C-PPy(water), $LiFePO_4$/C-PPy (ethanol) and $LiFePO_4$/C-PPy (ACN) are 0.77, 0.74 and 0.67 respectively. The R = 0.97 for $LiFePO_4$/C has already been presented in the section 4.1.6. The decrease in R values for all $LiFePO_4$/C-PPy composites shows higher fraction of the graphitic carbon as compared to that of $LiFePO_4$/C material. This is attributed to formation of H-bonds as a result of interaction between polypyrrole and defect sites of carbon [Singla et al, 2011]. H-bonding occurs when nearly spherical shaped ceramic particles were coated with polymer chains [Tanaka and Kozako, 2005]. A minimum value of R (= 0.67) has been obtained for sample $LiFePO_4$/C-PPy(ACN). This is because polypyrrole coating of minimum porosity grown in ACN solvent offers highest contact area with carbon coating on $LiFePO_4$ particles.

Hence large number of defects were interacted with polypyrrole coating resulting in decreased D-band intensity for $LiFePO_4/C$-PPy(ACN) composite.
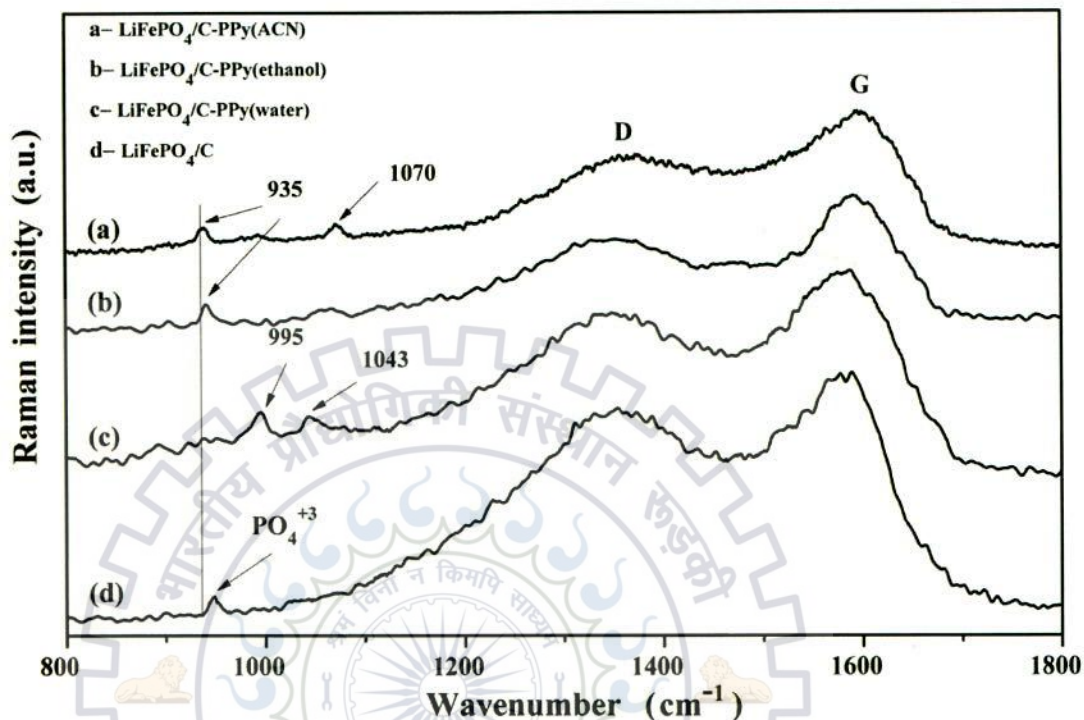

Fig. 5.6: Raman spectra of $LiFePO_4/C$ and $LiFePO_4/C$-PPy composites.

The growth and structure of polypyrrole has also been investigated by the Raman spectra analysis (Fig. 5.6) of $LiFePO_4/C$-PPy composites. Raman spectrum of $LiFePO_4/C$-PPy(water) composite has weak bands at 995 and 1043 cm^{-1} frequencies. The band at 995 cm^{-1} is associated with the ring deformation vibration which has a consequence of polaron formation. The low intensity peak at 1043 cm^{-1} is assigned to symmetric C–H in-plane bending vibration in the benzoid ring [Li et al, 2008]. The peaks at 935 and 937 cm^{-1} for the composites $LiFePO_4/C$-PPy(ACN) and $LiFePO_4/C$-PPy(ethanol) respectively arise due to C–H out of plane deformation in the quinoid ring and represent the bipolaron state of polypyrrole [Duchet et al, 1998]. The peak located at 1070 cm^{-1} for $LiFePO_4/C$-PPy(ACN) arises due to the C–H in-plane bending vibration occurred in the oxidized state of polypyrrole. Although polaron and bipolaron states give rise to the conductivity of polypyrrole, but bipolaron state favors the higher conductivity as compared to the polaron state [Hou et al, 2014]. Even though a single bipolaron peak at 935 cm^{-1} was observed for $LiFePO_4/C$-PPy(ethanol), but the detection of two peaks at 935 and 1070 cm^{-1} reflects the higher oxidation of polypyrrole in $LiFePO_4/C$-PPy(ACN) which supports the higher conductivity.
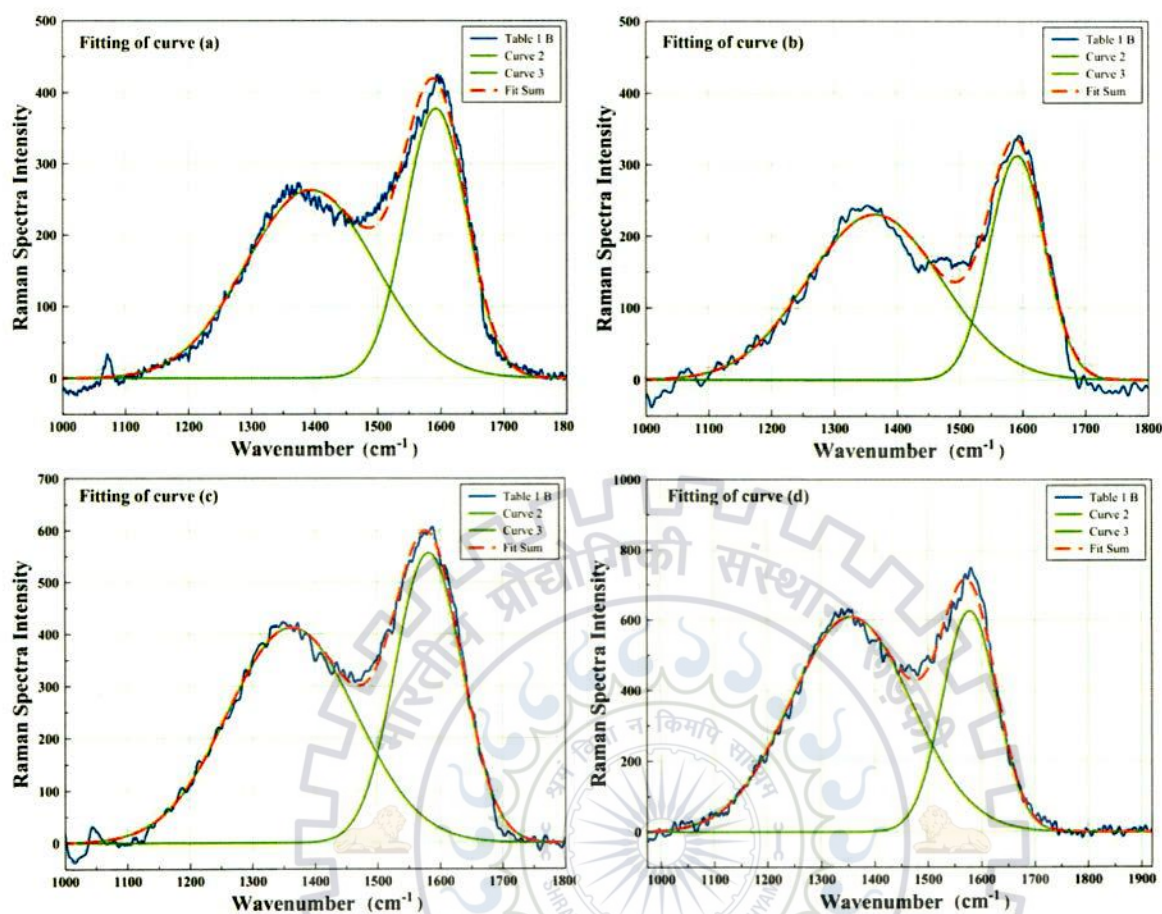
Fig. 5.7: Gaussian fitting and de-convoluted D-band and G-band of the Raman spectra (a), (b), (c) and (d) shown in Fig. 5.6.

5.1.2 Electrochemical testing

5.1.2.1 EIS analysis

EIS analyses were made to investigate the effect of solvents on the conductivity of all the LiFePO₄/C-PPy electrode materials. Fig. 5.8 shows the EIS profiles of LiFePO₄/C and LiFePO₄/C-PPy composite electrodes. The EIS profiles alongwith the equivalent circuit models as an inset are shown in the Fig. 5.8. The equivalent circuit has R_s in series with a parallel combination of *CPE*, and R_{ct} in series with Z_ω [Gao and Tang, 2008]. The low frequency response of EIS corresponds to the transport of Li-ion and electron into the electrode material [Shenouda and Liu, 2008]. The D_{Li+} has been calculated in the low frequency region of EIS using the similar method as explained under section 3.3.3.3 of chapter 3.

Fig. 5.8: Electrochemical impedance spectra of LiFePO$_4$/C, LiFePO$_4$/C-PPy(water), LiFePO$_4$/C-PPy(ethanol) and LiFePO$_4$/C-PPy(ACN).

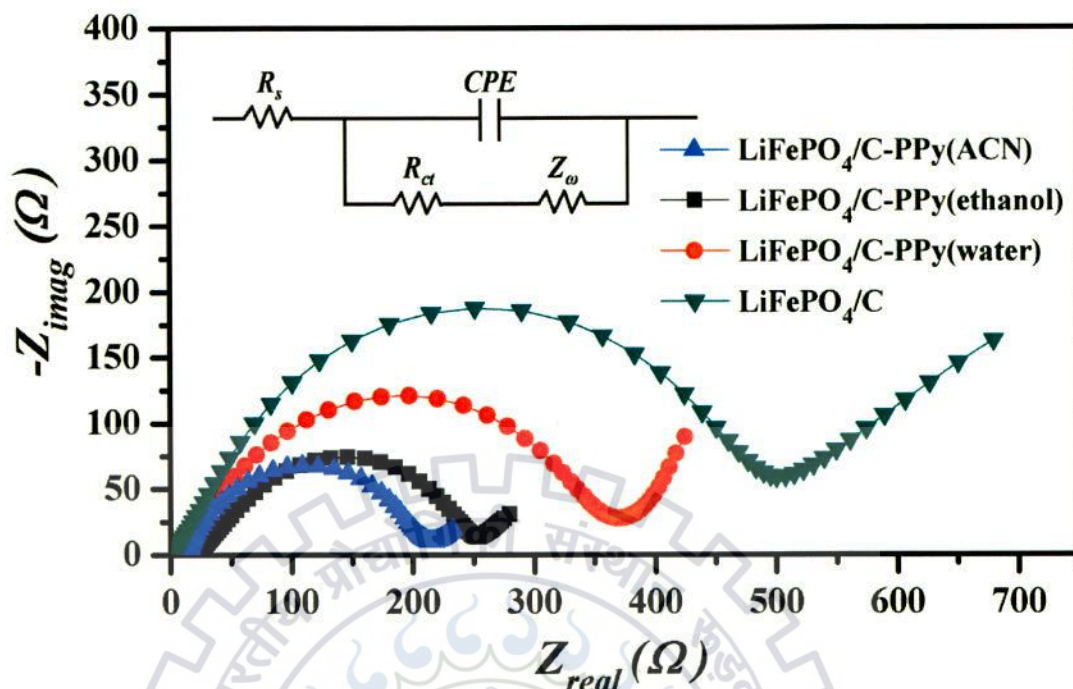The slope of the linearly fitted points in the low frequency region of the variation of Z_{real} vs. $\omega^{-1/2}$ in Fig. 5.9 yields the value of σ_ω. The slopes of the linear fitting of the points in the low frequency region have been calculated for each sample. The Table 5.2 contains the different EIS parameters such as R_{ct}, i_0, D_{Li+} and slopes for the LiFePO$_4$/C and LiFePO$_4$/C-PPy composite materials. Using the relations (3.4) and (3.5), the calculated values of D_{Li+} at room temperature are 7.56×10^{-14} cm^2/s, 4.00×10^{-13} cm^2/s and 6.23×10^{-13} cm^2/s for the samples LiFePO$_4$/C-PPy(water), LiFePO$_4$-PPy(ethanol) and LiFePO$_4$/C-PPy(ACN) respectively. Therefore D_{Li+} of nanocomposites are found higher than 7.37×10^{-15} cm^2/s for LiFePO$_4$/C. The highest D_{Li+} for LiFePO$_4$/C-PPy(ACN) composite can be explained by the Raman analysis and morphology studies. Raman spectra of all the LiFePO$_4$/C-PPy samples show decrease in the D-band intensity as compared to that of LiFePO$_4$/C. The interaction between polypyrrole and defect sites of carbon coating reduces the interaction of Li-ion with the defect sites [Sehrawat and Sil, 2015]. The reduced interaction facilitates fast movement of Li-ion on the graphitic carbon resulting in higher diffusivity to the LiFePO$_4$/C-PPy(ACN) material [Jana et al, 2014]. As confirmed by FESEM the low porosity on the polypyrrole synthesized in ACN solvent gives

better interconnection of chains and continuous path to facilitate Li-ion movement [Yin et al, 2012].

For all the materials synthesized, i_0s are calculated from the relation (3.6) and listed in the Table 5.2. The composite LiFePO$_4$/C-PPy(ACN) has the highest i_0 of 1.20×10^{-4} mA/cm^2 among all the composite materials studied, reflecting best electrochemical reversibility. The minimum R_{ct} value was obtained for LiFePO$_4$/C-PPy(ACN) and consequently electronic conductivity of this composite material is highest among all the composites prepared.
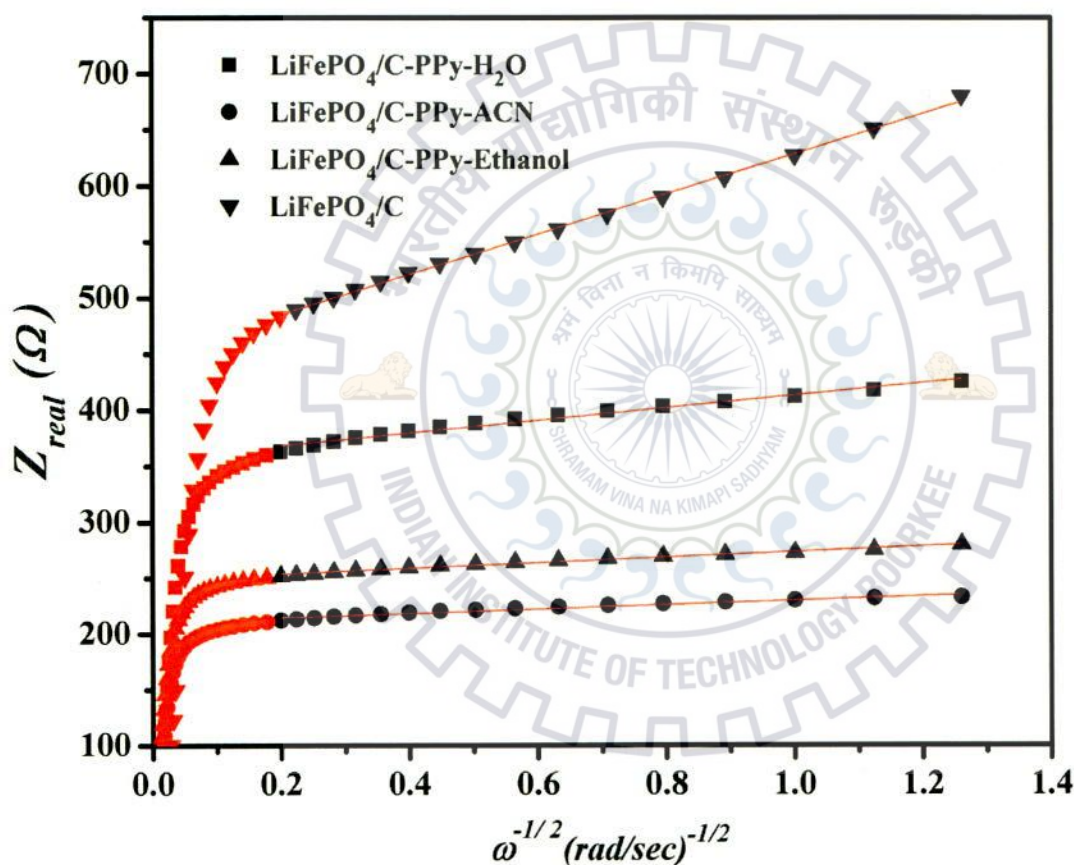
Fig. 5.9: Plot of Z_{real} vs. $\omega^{-1/2}$ for different composite materials

The higher electronic conductivity of the sample LiFePO$_4$/C-PPy(ACN) as compared to LiFePO$_4$/C-PPy(water) and LiFePO$_4$/C-PPy(ethanol) was attributed to the following effects of (i) the bipolaron formation in polypyrrole coating in ACN solvent as compared to polaron formation in water, (ii) generation of –OH and C=O groups during polymerization of pyrrole in water and ethanol solvents restrict the delocalization of polaron and bipolaron [Ko et al, 1990], (iii) the generated –OH and C=O groups during the synthesis attack the active sites which

restricts the pyrrole chain growth mechanism and resulting in the higher porosity [Ko et al, 1990]. On the other hand, higher porosity generated during the synthesis of pyrrole produces the discontinuity in the surface coating resulting in larger path length for the conducting species [Noh et al, 2003, Petrovsky et al, 2003]. As a result Fig. 5.8 shows $LiFePO_4/C$-PPy(ACN) composite giving a minimum value of R_{ct} = 215.6 Ω as compared to 500.3, 368.8 and 252.0 Ω for samples $LiFePO_4/C$, $LiFePO_4/C$-PPy(water) and $LiFePO_4/C$-PPy(ethanol) respectively.

Table 5.2: EIS parameter of electrodes $LiFePO_4/C$, $LiFePO_4/C$-PPy(water), $LiFePO_4/C$-PPy(ethanol) and $LiFePO_4/C$-PPy(ACN).

Sample	$R_s(\Omega)$	$R_{ct}(\Omega)$	$i_0(mA\ cm^{-2})$	$D_{Li^+}\ (cm^2\ s^{-1})$	$\sigma_\omega\ (\Omega\ rad^{1/2}\ sec^{-1/2})$
$LiFePO_4/C$	4.84	500.3	5.17×10^{-5}	7.37×10^{-15}	179.1
$LiFePO_4/C$-PPy(water)	13.4	368.8	7.01×10^{-5}	7.56×10^{-14}	55.9
$LiFePO_4/C$-PPy(ethanol)	19.7	252.0	1.02×10^{-4}	4.00×10^{-13}	24.31
$LiFePO_4/C$-PPy(ACN)	14.94	215.6	1.20×10^{-4}	6.23×10^{-13}	19.4

5.1.2.2 Electrochemical cell performance

The discharge profiles of the cathode materials $LiFePO_4/C$-PPy(ACN), $LiFePO_4/C$-PPy(ethanol), and $LiFePO_4/C$-PPy(water) measured at different current rates of 0.2, 0.5, 1, 2, 5, 10 and 20C rates are presented in comparison with that of $LiFePO_4/C$, in Fig. 5.10(a-c). It is seen that the rate capability has enhanced for all the polypyrrole coated composites as compared to $LiFePO_4/C$. For $LiFePO_4/C$-PPy(ACN), $LiFePO_4/C$-PPy(ethanol), $LiFePO_4/C$-PPy(water) and $LiFePO_4/C$ materials the discharge capacities are 139, 137, 138 and 142 mAh/g respectively obtained at low C-rate (0.2C), and 82, 60, 54 and 42 mAh/g respectively at high C-rate (20C). The measurements at 5, 10 and 20C rates for the composite $LiFePO_4/C$-PPy(ACN) show discharge capacities of 98, 91 and 82 mAh/g respectively. However the discharge capacities of $LiFePO_4/C$-PPy(ethanol) at 5, 10 and 20C rates are 83, 71 and 60 mAh/g respectively. All the $LiFePO_4/C$-PPy composites show a minor decrease in discharge capacity at low current rates. At low current rates the discharge capacities of $LiFePO_4/C$-PPy and $LiFePO_4/C$ are comparable as polypyrrole coating have no significant effect on the conduction because of slow movement of charge species. However the difference in capacities has substantially increased when current is increased into the steps of 2C, 5C, 10C and 20C. From

Fig. 5.10(a-c) one can infer that $LiFePO_4/C$-PPy(ACN) has higher rate capability than the materials $LiFePO_4/C$-PPy synthesized in other solvents such as water and ethanol.
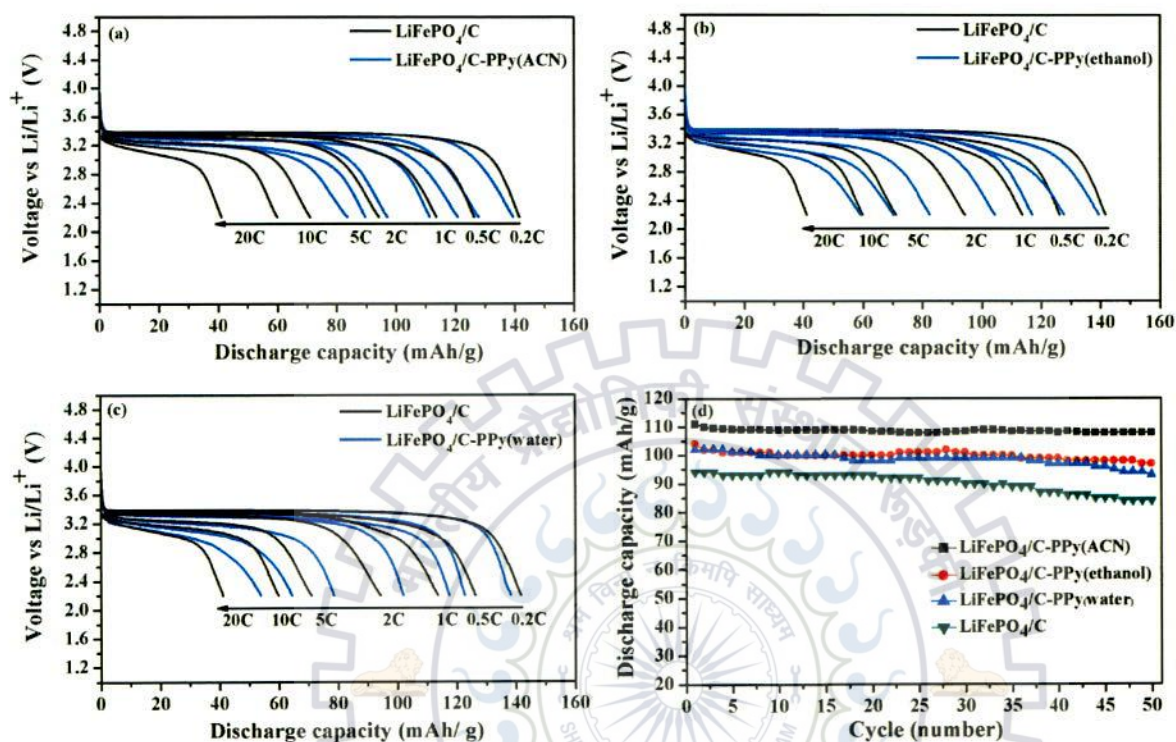
Fig. 5.10: Comparative plots of the capacities of composites (a) $LiFePO_4/C$-PPy(ACN), (b) $LiFePO_4/C$-PPy(ethanol), (c) $LiFePO_4/C$-PPy(water) with $LiFePO_4/C$. (d) Discharge capacities of $LiFePO_4/C$ and $LiFePO_4/C$-PPy composites at 2C rate for 50 cycles.

In order to investigate the higher rate capability of $LiFePO_4/C$-PPy(ACN), EIS measurements of all the samples have been discussed in section 5.1.2.1. It is observed that the results of the electrochemical measurements are consistent with EIS for all the samples. The higher R_{ct} values of the $LiFePO_4/C$-PPy(water) and $LiFePO_4/C$-PPy(ethanol) signify low charge transfer resistance. Also the improved Li-ion diffusion in the $LiFePO_4/C$-PPy(ACN) composite was supported by morphological and structural analysis of the polypyrrole coating. The low porosity and reduction in defect sites on carbon coating improves the Li-ion diffusion. From the morphology studies it was investigated that polypyrrole synthesized in ACN solvent has low porosity.
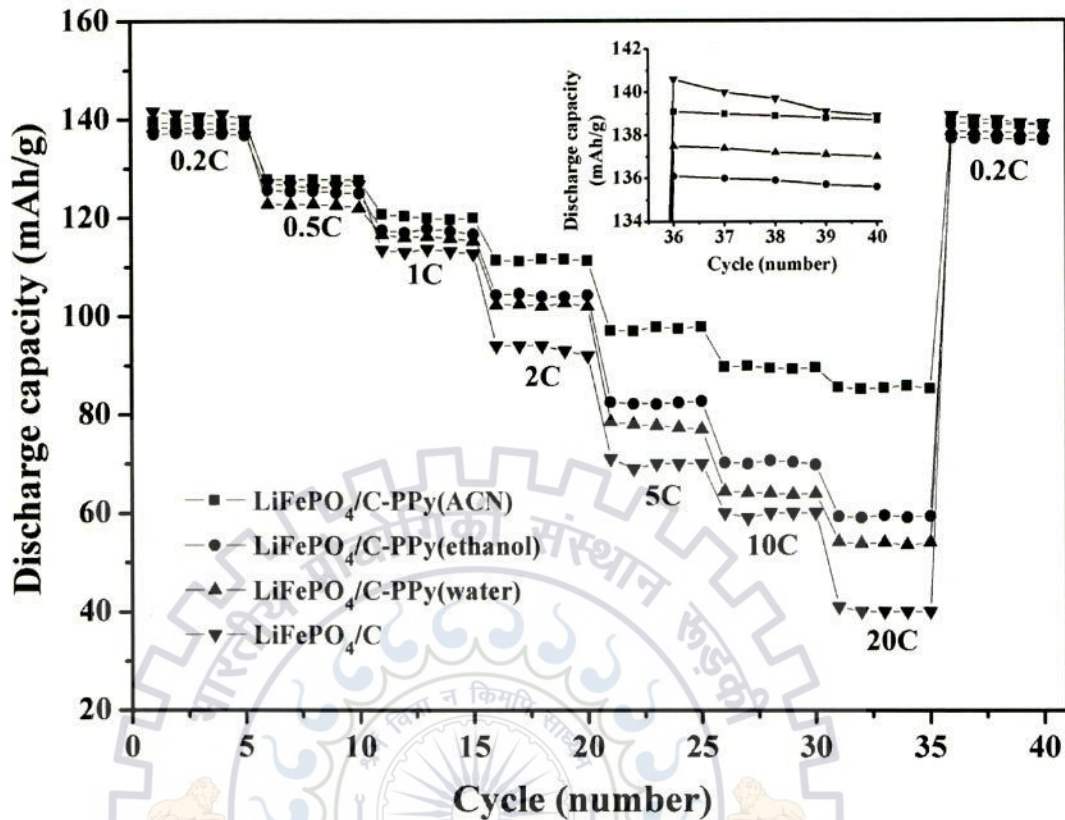
Fig. 5.11: Discharge capacity of LiFePO₄/C-PPy(ACN), LiFePO₄/C-PPy(ethanol), LiFePO₄/C-PPy(water) and LiFePO₄/C for 5 cycles at different 0.2, 0.5, 1, 2, 5, 10 and 20C rates.

The low porosity improves the Li-ion diffusion in two ways viz. (i) providing good interconnection and continuous path facilitating Li-ion movement, (ii) providing higher contact area with carbon coating resulting in minimum number of defect sites on the carbon coating. So, for sample LiFePO₄/C-PPy(ACN) the lower porosity of polypyrrole offers fast Li-ion movement as compared to that in LiFePO₄/C-PPy(ethanol), and LiFePO₄/C-PPy(water) materials.

It has been reported in many studies [Jana et al, 2014, Winter et al, 1998] that higher number of defects on carbon coating offers more sites for Li-ions occupancies, but there may be no de-intercalation from these sites due to which less number of Li-ions participate in the charging / discharging process, resulting in increased irreversible capacity of the electrode materials. The Raman analysis confirms the minimum number of defects on the carbon for LiFePO₄/C-PPy(ACN) cathode material, which may be occupied by the Li-ions contributing to the lowest

irreversible capacity among all the samples. The Fig. 5.10(d) compares the discharge capacities of LiFePO$_4$/C-PPy(ACN), LiFePO$_4$/C-PPy(ethanol) and LiFePO$_4$/C-PPy(water) composites at typically 2C rate for 50 cycles. All the LiFePO$_4$/C-PPy samples show superior cyclability as compared to LiFePO$_4$/C. The capacity fading of 2 %, 5 %, 9 % 11 % as compared to initial capacity were observed for LiFePO$_4$/C-PPy(ACN), LiFePO$_4$/C-PPy(ethanol), LiFePO$_4$/C-PPy(water) and LiFePO$_4$/C samples respectively over 50 cycles. This shows that polypyrrole addition to LiFePO$_4$/C improves the cyclability and rate capability for all the solvents.

Fig. 5.11 shows the discharge capacities of the materials measured at different C-rates and for every C-rate, measurements were made for 5 cycles. The Fig. 5.12 represents the plot of differential capacity (DC) versus C-rate. From the graph it can be inferred that the DC values are very close to zero, at lower current rates of 0.2C and 0.5C respectively. At moderate discharge rates of 1, 2 and 5C the DC of each samples starts increasing and shows maximum increase at the highest 20C rate. The sample LiFePO$_4$/C-PPy(water) shows a slight dip in DC at 10C rate showing a decrease in the rate capability as compared to that at 5C. The highest DC value of 1.08 has been obtained for LiFePO$_4$/C-PPy(ACN) composite material at 20C rate implying that it is a material able to withstand highest rate capability of all the synthesized materials.
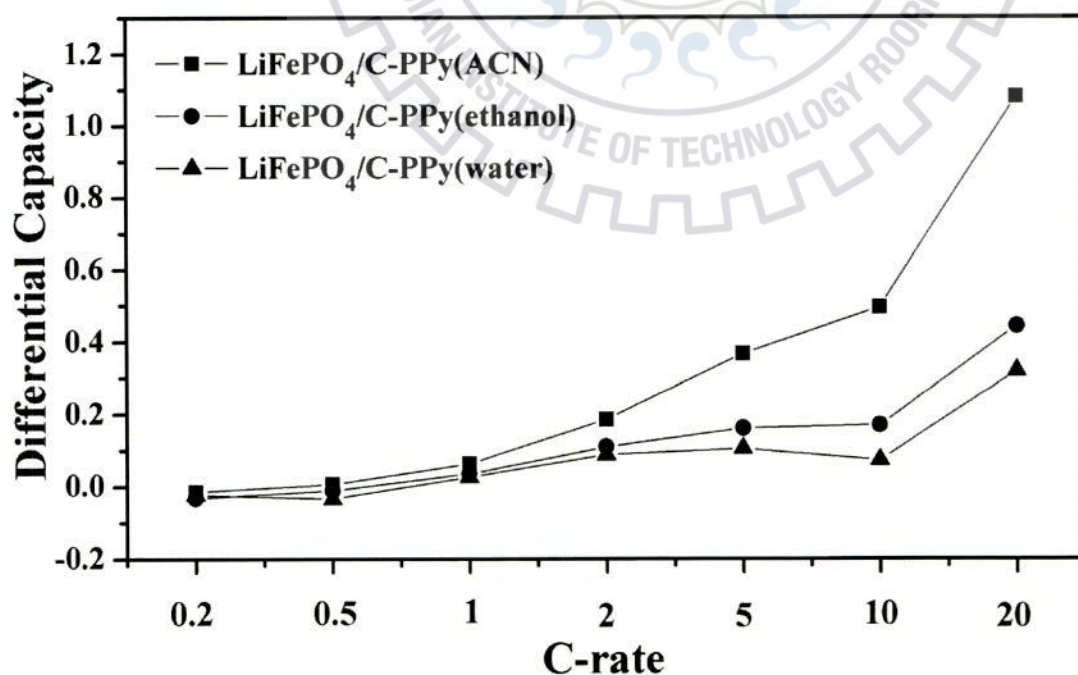
Fig. 5.12: DC variation with C-rate.
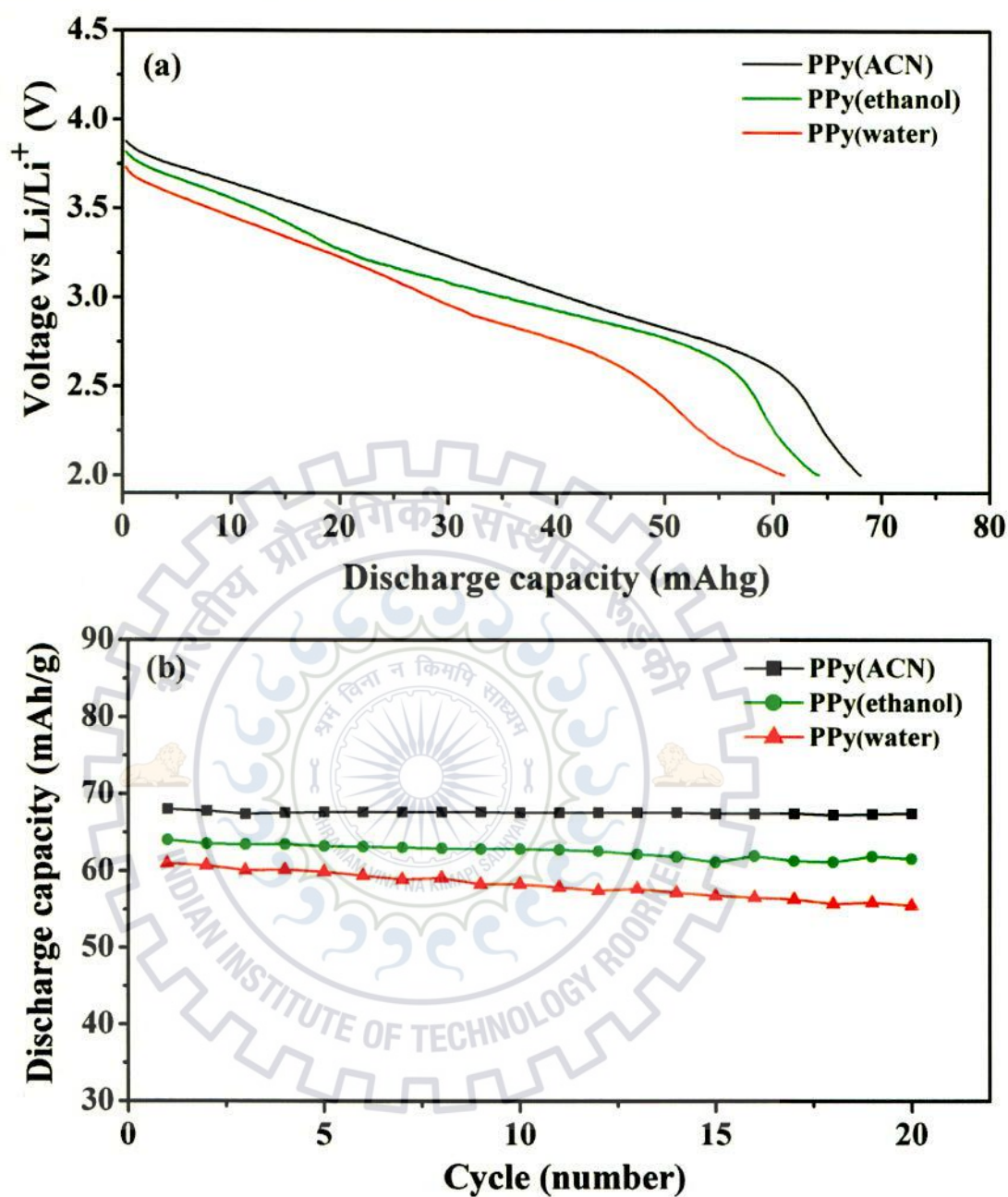
Fig. 5.13 (a) Discharge capacity vs. number of cycles and (b) voltage vs. discharge capacity of polypyrrole synthesized in water, ethanol and ACN solvents at 1 C rate.

Fig. 5.13(a) shows the discharge capacity of pure polypyrrole synthesized in water, ethanol and ACN solvents. The discharge profile shows that the polypyrrole samples are electrochemically active in the range of 4.2 – 2.0 V. The discharge capacities of 61, 64 and 68 mAh/g are observed at 1C rate for the polypyrrole samples synthesized in water, ethanol and ACN solvents respectively. The discharge capacity of polypyrrole is highest for ACN solvent

followed by those prepared in ethanol and water. This was due to the difference in morphology of polypyrrole samples obtained using various solvents. The electronic conductivity and Li-ion diffusivity were affected by morphology of polypyrrole. The continuous nature of polypyrrole coating derived in ACN solvent is the reason for higher capacity of the composite. In both coating and bulk, polypyrrole synthesized in ACN has denser structure as compared to that prepared in water and ethanol solvents. The discontinuity restricts the flow of conducting species due to which the overall conductivity of material decreases [Ko et al, 1990]. So, a continuous coating is required to achieve good electrical conductivity of the material. The discharge capacities upto 20 cycles for the cells of pure polypyrrole as cathode are presented in Fig. 5.13(b). The discharge capacities of polypyrrole synthesized in solvent ACN is almost constant upto 20 cycles. However, materials synthesized in water and ethanol solvents deliver 92 % and 96 % of the initial capacity respectively, after 20 cycles, showing the maximum stability of polypyrrole synthesized in ACN.
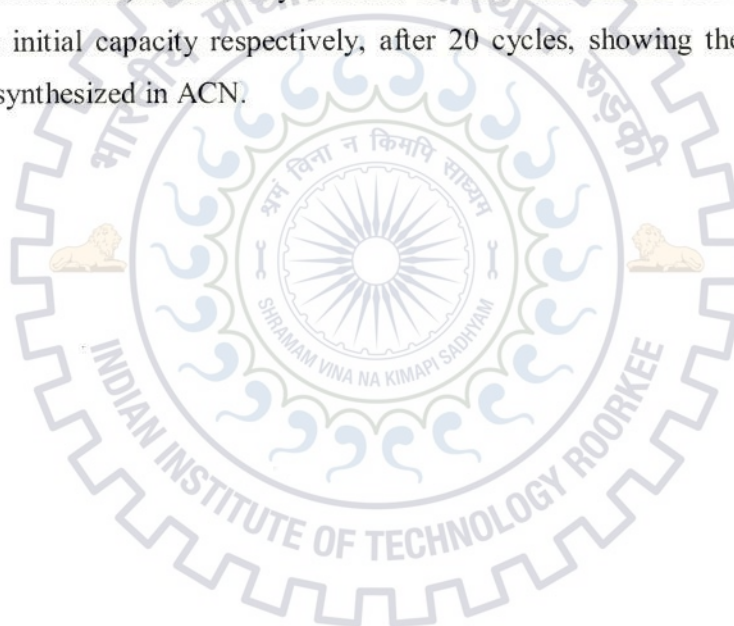
5.2 RESULTS AND DISCUSSION-
POLYTHIOPHENE COATED LiFePO$_4$/C

5.2 RESULTS AND DISCUSSION-POLYTHIOPHENE COATED LiFePO$_4$/C

Polythiophene is an electrochemically active conductive polymer with excellent environmental stability, good Li-ion storage capacity and long cyclability. Moreover mean discharge voltage of polythiophene is around of 3.7 V vs Li$^+$/Li, which is very close to the discharge voltage of LiFePO$_4$ (3.4 V) [Tang et al, 2008]. Therefore polythiophene coating on the surface of LiFePO$_4$/C particles would be suitable to improve the electronic conductivity and Li-ion diffusivity. This section presents the results and discussion on phase analysis, Raman spectroscopic analysis, morphology study and electrochemical analysis of the polythiophene coated LiFePO$_4$/C particles. In-situ polythiophene coating was deposited on LiFePO$_4$/C particles in the binary organic solvents of ACN and dichloromethane (CH$_2$Cl$_2$) at low temperature (0 – 5 °C). Polythiophene coating was performed on LiFePO$_4$/C with varying Li amount (95%, 100% and 105%) to suppress the growth of impurity phase(s). After this capacity and rate capability measurements of Polythiophene coated LiFePO$_4$/C samples were performed.

5.2.1 Physical characterization

5.2.1.1 Phase analysis

The XRD patterns of samples Li$_{1.00}$FePO$_4$/C and Li$_{1.00}$FePO$_4$/C-PTh are shown in Fig. 5.14 and Fig. 5.15 respectively. For Li$_{1.00}$FePO$_4$/C the XRD pattern reveals pure phase of olivine phosphates (JCPDS file no. 01-083-2092) without any detectable impurity. The XRD pattern of Li$_{1.00}$FePO$_4$/C-PTh composite shows the presence of three phases LiFePO$_4$, Li$_{0.05}$FePO$_4$ and Li$_3$PO$_4$. For the phase Li$_{0.05}$FePO$_4$, most of Fe has been oxidized from Fe^{2+} to Fe^{3+} due to delithiation during the polymerization and has electrochemical properties similar to that of LiFePO$_4$ [Yamada et al, 2006]. The weak intensity peaks at 22.32 ° and 23.16 ° (Fig. 5.14) correspond to electrochemically inactive Li$_3$PO$_4$ (with JCPDS no. 01-034-0358) impurity phase. To suppress the growth of Li$_3$PO$_4$ impurity, polythiophene coating was developed on Li-deficient Li$_{0.95}$FePO$_4$/C and Li-excess Li$_{1.05}$FePO$_4$/C materials using the similar method used for LiFePO$_4$. It has been observed that only the polythiophene coated Li-deficient Li$_{0.95}$FePO$_4$ material was capable of suppressing the formation of Li$_3$PO$_4$ impurity phase as compared to polythiophene coated LiFePO$_4$/C and Li-excess Li$_{1.05}$FePO$_4$/C materials.

The XRD patterns of $Li_{1.05}FePO_4/C$ and $Li_{0.95}FePO_4/C$ (Fig. 5.14) are similar to the $Li_{1.00}FePO_4/C$ and no peak corresponding to other phase is observed, hence excess lithium may have entered into the lattice of $LiFePO_4$ and deficiency of lithium has not changed the structure of $LiFePO_4$. The cell parameters of Li_xFePO_4 structure (for x = 0.95, 1.00 and 1.05) were determined by using the Bragg's law for the orthogonal system:

$$d = \left(\frac{h^2}{a^2} + \frac{k^2}{b^2} + \frac{l^2}{c^2}\right)^{-1/2}$$

(5.4)

where d is inter-planar spacing and a, b, c are the cell parameters. The calculations were performed using first, second and third highest intensity peaks and cell parameters are listed in Table 5.3.

Table 5.3: Unit cell parameters and volumes of Li_xFePO_4 (x=0.95, 1.00 and 1.05) compounds.

Sample	2θ	hkl	d-spacing (Å)	Lattice parameter (Å)	Unit cell volume (Å³)
	21.052	101	4.220	a = 10.299	
$Li_{0.95}FePO_4/C$	25.820	111	3.451	b = 5.994	285.57
	35.843	311	2.505	c = 4.626	
	20.880	101	4.255	a = 10.315	
$LiFePO_4/C$	25.668	111	3.471	b = 5.995	288.79
	35.704	311	2.515	c = 4.670	
	20.843	101	4.263	a = 10.321	
$Li_{1.05}FePO_4/C$	25.629	111	3.476	b = 6.004	289.95
	35.686	311	2.516	c = 4.679	

The cell volume of $Li_{1.00}FePO_4$ was calculated as $V = 288.79$ Å³ which is in excellent agreement with the value reported in literature ($V = 288.13$ Å³) [Moreno et al, 2001]. The samples $Li_{0.95}FePO_4$ and $Li_{1.05}FePO_4$ have the cell volumes of $V = 285.57$ Å³ and 289.95 Å³ respectively. The shift of the peak positions in the XRD patterns of Li-excess and Li-deficient samples of $LiFePO_4/C$ with respect to the parent compound was observed. The excess and deficiency of Li-ion develops a lattice strain in the material, which results in the change of the inter-planer spacing. Hence peak shifting in the XRD patterns towards lower Bragg angle for Li-excess and higher Bragg angle for Li-deficient samples were observed.
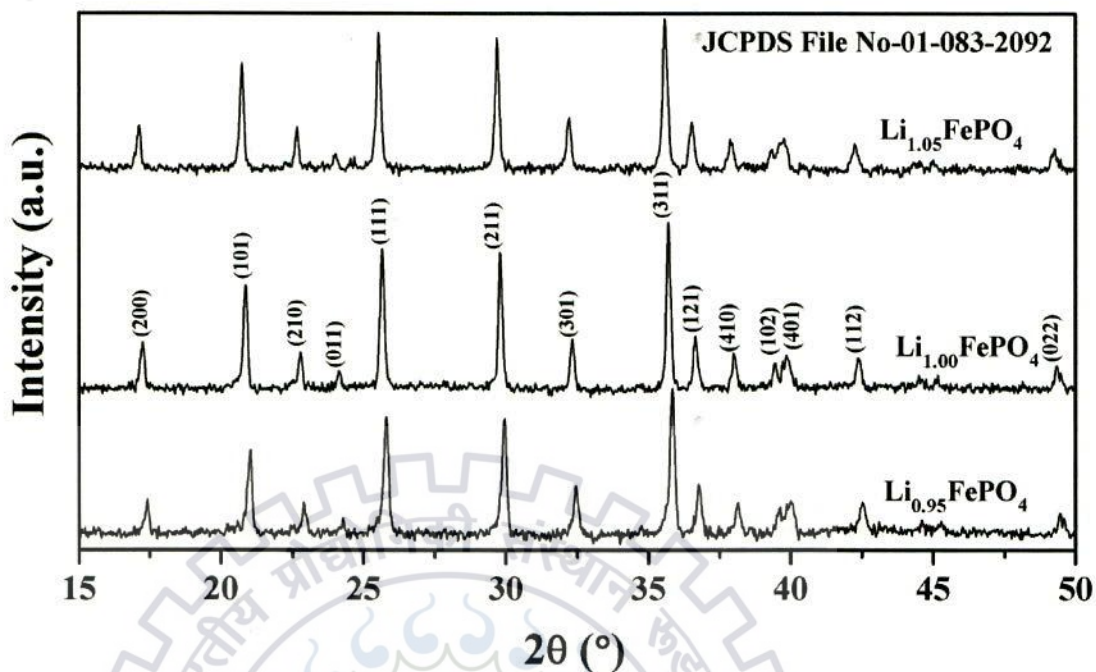
Fig. 5.14: XRD patterns of $Li_{0.95}FePO_4/C$, $Li_{1.00}FePO_4/C$ and $Li_{1.05}FePO_4/C$ composites.
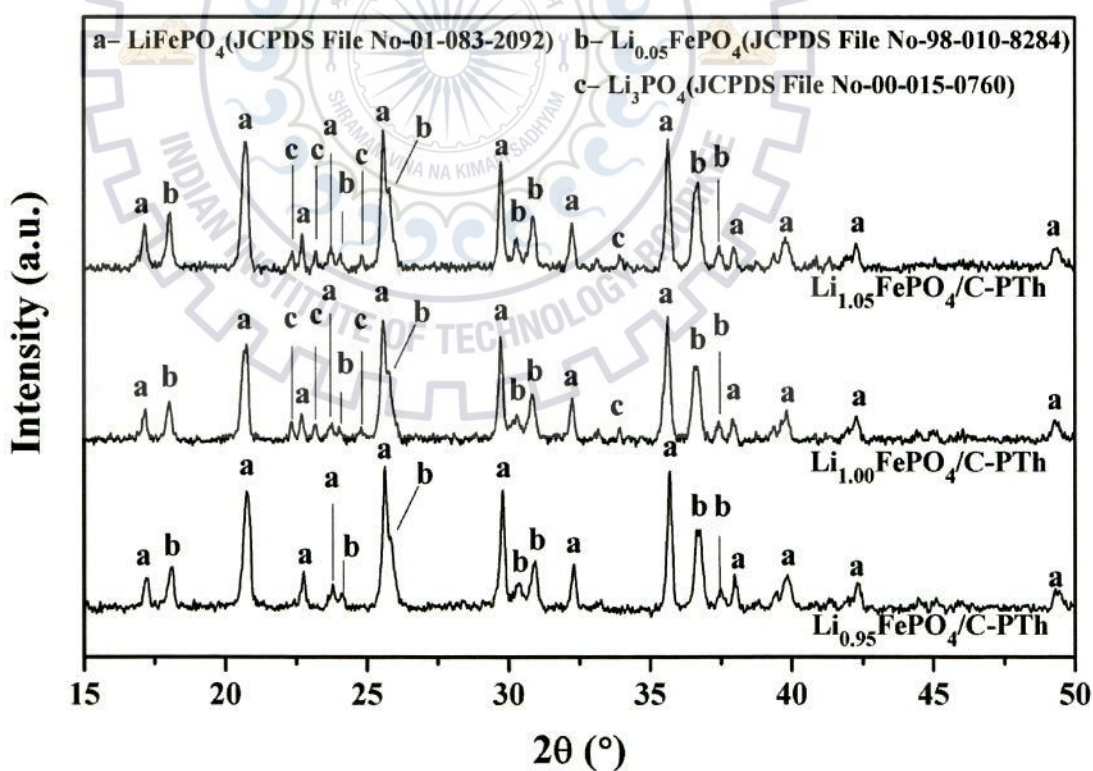
Fig. 5.15: XRD pattern of $Li_{0.95}FePO_4/C$-PTh, $Li_{1.00}FePO_4/C$-PTh and $Li_{1.05}FePO_4/C$-PTh composites.

The XRD results of sample $Li_{0.95}FePO_4/C$-PTh confirmed the presence of pure electrochemically active phases. Therefore the polythiophene coating of different contents on $Li_{0.95}FePO_4/C$ material has been investigated for the measurements of rate capability and specific capacity.

5.2.1.2 TG analysis

Fig. 5.16 shows the TG profiles of $Li_{0.95}FePO_4/C$-PTh composites from room temperature to 800 °C under Ar gas atmosphere. The weight loss from room temperature to 120 °C was due to removal of moisture content from the $Li_{0.95}FePO_4/C$-PTh composites. The gradual weight loss over the temperature range from 120 to 800 °C was attributed to decomposition of polythiophene present in $Li_{0.95}FePO_4/C$-PTh composites. During the TG analysis the polythiophene coated $Li_{0.95}FePO_4/C$ samples were held at 800 °C for 1 hour to decompose the entire polythiophene content. The polythiophene estimated from TG curves were about 4, 6, 8 and 10 wt%. The $Li_{0.95}FePO_4/C$-PTh composites containing ~ 4, 6, 8 and 10 wt% of polythiophene are denoted by $Li_{0.95}FePO_4/C$-PTh(4), $Li_{0.95}FePO_4/C$-PTh(6), $Li_{0.95}FePO_4/C$-PTh(8) and $Li_{0.95}FePO_4/C$-PTh(10) respectively.
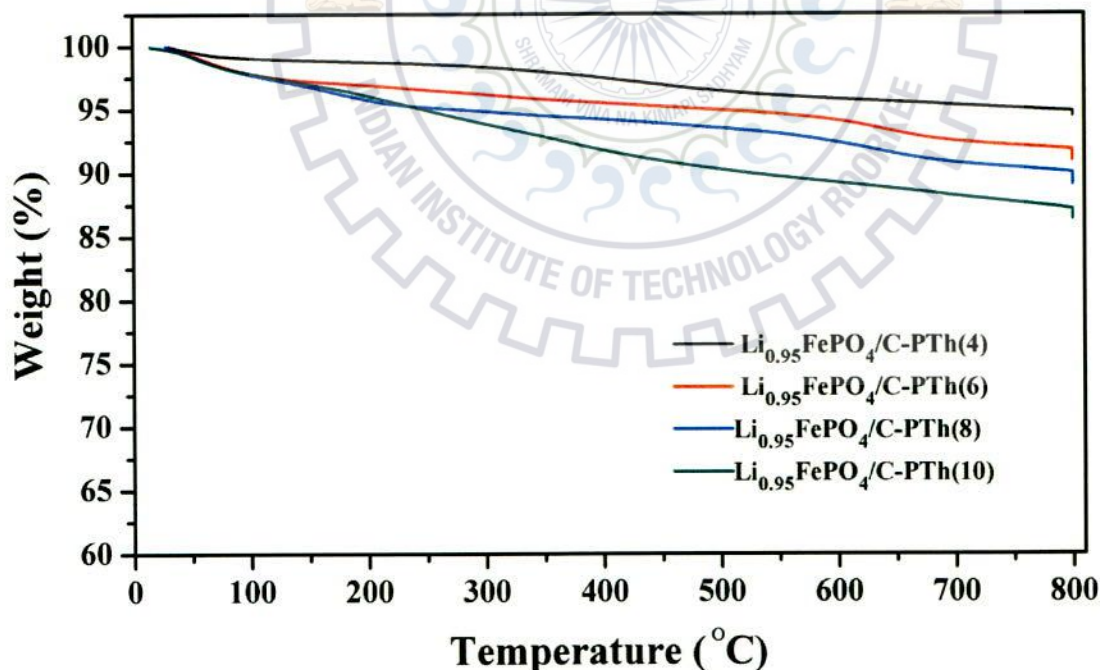
Fig. 5.16: TG plot of samples $Li_{0.95}FePO_4/C$-PTh(4), $Li_{0.95}FePO_4/C$-PTh(6), $Li_{0.95}FePO_4/C$-PTh(8) and $Li_{0.95}FePO_4/C$-PTh(10).

5.2.1.3 Morphologies

The FESEM micrographs of polythiophene coated Li$_{0.95}$FePO$_4$/C are shown in Fig 5.17(a-d). Fig. 5.17(a) and (b) show partially coated Li$_{0.95}$FePO$_4$/C particles of samples Li$_{0.95}$FePO$_4$/C-PTh(4) and Li$_{0.95}$FePO$_4$/C-PTh(6). So, the amount of polythiophene grown is not sufficient to cover all the LiFePO$_4$ and Li$_{0.05}$FePO$_4$ particles for these composites. The micrographs of Li$_{0.95}$FePO$_4$/C-PTh(6) composite show that there is inter-particle contact through carbon and polythiophene. However it appears from the micrograph of Li$_{0.95}$FePO$_4$/C-PTh(8) composite (Fig. 5.17(c)) that a continuous polythiophene coating has been developed and the inter-particle contact occurs over the particles of sample Li$_{0.95}$FePO$_4$/C through the polythiophene. Polymer coating appears to be still thicker for the sample Li$_{0.95}$FePO$_4$/C-PTh(10).

Fig. 5.17: FESEM micrograph of (a) Li$_{0.95}$FePO$_4$/C-PTh(4), (b) Li$_{0.95}$FePO$_4$/C-PTh(6), (c) Li$_{0.95}$FePO$_4$/C-PTh(8) and (d) Li$_{0.95}$FePO$_4$/C-PTh(10).

5.2.1.4 Raman spectroscopy

The Raman spectroscopy was performed to confirm the polymerization that has taken place with thiophene monomers and to characterize the structure of carbon. Raman spectra of all the $Li_{0.95}FePO_4$/C-PTh samples (Fig. 5.18) exhibit nine characteristic peaks at the wave numbers of 582, 650, 680, 900, 950, 1053 and 1154 along with the D and G-bands of carbon. The Raman band at 585 cm^{-1} corresponds to out of plane deformation vibration in the polythiophene ring [Louarn et al, 1996]. The bands at 650 and 680 cm^{-1} are assigned to the C_α–S–C_α in-plane deformation vibration in polythiophene ring [Louam et al 1995, Shi et al, 2002]. The Raman peak at 1053 cm^{-1} was assigned to the pure C_β–H in plane bending vibration [Shi et al, 2002]. The band at 950 cm^{-1} is attributed to stretching vibration of C_β–C_δ [Momo et al, 2012]. The band at 1154 cm^{-1} is due to inter-ring C_α–$C_{\alpha'}$ anti-symmetric stretching vibrations in the polythiophene chain [Shi et al, 2002].
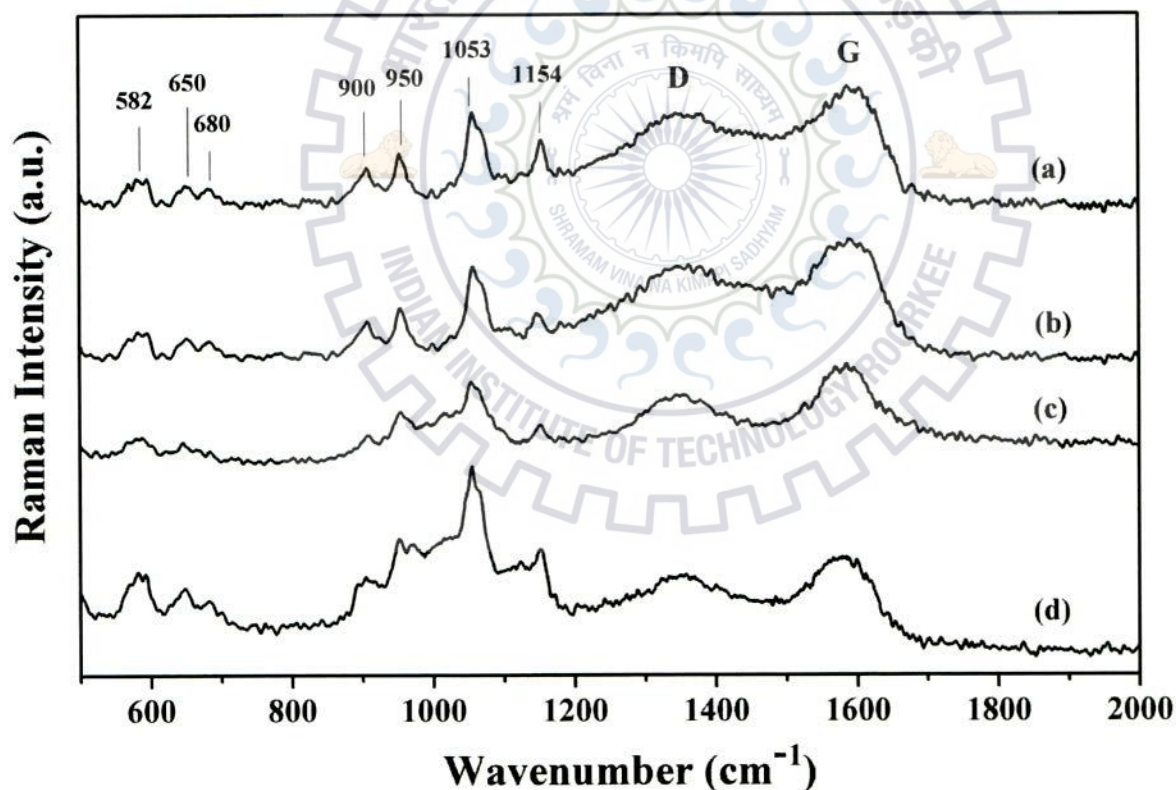
Fig. 5.18: Raman spectra of (a) $Li_{0.95}FePO_4$/C-PTh(4), (b) $Li_{0.95}FePO_4$/C-PTh(6), (c) $Li_{0.95}FePO_4$/C-PTh(8) and (d) $Li_{0.95}FePO_4$/C-PTh(10).

It can be seen from the graph that overall intensity of D-band and G-band get suppressed due to the polymer coating over the carbon. The intensity of these bands keeps on decreasing with the

increase in the amount of polythiophene in the composite materials. It can also be observed that the presence of polymer coating does not change the basic nature of D-band and G-bands. There is small shift in the bands which may be due to the interaction between carbon and polythiophene. The relative wave number (cm^{-1}) shift observed in the carbon bands after polymer coating has been presented in Table 5.4.

Table 5.4: Positions of D-band and G-band for $Li_{0.95}FePO_4/C$-PTh(4), $Li_{0.95}FePO_4/C$-PTh(6), $Li_{0.95}FePO_4/C$-PTh(8) and $Li_{0.95}FePO_4/C$-PTh(10) samples.

Observed for sample	D-band(cm^{-1})	G-band (cm^{-1})
$LiFePO_4/C$	1358	1573
$LiFePO_4/C$-PTh (4)	1382	1584
$LiFePO_4/C$-PTh (6)	1386	1586
$LiFePO_4/C$-PTh (8)	1350	1579
$LiFePO_4/C$-PTh (10)	1371	1581

It is examined from the Fig. 5.19 that polythiophene coating decreases the R (= I_D/I_G) for all the levels of polythiophene in $LiFePO_4/C$-PTh. The R values were estimated by the Gaussian fitting of D-band and G-band of Raman spectra. Such fitting has yielded R values of 0.86, 0.71, 0.66 and 0.64 for the samples $LiFePO_4/C$-PTh(4), $LiFePO_4/C$-PTh(6), $LiFePO_4/C$-PTh(8) and $LiFePO_4/C$-PTh(10) respectively. The estimated R is 0.97 for $LiFePO_4/C$, and this has been reported in section 4.1.1. The reduction of R for the polymer coated composites is perhaps the reduction of defect sites of the carbon due to polythiophene coating. Polythiophene and graphitic carbon were interacted through the defect sites such as dangling bonds on carbon and the α-position of polythiophene. The α-position is 100 times more reactive as compared to β-position [Joule and Mills, 2010, page no. 22]. The polymerization initiates as $FeCl_3$ oxidize the thiophene monomer to produce a radical cation. This radical cation couples with the other similar radical cation to form dication. The dication releases the two protons to form a dimer. The dimer has higher ability to get oxidized further by Fe^{3+} than monomer and go further addition of radical cation for chain propagation as shown in Fig. 5.20 (a). The polymer radical cation either isolated or at the head of propagation polymer chain could couple with the defect sites such as dangling bond on the carbon coating to form coupling as shown in Fig. 5.20 (b). This coupling decreases the dangling bond density on carbon coating arising due to finite graphitic size and diamond like carbon, to reduce the A_{1g} mode of vibration, resulting in the

decrease of the D-band intensity (or R value) of the Raman spectrum. The R value decreases upto 8 wt% of polythiophene addition to Li$_{0.95}$FePO$_4$/C. This is because 8 wt% of polythiophene coating gives maximum coverage to particles of sample Li$_{0.95}$FePO$_4$/C as compared to coating with 4 wt% and 6 wt% of polythiophene.
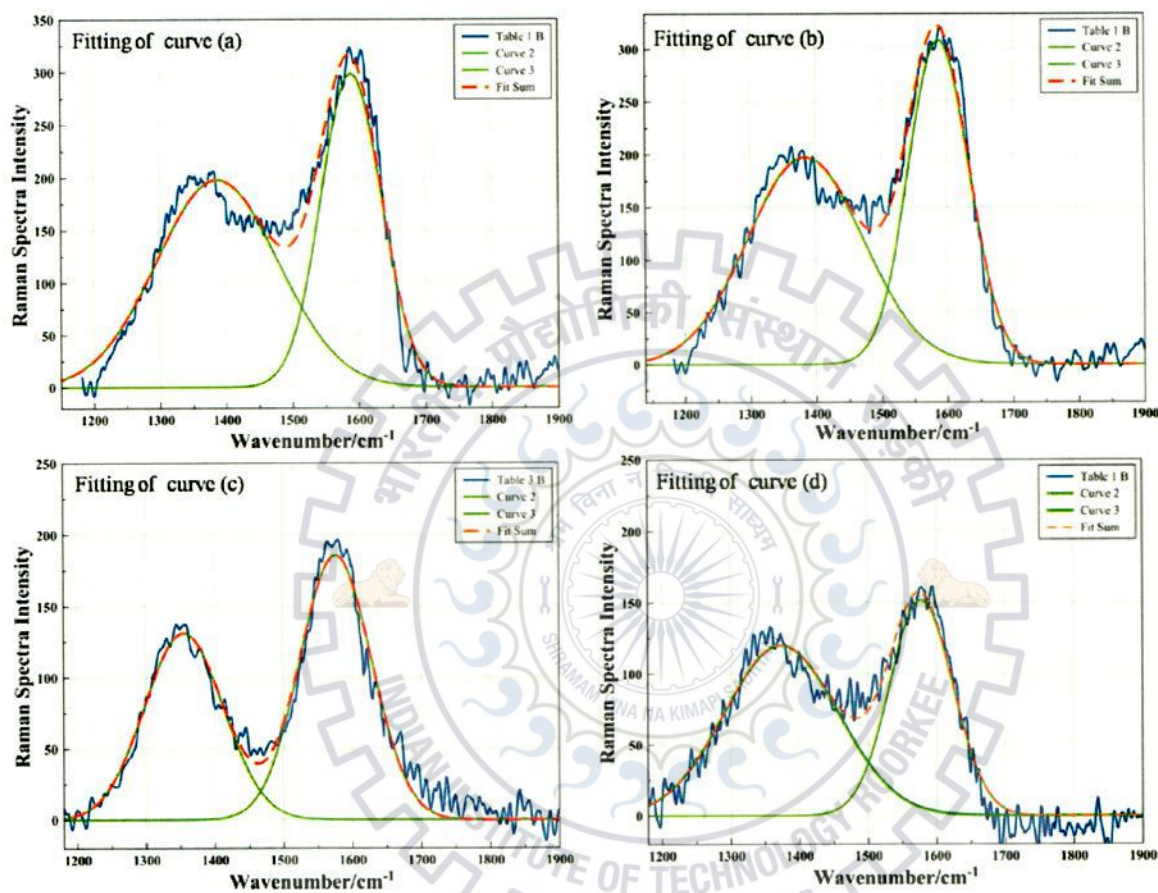
Fig. 5.19: The peak resolution and Gaussian fit of the D and G-bands of the curves shown in Fig.5.18.

The full coverage of particles of Li$_{0.95}$FePO$_4$/C by polythiophene offers highest contact area with carbon coating covering largest number of defects on carbon to give minimum R values. Since, the behavior of polythiophene is considered at four different quantities of 4, 6, 8 and 10 wt%. If this approach is valid then 8 wt% give maximum coverage of the discrete points. If the interaction between polythiophene and dangling bond of carbon is a valid approach to explain the intensities of D-band and G-band to give minimum R value, then lowest R value that has resulted with 8 wt% of polythiophene coating implies that maximum coverage of carbon with polythiophene has taken place. While any further increase from 8 wt% content does seem not significant reduction of D-band intensity. Though the study was limited upto 10 wt% addition

therefore 8 wt% is minimum content of polythiophene which can be considered to be optimum level of coating to give minimum R value and full coverage.
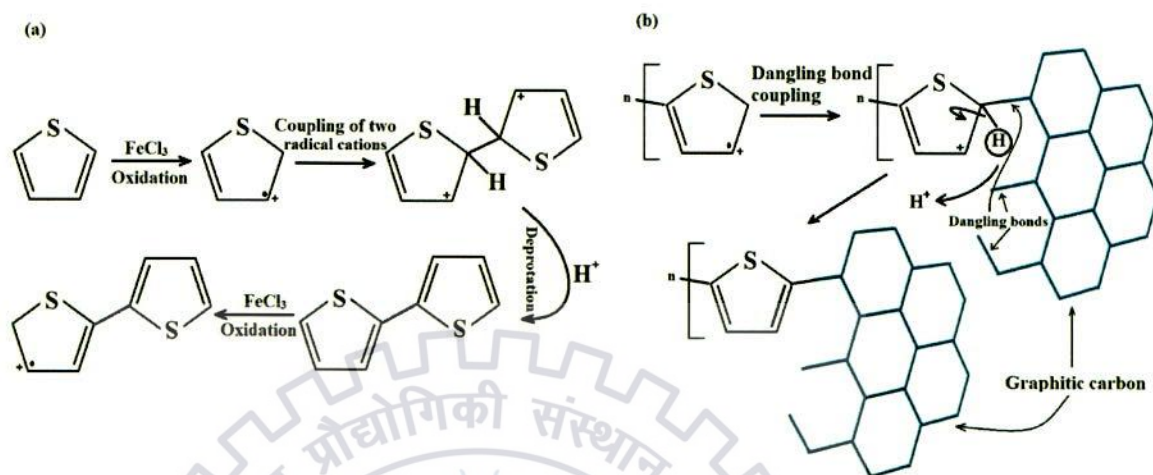
Fig. 5.20 (a) Mechanism of polymerization of thiophene monomers, (b) coupling of polythiophene chains with the defect site on graphic carbon.

5.2.2 Electrochemical testing

5.2.2.1 EIS analysis

EIS measurement was performed to investigate the effect of polythiophene on the electronic conductivity and Li-ion diffusivity of polythiophene coated $LiFePO_4/C$ composites. The EIS spectra of $Li_{0.95}FePO_4/C$ and $Li_{0.95}FePO_4/C$-PTh (Fig 5.21) can be resolved into two segments. The one segment is a semi-circular profile over higher to medium frequency range, which is electronic conductivity dominating region and the other segment is a straight line over the medium to low frequency region giving rise to Li-ion diffusion controlled behavior [Shenouda et al, 2008]. R_{ct} has been estimated from Fig. 5.21 and the values are 472, 360, 230, 130 and 111 Ω for $Li_{0.95}FePO_4/C$, $Li_{0.95}FePO_4/C$-PTh(4), $Li_{0.95}FePO_4/C$-PTh(6), $Li_{0.95}FePO_4/C$-PTh(8) and $Li_{0.95}FePO_4/C$-PTh(10) composite materials respectively. All the $Li_{0.95}FePO_4/C$-PTh electrodes show the low R_{ct} as compared to $Li_{0.95}FePO_4/C$ in a manner that R_{ct} decreases with the increase in weight fraction of polythiophene. The D_{Li+} has been calculated using the equations (3.5) and (3.6) mentioned in the section 3.4.3.4 of chapter 3. Fig. 5.22 shows the Z_{real} as a function of $\omega^{-1/2}$ in the low frequency region for $Li_{0.95}FePO_4/C$ and $Li_{0.95}FePO_4/C$-PTh composites. The calculated values of σ_ω for $Li_{0.95}FePO_4/C$ and $Li_{0.95}FePO_4/C$-PTh(4), $Li_{0.95}FePO_4/C$-PTh(6), $Li_{0.95}FePO_4/C$-PTh(8) and $Li_{0.95}FePO_4/C$-PTh(10) composite materials are 400, 209, 129, 83 and 73 Ω rad$^{1/2}$/sec$^{1/2}$ respectively. The values of D_{Li+} for $Li_{0.95}FePO_4/C$

and Li$_{0.95}$FePO$_4$/C-PTh have been calculated and are presented in the Table 5.5. It is seen from the Table 5.5 that Li$_{0.95}$FePO$_4$/C-PTh material yields higher D_{Li+} for all the concentrations of polythiophene. The D_{Li+} increases with the increase in polythiophene in Li$_{0.95}$FePO$_4$/C-PTh composite. The presence of polythiophene has improved the graphitization of underneath carbon as confirmed by the Raman analysis. Further the polythiophene coating also improves the electronic and ionic contact between Li$_{0.95}$FePO$_4$/C particles.
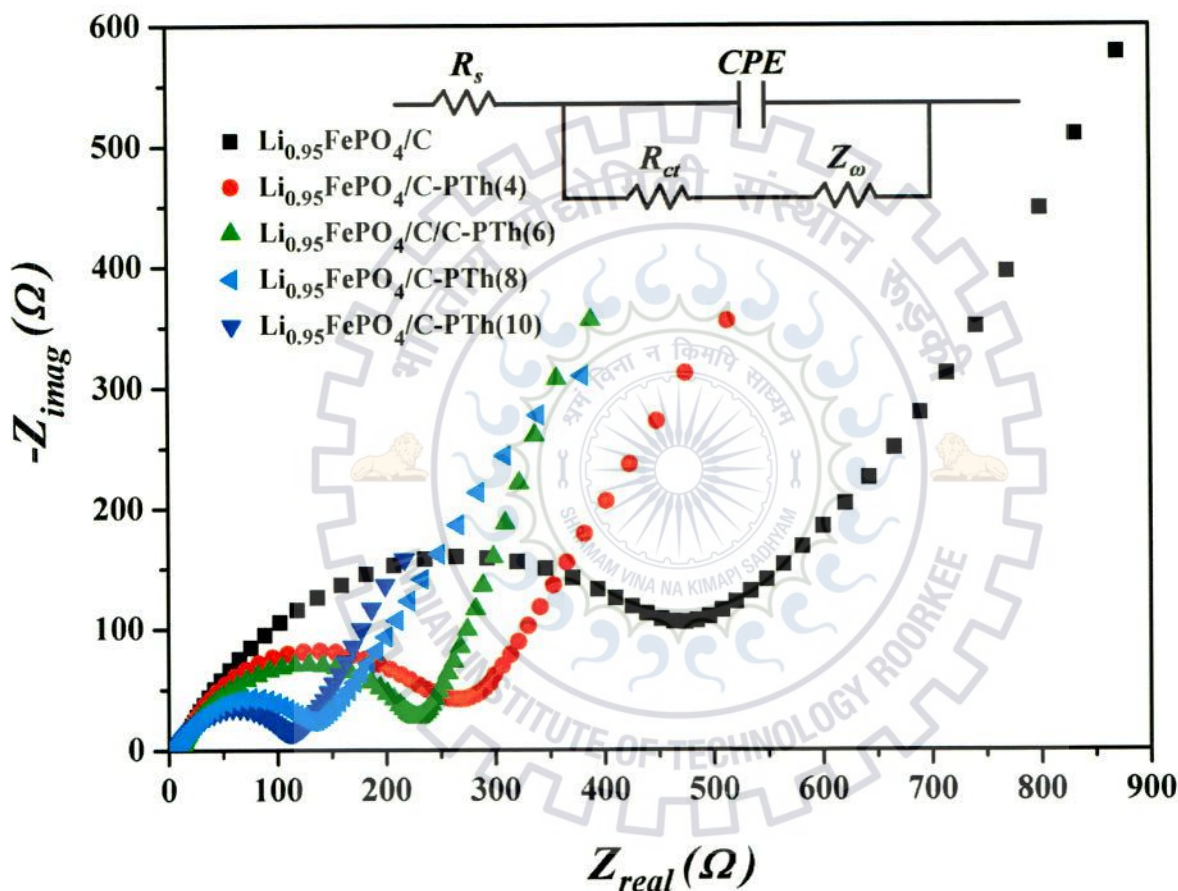
Fig. 5.21: Electrochemical impedance spectra of Li$_{0.95}$FePO$_4$/C and polythiophene coated Li$_{0.95}$FePO$_4$/C samples.

The polythiophene coating has the advantage of both the π-conjugation and one-dimensional chain morphology. These advantages enhanced the electronic and ionic contact between the particles of sample Li$_{0.95}$FePO$_4$/C-PTh resulting in higher electrical conductivity and Li-ion diffusion of Li$_{0.95}$FePO$_4$/C-PTh composites [Yin et al, 2012]. While the reduced R values for samples Li$_{0.95}$FePO$_4$/C-PTh calculated from Raman analysis has confirmed the decreased number of defect sites on the carbon coating resulting in improved graphitization of carbon.

The defect sites present on the carbon coating restrict the Li-ion diffusion either through the interaction or / and it may impede with defect site [Jana et al, 2014]. In both the processes Li-ion transport slows down through the carbon coating. The low R_{ct} for $Li_{0.95}FePO_4$/C-PTh samples shows higher electronic conductivity due to the improved graphitization of the carbon [Wang and Sun, 2012].
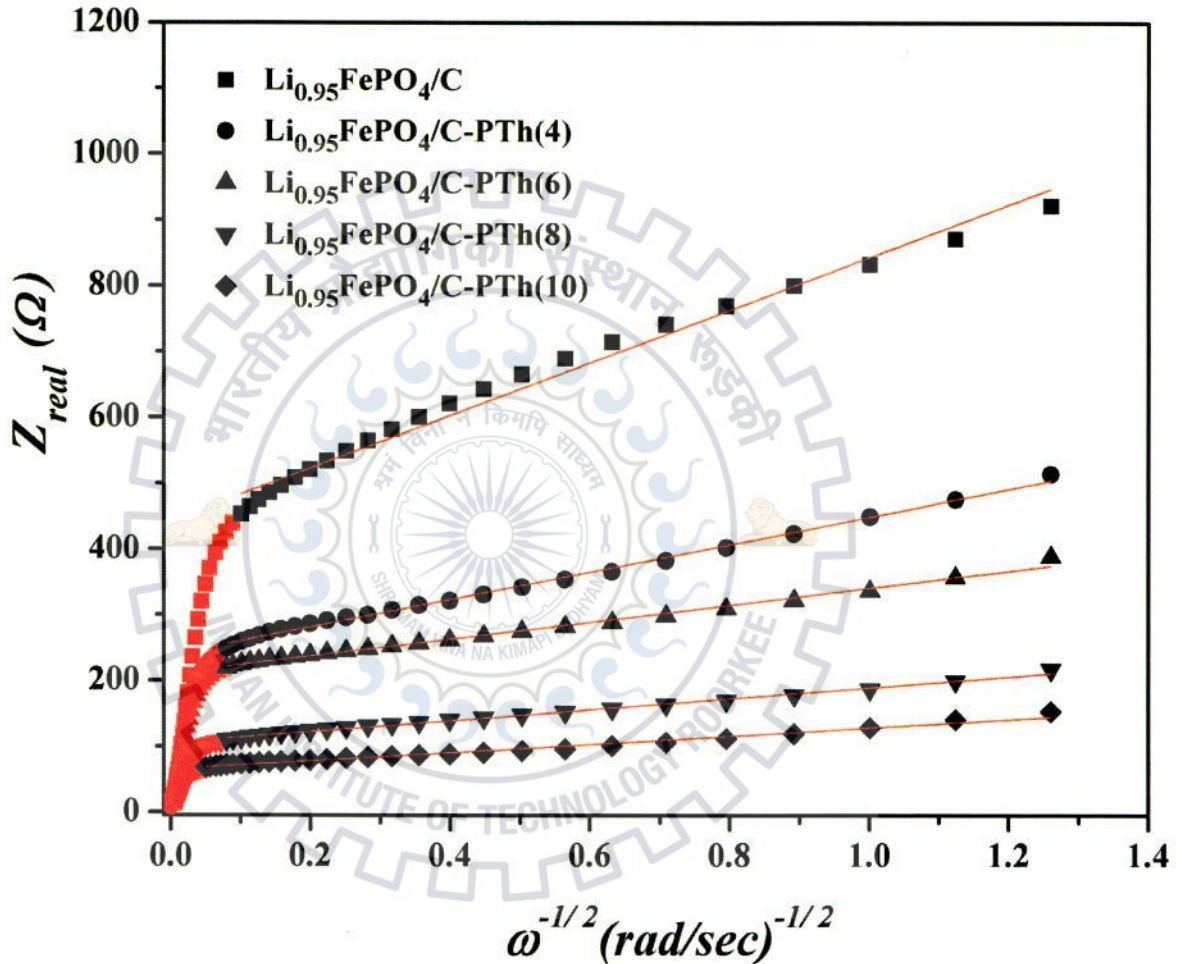
Fig. 5.22: Plot of Z_{real} vs. $\omega^{-1/2}$ for different composite materials.

From the EIS measurements it is confirmed that upto 8 wt% of polythiophene addition to $Li_{0.95}FePO_4$/C imparts appreciable improvement in charge transfer and D_{Li+}. The further addition of polythiophene (10 wt%) marginally improves the conductivity and D_{Li+} for $Li_{0.95}FePO_4$/C sample. This is because 8 wt% of polythiophene content gives maximum coverage to $Li_{0.95}FePO_4$/C particles, providing highest interface area between carbon and polythiophene covering a large no of defect sites on carbon coating. On the other hand coating of 10 wt% of polythiophene addition does not improve the interface area instead the

polythiophene coating becomes thicker. So no significant improvement in the electronic conductivity was observed due to higher fraction of more conductive polythiophene to $Li_{0.95}FePO_4$/C-PTh composite material.

Table 5.5: EIS parameter of electrodes $Li_{0.95}FePO_4$/C and $Li_{0.95}FePO_4$/C-PTh

Sample	$R_s(\Omega)$	$R_{ct}(\Omega)$	$D_{Li+}(cm^2 s^{-1})$	σ_ω $(\Omega\ rad^{1/2}/sec^{1/2})$
LiFePO₄/C	12.9	472	1.48×10^{-15}	400
LiFePO₄/C-PTh(4)	10.9	360	5.41×10^{-15}	209
LiFePO₄/C- PTh(6)	11.3	230	1.42×10^{-14}	129
LiFePO₄/C- PTh(8)	8.6	130	3.42×10^{-14}	83
LiFePO₄/C- PTh(10)	8.9	111	3.94×10^{-14}	73

5.2.2.2 Electrochemical cell performance

Fig. 5.23(a-d) present the comparative performances of the discharge capacities of $Li_{0.95}FePO_4$/C with $Li_{0.95}FePO_4$/C-PTh composites at different current rates. From the Fig. 5.23(a-d) it is observed that specific capacities of the samples $Li_{0.95}FePO_4$/C and $Li_{0.95}FePO_4$/C-PTh are similar at 0.2C rate. This is because, a low discharging rate of 0.2C does not require higher electronic and Li-ion movements in the cathode material. So the higher electronic conductivity and Li-ion diffusivity due to polythiophene have insignificant effect on discharge capacity. When the discharge rates were progressively increased in the steps of 0.2C, 0.5C, 1C, 2C, 5C, 10C and 20C, the composite materials $Li_{0.95}FePO_4$/C-PTh show higher discharge capacity as compared to that of $Li_{0.95}FePO_4$/C. Fig. 5.23(a-d) shows that at fastest 20C rate highest discharge capacity of 90 mAh/g was delivered by sample $Li_{0.95}FePO_4$/C-PTh(8) which is greatest among the $Li_{0.95}FePO_4$/C-PTh samples. This might be due to optimum content (8 wt%) of polythiophene which provides full coverage to LiFePO₄/C particles and facilitates to deliver higher conductivity and faster Li-ion diffusion as discussed in the conductivity measurements of section 5.2.2.1. However the higher content (10 wt%) of polythiophene decreases the discharge capacity of LiFePO₄/C-PTh(10) composite. This is because polythiophene has lower theoretical discharge capacity of 90 mAh/g as compared to the theoretical discharge capacity of 170 mAh/g for LiFePO₄ core particles [Tang et al, 2008]. If the content of polythiophene in LiFePO₄/C-PTh composite is higher (10 wt%) than the content (8 wt%) required for full coverage of LiFePO₄/C particles, then addition of lower capacity polythiophene removes the higher capacity LiFePO₄ material from the LiFePO₄/C-PTh

composite material. Consequently this reduces the overall capacity of LiFePO$_4$/C-PTh electrode.
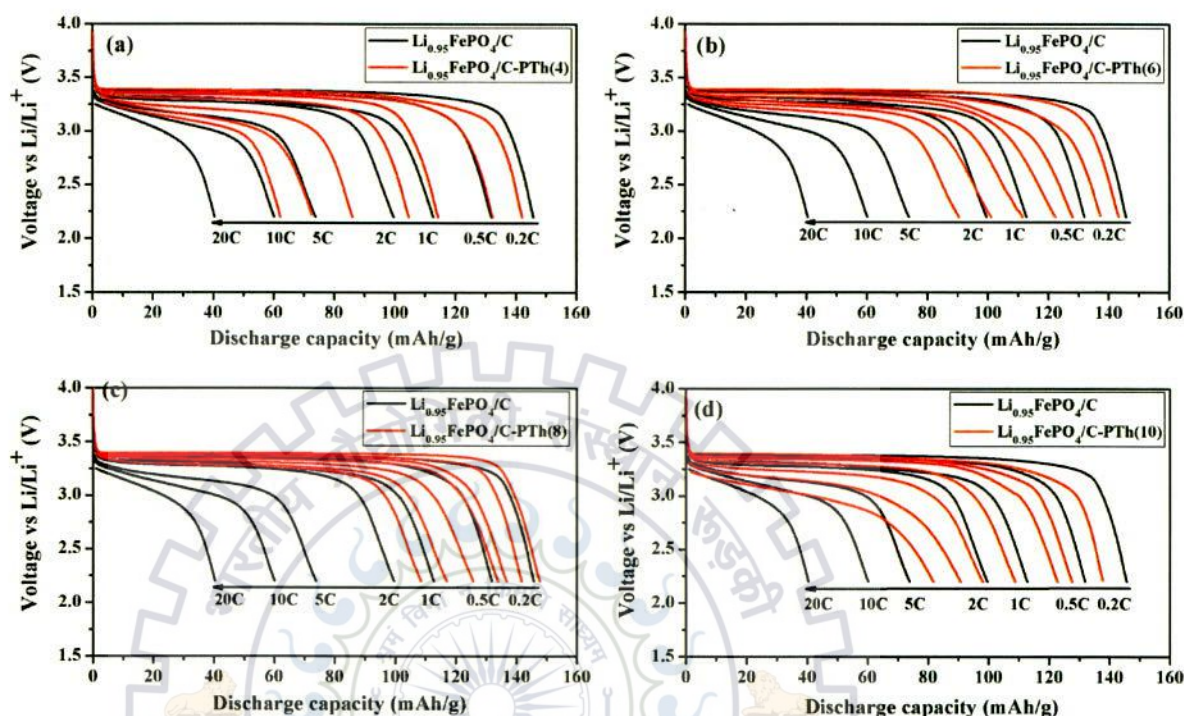
Fig. 5.23: Discharge capacities of Li$_{0.95}$FePO$_4$/C-PTh samples at 0.2C, 0.5C, 1C, 2C, 5C, 10C and 20C rates.

As discussed in section 5.2.1.4 the 8 wt% content of polythiophene appears to be optimum to cover the LiFePO$_4$/C particles from all directions and interconnect the coated particles through conducting polythiophene chains. These polythiophene chains allow fast movement of electron and Li-ion as discussed in the EIS of the composite materials. The interconnection of LiFePO$_4$/C-PTh coated particles through the chain morphology removes the lower capacity polythiophene from the composite and improves the utilization of LiFePO$_4$.

The stability of Li$_{0.95}$FePO$_4$/C and Li$_{0.95}$FePO$_4$/C-PTh as cathode materials has been estimated by measuring the discharge capacity in the form of their electrodes at 0.2C rate. These samples were tested for 35 cycles of charging / discharging at progressively increasing rates of 0.2C, 0.5C, 1C, 2C, 5C, 10C and 20C, where measurements were performed for 5 cycles at a particular C-rate. After 35 cycles the cell was again tested at 0.2C and the discharge capacities were compared with those of starting cycles tested at same (0.2C) rate.
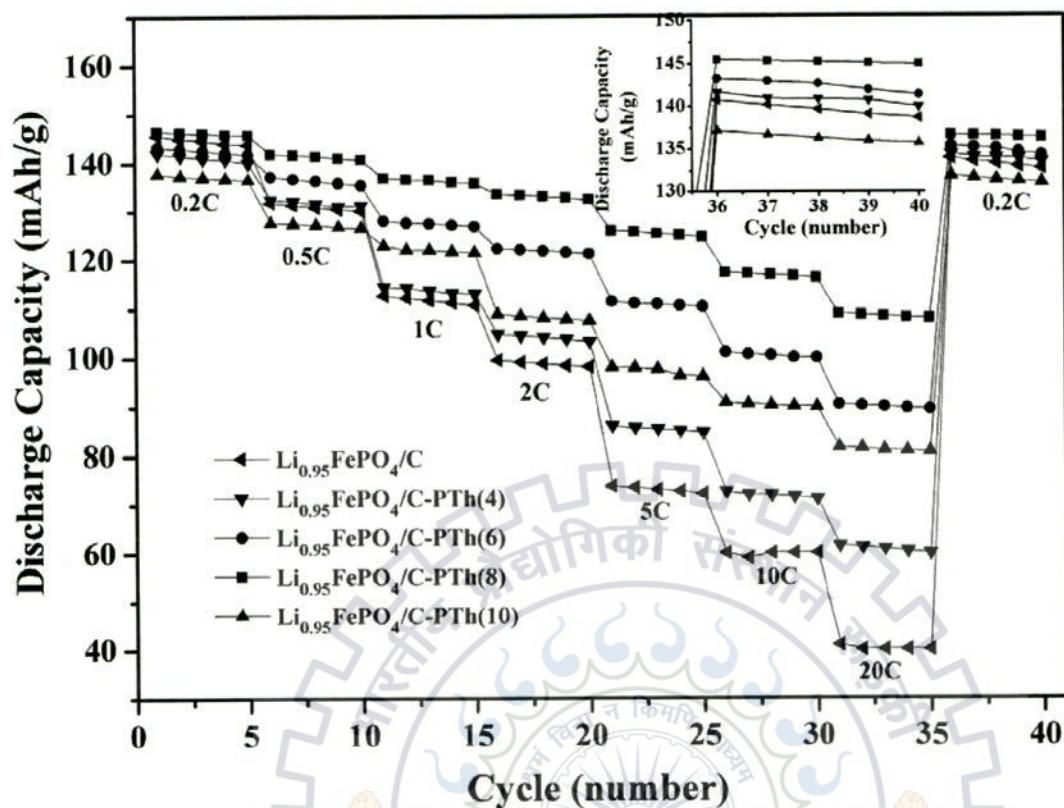
Fig. 5.24: Discharge capacity of $Li_{0.95}FePO_4/C$ and $Li_{0.95}FePO_4/C$-PTh at different 0.2C, 0.5 C, 1 C, 2 C, 5 C, 10 C and 20C rate.
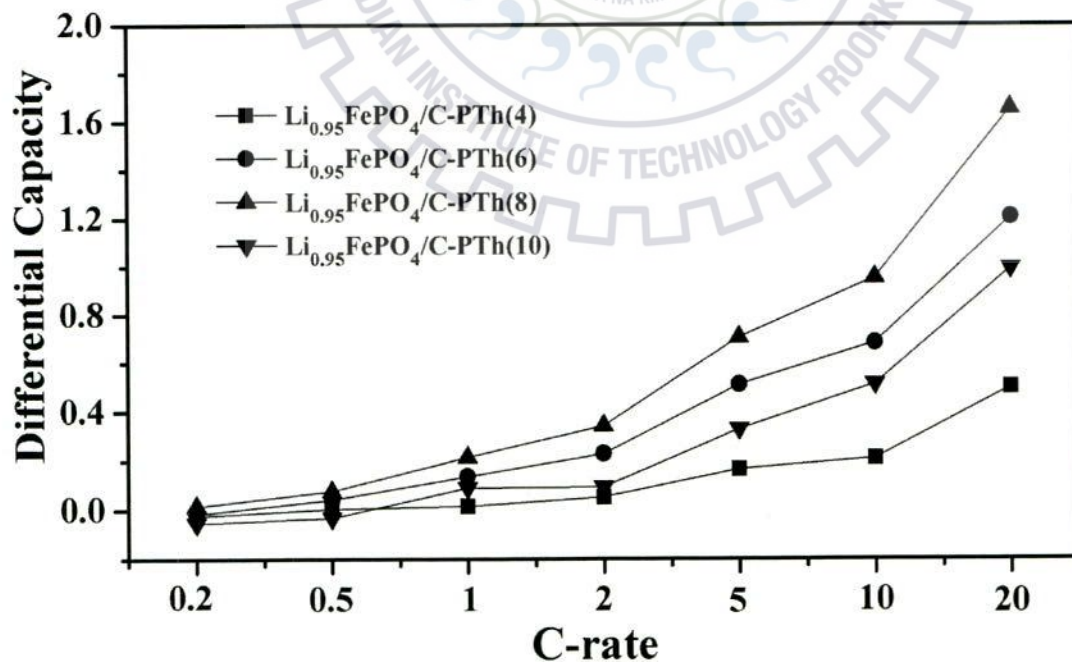
Fig. 5.25: DC variation with C-rates, for $Li_{0.95}FePO_4/C$-PTh samples.

The columbic efficiency of 98.1, 98.6, 99 and 97.7 % were observed (Fig 5.24) for $Li_{0.95}FePO_4$/C-PTh(4), $Li_{0.95}FePO_4$/C-PTh(6), $Li_{0.95}FePO_4$/C-PTh(8) and $Li_{0.95}FePO_4$/C-PTh(10) samples respectively as compared to 95.1 for $Li_{0.95}FePO_4$/C. Thus all the $Li_{0.95}FePO_4$/C-PTh composites have good cyclic stability.

The Fig. 5.25 represents the DC values of the $Li_{0.95}FePO_4$/C-PTh composites at different C-rates. From the graph it may be seen that at 0.2C and 0.5C rates the DC values are very close to zero. The DC values of all the $Li_{0.95}FePO_4$/C-PTh samples start spreading from the discharging rates 2C to 20C. The highest DC value of 1.63 was calculated for the $Li_{0.95}FePO_4$/C-PTh(8) at 20C-rate, which reveals that the material is suitable for the high rate capability cathode.

5.3 RESULTS AND DISCUSSION-
POLYANILINE COATED LiFePO$_4$/C
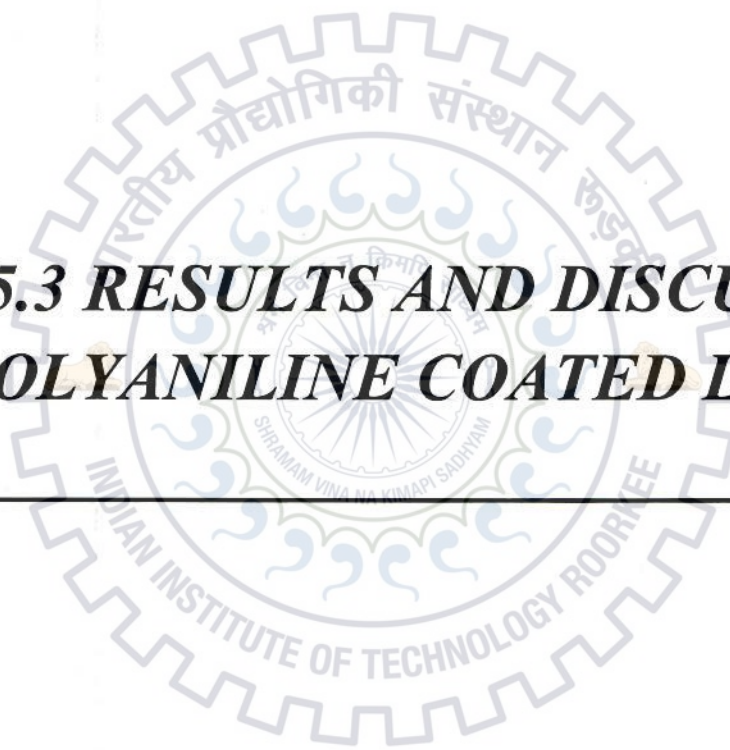
5.3 RESULTS AND DISCUSSION-POLYANILINE COATED LiFePO₄/C

The conducting form of polyaniline (emerladine salt) is one of the promising polymer due to its ease of synthesis, inexpensive monomer units, high stability and good conductivity [Yang et al, 1993, Sivakkumar et al 2006]. There are a total of five different form of polyaniline. Among them emerladine salt and emerladine base forms are most important. Emerladine base form is the insulating form of polyaniline, which can be converted to emerladine salt form through the inorganic acid doping. Emerladine salt has good conductivity moreover its conductivity can be tailored from 10^{-10} to 10 S/cm depending upon the level of inorganic acid doping [Yang et al, 1996]. Also both the forms of polymers can be interchanged by inorganic acid doping and de-doping. In view of the battery application polyaniline is the material of importance since it is electrochemically active in the voltage range of 2 – 4 V and has lithium storage ability. The theoretical capacity of polyaniline is ~ 100 mAh/g [Novak et al, 1997]. Herein, *in-situ* polyaniline synthesis on the surface of LiFePO₄/C composite material using $KMnO_4$, $K_2Cr_2O_7$ and $(NH_4)_2S_2O_8$ as oxidizing agent has been reported. The polyaniline coated LiFePO₄/C samples synthesized using $KMnO_4$, $K_2Cr_2O_7$ and $(NH_4)_2S_2O_8$ as oxidizer are designated as LiFePO₄/C-PANI($KMnO_4$), LiFePO₄/C-PANI($K_2Cr_2O_7$) and LiFePO₄/C-PANI($(NH_4)_2S_2O_8$), where for one / all polyaniline coated LiFePO₄/C are denoted as LiFePO₄/C-PANI.

5.3.1 Physical characterizations

5.3.1.1 Phase analysis

XRD patterns of all the synthesized LiFePO₄/C-PANI composite materials and pristine polyaniline are shown in Fig. 5.26. All the peaks of XRD patterns are well indexed as orthorhombic olivine structure of LiFePO₄ (JCPDS card no-01-083-2092) and $Li_{0.05}FePO_4$ (JCPDS code no 98-010-8284) phases with space group of Pnma. The charatersitic broad peak of polyaniline which appears centring at $2\theta = 25$ ° is not present in the diffraction patterns of LiFePO₄/C-PANI composites. This perhaps due to amorphus state of polyaniline in the LiFePO₄/C-PANI composite.
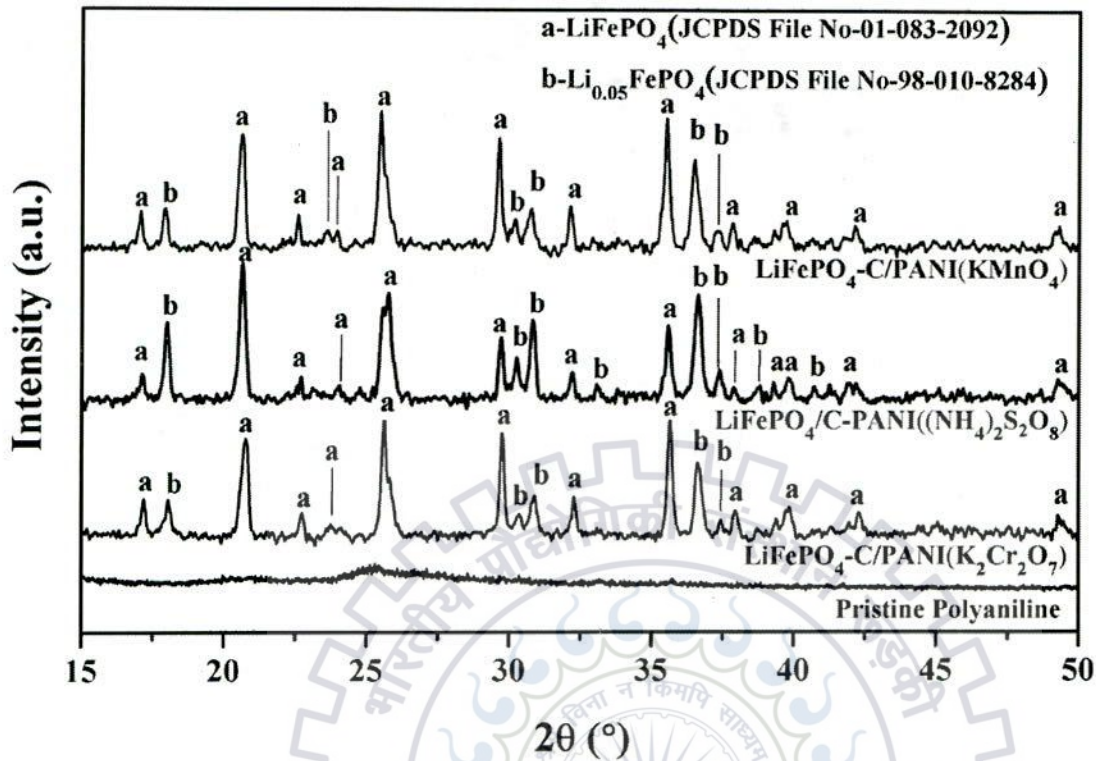
Fig. 5.26: XRD patterns of LiFePO$_4$/C-PANI((NH$_4$)$_2$S$_2$O$_8$), LiFePO$_4$/C-PANI(K$_2$Cr$_2$O$_7$), LiFePO$_4$/C-PANI(KMnO$_4$) and pristine polyaniline samples.

5.3.1.2 Particles morphology

Fig. 5.27(b-d) shows the FESEM micrographs of synthesized LiFePO$_4$-C/PANI composites. For all the LiFePO$_4$-C/PANI composites, polyaniline gives full coverage to LiFePO$_4$ particles. It is further estimated from the micrograph of Fig. 5.27(d) that powder of LiFePO$_4$-C/PANI((NH$_4$)$_2$S$_2$O$_8$) composite shows plate like microstructure. The magnified image of Fig. 5.27(d) is inserted in the inset which clearly shows that each plate consist of single layer of LiFePO$_4$/C particles covered by polyaniline.
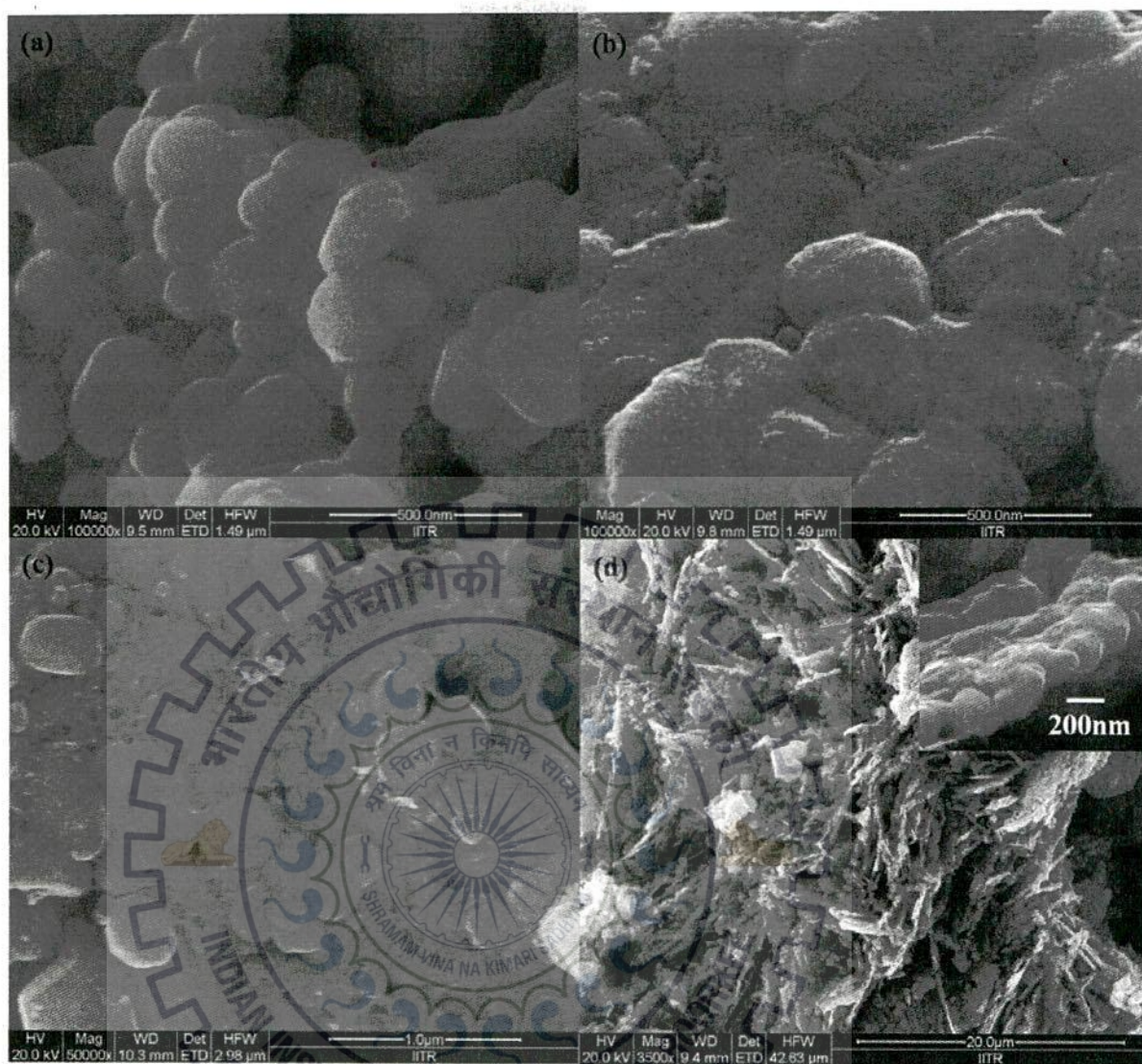
Fig. 5.27: FESEM micrograph of (a) LiFePO$_4$-C, (c) LiFePO$_4$-C/PANI(KMnO$_4$), (d) LiFePO$_4$-C/PANI(K$_2$Cr$_2$O$_7$) and (b) LiFePO$_4$-C/PANI((NH$_4$)$_2$S$_2$O$_8$).

5.3.1.3 TG analysis

Fig 5.28 shows the TG plots of LiFePO$_4$/C-PANI composites. The TG trace shows that weight loss occurs in three steps. The first step starts from room temperature and continues upto 110 °C showing a weight loss of nearly 1 % due to moisture removal from the material. The second step begins at 110 °C and continues up to 800 °C which arises due to polyaniline decomposition. This weight loss continues in the third step due to polyaniline decomposition for the samples held at 800 °C for 1 hour. The polyaniline contents are 16.5, 15.1 and 14.3 wt% as estimated for LiFePO$_4$-C/PANI((NH$_4$)$_2$S$_2$O$_8$), LiFePO$_4$-C/PANI(KMnO$_4$) and LiFePO$_4$-C/PANI(K$_2$Cr$_2$O$_7$) composite materials respectively.
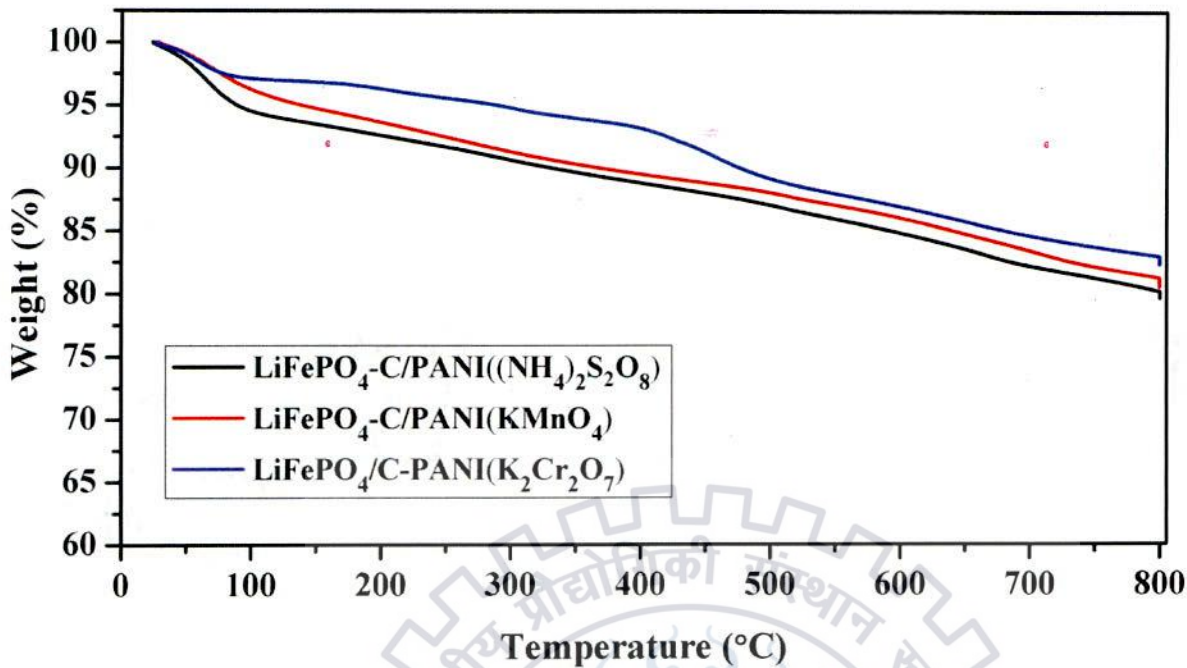
Fig. 5.28: TG plots of all the LiFePO₄/C-PANI composites.

5.3.1.4 Raman analysis

Fig. 5.29 shows the Raman spectra of all the LiFePO₄/C-PANI composites. The peaks at 1156 cm^{-1}, 1158 cm^{-1} and 1159 cm^{-1} for the LiFePO₄-C/PANI((NH₄)₂S₂O₈), LiFePO₄-C/PANI(KMnO₄) and LiFePO₄-C/PANI(K₂Cr₂O₇) composite materials respectively corresponds to the inplane deformation of C–N–C bonds. Where the peaks at 1237 cm^{-1}, 1233 cm^{-1} and 1236 cm^{-1} for LiFePO₄/C-PANI((NH₄)₂S₂O₈), LiFePO₄/C-PANI(KMnO₄) and LiFePO₄/C-PANI(K₂Cr₂O₇) composites respectively are due to inplane deformation of Quinoid ring of polyaniline [Cochet et al, (2000)]. Both the above mentioned deformations correspond to the bipolaron formations which exist in the emeraldine salt form of polyaniline. The polaron and bipolaron formation in the polyaniline depends up on the level of protonic acid doping. The protonic acid doping has resulted in the bipolaron formation in polyaniline emeraldine salt which is confirmed by the Raman spectra of LiFePO₄/C-PANI. The peaks at near to 1158 and 1236 cm^{-1} are the characteristic peaks of polyaniline.
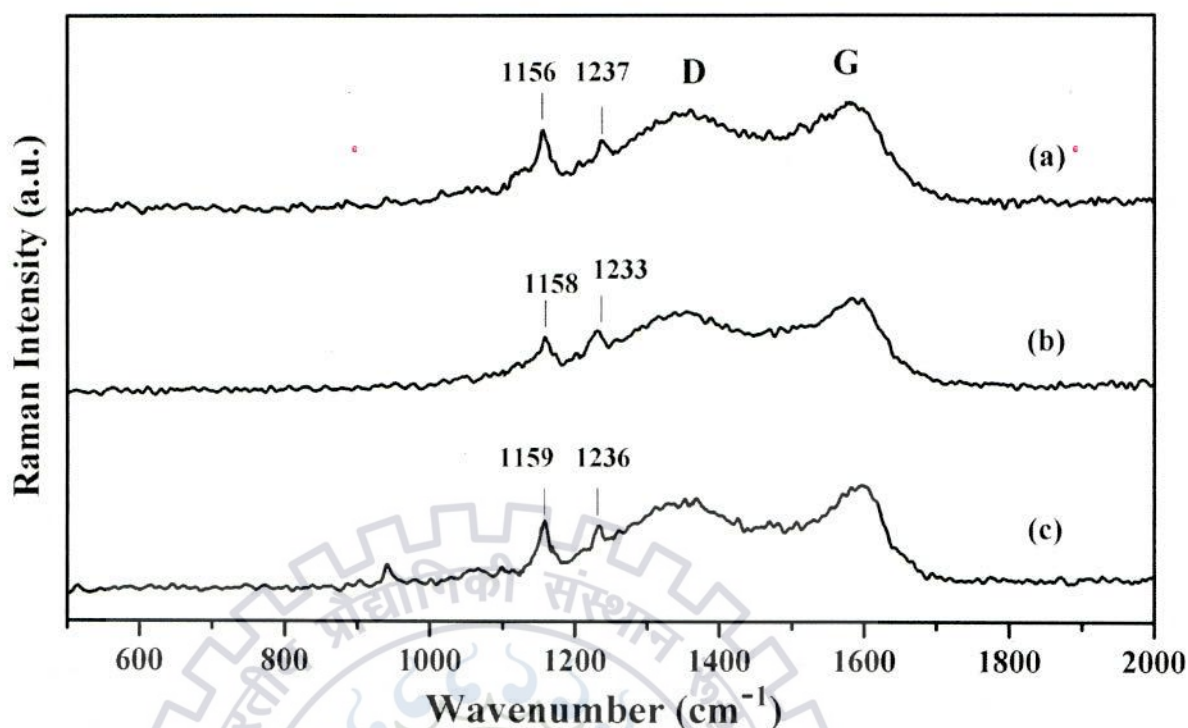
Fig. 5.29: Raman spectra of (a) LiFePO$_4$/C-PANI((NH$_4$)$_2$S$_2$O$_8$) (b) LiFePO$_4$/C-PANI(K$_2$Cr$_2$O$_7$) and (c) LiFePO$_4$/C-PANI(KMnO$_4$).

5.2.2 Electrochemical testing

5.2.2.1 EIS analysis

EIS of LiFePO$_4$/C-PANI composite materials have been compared with bare LiFePO$_4$/C in Fig. 5.30. The EIS plot of LiFePO$_4$/C-PANI composites show smaller diameter of the semi-circles as compared to LiFePO$_4$/C which reflects low R_{ct} consequently resulting in higher conductivity. The observed values of R_{ct} for LiFePO$_4$/C-PANI((NH$_4$)$_2$S$_2$O$_8$), LiFePO$_4$/C-PANI(K$_2$Cr$_2$O$_7$) and LiFePO$_4$/C-PANI(KMnO$_4$) are 151, 175 and 244 Ω respectively. Where, the observed R$_{ct}$ value for bare LiFePO$_4$/C is ~ 500 Ω. The improved conductivity of LiFePO$_4$/C-PANI composites was due to highly conducting protonic acid doped polyaniline coating on LiFePO$_4$/C particles. Although all the three are strong oxidizing agents but (NH$_4$)$_2$S$_2$O$_8$ is strongest as it has highest standard electrode potential (1.95 V) as compared to KMnO$_4$ (1.49 V) and K$_2$Cr$_2$O$_7$ (1.29 V) [Yasuda and Shimidzu, 1993]. So for equal amount of aniline monomers, (NH$_4$)$_2$S$_2$O$_8$ has yielded higher quantity of polyaniline as compared to that obtained using other two oxidizing agents. The lower R$_{ct}$ observed for the composite LiFePO$_4$/C-PANI((NH$_4$)$_2$S$_2$O$_8$) may be due to higher fraction of conducting polyaniline.

The equivalent circuit of the EIS profiles is shown in the inset of Fig. 5.30. The factors such as σ_ω, i_0 and D_{Li+} of the cathode for all the LiFePO$_4$/C-PANI composites are calculated by using the method discussed under section 3.4.3.4 of chapter 3 and their values are presented in the Table 5.5. The slop of linear fitted straight line is the σ_ω which has been calculated from Fig. 5.31. The D_{Li+} are found to be higher for all the LiFePO$_4$/C-PANI samples as compared to LiFePO$_4$/C implying that polyaniline incorporation results in improved Li-ion kinetics. The highest i_0 reflects better reversibility of LiFePO$_4$/C-PANI($(NH_4)_2S_2O_8$) of cathode material.

Table 5.6: EIS parameter of electrodes of LiFePO$_4$/C and LiFePO$_4$/C-PANI

Sample	$R_s(\Omega)$	$R_{ct}(\Omega)$	i_0 (mA cm^{-2})	D_{Li+} (cm^2 sec^{-1})	σ_ω (Ωrad$^{1/2}$sec$^{-1/2}$)
LiFePO$_4$/C	12.9	472	5.47×10^{-5}	1.48×10^{-15}	400
LiFePO$_4$/C-PANI(K$_2$Cr$_2$O$_7$)	7.2	244	1.06×10^{-4}	4.41×10^{-15}	233
LiFePO$_4$/C-PANI(KMnO$_4$)	9.6	175	1.48×10^{-4}	5.47×10^{-15}	209
LiFePO$_4$/C-PANI($(NH_4)_2S_2O_8$)	9.8	151	1.72×10^{-4}	1.17×10^{-14}	143
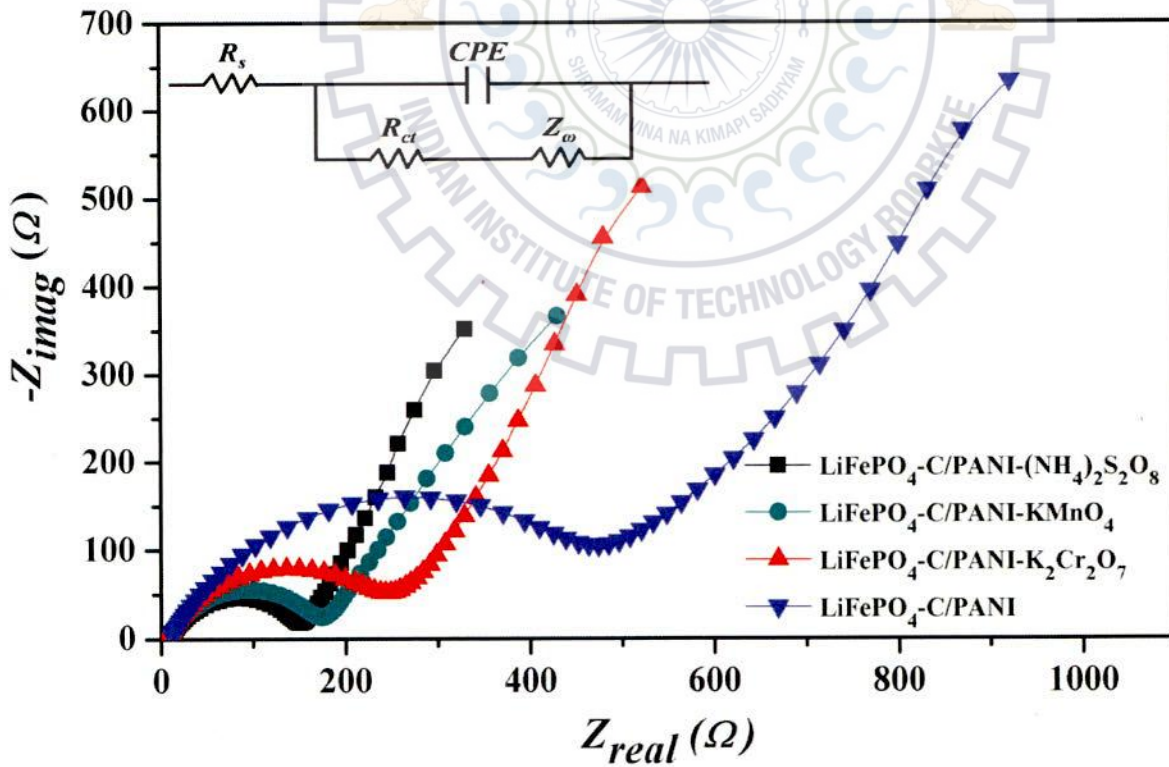
Fig. 5.30: Electrochemical impedance spectra of LiFePO$_4$/C and polyaniline coated LiFePO$_4$/C samples.
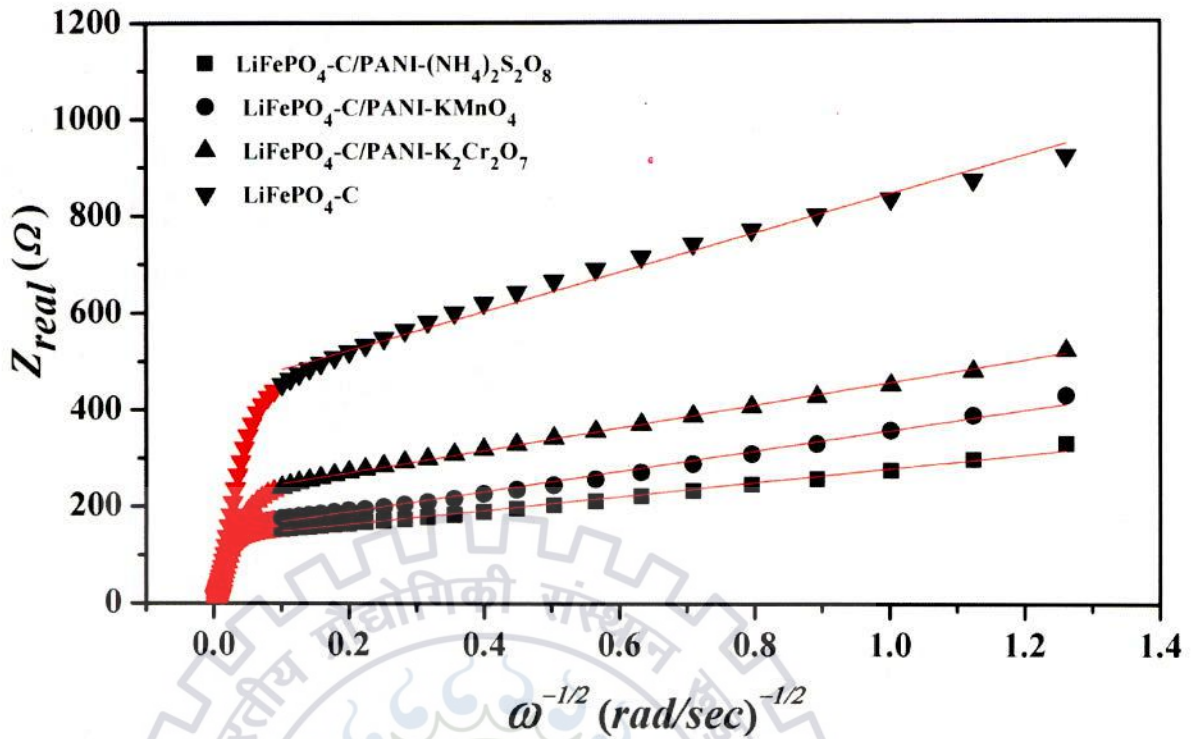
Fig. 5.31: Linear fitting of Warburg impedance.

5.2.2.2 Electrochemical cell performance

The discharge capacities of LiFePO$_4$/C and LiFePO$_4$/C-PANI have been measured at different C-rates and are plotted in Fig 5.32. All LiFePO$_4$/C-PANI composites show a small decrease in the discharge capacities at slow discharge rate of 0.2C. However, if the charging / discharging rate is gradually increased in steps of 0.5, 1, 2, 5, 10 and 20C, the composites LiFePO$_4$/C-PANI show higher discharge capacity as compared to LiFePO$_4$/C. The composite LiFePO$_4$/C-PANI((NH$_4$)$_2$S$_2$O$_8$) delivers highest discharge capacities of 109, 100, and 93.8 mAh/g at 5C, 10C and 20C rates respectively with respect to the other composites. The results of capacity measurements at higher discharging rates are consistent with the conductivity measurements for all the LiFePO$_4$/C-PANI samples. The higher conductivity of LiFePO$_4$/C-PANI((NH$_4$)$_2$S$_2$O$_8$) sample supports better rate capability as cathode material which is followed by LiFePO$_4$/C-PANI(KMnO$_4$), LiFePO$_4$/C-PANI(K$_2$Cr$_2$O$_7$) respectively in terms of conductivity.

To evaluate the cyclic performance the discharge capacities for all LiFePO$_4$/C-PANI and LiFePO$_4$/C composites are compared (Fig. 5.32(d)) at typically 2C-rate for 50 cycles. All the LiFePO$_4$/C-PANI samples show superior cyclability of ~ 98 % in comparison to initial capacity as compared with 88 % for LiFePO$_4$/C material over 50 cycles. This shows that polyaniline

addition to LiFePO$_4$/C improves the cyclability and rate capability for all the oxidizing agents used for polymerization.

The rate performances of LiFePO$_4$/C-PANI and LiFePO$_4$/C electrodes were estimated using discharge capacities of the materials at different C-rates and for every C-rate, measurements were made for 5 cycles (Fig. 5.33 (a)). The observed DC values were plotted for different C-rate for the composites LiFePO$_4$/C-PANI((NH$_4$)$_2$S$_2$O$_8$), LiFePO$_4$/C-PANI(KMnO$_4$) and LiFePO$_4$/C-PANI(K$_2$Cr$_2$O$_7$). The DC has been calculated for these composites using the relation (3.4) presented under section 3.4.3.2 of chapter 3 and were plotted with different C-rates in Fig. 5.33(b). The DC values are very close to zero at lower discharging rates of 0.2C and 0.5C showing the insignificant capacity improvement at these C-rates. At moderate discharge rates of 1, 2 and 5C the DC of each samples start spreading and shows maximum spread at highest 20C rate. The highest DC value of 1.32 have been obtained for LiFePO$_4$/C-PANI((NH$_4$)$_2$S$_2$O$_8$) composite material at 20C rate implying that it is a high rate capability material followed by LiFePO$_4$/C-PANI(KMnO$_4$) and LiFePO$_4$/C-PANI(K$_2$Cr$_2$O$_7$).
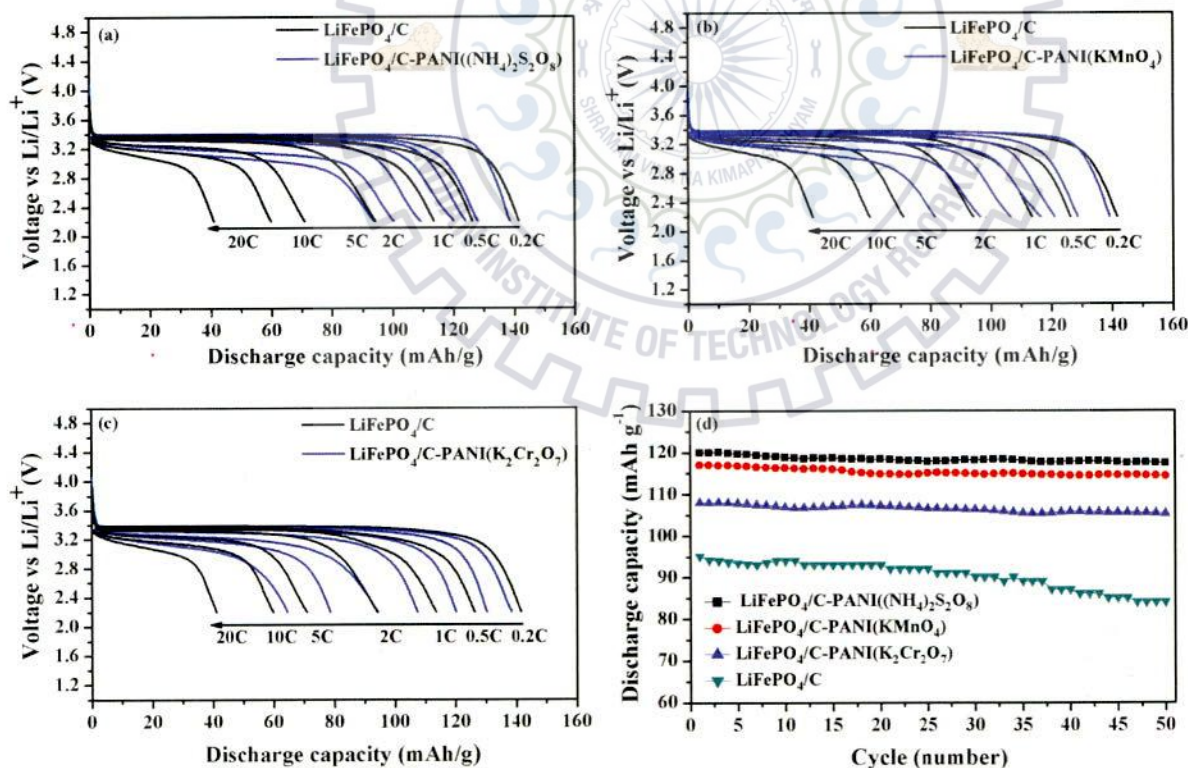
Fig. 5.32: Comparative plots of the capacities of composites (a) LiFePO$_4$/C-PANI((NH$_4$)$_2$S$_2$O$_8$), (b) LiFePO$_4$/C-PANI(KMnO$_4$), (c) LiFePO$_4$/C-PANI(K$_2$Cr$_2$O$_7$) with LiFePO$_4$/C. (d) Discharge capacities of LiFePO$_4$/C and LiFePO$_4$/C-PANI composites at 2C rate for 50 cycles

(a)

(b)
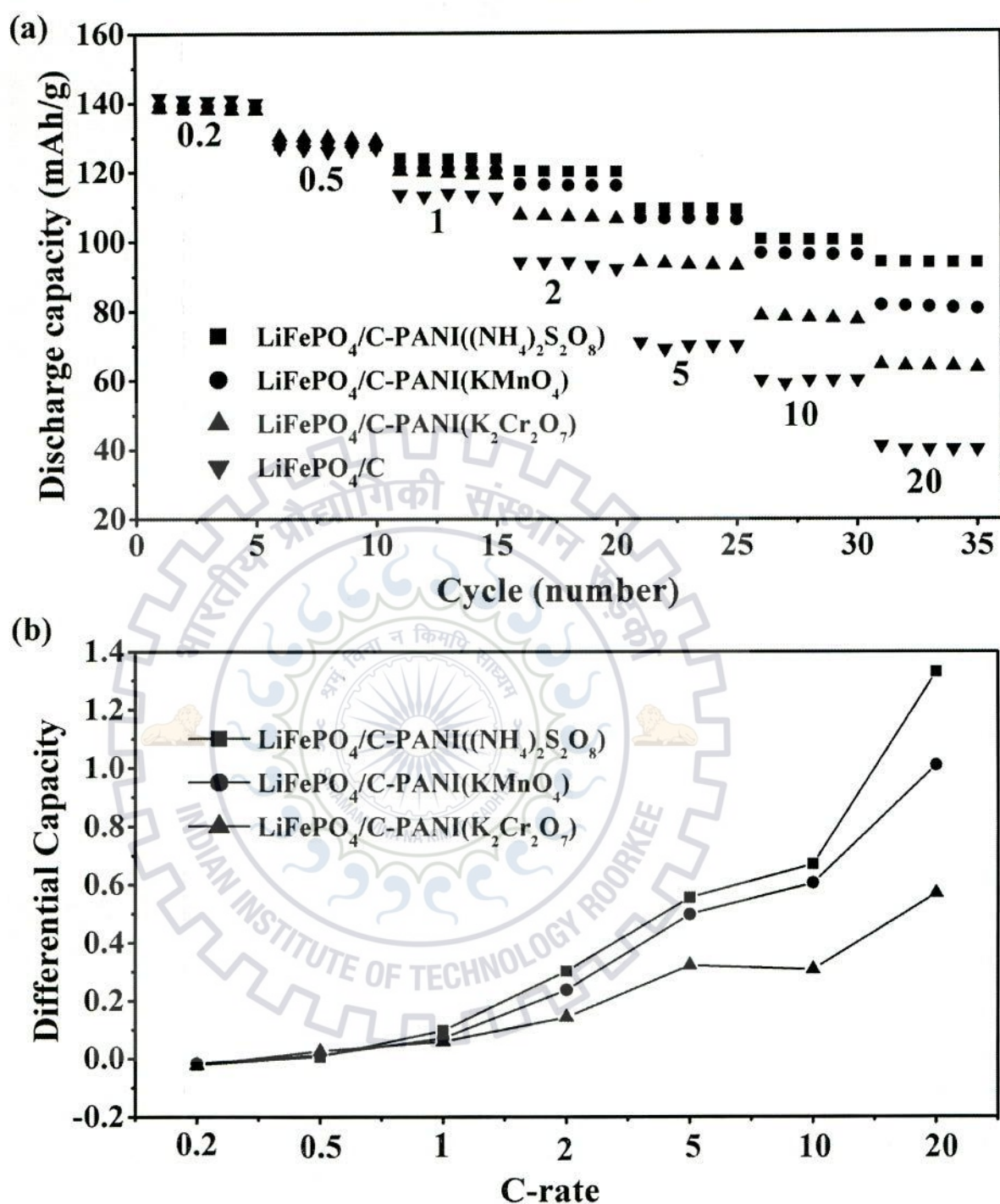
Fig. 5.33: (a) Cyclic performances of LiFePO₄/C and LiFePO₄/C-PANI samples at different C-rates, and (b) DC variation of LiFePO₄/C-PANI, with C-rate.

Summary

Polypyrrole coating on the surface of LiFePO₄/C has been grown in three different solvents water, ethanol, and ACN. Minimum porosity was observed for the polypyrrole coating grown using ACN solvent which has covered larger number of defects on carbon coating. The

interaction between polypyrrole and defect site on carbon coating was confirmed by the reduced R (= I_D/I_G) values of D-band to G-band for samples $LiFePO_4/C$-PPy as compared to $LiFePO_4/C$. The higher electrical conductivity of sample $LiFePO_4/C$-PPy(ACN) was attributed to the formation of bipolaron in the polypyrrole chains synthesized in ACN solvent. The $LiFePO_4/C$-PPy samples synthesized in water and ethanol solvent, generate –OH and C=O groups during polymerization of pyrrole. These groups restrict the delocalization of polaron and bipolaron for samples $LiFePO_4/C$-PPy(ethanol) and $LiFePO_4/C$-PPy(water) leading to the decrease in conductivity. Incorporation of polypyrrole with $LiFePO_4/C$ has been found to show appreciable improvement in rate capabilities. The composite $LiFePO_4/C$-PPy(ACN) produces best electrochemical performance, which gives a rate capability of 82 mAh/g at 20C. The superior rate capability of $LiFePO_4/C$-PPy(ACN) was attributed to the better electronic conductivity and enhanced Li-ion diffusivity through the polypyrrole and carbon coating.

Polythiophene coating was performed on Li-excess ($Li_{1.05}FePO_4/C$), $LiFePO_4/C$ and Li-deficient ($Li_{0.95}FePO_4/C$) compounds in the binary solvent of CH_2Cl_2 and ACN. The Li-deficient $Li_{0.95}FePO_4/C$ was only sample that contains pure electrochemically active phases. Polythiophene coating on $Li_{0.95}FePO_4/C$ reduces the R values in all the cases. The interaction between polythiophene and graphitic carbon improves the graphitization of carbon coating, resulting in reduction of R values. From EIS measurements it was found that polythiophene addition to $Li_{0.95}FePO_4/C$ imparts appreciable improvement in the electrical conductivity and Li-ion diffusivity. The electrical conductivity and Li-ion diffusivity improved with 4, 6 and 8 wt.% addition of polythiophene while marginal improvement was observed for 10 wt.% addition of polythiophene. The higher electrical conductivity and Li-ion diffusivity for $Li_{0.95}FePO_4/C$-PTh composites are because of polythiophene coating which enhanced the electronic and ionic contact between $Li_{0.95}FePO_4/C$ particles, and improves the graphitization of carbon coating. The optimized wt.% of polythiophene content (8 wt%) have facilitated to deliver higher conductivity and faster Li-ion diffusion. Due to this significant improvement in rate capability was observed for the sample $Li_{0.95}FePO_4/C$-PTh(8) at 20C rate.

The polyaniline coated $LiFePO_4/C$ cathode materials was prepared by using $(NH_4)_2S_2O_8$, $K_2Cr_2O_7$ and $KMnO_4$ oxidizing agents. All the $LiFePO_4/C$-PANI composites have resulted in pure electrochemically active phases of $LiFePO_4$ and $Li_{0.05}FePO_4$. The protonic acid doping has resulted in the bipolaron formation for all the $LiFePO_4/C$-PANI composites. All the $LiFePO_4/C$-PANI composites show improved electrical conductivity and Li-ion diffusion. This

is due to the addition of doped conducting polyaniline which facilitates fast charge transport resulting higher conductivity and Li-ion diffusion. $LiFePO_4/C-PANI((NH_4)_2S_2O_8)$ composite delivers highest rate capability of 94 mAh/g at 20C among all the polyaniline coated $LiFePO_4/C$ samples. This is due to higher content of conducting polyaniline deposited in the presence of $(NH_4)_2S_2O_8$ oxidizing agent.

CONCLUSIONS AND SCOPE OF FUTURE WORK
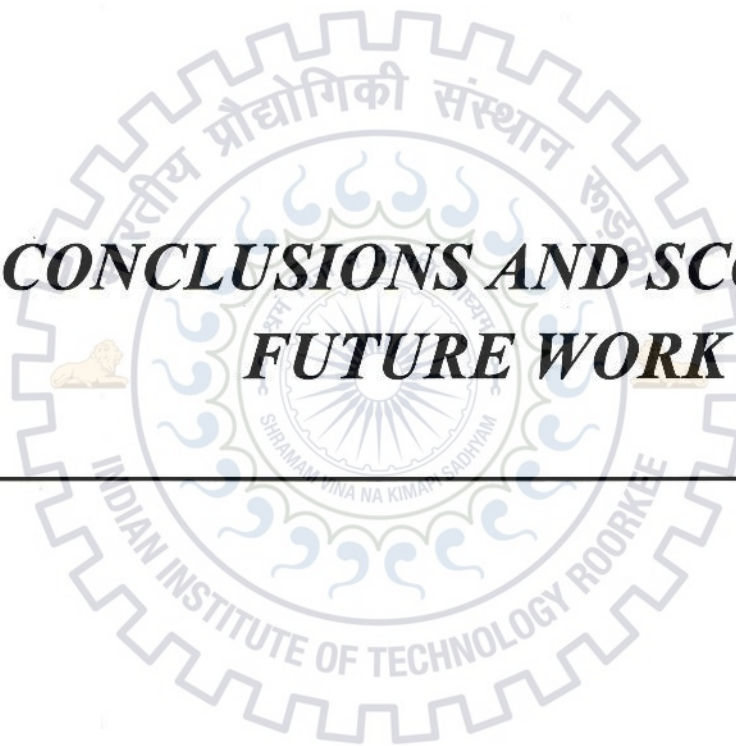
The present investigation has focused on the growth of LiFePO$_4$/C using chemical precipitation method and to develop in-situ polymer coating on LiFePO$_4$/C particles by oxidation polymerization method. Then LiFePO$_4$/C and polymer coated LiFePO$_4$/C have been investigated for their electrochemical performance in order to examine their potentiality for the application in cathode for Li-ion battery to enhance their rate capability. The morphology, structure, thermal analysis, spectroscopic analysis and electrochemical behavior of samples were determined and discussed.

6.1.1 Conclusion on LiFePO$_4$/C

The growth of (NH$_4$)Fe(HPO$_4$)$_2$ and LiFePO$_4$ particles were restricted by the polymer and carbon coatings respectively. The polymer coating has decomposed to carbon coating on LiFePO$_4$ particles with coating thickness of ~ 3 nm and ~ 7 nm for 0.5 ml and 1.0 ml of aniline respectively. The addition of 0.2 ml of aniline leads to partially coated (NH$_4$)Fe(HPO$_4$)$_2$ particles where 1.5 ml of aniline resulted in full coating on (NH$_4$)Fe(HPO$_4$)$_2$ particles along with the individual polyaniline rods. The Raman spectroscopy analysis showed that the structure of carbon coating on LiFePO$_4$ particles were found similar for samples prepared using 1.0 ml and 0.5 ml of aniline. At slow C-rate the sample LFP(0.5) shows higher discharge capacity as compared to LFP(1.0), but at the faster C-rate LFP(1.0) shows better rate capability and cyclic stability as compared to sample LFP(0.5). The higher rate capacity and cyclability of LFP(1.0) is attributed by small particle size and uniform carbon coating. Cyclic voltammetry tests reveal the narrow voltage difference between peak currents in a cycle. This confirms that sample LFP(1.0) has better reversibility at the scan rate of 0.1 mV/s.

6.1.2 Conclusion on Polypyrrole coated LiFePO$_4$/C composites.

The polypyrrole coating on the surface of LiFePO$_4$/C has been produced by chemical oxidation method using FeCl$_3$ as oxidizing agent in three different solvents water, ethanol, and ACN. The diffraction patterns of all LiFePO$_4$/C-PPy composites show the presence of pure electrochemically active LiFePO$_4$ and Li$_{0.05}$FePO$_4$ phases. The particles of polypyrrole

synthesized in ACN solvent are found to possess lower porosity as compared to polypyrrole synthesized separately in water and ethanol solvent. This was due to the formation of $-OH$ and $C=O$ nucleophilic end groups in water and ethanol which stop the polymer chain propagation. The reduced R $(= I_D/I_G)$ values of D-band to G-band for samples $LiFePO_4$/C-PPy as compared to $LiFePO_4$/C were due to interaction of polypyrrole with the defect site on carbon coating. The polypyrrole coating of minimum porosity grown using ACN solvent offers highest contact area with carbon coating on $LiFePO_4$ particles covering largest number of defects on carbon coating. Due to this polypyrrole grown in ACN solvent are found to have a minimum R value. The higher electrical conductivity of sample $LiFePO_4$/C-PPy(ACN) was attributed to the formation of bipolaron in the polypyrrole chains synthesized in ACN solvent. The $LiFePO_4$/C-PPy samples synthesized in water and ethanol solvent, generate $-OH$ and $C=O$ groups during polymerization of pyrrole. These groups restrict the delocalization of polaron and bipolaron for samples $LiFePO_4$/C-PPy(ethanol) and $LiFePO_4$/C-PPy(water) leading to the decrease in conductivity. The highest D_{Li+} was obtained for sample $LiFePO_4$/C-PPy(ACN) and this was due to the decrease in the D-band intensity as a result of interaction of polypyrrole with the defect sites of carbon coating. All the $LiFePO_4$/C-PPy samples are found to show appreciable rate capabilities as compared to $LiFePO_4$/C. The composite $LiFePO_4$/C-PPy(ACN) produces highest rate capability of 82 mAh/g at 20C. The superior rate capability of $LiFePO_4$/C-PPy(ACN) was attributed to the better electronic conductivity and enhanced Li-ion diffusivity through the polypyrrole and carbon coating.

6.1.3 Conclusion on polythiophene coated $LiFePO_4$/C

Polythiophene coating was performed on Li-excess $(Li_{1.05}FePO_4$/C), $LiFePO_4$/C and Li-deficient $(Li_{0.95}FePO_4$/C) compounds. After polythiophene coating, Li-deficient $Li_{0.95}FePO_4$/C was the only sample that contains pure electrochemically active phases. The FESEM micrographs show that 4 and 6 wt% of polythiophene give rise to partial coverage to $Li_{0.95}FePO_4$/C particles whereas 8 and 10 wt% of polythiophene show full coverage. Polythiophene coating on $Li_{0.95}FePO_4$/C reduces the R values in all the cases. The interaction between polythiophene and graphitic carbon improves the graphitization of carbon coating, resulting in reduction of R values. From EIS measurements it is found that upto 8 wt% of polythiophene addition to $Li_{0.95}FePO_4$/C imparts appreciable lower in R_{ct} and higher D_{Li+}. The further addition of polythiophene (10 wt%) marginally improves R_{ct} and and higher D_{Li+} of $Li_{0.95}FePO_4$/C-PTh. The low R_{ct} and higher D_{Li+} for $Li_{0.95}FePO_4$/C-PTh composites are because

of polythiophene coating which enhanced the electronic and ionic contact between $Li_{0.95}FePO_4/C$ particles, and improves the graphitization of carbon coating. The enhanced rate capability of sample $Li_{0.95}FePO_4/C$-PTh(8) at 20C rate might be due to optimum content (8 wt%) of polythiophene which provides full coverage to $LiFePO_4/C$ particles and facilitates to deliver higher conductivity and faster Li-ion diffusion.

6.1.4 Conclusion on Polyaniline coated LiFePO₄/C

The polyaniline coating on $LiFePO_4/C$ prepared by using the oxidizing agents $(NH_4)_2S_2O_8$, $K_2Cr_2O_7$ and $KMnO_4$ has resulted in pure electrochemically active phases of $LiFePO_4$ and $Li_{0.05}FePO_4$. The composite $LiFePO_4/C$-PANI synthesized using $(NH_4)_2S_2O_8$ oxidizing agent have elongated structure as compared to the composites synthesized using other oxidizing agents. The protonic acid doping has resulted in the bipolaron formation for all the $LiFePO_4/C$-PANI composites. All the $LiFePO_4/C$-PANI composites show improved electrical conductivity and Li-ion diffusion. This is due to the addition of doped conducting polyaniline which facilitates fast charge transport resulting higher conductivity and Li-ion diffusion. $LiFePO_4/C$-PANI($(NH_4)_2S_2O_8$) composite delivers highest rate capability of 94 mAh/g at 20C among all the polyaniline coated $LiFePO_4/C$ samples. This is due to higher content of conducting polyaniline deposited in the presence of $(NH_4)_2S_2O_8$ oxidizing agent.

REFERENCES

REFERENCES

Amine, K., Yasuda, H., Yamachi, M., Olivine $LiCoPO_4$ as 4.8 V electrode material for lithium batteries. Electrochemical and Solid-State Letters, 3 (4) (2000) 178 – 179.

Andersson, A.S., Thomas, J.O., Kalska, B., Haggstrom, L., Thermal stability of $LiFePO_4$-based cathodes. Electrochemical and Solid-State Letters, 3 (2) (2000) 66 – 68.

Aurbach, D., Levi, M.D., Gamulski, K., Markovsky, B., Salitra, G., Levi, E., Heider, U., Heider, L., Oesten, R., Capacity fading of LiMnO spinel electrodes studied by XRD and electroanalytical techniques. Journal of Power Sources, 81 – 82 (1999) 472 – 479.

Bai, Y., Chang, Q., Yu, Q., Zhao, S., Jiang, K., A novel approach to improve the electrochemical performances of layered $LiNi_{1/3}Co_{1/3}Mn_{1/3}O_2$ cathode by YPO_4 surface coating. Electrochimica Acta, 112 (2013) 414 – 421.

Bai, Y.M., Qiu, P., Wen, Z.L., Han, S.C., Improvement of electrochemical performances of $LiFePO_4$ cathode materials by coating of polythiophene. Journal of Alloys and Compounds, 508 (2010) 1 – 4.

Balaya, P., Bhattacharyya, A.J., Jamnik, J., Zhukovskii, Y.F., Kotomin, E.A., Maier, J., Nano-ionics in the context of lithium batteries. Journal of Power Sources, 159 (2006) 171 – 178.

Balint, R., Cassidy, N.J., Cartmell, S.H., Conductive polymers: Towards a smart biomaterial for tissue engineering. Acta Biomaterialia, 10 (2014) 2341 – 2353.

Bhargava, S., Bist, H.D., Narlikar, A.V., Samanta, S.B., Narayan, J., Tripathi, H.B., Effect of substrate temperature and heat treatment on the microstructure of diamond like carbon films. Journal of Applied Physics, 79 (1996) 1917 – 1925.

Biendicho, J.J., West, A.R., Impedance characterisation of $LiFePO_4$ ceramics. Solid State Ionics, 226 (2012) 41 – 52.

Biendicho, J.J., West, A.R., Thermally-induced cation disorder in $LiFePO_4$. Solid State Ionics, 203 (2011) 33 – 36.

Bramnik, N.N., Nikolowski, K., Baehtz, C., Bramnik, K.G., Ehrenberg, H., Phase transitions occurring upon lithium insertion-extraction of $LiCoPO_4$. Chemistry of Materials, 19 (2007) 908 – 915.

Brownson, D.A.C., Kampouris, D.K., Banks, C.E., An overview of graphene in energy production and storage applications. Journal of Power Sources, 196 (2011) 4873 – 4885.

Bruce, P.G., Scrosati, B., Tarascon, J.M., Nanomaterials for rechargeable lithium batteries. Angewandte Chemie International Edition, 47 (2008) 2930 – 2946.

Cao, Q., Zhang, H.P., Wang, G.J., Xia, Q., Wu, Y.P., Wu, H.Q., A novel carbon-coated $LiCoO_2$ as cathode material for lithium ion battery. Electrochemistry Communications, 9 (2007) 1228 – 1232.

Chabukswar, V., Bhavsar, S., Synthesis and characterization of organically soluble and electrically conducting acids doped polyaniline. Chemistry & chemical technology, 4 (4) (2010) 277 – 280.

Chandrakanthi, N., Careem, M.A., Thermal stability of polyaniline. Polymer Bulletin, 44 (2000) 101 – 108.

Chang, H.H., Chang, C.C., Sub, C.Y., Wub, H.C., Yang, M.H., Wu, N.L., Effects of TiO_2 coating on high-temperature cycle performance of $LiFePO_4$-based lithium-ion batteries. Journal of Power Sources, 185 (2008) 466 – 472.

Chang, Z.R., Lv, H.J., Tang, H.W., Li, H.J., Yuan, X.Z., Wang, H., Synthesis and characterization of high-density $LiFePO_4/C$ composites as cathode materials for lithium-ion batteries. Electrochimica Acta, 54 (2009) 4595 – 4599.

Chen, J., Zou, Y.C., Zhang, F., Zhang, Y.C., Guo, F.F., Li, G.D., Superior electrode performance of $LiFePO_4/C$ composite prepared by an in situ polymerization restriction method. Journal of Alloys and Compounds, 563 (2013) 264 – 268.

Chen, R., Wu, Y., Kong, X.Y., Monodisperse porous $LiFePO_4/C$ microspheres derived by microwave assisted hydrothermal process combined with carbothermal reduction for high power lithium-ion batteries. Journal of Power Sources, 258 (2014) 246 – 252.

Chen, Z., Qin, Y., Amine, K., Sun, Y.K., Role of surface coating on cathode materials for lithium-ion batteries. Journal of Materials Chemistry, 20 (2010) 7606 – 7612.

Chena Z., Dahna, J.R., Reducing carbon in $LiFePO_4$ /C composite electrodes to maximize specific energy, volumetric energy, and tap density. Journal of The Electrochemical Society, 149 (9) (2002) A1184 – A1189.

Cho, J., Kim, Y.J., Kim, T.J., Park, B., Zero-strain intercalation cathode for rechargeable Li-ion cell. Angewandte Chemie International Edition, 40 18 (2001) 3367 – 3369.

Cho, J., Kim, Y.W., Kim, B., Lee, J.G., Park, B., A breakthrough in the safety of lithium secondary batteries by coating the cathode material with $AlPO_4$ nanoparticles. Angewandte Chemie International Edition, 42 (2003) 1618 – 1621.

Cho, Y.D., Fey, G.T.K., Kao, H.M., The effect of carbon coating thickness on the capacity of $LiFePO_4$/C composite cathodes. Journal of Power Sources, 189 (2009) 256 – 262.

Corradini, A., Mastragostino, M., Electrochemical stability of electro synthesized heterocyclic semiconducting polymers as cathode-active materials in advanced batteries. Synthetic Metals, 18 (1987) 625 – 630.

Croce, F., Epifanio, A.D., Hassoun, J., Deptula, A., Olczac, T., Scrosatia, B., A novel concept for the synthesis of an improved $LiFePO_4$ lithium battery cathode. Electrochemical and Solid-State Letters, 5 (3) (2002) A47 – A50.

Das, S.R., Fachini, I.R., Majumder, S.B., Katiyar, R.S., Structural and electrochemical properties of nanocrystalline $Li_xMn_2O_4$ thin film cathodes (x = 1.0 – 1.4). Journal of Power Sources, 158 (2006) 518 – 523.

Delacourt, C., Laffont, L., Bouchet, R., Wurm, C., Leriche, J.B., Morcrette, M., Tarascon, J.M., Masqueliera, C., Toward understanding of electrical limitations (electronic, ionic) in $LiMPO_4$ (M = Fe, Mn) electrode materials. Journal of The Electrochemical Society, 152 (5) (2005) A913 – A921.

Delacourt, C., Poizot, P., Masquelier, C., Crystalline nanometric $LiFePO_4$, United States Patent Application 20080241690, Application No PCT/EP2006/005725, Date of filling: 15/01/2006.

Delacourt, C., Poizot, P., Morcrette, M., Tarascon, J.M., Masquelier, C., One-step low-temperature route for the preparation of electrochemically active $LiMnPO_4$ powders. Chemistry of Materials, 16 (2004) 93 – 99.

Delacourt, D., Poizot, P., Levasseur, S., Masqueliera, C., Size effects on carbon-free $LiFePO_4$ powders the key to superior energy density. Electrochemical and Solid-State Letters, 9 (7) (2006) A352 – A355.

Ding, Y., Jiang, Y., Xua, F., Yin, J., Ren, H., Zhuo, Q., Long, Z., Zhang, P., Preparation of nano-structured $LiFePO_4$/graphene composites by co-precipitation method. Electrochemistry Communications, 12 (2010) 10 – 13.

Doeff, M.M., Hu, Y., McLarnon, F., Kostecki, R., Effect of surface carbon structure on the electrochemical performance of $LiFePO_4$. Electrochemical and Solid-State Letters, 6 (10) (2003) A207 – A209.

Drezen, T., Kwon, N.H., Bowen, P., Teerlinck, I., Isono, M., Exnar, I., Effect of particle size on LiMnPO$_4$ cathodes. Journal of Power Sources, 174 (2007) 949 – 953.

Ellis, B., Kan, W.H., Makahnouk, W.R.M., Nazar, L.F., Synthesis of nanocrystals and morphology control of hydrothermally prepared LiFePO$_4$. Journal of Materials Chemistry, 17 (2007) 3248 – 3254.

Fang, T., Duh, J.G., Effect of calcination temperature on the electrochemical behavior of ZnO-coated LiCoO$_2$ cathode. Surface & Coatings Technology, 201 (2006) 1886 – 1893.

Focke, W.W., Wnek, G.E., Wei, Y., Influence of oxidation state, pH, and counterion on the conductivity of polyaniline. The Journal of Physical Chemistry, 91 (22) (1987) 5813 – 5818.

Franger, S., Cras, F.L., Bourbon, C., Rouault, H., Comparison between different LiFePO$_4$ synthesis routes and their influence on its physico-chemical properties. Journal of Power Sources, 119–121 (2003) 252 – 257.

Freund, M.S., Deore, B. A., Self doped conducting polymers. John Wiley & Sons Ltd, The Atrium, Southern Gate, Chichester, West Sussex PO19 8SQ, England, Copy right 2007.

Ghosh, P., Mahanty, S., Basu, R.N., Lanthanum-doped LiCoO$_2$ cathode with high rate capability. Electrochimica Acta, 54 (2009) 1654 – 1661.

Gibot, P., Masquelier, C., Tarascon, J.M., Levasseur, S., Carlach, P., Room temperature single phase Li insertion / extraction material for use in Li-based battery, Date of filling: 19/03/2008 Application No.: PCT/EP2008/002195 Publication number WO2008113570 A1.

Goodenough, J.B., Padhi, A.K., Nanjundaswamy, K.S., Masquelier, C., Cathode of mixed oxide containing lithium, phosphorus and transition metal, Date of filling: 21/04/1997, Application number US 08/840,523, Publication number US5910382 A.

Goriparti, S., Miele, E., Angelis, F.D., Fabrizio, E.D., Zaccaria, R.P., Capiglia, C., Review on recent progress of nanostructured anode materials for Li-ion batteries. Journal of Power Sources, 257 (2014) 421 – 443.

Groenendaal, L.B., Jonas, F., Freitag, D., Pielartzik, H., Reynolds, J.R., Poly(3,4-ethylenedioxythiophene) and its derivatives: past, present, and future. Advanced Materials, 12 (7) (2000) 481 – 494.

Gu, F., Chen, G., Carbon coating with oleic acid on Li$_4$Ti$_5$O$_{12}$. International Journal of Electrochemical Science, 7 (2012) 6168 – 6179.

Guimard, N.K., Gomez, N., Schmidt, C.E., Conducting polymers in biomedical engineering. Progress in Polymer Science, 32 (2007) 876 – 921.

Guo, H., Liu, L., Shu, H., Yang, X., Yang, Z., Zhou, M., Tan, J., Yan, Z., Hu, H., Wang, X., Synthesis and electrochemical performance of LiV_3O_8/polythiophene composite as cathode materials for lithium ion batteries. Journal of Power Sources, 247 (2014) 117 – 126.

Guo, Y.G., Hu, J.S., Wan, L.J., Nanostructured materials for electrochemical energy conversion and storage devices. Advanced Materials, 20 (2008) 2878 – 2887.

Han, C.C., Lu, C.H., Hong, S.P., Yang, K.F., Highly conductive and thermally stable self-doping propylthiosulfonated polyanilines. Macromolecules, 36 (2003) 7908 – 7915.

Heeger, A.J., Semiconducting and metallic polymers: The fourth generation of polymeric materials (nobel lecture). Angewandte Chemie International Edition, 40 (2001) 2591 – 2611.

Hou, Y., Zhang, L., Chen, L.Y., Liu, P., Hirat, A., Chen, M.W., Raman characterization of pseudocapacitive behavior of polypyrrole on nanoporous gold. Physical Chemistry Chemical Physics, 16 (2014) 3523 – 3528.

Hu, Y., Doeff, M.M., Kostecki, R., Finonesa, M.M., Electrochemical performance of sol-gel synthesized $LiFePO_4$ in lithium batteries. Journal of The Electrochemical Society, 151 (8) (2004) A1279 – A1285.

Huang, H., Yin, S.C., Nazar, L.F., Approaching theoretical capacity of $LiFePO_4$ at room temperature at high rates. Electrochemical and Solid-State Letters, 4 (10) (2001) A170 – A172.

Huang, J., Virji, S., Weiller, B.H., Kaner, R.B., Polyaniline nanofibers: facile synthesis and chemical sensors. Journal of American Chemical Society, 125 (2003) 314 – 315.

Huang, Y.H., Goodenough, J.B., High-rate $LiFePO_4$ lithium rechargeable battery promoted by electrochemically active polymers. Chemistry of Materials, 20 (2008) 7237 – 7241.

Huang, Y.H., Park, K.S., Goodenough, J.B., Improving lithium batteries by tethering carbon-coated $LiFePO_4$ to polypyrrole. Journal of The Electrochemical Society, 153 (12) (2006) A2282 – A2286.

Ibarra, L.E., Tarres, L., Bongiovanni, S., Barbero, C.A., Kogan, M.J., Rivarola, V.A., Bertuzzi, M.L., Yslas, E.I., Assessment of polyaniline nanoparticles toxicity and teratogenicity in aquatic environment using Rhinella arenarum model. Ecotoxicology and Environmental Safety 114 (2015) 84 – 92.

Islam, M.S., Driscoll, D.J., Fisher, C.A.J., Slater, P.R., Atomic-scale investigation of defects, dopants, and lithium transport in the $LiFePO_4$ olivine-type battery material. Chemistry of Materials, 17 (2005) 5085 – 5092.

Jeon, S.S., Yang, S.J., Lee, K.J., Im, S.S., A facile and rapid synthesis of unsubstituted polythiophene with high electrical conductivity using binary organic solvents. Polymer, 51 (2010) 4069 – 4076.

Jiang, Z., Jiang, Z.J., Effects of carbon content on the electrochemical performance of $LiFePO_4$/C core/shell nanocomposites fabricated using $FePO_4$/polyaniline as an iron source. Journal of Alloys and Compounds, 537 (2012) 308 – 317.

Jiao, F., Bao, J., Hill, A.H., Bruce, P.G., Synthesis of ordered moesoporous Li–Mn–O spinel as a positive electrode for rechargeable lithium batteries. Angewandte Chemie International Edition, 47 (2008) 9711 – 9716.

Jin, E.M., Jina, B., Jun, D.K., Park, K.H., Gua, H.B., Kim K.W., A study on the electrochemical characteristics of $LiFePO_4$ cathode for lithium polymer batteries by hydrothermal method. Journal of Power Sources, 178 (2008) 801 – 806.

John A. Joule, Keith Mills, Heterocyclic Chemistry. John Wiley & Sons Ltd, Copy right 2010

Jung, Y.S., Cavanagh, A.S., Dillon, A.C., Groner, M.D., George, S.M., Lee S.H., Enhanced stability of $LiCoO_2$ cathodes in lithium-ion batteries using surface modification by atomic layer deposition. Journal of The Electrochemical Society, 157 (1) (2010) A75 – A81.

Jurcakova, D.H., Seredych, M., Lu, G.Q., Bandosz, T.J., Combined effect of nitrogen- and oxygen-containing functional groups of microporous activated carbon on its electrochemical performance in supercapacitors. Advanced Functional Materials, 19 (2009) 438 – 447.

Kang, H.C., Geckeler, K.E., Enhanced electrical conductivity of polypyrrole prepared by chemical oxidative polymerization: effect of the preparation technique and polymer additive. Polymer, 41 (2000) 6931 – 6934.

Katare, R.K., Pandey, L., Thakur, O.P., Om P., Kumar, D., Equivalent circuit model of $Ca_{1-x}Y_xTi_{1-x}Co_xO_3$ using impedance spectroscopy. Modern Physics Letters B, 17 (8) (2003) 339 – 346.

Katare, R.K., Pandey, L., Thakur, O.P., Om P., Kumar, D., Impedance spectroscopic study of $Ca_{1-x}Y_xTi_{1-x}Co_xO_3$ ceramics based humidity sensor. International Journal of Modern Physics B, 19 (10) (2005) 1783 – 1791.

Kavan, L., Prochazka, J., Spitler, T.M., Kalbac, M., Zukalova, M., Drezen, T., Gratzel, M., Li insertion into $Li_4Ti_5O_{12}$ (Spinel) charge capability vs. particle size in thin-film electrodes. Journal of The Electrochemical Society, 150 (7) (2003) A1000 – A1007.

Kawai, H., Nagata, M., Tukamoto, H., West, A.R., High-voltage lithium cathode materials. Journal of Power Sources, 81 – 82 (1999) 67 – 72.

Kaynak, A., Decay of electrical conductivity in p-toluene sulfonate doped polypyrrole films. Fibers and Polymers, 10 (5) (2009) 590 – 593.

Kim, J.K., Cheruvally, G., Ahn, J.H., Ahn, H.J., Kim, J.K., Cheruvally, G., Ahn, J.H., Ahn, H.J., Electrochemical properties of $LiFePO_4$/C composite cathode material: Carbon coating by the precursor method and direct addition. Journal of Physics and Chemistry of Solids 69 (2008) 1257 – 1260.

Kim, J.K., Choi, J.W., Chauhan, G.S., Ahn, J.H., Hwang, G.C., Choi, J.B., Ahn, H.J., Enhancement of electrochemical performance of lithium iron phosphate by controlled sol–gel synthesis. Electrochimica Acta, 53 (2008) 8258 – 8264.

Ko, J.M., Rhee, H.W., Park, S.M., Kim, C.Y., Morphology and electrochemical properties of polypyrrole films prepared in aqueous and nonaqueous solvents. Journal of The Electrochemical Society, 137 (3) (1990) 905 – 909.

Kulkarni, M., Kale, B., Apte, S., Naik, S., Mulik, U., Amalnerkar, D., Synthesis and characterization of polyaniline nanofibres by rapid liquid-liquid interfacial polymerization method. Chemistry & Chemical Technology, 5 (2011) 55 – 58.

Kumar, A., Thomas, R., Karan, N.K., Saavedra-Arias, J.J., Singh, M.K., Majumder, S.B., Tomar, M.S., Katiyar, R.S., Structural and electrochemical characterization of pure $LiFePO_4$ and nanocomposite C-$LiFePO_4$ cathodes for lithium ion rechargeable batteries. Volume 2009, Article ID 176517, 10 pages.

Lee, J., Kumar, P., Lee, J., Moudgil, B.M., Singh, R.K., ZnO incorporated $LiFePO_4$ for high rate electrochemical performance in lithium ion rechargeable batteries. Journal of Alloys and Compounds, 550 (2013) 536 – 544.

Li, H., Wang, Z., Chen, L., Huang, X., Research on Advanced Materials for Li-ion Batteries. Advanced Materials, 21 (2009) 4593 – 4607.

Li, X., Wang, C., Engineering nanostructured anodes via spray deposition for high performance lithium ion battery application. Journal of Materials Chemistry A, 1 (2013) 165 – 182.

Li, X., Xua, Y., Wang, C., Suppression of Jahn–Teller distortion of spinel $LiMn_2O_4$ cathode. Journal of Alloys and Compounds, 479 (2009) 310 – 313.

Ohzuku, T., Makimura, Y., Layered lithium insertion material of $LiNi_{1/2}Mn_{1/2}O_2$: A possible alternative to $LiCoO_2$ for advanced lithium-ion batteries. Chemistry Letters, 642 (30) (2001) 744 – 745.

Okada, S., Sawa, S., Egashira, M., Yamaki, J., Tabuchi, M., Kageyama, H., Konishi, T., Yoshino, A., Cathode properties of phosphor-olivine $LiMPO_4$ for lithium secondary batteries. Journal of power sources, 97 – 98 (2011) 430 – 432.

Osaka, T., Mamma, T., Nishimura, K., Kakuda, S., Ishii, T., Application of solid polymer electrolyte to lithium/polypyrrole secondary battery system. Journal of The Electrochemical Society, 141 (8) (1994) 1994 – 1998.

Ouyang, C.Y., Shi, S.Q., Wang, Z.X., Li, H., Huang, X.J., Chen, L.Q., The effect of Cr doping on Li ion diffusion in $LiFePO_4$ from first principles investigations and Monte Carlo simulations. Journal of Physics: Condense Matter, 16 (2004) 2265 – 2272.

Padhi, A. K., Nanjundaswamy, K., Goodenough, J. B., Phospho-olivines as positive-electrode materials for rechargeable lithium batteries. Journal of The Electrochemical Society, 144 (4) (1997) 1188 – 1194.

Pan, D., Wang, S., Zhao, B., Wu, M., Zhang, H., Wang, Y., Jiao, Z., Li storage properties of disordered graphene nanosheets. Chemistry of Materials, 21 (2009) 3136 – 3142.

Park, C.M., Kim, J.H., Kim H., Sohn, H.J., Li-alloy based anode materials for Li secondary batteries. Chemical Society Review, 39 (2010) 3115 – 3141.

Park, K.S, Benayad, A., Kang, D.J., Doo, S.G., Nitridation-driven conductive $Li_4Ti_5O_{12}$ for lithium ion batteries. Journal of American Chemical Society, 130 (2008) 14930 – 14931.

Park, K.S., Son, J.T., Chung, H.T., Kim, S.J., Lee, C.H., Kang, K.T., Kim, H.G., Surface modification by silver coating for improving electrochemical properties of $LiFePO_4$. Solid State Communications, 129 (2004) 311 – 314.

Pei, B., Yao, H, Zhang, W., Yang, Z., Hydrothermal synthesis of morphology-controlled $LiFePO_4$ cathode material for lithium-ion batteries. Journal of Power Sources, 220 (2012) 317 – 323.

Petrovsky, V., Anderson, H.U., Petrovsky, T., Low temperature technologies for SOFC, Solid Oxide Fuel Cells, Electrochemical Society proceedings, 8 (2003) 976 – 983.

Poizot, P., Laruelle, S., Grugeon, S., Tarasconz, J.M., Rationalization of the low-potential reactivity of 3d-metal-based inorganic compounds toward Li. Journal of The Electrochemical Society, 149 (9) (2002) A1212 – A1217.

Pron, A., Genoud, F., Menardo, C., Nechtschein, M., The effect of the oxidation conditions on the chemical polymerization of polyaniline. Synthetic Metals, 24 (1988) 193 – 201.

Raja, M.W., Mahanty, S., Basu, R.N., Filter paper templated interconnected nanocrystalline $LiMn_2O_4$ with high Columbic efficiency and rate capability. Journal of Materials Chemistry, 34 (2009) 6161 – 6166.

Rajeev Sehrawat, Anjan Sil "Effect of solvents on electrochemical performance of polypyrrole coated $LiFePO_4$/C cathode materials", Journal of Materials Science: Materials in Electronics, 26 (2015) 5175 - 5185.

Ramar, V., Balaya, P., Enhancing the electrochemical kinetics of high voltage olivine $LiMnPO_4$ by isovalent co-doping. Physical Chemistry Chemical Physics, 15 (2013) 17240 – 17249.

Ravet, N., Abouimrane, A., Armand, M., From our readers: On the electronic conductivity of phospho-olivines as lithium storage electrodes. Nature Materials, 2 (2003) 702 – 703.

Ravet, N., Chouinard, Y., Magnan, J.F., Besner, S., Gauthier, M., Armand, M., Electroactivity of natural and synthetic triphylite. Journal of power sources, 97 – 98 (2001) 503 – 507.

Rengan, A., Narayan, J., Jahnke, C., Bedge, S., Park, J.L., Li, M., Characteristics of diamond-like carbon films formed by a hybrid laser-plasma ablation of graphite. Materials Science and Engineering, B15 (1992) 15 – 24.

Rho, Y.H., Nazar, L.F., Perry, L., Ryan, D., Surface chemistry of $LiFePO_4$ studied by Mössbauer and X-Ray photoelectron spectroscopy and its effect on electrochemical properties. Journal of The Electrochemical Society, 154 (4) (2007) A283 – A289.

Ryu, K.S., Lee, Y., Han, K.S., Kim, M.G., The electrochemical performance of polythiophene synthesized by chemical method as the polymer battery electrode. Materials Chemistry and Physics, 84 (2004) 380 – 384.

Sarkar, S., Banda, H., Mitra, S., High capacity lithium-ion battery cathode using LiV_3O nanorods. Electrochimica Acta, 99 (2013) 242 – 252.

Sarkar, S., Mitra, S., Carbon coated submicron sized-$LiFePO_4$: Improved high rate performance lithium battery cathode. Energy Procedia, 54 (2014) 718 – 724.

Scrosati, B., Garche, J., Lithium batteries: Status, prospects and future. Journal of Power Sources, 195 (2010) 2419 – 2430.

Sen, U.K., Shaligram, A., Mitra, S., Intercalation Anode Material for Lithium-ion Battery Based on Molybdenum Di-oxide. ACS Applied Materials and Interfaces, 6 (16) (2014) 14311 – 14319.

Sengodu, P., Deshmukh, A.D., Conducting polymers and their inorganic composites for advanced Li-ion batteries: a review. RSC Adv., 5 (2015) 42109 – 42130.

Seredych, M., Jurcakova, D.H., Lu, G.Q., Bandosz, T.J., Surface functional groups of carbons and the effects of their chemical character, density and accessibility to ions on electrochemical performance. Carbon, 46 (2008) 1475 – 1488.

Shaju, K.M., Bruce, P.G., A stoichiometric nano-$LiMn_2O_4$ spinel electrode exhibiting high power and stable cycling. Chemistry of Materials, 20 (2008) 5557 – 5562.

Shaju, K.M., Bruce, P.G., Nano-$LiNi_{0.5}Mn_{1.5}O_4$ spinel: a high power electrode for Li-ion batteries. Dalton Transactions, (2008) 5471 – 5475.

Shen, L., Yuan, C., Luo, H., Zhang, X., Xu, K., Xia, Y., Facile synthesis of hierarchically porous $Li_4Ti_5O_{12}$ microspheres for high rate lithium ion batteries. Journal of Materials Chemistry, 20 (2010) 6998 – 7004.

Singh, D.P., Mulder, F.M., Wagemaker, M., Templated spinel $Li_4Ti_5O_{12}$ Li-ion battery electrodes combining high rates with high energy density. Electrochemistry Communications, 35 (2013) 124 – 127.

Singh, G., Gupta, S.L., Prasad, R., Auluck, S., Gupta, R., Sil, A., Suppression of Jahn–Teller distortion by chromium and magnesium doping in spinel $LiMn_2O_4$: A first-principles study using GGA and GGA+U. Journal of Physics and Chemistry of Solids, 70 (2009) 1200 – 1206.

Sivaprakash, S., Majumder, S.B., Understanding the role of Zr^{4+} cation in improving the cyclability of $LiNi_{0.8}Co_{0.15}Zr_{0.05}O_2$ cathodes for Li ion rechargeable batteries. Journal of Alloys and Compounds, 479 (2009) 561 – 568.

Snively, C.M., Koenig, J.L., Polymer applications of IR and Raman spectroscopy, Encyclopedia of spectroscopy and spectrometry. Academics Press San Diego, 3 (1999) 1858 – 1864.

Song, H.K., Lee, K.T., Kim, M.G., Nazar, L.F. Cho, J., Recent progress in nanostructured cathode materials for lithium secondary batteries. Advanced Functional Materials, 20 (2010) 3818 – 3834.

Sood, A.K., Gupta, R., Asher, S.A., Origin of the unusual dependence of Raman D band on excitation wavelength in graphite-like materials. Journal of Applied Physics, 90 (2001) 4494 – 4497.

Srinivasan, V., Newman J., Discharge model for the lithium iron-phosphate electrode. Journal of The Electrochemical Society, 151 (10) (2004) A1517 – A1529.

Su, F.Y., You, C., He, Y.B., Lv, W., Cui, W., Jin, F., Li, B., Yang, Q.H., Kang, F., Flexible and planar graphene conductive additives for lithium-ion batteries. Journal of Materials Chemistry, 20 (2010) 9644 – 9650.

Takahashi, M., Yoshida, T., Ichikawa, A., Kitoh, K., Katsukawa, H., Zhang, Q., Yoshio, M., Effect of oxygen deficiency reduction in Mg-doped Mn-spinel on its cell storage performance at high temperature. Electrochimica Acta, 51 (2006) 5508 – 5514.

Tang, J., Kong, L., Zhang, J., Zhan, L., Zhan, H., Zhou, Y., Zhan, C., Solvent-free, oxidatively prepared polythiophene: High specific capacity as a cathode active material for lithium batteries. Reactive & Functional Polymers, 68 (2008) 1408 – 1413.

Tang, K., Yu, X., Sun, J., Li, H., Huang, X., Kinetic analysis on $LiFePO_4$ thin films by CV, GITT, and EIS. Electrochimica Acta, 56 (2011) 4869 – 4875.

Tarascon, J.M., Armand, M., Issues and challenges facing rechargeable lithium batteries. Nature, 414 (2001) 359 – 367.

Thackeray, M.M., David, W.I.F., Bruce, P.G., Goodenough, J.B., Lithium insertion into manganese spinels. Materials Research Bulletin, 18 (1983) 461 – 472.

Tuinstra, F., Koenig, J. L., Raman spectrum of graphite. The Journal of Chemical Physics, 53 (1970) 1126 – 1130.

Vernitskaya, T.V., Efimov, O.N., Polypyrrole: a conducting polymer; its synthesis, properties and applications. Russian Chemical Reviews, 66 (5) (1997) 443 – 457.

Wagemaker, M., Ellis, B.L., Lutzenkirchen-Hecht, D., Mulder, F.M., Nazar, L.F., Proof of Supervalent doping in Olivine $LiFePO_4$. Chemistry of Materials, 20 (2008) 6313 – 6315.

Wagemaker, M., Mulder, F.M., Properties and promises of nanosized insertion materials for Li-ion batteries. Accounts of chemical research, 46 (5) (2013) 1206 – 1215.

Wanekaya, A.K., Lei, Y., Bekyarova, E., Chen, W., Haddon, R., Mulchandani, A., Myung, N.V., Fabrication and properties of conducting polypyrrole/SWNT-PABS composite films and nanotubes. Electroanalysis, 18 (11) (2006) 1047 – 1054.

Wang, C., Hong, J., Ionic/electronic conducting characteristics of $LiFePO_4$ cathode materials, the determining factors for high rate performance. Electrochemical and Solid-State Letters, 10 (3) (2007) A65 – A69.

Wang, D., Li, H., Shi, S., Huang, X., Chen, L., Improving the rate performance of $LiFePO_4$ by Fe-site doping. Electrochimica Acta, 50 (2005) 2955 – 2958.

Wang, G.X., Bewlay, S., Needham, S.A., Liu, H.K., Liu, R.S., Drozd, V.A., Lee, J.F., Chend, J.M., Synthesis and characterization of $LiFePO_4$ and $LiTi_{0.01}Fe_{0.99}PO_4$ cathode materials. Journal of The Electrochemical Society, 153 (1) (2006) A25 – A31.

Wang, G.X., Yang, L., Chen, Y., Wang, J.Z., Bewlay, S., Liu, H.K., An investigation of polypyrrole-$LiFePO_4$ composite cathode materials for lithium-ion batteries. Electrochimica Acta, 50 (2005) 4649 – 4654.

Wang, H., Jang, Y.I., Huang, B., Sadoway, D.R., Chiang, Y.M., TEM study of electrochemical cycling-induced damage and disorder in $LiCoO_2$ cathodes for rechargeable lithium batteries. Journal of The Electrochemical Society, 146 (2) (1999) 473 – 480.

Wang, J., Liu, J.L., Wang, Y.G., Wang, C.X., Xia, Y.Y., Pitch modified hard carbons as negative materials for lithium-ion batteries. Electrochim. Acta 74 (2012) 1 – 7.

Wang, J., Sun, X., Understanding and recent development of carbon coating on $LiFePO_4$ cathode materials for lithium-ion batteries. Energy and Environmental Science, 5 (2012) 5163 – 5185.

Wang, Y., Wang, Y., Hosono, E., Wang, K., Zhou, H., The design of a $LiFePO_4$/carbon nanocomposite with a core–shell structure and its synthesis by an in situ polymerization restriction method. Angewandte Chemie International Edition, 47 (2008) 7461 – 7465.

Wang, Y., Yang, Y., Yang, Y., Shao, H., Enhanced electrochemical performance of unique morphological $LiMnPO_4$/C cathode material prepared by solvothermal method. Solid State Communications, 150 (2010) 81 – 85.

Wei, Q., Sharma, A.K., Sankar, J., Narayan, J., Mechanical properties of diamond-like carbon composite thin films prepared by pulsed laser deposition. Composites: Part B, 30 675 – 684 (1999).

Wilcox, J.D., Doeff, M.M., Marcinek, M., Kostecki, R., Factors influencing the quality of carbon coatings on $LiFePO_4$. Journal of The Electrochemical Society, 154 (5) (2007) A389 – A395.

Wolfenstine, J., Allen J.L., Electrical conductivity and charge compensation in Ta doped $Li_4Ti_5O_{12}$. Journal of Power Sources, 180 (2008) 582 – 585.

Wolfenstine, J., Allen, J., Ni^{3+}/Ni^{2+} redox potential in $LiNiPO_4$. Journal of Power Sources, 142 (2005) 389 – 390.

Wolska, E., Tovar, M., Andrzejewski, B., Nowicki, W., Darul, J., Piszora, P., Knapp, M., Structural and magnetic properties of the iron substituted lithium–manganese spinel oxides. Solid State Sciences, 8 (2006) 31 – 36.

Wu, F., Chen, J., Chen, R., Wu, S., Li, L., Chen, S., Zhao, T., Sulfur/polythiophene with a core/shell structure: synthesis and electrochemical properties of the cathode for rechargeable lithium batteries. Journal of Physical Chemistry C, 115 (2011) 6057 – 6063.

Wu, X.L., Jiang, L.Y., Cao, F.F., Guo, Y.G., Wan, L.J., $LiFePO_4$, Nanoparticles embedded in a nanoporous carbon matrix: superior cathode material for electrochemical energy-storage devices. Advanced Materials, 21 (2009) 2710 – 2714.

Xie, H.M., Wang, R.S., Ying, J.R., Zhang, L.Y., Jalbout, A.F., Yu, H.Y., Yang, G.L., Pan, X.M., Su, Z. M., Optimized $LiFePO_4$–polyacene cathode material for lithium ion batteries. Advanced Materials, 18 (2006) 2609 – 2613.

Xu, B., Qian, D., Wang, Meng, Y.S., Recent progress in cathode materials research for advanced lithium ion batteries. Materials Science and Engineering R, 73 (2012) 51 – 65.

Yamada, A., Chung, S.C., Hinokuma, K., Optimized $LiFePO_4$ for lithium battery cathodes. Journal of The Electrochemical Society, 148 (3) (2001) A224 – A229.

Yang, J., Xu, J.J., Nonaqueous sol-gel synthesis of high-performance $LiFePO_4$. Electrochemical and Solid-State Letters, 7 (12) (2004) A515 – A518.

Yang, L., Qiu, W., Liu, Q., Polyaniline cathode material for lithium batteries. Solid State Ionics, 86 – 88 (1996) 819 – 824.

Yang, L., Wang, S., Mao, J., Deng, D., Gao, Q., Tang, Y., Schmidt O.G., Hierarchical MoS_2/Polyaniline nanowires with excellent electrochemical performance for lithium-ion batteries. Adv. Mater., 25 (2013) 1180 – 1184.

Yang, R., Song, X., Zhao, M., Wang, F., Characteristics of $Li_{0.98}Cu_{0.01}FePO_4$ prepared from improved co-precipitation. Journal of Alloys and Compounds, 468 (2009) 365 – 369.

Yin, Z., Zheng, Q., Controlled synthesis and energy applications of one-dimensional conducting polymer nanostructures: An overview. Advanced Energy Materials, 2 (2012) 179 – 218.

Yonemura, M., Yamada, A., Takei, Y., Sonoyama, N., Kanno, R., Comparative kinetic study of olivine Li_xMPO_4. M=Fe, Mn. Journal of the Electrochemical Society, 151 (9) (2004) A1352 – A1356.

Zeng, L., Fan, C., Structure of polyaniline and its influences on the electrochemical performance of $LiCoO_2$ cathode for lithium ion batteries. Asian Journal of Chemistry, 25 (7) (2013) 3553 – 3556.

Zhang, S.S., Allen, J.L., Xu, K., Jow, T.R., Optimization of reaction condition for solid-state synthesis of LiFePO$_4$-C composite cathodes. Journal of Power Sources, 147 (2005) 234 – 240.

Zhang, W., Hu, Y., Tao, X., Huang, H., Gan, Y., Wang, C., Synthesis of spherical LiFePO$_4$/C via Ni doping. Journal of Physics and Chemistry of Solids, 71 (2010) 1196 – 1200.

Zhang, Y., Feng, H., Wu, X., Wang, L., Zhang, A., Xia, T., Dong, H., Liu, M., One-step microwave synthesis and characterization of carbon-modified nanocrystalline LiFePO$_4$. Electrochimica Acta, 54 (2009) 3206 – 3210.

Zhang, Z., Wei, Z., Wan, M., Nanostructures of polyaniline doped with inorganic acids. Macromolecules, 35 (2002) 5937 – 5942.

Zhao, S.L., Chen, H.Y., Wen, J.B., Li, D.X., Electrochemical properties of spinel LiCo$_x$Mn$_{2-x}$O$_4$ prepared by sol–gel process. Journal of Alloys and Compounds, 474 (2009) 473 – 476.